

University of Alberta

Structure-function relation of isolated preBötC inspiratory networks
in newborn rats

by

Araya Ruangkittisakul



A thesis submitted to the Faculty of Graduate Studies and Research
in partial fulfillment of the requirements for the degree of

Doctor of Philosophy

Department of Physiology

Edmonton, Alberta

Fall 2008



Library and
Archives Canada

Published Heritage
Branch

395 Wellington Street
Ottawa ON K1A 0N4
Canada

Bibliothèque et
Archives Canada

Direction du
Patrimoine de l'édition

395, rue Wellington
Ottawa ON K1A 0N4
Canada

Your file *Votre référence*
ISBN: 978-0-494-46414-4
Our file *Notre référence*
ISBN: 978-0-494-46414-4

NOTICE:

The author has granted a non-exclusive license allowing Library and Archives Canada to reproduce, publish, archive, preserve, conserve, communicate to the public by telecommunication or on the Internet, loan, distribute and sell theses worldwide, for commercial or non-commercial purposes, in microform, paper, electronic and/or any other formats.

The author retains copyright ownership and moral rights in this thesis. Neither the thesis nor substantial extracts from it may be printed or otherwise reproduced without the author's permission.

AVIS:

L'auteur a accordé une licence non exclusive permettant à la Bibliothèque et Archives Canada de reproduire, publier, archiver, sauvegarder, conserver, transmettre au public par télécommunication ou par l'Internet, prêter, distribuer et vendre des thèses partout dans le monde, à des fins commerciales ou autres, sur support microforme, papier, électronique et/ou autres formats.

L'auteur conserve la propriété du droit d'auteur et des droits moraux qui protègent cette thèse. Ni la thèse ni des extraits substantiels de celle-ci ne doivent être imprimés ou autrement reproduits sans son autorisation.

In compliance with the Canadian Privacy Act some supporting forms may have been removed from this thesis.

Conformément à la loi canadienne sur la protection de la vie privée, quelques formulaires secondaires ont été enlevés de cette thèse.

While these forms may be included in the document page count, their removal does not represent any loss of content from the thesis.

Bien que ces formulaires aient inclus dans la pagination, il n'y aura aucun contenu manquant.


Canada

To my family and friends,

Thank you

For being the center of my inspiration

Abstract

Breathing movements are initiated and controlled by the hypothesized pre-Bötzinger Complex (preBötC) inspiratory center in the lower brainstem. Using established newborn rat brainstem-spinal cords and brainstem slices, this thesis examined primarily how preBötC activity is influenced by systematic variation of the rostrocaudal boundaries of these models or variation of superfusate $\text{Ca}^{2+}/\text{K}^{+}$ content. It was found that rostrocaudal extents of respiratory brainstem marker nuclei and ventral brainstem surface markers are constant in 0-4 days-old rats. This enables, with the help of a novel brainstem reference atlas, the generation of preBötC-containing preparations with “calibrated” boundaries. Slices with the preBötC in the center and 500 or 600 μm thickness generate stable inspiratory (motor) rhythm in physiological (3 mM) K^{+} and show a high sensitivity to neuromodulators, in particular opioids.

The rostrocaudal area sufficient (in thin slices) or necessary (in thicker slices) for a functional preBötC is $<200 \mu\text{m}$ and $<100 \mu\text{m}$, respectively, centered at 0.5 mm caudal to the facial nucleus. Slices containing the preBötC plus caudal structures produce a eupnea-like burst pattern, whereas slices containing the preBötC plus rostral tissue generate a mixed eupnea-sigh pattern. Spontaneous arrest of inspiratory bursting in 3 mM K^{+} occurring after several hours (“in vitro apnea”) is reversed by either elevated K^{+} or excitatory neuromodulators. Multineuronal multiphoton Ca^{2+} imaging revealed that preBötC neurons reconfigure their activity between the eupnea and the eupnea-sigh burst pattern induced upon in vitro apnea by thyrotropin-releasing hormone and substance-P,

respectively. Depression of preBötC rhythms in 3 mM K^+ in both the slice and en bloc model by elevation of superfusate Ca^{2+} above physiological (1.2 mM) levels was reversed by raised K^+ .

In summary, this thesis provided novel information regarding the structure-function relationship of rhythmogenic preBötC inspiratory neuronal networks. The findings indicate that endogenous rhythm of the isolated preBötC depends on an extracellular Ca^{2+}/K^+ antagonism. The findings also suggest a (gradient-like) spatiochemical organization of regions adjacent to the preBötC, such that a small preBötC inspiratory-related oscillator generates eupnea under the predominant influence of caudal structures or thyrotropin-releasing hormone-like transmitters, but eupnea-sigh activity when the influence of rostral structures or substance-P-like transmitters predominates.

Acknowledgments

First and foremost, I would like to thank my supervisor, Dr. Klaus Ballanyi, for his tremendous supports and encouragements throughout the years. This work would not be possible without his helps. I truly appreciate the opportunity he has given me to work here and be a part of this exciting research. I would also like to give a special thank to Lucia Secchia for her kindness, supports, and every little things she has helped me with. To the past and present members of the Ballanyi laboratory: Nicoleta Bobocea, Bogdan Panaitescu, Yonglie Ma, Denise Ng, Troy Bornes, and Darren Palathinkal, many thanks for all their helps and for making my journey an enjoyable experience.

I would like to thank my committee members, Drs. John Greer and William Colmers, for their valuable suggestions throughout my graduate program. To the rest of the candidacy and defense examining committee, Drs. Greg Funk, Peter Smith, Christina Benishin, and Jean Champagnat, for taking the time out of their busy schedules to be a part of my committee and for their helpful suggestions and feedbacks.

I would also like to thank Drs. Greg Funk, Stephan Schwarzacher, and Hiroshi Onimaru. I have learnt a lot from them through our collaborations. A special thank to Dr. Xue-jun Sun for his expertise and his continuous willingness to help out with the two-photon system. Also, many thanks to Dr. Silvia Pagliardini for her expertise in immunohistochemistry and for teaching me the technique.

Last but not least, I would like to thank the funding agencies, the CIHR/Maternal-Fetal-Newborn Health and the AHFMR/Hotchkiss Brain Institute, for giving me the opportunity to do research and for their excellent training program that I am thankful to be a part of.

Table of Contents

Chapter I: General Introduction	1
1.1 Overview	2
1.2 Respiratory Network Organization	3
1.3 In Vitro Identification of Respiratory Centers	5
1.3.1 preBötC Inspiratory Center	6
1.3.2 pFRG Expiratory Center	7
1.3.3 Dual preBötC/pFRG Respiratory Center	8
1.4 Mechanisms of Respiratory Rhythm Generation	10
1.4.1 Rhythmogenic Role of Mutual Inhibition	10
1.4.2 Rhythmogenic Role of Pacemaker Neurons	11
1.5 Respiratory Modulation	12
1.5.1 Opioids	13
1.5.2 Substance-P	13
1.5.3 Thyrotropin-releasing Hormone	15
1.5.4 Ca ²⁺	16
1.5.5 cAMP	17
1.6 Respiratory Network Visualization	18
1.7 Open Questions of Respiratory Network Organization	20
1.7.1 Rostrocaudal preBötC and pFRG Extension	21
1.7.2 Endogeneous Rhythmogenic Property of the Isolated preBötC and pFRG	23
1.7.2 Modulation of preBötC Activity Patterns by Neighboring Structures	25
1.8 Objectives and Hypotheses	26
1.9 References	36

Chapter II: High Sensitivity to Neuromodulator-Activated Signaling Pathways at Physiological [K⁺] of Confocally Imaged Respiratory Center Neurons in On-Line-Calibrated Newborn Rat Brainstem Slices	50
2.1 Introduction	51
2.2 Material and Methods	52
2.2.1 Preparation and Solutions	52
2.2.2 Agents	53
2.2.3 Electrophysiological Recording	53
2.2.4 Two-Photon/Confocal Ca ²⁺ Imaging	54
2.2.5 Histological Procedures	55
2.2.6 Data Analysis	55
2.3 Results	56
2.3.1 Anatomical Relationship between Neonatal Rat Brainstem Nuclei and preBötC	56
2.3.2 On-line Histology for Generating Calibrated preBötC Slices	57
2.3.3 Generation of Calibrated 500- μ m-Thick preBötC Slices	57
2.3.4 Rhythm in Calibrated preBötC Slices at 3 mM [K ⁺]	58
2.3.5 Neuromodulation of preBötC Inspiratory Networks	59
2.3.5.1 Inhibition by opiates	59
2.3.5.2 Neurostimulants	60
2.3.6 Ca ²⁺ Imaging of Neuromodulator-Induced Rhythmic Activities in Assemblies of VRC/preBötC Neurons	61
2.4 Discussion	62
2.4.1 Calibrated preBötC Slices	62
2.4.2 High Sensitivity to Neuromodulators of Rhythm in 3 mM [K ⁺]	63
2.4.3 Imaging of VRC/preBötC Neurons	65
2.5 Summary	66
2.6 References	79

Chapter III: Generation of Eupnea and Sighs by a Spatiochemically Organized Inspiratory Network	84
3.1 Introduction	85
3.2 Material and Methods	86
3.2.1 Preparation and Solutions	86
3.2.2 Agents	88
3.2.3 Histological Procedures	88
3.2.4 Electrophysiological Recording	89
3.2.5 Multiphoton/Confocal Ca ²⁺ Imaging	89
3.2.6 Data Analysis	89
3.2.7 Anatomical preconditions for determination of necessary and sufficient preBötC boundaries	90
3.2.8 Criteria for identification and classification of inspiratory-related bursting	91
3.3 Results	92
3.3.1 Slice Thickness Sufficient for Inspiratory-Related Rhythm in 3 mM K ⁺	92
3.3.2 Necessary preBötC Boundaries in 700 μm Slices with Exposed preBötC	94
3.3.3 Distinct Inspiratory Patterns in 700 μm Slices with Exposed preBötC	95
3.3.4 Effects of NK1 Receptor Antagonism on preBötC Activity	96
3.3.5 Ca ²⁺ Imaging of Reconfiguring preBötC Neurons	97
3.4 Discussion	98
3.4.1 A Closer Look at the preBötC	98
3.4.2 A Reconfiguring preBötC Kernel	99
3.4.3 Origin of Sighs versus Biphasic Bursts	99
3.4.4 Spatiochemical Organization of Inspiratory Networks	100
3.5 Summary	102
3.6 References	113

Chapter IV: Dependence on Extracellular Ca²⁺/K⁺ Antagonism of Inspiratory Centre Rhythms in Slices and En Bloc Preparations of Newborn Rat Brainstem	117
4.1 Introduction	118
4.2 Material and Methods	120
4.2.1 Preparation and Solutions	120
4.2.2 Electrophysiological Recording	122
4.2.3 Data Analysis	122
4.2.4 Histology	123
4.2.5 Defined Sectioning of Brainstem-Spinal Cord	123
4.2.5 Ventral Respiratory Column Structures in Newborn Rat Brainstem-Spinal Cords	124
4.3 Results	125
4.3.1 Inspiratory Cervical Rhythm in Transected Brainstem-Spinal Cords	125
4.3.2 Pre/postinspiratory Lumbar Rhythm in Transected Brainstem-Spinal Cords	127
4.3.3 Hypoglossal Nerve Activity in Transected Brainstem-Spinal Cords	127
4.3.4 Rhythm in preBötC Slices	128
4.3.5 Ca ²⁺ Sensitivity of Inspiratory Rhythms in Transected Brainstem-Spinal Cords	129
4.3.6 Ca ²⁺ Block of preBötC Slice Rhythm	131
4.4 Discussion	132
4.4.1 Implications from Defined Sectioning of Isolated Brainstem-Spinal Cords	132
4.4.2 Modulation of preBötC Rhythms by Neighboring Brainstem Regions	133
4.4.3 Ca ²⁺ /K ⁺ Antagonism of preBötC Rhythms	135
4.4.4 Relation of Hypoglossal Bursting with Cervical and preBötC Rhythms	136
4.4.5 Influence of Restricted Diffusion on Respiratory Activities in En Bloc Medullas	137
4.5 Summary	139
4.6 References	156

Chapter V: General Discussion & Conclusions	163
5.1 Summary of Findings	164
5.2 Necessity of Calibrated in vitro Brainstem Preparations	165
5.3 preBötC Rhythm in Physiological Ion Solution	168
5.4 Generation of Eupnea versus Eupnea-Sigh Burst Pattern	170
5.5 Determination of the preBötC Excitability by Ca ²⁺ /K ⁺ Antagonism	173
5.6 Conclusions and Future Perspectives	174
5.7 References	178
Appendix I: Atlas of Newborn Rat Medulla Oblongata	183
Appendix II: Inspiratory burst patterns in 3 mM K⁺ in newborn rat preBötC slices	190
Appendix III: Generation of newborn rat brainstem-spinal cord preparations with defined rostral boundary	200

List of Figures

Figure 1-1	28
Figure 1-2	30
Figure 1-3	31
Figure 1-4	32
Figure 1-5	33
Figure 1-6	34
Figure 1-7	35
Figure 2-1	67
Figure 2-2	68
Figure 2-3	69
Figure 2-4	70
Figure 2-5	71
Figure 2-6	72
Figure 2-7	73
Figure 2-8	74
Figure 2-9	75
Figure 2-10	76
Figure 2-11	77
Figure 2-12	78
Figure 3-1	103
Figure 3-2	105
Figure 3-3	107
Figure 3-4	108
Figure 3-5	109
Figure 3-6	110
Figure 3-7	111

Figure 3-8	112
Figure 4-1	140
Figure 4-2	142
Figure 4-3	143
Figure 4-4	144
Figure 4-5	145
Figure 4-6	146
Figure 4-7	147
Figure 4-8	148
Figure 4-9	149
Figure 4-10	150
Figure 4-11	151
Figure 4-12	152
Figure 4-13	153
Figure 4-14	154
Figure 4-15	155
Figure A2-1	195
Figure A2-2	196
Figure A2-3	197
Figure A2-4	198
Figure A2-5	199
Figure A3-1	202
Figure A3-2	203
Figure A3-3	204
Figure A3-4	205

List of Abbreviations

5HT	5-hydroxytryptamine or serotonin
ACh	acetylcholine
AMPA	α -amino-3-hydroxy-5-methyl-4-isoxazolepropionic acid
AP	area postrema
BA	basilar artery
BAPTA	1,2-bis(o-aminophenoxy)ethane-N,N,N',N'-tetraacetic acid
BötC	Bötzinger complex
c	caudal
c+preBötC	slice containing "caudal" tissue plus the preBötC
cAMP	cyclic-adenosine monophosphate
CCA	caudal cerebellar artery
d	dorsal
DAMGO	[D-Ala ² , N-Me-Phe ⁴ , Gly ⁵ -ol] Enkephalin
DHPG	3,5-dihydroxy-phenylglycine
DMCC	dorsomedial cell column of inferior olive
DMX	dorsal vagal motonucleus
DRG	dorsal respiratory group
EGTA	ethylene glycol tetraacetic acid
GABA	γ -aminobutyric acid
IO	inferior olive
IOD	dorsal inferior olive
IOM	medial inferior olive
IOM _c	caudal end of IOM
IOP	principal inferior olive
IOP _{loop}	lateral loop of IOP
IX	glossopharyngeal nerve
LRN	lateral reticular nucleus
LRN _{div}	LRN divided in medial and lateral subnucleus
m-preBötC	slices containing the preBötC in the middle

NA	nucleus ambiguous
NA _c	compact subdivision of nucleus ambiguous
NK1	neurokinin-1
NK3	neurokinin-3
NMDA	N-methyl-D-aspartic acid
NTB	nucleus trapazoid body
pFRG	parafacial respiratory group
preBötC	pre-Bötzinger complex
PRG	pontine respiratory group
r	rostral
r+preBötC	slice containing “rostral” tissue plus the preBötC
RFN	retrofacial nucleus
RTN	retrotrapezoid nucleus
SD	Sprague Dawley
SP	substance-P
TRH	thyrotropin releasing hormone
v	ventral
V ₄	fourth ventricle
V	trigeminal nerves
VGLUT	vesicular glutamate transporter
VI	abducen nerves
VII	facial motonucleus, nerves
VII _c	caudal end of facial motonucleus
VII _r	rostral end of facial motonucleus
VII _{dor}	dorsal subnucleus of VII
VII _{med}	medial subnucleus of VII
VII _{lat}	lateral subnucleus of VII
VIII	vestibulocochlear nerves
VRC	ventral respiratory column
VRG	ventral respiratory group
W	Wistar

- X vagal nerves
- XI accessory nerves
- XII hypoglossal motonucleus/nerves

CHAPTER I

General Introduction

1.1 Overview

Rhythmic ventilation of the lungs for oxygen uptake and carbon dioxide removal is mediated by contraction of respiratory muscles. Such breathing movements are controlled by a multicomponent neural respiratory network in the lower brainstem. This network not only needs to generate an ongoing robust rhythm since its arrest would lead to death within minutes, but must also be able to rapidly adapt to changes in behavioural states such as those occurring during speaking or exercise. A respiratory network component located in the medulla oblongata is the hypothesized pre-Bötzinger complex (preBötC) inspiratory center. Less is known about the function and location of a presumable expiratory center comprised of neurons of the parafacial respiratory group (pFRG). The preBötC and pFRG may form a dual respiratory center, at least in newborn mammals.

Numerous studies on the preBötC, pFRG, and their interactions are done on brainstem-spinal cord preparations from newborn rats. Sectioning of this en bloc preparation led to the discovery that the preBötC continues to operate in a more reduced transverse slice. Several findings on the en bloc and slice models differ between research groups. For example, some groups propose that the preBötC does not generate a robust rhythm in physiological K^+ in vitro following transection of the pFRG, whereas findings by others argue against this view. These discrepancies may be partly related to a lack of consistent physical dimensions of these models, which may result in differences regarding the content of respiratory groups and modulatory structures such as those mediating central respiratory chemosensitivity. Also, the ionic composition of the superfusate for studying these models varies between groups, particularly with respect to the potent neuromodulators K^+ and Ca^{2+} . It is ultimately desirable to study the neural control of breathing in these models under conditions that resemble those in intact mammals as closely as possible, while providing precise information on their histological content. Under these premisses, such studies will likely provide valuable information on the basic operation of the respiratory network. Knowledge gained from these studies may be applicable to the development of a more efficient treatment of respiratory disturbances such as those associated with apnea of prematurity or sleep apnea.

1.2 Respiratory Network Organization

Breathing movements in mammals are controlled by complex interactions between various classes of respiratory neurons, with a yet unclear contribution from associated glial cells (Feldman, 1986; Bianchi et al., 1995). The rhythm generated by this respiratory network is very robust as it must continue throughout life, while remaining capable of rapidly adapting to changes in behavioural states. The sensory information triggering such alteration in breathing pattern is transmitted to the central respiratory network via afferent input from multiple receptors, most of which are located in the periphery. Examples of these sensors are chemoreceptors in the carotid and aortic bodies, and mechanoreceptors such as those mediating the lung stretch (“Hering-Breuer”) reflex (Feldman et al., 2003; Kubin et al., 2006).

The multiphase organization of the respiratory pattern is a precondition enabling the respiratory network to adapt to the various ventilatory behaviours. Specifically, respiratory muscles are active during one or two of principally three respiratory phases, labelled inspiratory, early-expiratory (or post-inspiratory), and late-expiratory (or pre-inspiratory) (Bianchi et al., 1995; Richter & Spyer, 2001) (Figure 1-1). The specific patterns of neuronal activities, which are transmitted to different respiratory muscles, result from interaction between bilateral columns of rhythmically active neurons in three different brainstem regions. These neuronal arrays form the dorsal respiratory group, the pontine respiratory groups, and the ventral respiratory group, which is considered by several groups as a subregion within the ventral respiratory column (VRC) (Figure 1-1) (Feldman, 1986; Bianchi et al., 1995; Alheid et al., 2004). While these three respiratory groups are directly involved in the neural control of breathing, higher brain structures also influence breathing as indicated by emotionally-driven respiratory behaviours such as crying or some forms of sighs (Ley, 1999; Homma & Masaoka, 2008).

The dorsal respiratory group is comprised of neurons in the region of the nucleus of the solitary tract (Figure 1-1). This nucleus serves as a relay structure for peripheral chemo- and mechanosensory information from the carotid bodies and pulmonary receptors to

structures such as the nucleus ambiguus, the dorsal vagal nucleus, the area postrema and various regions of the pons (Finley & Katz, 1992; Bianchi et al., 1995). The nucleus of the solitary tract also forms reciprocal connections with the retrotrapezoid nucleus (RTN) (Figure 1-1), raphe nuclei, and the ventral respiratory group (Smith et al., 1989; Ellenberger & Feldman, 1990; Bodineau et al., 2000).

The pontine respiratory group is constituted by neurons of the Kölliker-Fuse and parabrachial nucleus that are located dorsolaterally within the rostral pons (Figure 1-1). In addition to input from slowly-adapting lung stretch receptors via the nucleus of the solitary tract, the pontine respiratory group also receives afferent projections from carotid chemoreceptors, nociceptive somatic and visceral stimuli, and the reticular system controlling sleep and wakefulness (Bianchi et al., 1995; Dutschmann et al., 2004). This suggests a role of this neuronal group in complex behaviours such as respiratory reflexes, control of airway muscles during sleep and exercise, vocalization, and respiratory responses to nociceptive stimuli. Stimulation or lesion of these areas transforms normal (eupneic) breathing patterns into tachypnea (fast breathing), bradypnea (slow breathing), apneusis (prolonged inspiration), or apnea (arrest of breathing) (Alheid et al., 2004; Dutschmann et al., 2004). A subset of pontine respiratory neurons is phasically active with most intense bursting during the transition between the inspiratory and expiratory phase (Bertrand et al., 1973; Bianchi et al., 1995). This suggests an involvement of this respiratory group in the regulation of respiratory phase transitions (Rybak et al., 2004). Phasic pontine respiratory group neurons may have polysynaptic connections with medullary respiratory neurons (Bianchi & St.-John, 1982; Segers et al., 1985). Conversely, non-phasically active pontine respiratory neurons seem to project directly to medullary respiratory neurons and are thought to provide tonic input to those neurons (Alheid et al., 2004).

In vivo studies have presented evidence that breathing movements continue when either the dorsal or the pontine respiratory group are extensively lesioned (Feldman 1986; Bianchi et al., 1995). This led to the hypothesis that the essential respiratory rhythm is generated by neuronal networks within the VRC. The notion of a highly-localized

respiratory center in the lower brainstem has been hypothesized for over a century (Flourens, 1858; see also Feldman, 1986). As dealt with in the next section, this hypothesis has gained support from sectioning studies using isolated newborn rat brainstem preparations generating endogenous fictive respiratory activity.

1.3 In Vitro Identification of Respiratory Centers

More than eight decades ago, *in vivo* sectioning experiment of the cat brainstem has presented evidence for a rostrocaudal hierarchy of rhythmogenic neural networks that are responsible for distinct respiratory behaviours such as eupnea, sighs, gasps or apneusis (Lumsden, 1923). More recent work indicated that these findings depended very much on experimental conditions in the *in vivo* models, such as the use of vagotomised versus non-vagotomised animals (Feldman, 1986; Bianchi et al., 1995). The development of respiratory active *in vitro* models from perinatal rodents was a major step toward a quantitative analysis of both the location and functional properties of the hypothesized rostrocaudally organized respiratory centers.

A widely used *in vitro* model for studying the neural control of breathing in mammals is the isolated brainstem-spinal cord preparation from newborn rats that was developed by Suzue (1984). This *en bloc* medulla preparation spontaneously generates a multiphase respiratory rhythm that can be recorded from various cranial and spinal nerves for several hours (Smith et al., 1990; Ballanyi et al., 1999). The *in vitro* respiratory rhythm in this preparation is notably slower than that of intact newborn rats *in vivo*. In addition, *in vitro* inspiratory-related nerve activities show a decremting pattern in contrast to the incrementing patterns seen *in vivo*. However, these differences are primarily related to the use of a lower temperature *in vitro* (25-28 °C) and deafferentation of sensory inputs in the course of the isolation of the medulla (Smith et al., 1990; Ballanyi et al., 1999). The *en bloc* medulla model shows responses to a large number of neuromodulators and clinically-relevant respiratory depressants such as opioids and hypoxia/anoxia, that resemble changes in breathing patterns *in vivo* in response to such treatments (Morin-

Surun et al., 1984; Ballanyi et al., 1999; Solomon, 2002; Mellen et al., 2003; Ballanyi, 2004a,b; Ren et al., 2006).

In line with in vivo lesion studies, removal or lesioning of the dorsal aspect of the newborn rat brainstem-spinal cord preparation did not change inspiratory-related cervical nerve activity (Arata et al., 1990; Hilaire et al., 1990; Smith et al., 1991). Similarly, cervical spinal nerve rhythm persisted upon removal of the pons, although the transection increased inspiratory burst rate (Hilaire et al., 1989). It was concluded in that report that the pons exerts a tonic inhibitory influence on inspiratory networks of the ventral respiratory group. These studies support the hypothesis based on in vivo work (see above) that the primary respiratory rhythm is not generated by the pontine or the dorsal respiratory group.

1.3.1 preBötC Inspiratory Center

A brainstem section study on the newborn rat en bloc model identified a subregion within the VRC that may be a pivotal inspiratory center (Smith et al., 1991). Specifically, that work revealed that inspiratory-related bursting of spinal or cranial nerves stops when the transection in either a rostral-to-caudal or caudal-to-rostral direction approaches a certain region (Figure 1-2) (Smith et al., 1991). This limited brainstem region critical for generation of fictive inspiratory activity is termed the pre-Bötzinger Complex (preBötC) and is located caudal to the Bötzinger Complex (BötC). The BötC constitutes a ventrolateral brainstem area within the VRC caudal to the facial (VII) motor nucleus and is characterized by abundant expiratory neurons (Sun et al., 1997; Fortuna et al., 2008). Findings from in vivo studies indicated that the BötC may contain neuronal networks that are pivotal for the neural control of breathing (Jiang & Lipski, 1990; Bianchi et al., 1995; Sun et al., 1997). The findings of Smith et al. (1991) indicated indirectly the preBötC had a rostrocaudal thickness of 225 μm (Figure 1-2). This suggested that a transverse brainstem slice containing this region may be capable of generating inspiratory-related rhythm. In fact, neurons in the ventrolateral aspect of 350-600 μm thick slices containing the preBötC generated rhythmic bursts of action potentials (Smith et al., 1991). These cellular bursts were synchronous with rhythmic activity of hypoglossal (XII) nerve roots

that innervate inspiratory muscles in the tongue for maintenance of upper airway patency (Smith et al., 1990; Li et al., 2003; Greer & Funk, 2005).

The hypothesis that the preBötC constitutes a pivotal inspiratory center is supported by numerous *in vivo* and *in vitro* studies (Feldman et al., 2003; Feldman & Del Negro, 2006). For example, focal injection of antagonists of kainate/AMPA-type ionotropic glutamate receptors into the preBötC decreased XII nerve burst rate and amplitude in neonatal rat medullary slices (Funk et al., 1993). Furthermore, a study on newborn rat and mouse slices indicated that rhythmogenic preBötC neurons are characterized by postsynaptic responses to opioids acting on μ -receptors, substance-P (SP) acting on neurokinin-1 (NK1) receptors, and thyrotropin-releasing hormone (TRH) acting on yet unknown receptors (Gray et al., 1999). A follow-up study by the same group demonstrated that bilateral injections of the toxin saporin conjugated with SP, which targets NK1 receptor-expressing preBötC neurons, into the brainstem of awake adult rats severely disturbed breathing regularity (Gray et al., 2001). Recently, similar results were obtained upon activation of viral-induced expression of allosterin receptors in neurons in the preBötC region (Tan et al., 2008). The latter findings were consistent with the previous observation that injection of the voltage-activated Ca^{2+} channel blocker ω -conotoxin GVIA into the preBötC of adult cats blocked rhythmic activity of the phrenic nerve which drives the most important inspiratory muscle, the diaphragm (Ramirez et al., 1998). On the other hand, focal application of the ionotropic glutamate receptor agonist DL-homocysteic acid to the preBötC of adult cats stimulated phrenic nerve bursting (Solomon et al., 1999).

1.3.2 pFRG Expiratory Center

Since its discovery, the preBötC inspiratory center and its rhythm generating mechanism have been a major focus in research on the neural control of breathing. However, for more than fifteen years, findings in the newborn rat *en bloc* model have revealed that inspiratory neurons receive rhythmic excitatory drive from more rostrally located “Pre-I neurons” of the ventrolateral medulla that are active during both the pre- and post-inspiratory phase (Onimaru et al., 1992). In fact, it was shown some years earlier that

lesioning or stimulation of this rostral VRC area depresses or resets the inspiratory rhythm, respectively (Onimaru & Homma, 1987; Onimaru et al., 1987). Accordingly, it has been proposed that Pre-I neurons provide a pivotal rhythmic excitatory synaptic drive to inspiratory neuronal networks, and may therefore constitute the primary respiratory rhythm generator (Onimaru & Homma, 1987; Onimaru et al., 1987, 1997). This view has gained support from a more recent voltage-sensitive dye-imaging study in the newborn rat en bloc model by the same group (Onimaru & Homma, 2003). Specifically, they analyzed the spatiotemporal relation between the activity of the preBötC and a group of Pre-I neurons located several hundred micrometers rostral to the preBötC in a region that overlaps with (the ventrolateral aspect of) the VII nucleus. The authors hypothesized that Pre-I neurons in that area constitute the parafacial respiratory group (pFRG), which generates the primary respiratory rhythm (Figure 1-3) (Onimaru & Homma, 2003). Onimaru's group also showed recently that a rostral brainstem block obtained by transection of the newborn rat en bloc preparation between the preBötC and the VII nucleus generates rhythmic VII nerve activity that is presumably driven by the pFRG (Figure 1-3) (Onimaru et al., 2006). Findings from the newborn rat en bloc model also indicated that the pFRG constitutes an expiratory center (Janczewski et al., 2002). This view was based on the finding that pre/post-inspiratory bursting of lumbar nerve roots innervating abdominal expiratory muscles (Iscoe, 1998) is transmitted from rhythmogenic Pre-I interneurons via ipsilateral premotoneurons in the caudal medulla to contralateral lumbar motoneurons. The rhythmic bursting in such pFRG slices may correspond primarily to pre-inspiratory and inspiratory activity since branches of the VII nerve innervating muscles of the alae nasi were found to be active in cats and dogs during these respiratory periods in order to decrease nasal airway resistance during inspiration (Strohl, 1985; Hwang et al., 1988; Bianchi et al., 1995).

1.3.3 Dual preBötC/pFRG Respiratory Center

The studies mentioned above indicated that the pFRG constitutes a rhythmogenic expiratory center. However, the proposal that the preBötC and pFRG form a dual respiratory center within the VRC has only been explicitly stated recently. Specifically, brainstem transection in juvenile rats in vivo at the level of the caudal end of the VII

nucleus (VII_c) abolished pre/post-inspiratory activity of expiratory abdominal muscles, but not inspiratory activity, whereas opioids depressed inspiratory breathing movements, but not the rhythmic abdominal muscle activity (Janczewski & Feldman, 2006). The authors hypothesized that Pre-I neurons of the pFRG represent an expiratory center in addition to the preBötC inspiratory center and that both rhythmogenic VRC areas can operate independently of each other in vivo. Uncoupling of the preBötC and pFRG via opioid-induced “quantal” depression of inspiratory rhythm in the en bloc model and in juvenile rats in vivo presumably results from failure of rhythmic drive from Pre-I neuronal (i.e. pFRG) networks to rhythmogenic preBötC neurons, in addition to direct inhibition of the preBötC neurons via postsynaptic μ receptors (Mellen et al., 2003). The dual pFRG/preBötC respiratory center hypothesis has been supported by findings from several recent studies. For example, slowing of respiratory rhythm in the newborn rat brainstem-spinal cord preparation by anoxia is accompanied by the occurrence of repetitive inspiratory-related cervical nerve bursts and augmentation of post-inspiratory component of lumbar nerve bursts (Taccola et al., 2007). Since both events were abolished in preparations transected between the preBötC and VII_c, this led to the hypothesis that both phenomena, but not the persistent anoxic slowing of inspiratory rhythm, are due to synchronization of the pFRG and preBötC rhythm generators (Taccola et al., 2007).

Although the hypothesis of a dual inspiratory-expiratory rhythm generator constituted by rostrocaudally neighboring rhythmogenic VRC groups appears sound, this concept is not generally accepted. The reason for this is that neurons with a pre/post-inspiratory activity pattern characteristic of pFRG neurons have not been found in adult mammals in vivo to date (Fortuna et al., 2008). Accordingly, it has been hypothesized that the pFRG in neonate corresponds to either the RTN in adults, which mediates central respiratory chemosensitivity, or to expiratory neurons in the BötC (Feldman & Del Negro, 2006; Fortuna et al., 2008). Possibly, the pFRG is particularly important in newborns to compensate for depression of breathing by endogenous opioids that are released during the process of birth (Feldman & Del Negro, 2006; Janczewski & Feldman, 2006). Moreover, Krox20 gene knockout mice, which lack the rhombomeres 3 and 5

consequently resulting in a substantial lesion of the pFRG, can survive into adulthood provided that the opioid receptor antagonist naloxone is applied to overcome the effect of the opioid surge at birth (Borday et al., 2004). These and other findings imply that the respiratory rhythm in adult mammals is normally dominated by the preBötC (Feldman & Del Negro, 2006). However, more work is necessary to define the roles not only of the pFRG, but also of the preBötC and other (modulatory) respiratory groups for breathing in intact animals.

1.4 Mechanisms of Respiratory Rhythm Generation

In intact animals, rhythmogenic respiratory neuron groups are embedded within a larger network of the rostrocaudal columns of respiratory (modulated) neurons in the VRC. Most of these neurons communicate, often mutually, with the dorsal and pontine respiratory groups (Figure 1-1). Accordingly, rhythmogenic VRC neurons integrate a large amount of afferent synaptic inputs. This complexity of respiratory activity in vivo impedes the unraveling of mechanisms of respiratory rhythm generation. Therefore, understanding how the preBötC operates in a reduced system, such as medullary slices, is an important step toward gaining insight into the mechanisms of generation of respiratory rhythm in more intact preparations.

1.4.1 Rhythmogenic Role of Mutual Inhibition

A large number of in vivo and in vitro studies established that glutamate is the major neurotransmitter involved in excitatory connectivity between distinct groups of respiratory neurons (Greer et al., 1991; Funk et al., 1993; Pace et al., 2007b). Some of these, and other studies (Schwarzacher et al., 1991; Johnson, 2007; Ireland et al., 2008; Mironov, 2008) demonstrated that both ionotropic and metabotropic glutamate receptors are involved in recurrent excitation within inspiratory networks, and also between respiratory neurons and cells of the reticular formation that provide (tonic) drive to respiratory networks.

Findings from *in vivo* membrane potential recording of cat VRC neurons led to the “network hypothesis” for generation of respiratory rhythm. According to this hypothesis, mutual inhibition instead of excitation dominates the connectivity of VRC neurons, and is particularly important for interactions between early-inspiratory and post-inspiratory neurons that presumably constitute the primary respiratory oscillator (Figure 1-4) (Richter et al., 1992; Richter & Spyer, 2001). Such (mutual) respiratory inhibition is mediated by ionotropic glycine or γ -aminobutyric acid_A (GABA_A) receptors that are coupled to anion channels, and by metabotropic GABA_B receptors that modulate (presynaptic) Ca²⁺ and K⁺ channels (Kaila, 1994; Brockhaus & Ballanyi, 1998). Consistent with the network hypothesis, blockade of anion channel-mediated inhibition with the GABA_A receptor antagonist bicuculline and the glycine receptor antagonist strychnine, or perfusion of low Cl⁻ saline greatly disturbs respiratory activities or changes their phase relationships in both *in vivo* and *in situ* preparations, such as the working-heart-brainstem preparation (Champagnat et al., 1982; Schwarzacher et al., 1991; Haji et al., 1992; Ramirez et al., 1998; Busselberg et al., 2003). The network hypothesis was, however, challenged by studies showing that respiratory rhythm is not substantially changed by these procedures in the brainstem spinal cord or the slice model (Feldman & Smith, 1989; Onimaru et al., 1990; Ramirez et al., 1997; Shao & Feldman, 1997; Brockhaus & Ballanyi, 1998, 2000).

1.4.2 Rhythmogenic Role of Pacemaker Neurons

The latter observation that the *in vitro* respiratory rhythms persist upon blockade of synaptic inhibition led to the hypothesis that VRC neurons with intrinsic bursting properties, i.e., “conditional burster” or “pacemaker” cells, generate the rhythm (Smith et al., 1991, 2000). In particular, the persistent Na⁺ current (Ballanyi et al., 1999; Del Negro et al., 2002; Pace et al., 2007a) and the Ca²⁺-activated nonspecific cation current (Peña et al., 2004; Pace et al., 2007b) contribute to intrinsic bursting of medullary respiratory neurons, as revealed in the newborn rodent *en bloc* and slice models. Thorough analysis of these currents showed on the one hand that pacemaker neurons expressing the persistent Na⁺ current were insensitive to the voltage-activated Ca²⁺ channel blocker Cd²⁺, while their activity was inhibited by the persistent Na⁺ current blocker riluzole (Del

Negro et al., 2002; Ptak et al., 2005). On the other hand, pacemaker neurons with Ca^{2+} -activated nonspecific cation current were inactivated by both Cd^{2+} and the more specific antagonist flufenamic acid (Peña et al., 2004; Del Negro et al., 2005). The specific expression of these currents in distinct respiratory neurons may depend on both the developmental stage of animals and the species studied (Peña et al., 2004; Del Negro et al., 2005; Pace et al., 2007b).

In summary, the latter reports and various other studies showed that respiratory neurons possess intrinsic bursting properties. However, administration of AMPA or SP re-establishes the rhythm after blockade of these pacemaker currents (Del Negro et al., 2005), suggesting that respiratory rhythmogenesis may depend on neuronal excitability of preBötC neurons, including those without intrinsic bursting properties, rather than on a specialized set of pacemaker neurons per se. Therefore, according to the “group-pacemaker hypothesis” (Del Negro et al., 2002, 2005; Feldman & Del Negro, 2006), respiratory rhythm is an emergent behavior, generated primarily by recurrent excitation among preBötC neurons (Figure 1-4). Arguments for and against the role of pacemakers in generation of eupnea and gasping have been recently discussed (Paton & St-John, 2007; Ramirez & Garcia, 2007).

1.5 Respiratory Modulation

Respiratory network activity is influenced by a variety of excitatory and inhibitory neuromodulators (Figure 1-5). This probably reflects, at the cellular level, the necessity to rapidly adapt breathing to a wide range of behavioural states. It is beyond the scope of this document to provide a comprehensive overview of all classes of respiratory neuromodulators that include among others peptides, biogenic amines, purines and acetylcholine. Instead, the focus here will be on those neuromodulators that are considered as potential markers for rhythmogenic respiratory neurons. As stated above, these markers are peptides, specifically opioids, SP and TRH. Additionally, the second-messengers Ca^{2+} and cyclic adenosine monophosphate (cAMP) will be dealt with as they

function as signalling molecules that mediate the downstream effects of opioids, SP and TRH, among other neuromodulators (Figure 1-5) and are considered to be most relevant for respiratory network function.

1.5.1 Opioids

In vivo experiments on VRC neurons in adult mammals have established that both, μ and δ types of opioid receptors are involved in depression of breathing (Morin-Surun et al., 1984). In the rat brainstem, μ receptors are expressed at high density in cardiorespiratory-related nuclei already at birth, when δ receptors are scarce (Xia & Haddad, 1991). Accordingly, depression of inspiratory-related rhythms by opioids in vitro and in vivo is mediated by μ receptors in newborns, while δ receptors contribute to such depression after approximately the first postnatal week (Greer et al., 1995). A study on newborn rat brainstem-spinal cords showed that opioid-induced frequency depression of cervical inspiratory nerve bursts was not accompanied by a major effect on membrane potential or conductance in the vast majority of respiratory neurons (Ballanyi et al., 1997). It was concluded by these authors that the inhibitory action of these drugs might be primarily due to presynaptic effects on synaptic transmission, possibly involving block of voltage-activated Ca^{2+} currents. A thorough study with intracellular recordings showed that Pre-I neurons in the newborn rat en bloc model are not affected by opioids, whereas different types of inspiratory VRC neurons show either no response or a modest hyperpolarization and conductance increase in response to activation of μ or κ receptors (Takeda et al., 2001). Finally, a seminal study using both the en bloc and the slice model, and also juvenile rats in vivo (Mellen et al., 2003) indicated that quantal depression of inspiratory rhythm by opioids is due to a failure of rhythmic drive from the pFRG to the preBötC that is also inhibited via postsynaptic μ receptors, a hypothesized marker for rhythmogenic inspiratory cells (Gray et al., 1999). As outlined above, these findings support the hypothesis that breathing is regulated by a dual respiratory center.

1.5.2 Substance-P

Application of capsaicin depletes SP and glutamate from presynaptic terminals and slows inspiratory frequency in brainstem slice preparation, suggesting that endogenous (tonic)

release of SP and glutamate is important for rhythm generation (Morgado-Valle & Feldman, 2004). In addition, application of SP itself stimulates respiratory rhythm (Murakoshi et al., 1985; Johnson et al., 1996). In the report by Murakoshi et al. (1985), and also in a more recent study (Yamamoto et al., 1992), SP produced an excitatory effect mainly in preparations with a low baseline frequency, whereas it could reduce respiratory burst rate in preparations with a high inspiratory burst rate. Observations made with selective agonists and antagonists of tachykinin receptors indicated that both NK1 and NK3 receptors are involved in the stimulatory effect on isolated respiratory networks (Monteau et al., 1996). SP is also capable of reversing depression of inspiratory frequency induced by the α_2 adrenergic receptor agonist clonidine (Yamamoto et al., 1992). In the latter study on the newborn rat en bloc model, the drug induced tonic nerve activity at higher ($>0.1 \mu\text{M}$) concentrations as reported earlier (Murakoshi et al., 1985). Furthermore, SP restored or potentiated extracellularly recorded burst activity of Pre-I or inspiratory neurons after suppression of synaptic transmission in the en bloc model (Yamamoto et al., 1992) and mouse slices in elevated K^+ (Del Negro et al., 2005), respectively, or after spontaneous arrest of slice rhythm in 3 mM K^+ (Peña & Ramirez, 2004). Finally, bath administration of SP in the en bloc preparation increased the frequency of “biphasic” bursts, which were hypothesized to underlie the inspiratory-related sigh pattern in vivo (Shvarev et al., 2003) (Figure 1-6), suggesting that SP also plays a role in modulation of inspiratory patterns.

Consistent with the role of SP in respiratory modulation, NK1 receptor antagonism depressed inspiratory rhythm in mouse slices (Telgkamp et al. 2002). A milestone slice study reported that NK1 receptors, in addition to μ opioid receptors, are characteristic feature of rhythmogenic newborn mouse “type-I” preBötC inspiratory neurons (Gray et al., 1999). Moreover, depolarization induced by both SP and TRH is also another characteristic of these rhythmogenic “type-I” neurons (Gray et al., 1999). A follow-up study by the same group demonstrated that depressed breathing occurred following toxin-targeting of NK1 receptor-expressing preBötC neurons (Gray et al., 2001). Similar to the in vitro models, medullary respiratory neurons were excited in adult cats in vivo upon SP microinjection into the VRC (Rampin et al., 1993). According to the hypothesis that NK1

receptors are a marker for rhythmogenic neurons, attempts have been made to identify the specific location of the preBötC and its cellular elements in adults and also during perinatal development via immunohistochemical labelling of these receptors (Wang et al., 2001, Pagliardini et al., 2003; Thoby-Brisson et al., 2003; Greer et al., 2006). However, there is increasing evidence that NK1 receptors are expressed in various neurons of brainstem structures that partially overlap with the preBötC, such as ambigular motoneurons (Gray et al., 1999) and expiratory neurons of the BötC and preBötC region, while some inspiratory preBötC neurons lack these receptors (Hayes & Del Negro, 2007).

1.5.3 Thyrotropin-releasing Hormone

Intracerebroventricular injection of TRH had a strong stimulatory effect on breathing in adult rodents (Hedner et al. 1981; Homma et al., 1984). Similar TRH induced respiratory frequency potentiation effects were seen in fetal, neonatal and adult animals of a diversity of species (for references, see Greer et al., 1996). The respiratory stimulant effect of TRH is hypothesized to result from direct TRH action on the preBötC as suggested from finding in rhythmic slices from newborn rats that local injection of TRH into the preBötC increases respiratory frequency (Greer et al., 1996). TRH also exerts its effect on other respiratory (modulated) regions such as the BötC, caudal ventral respiratory group, nucleus of the solitary tract, and area postrema (Mutolo et al., 1999). In line with this, synaptic terminals containing TRH were found to have a differential distribution within the ventrolateral medulla (McCown et al., 1986; Sun et al., 1996). At the XII motonucleus level, local administration of the drug changed the amplitude of XII nerve discharge but not inspiratory burst rate of rhythmic slices from neonatal mice (Funk et al., 1994).

In newborn rat brainstem-spinal cords, it was first described by Murakoshi et al. (1985) that TRH accelerates respiratory frequency. In the report of Greer et al. (1996), TRH had a stronger excitatory effect in fetal preparations, in which baseline frequency of respiratory rhythm is much slower than in those from newborn rats. The assumption by the latter authors that the rate of rhythm before birth depends on the tonic excitatory drive to the ventral respiratory group neurons (Greer et al., 1996) is consolidated by the recent

findings that not only TRH, but also other depolarizing drugs, such as Ba^{2+} and muscarine, accelerate fictive inspiratory activity in fetal rats (Ballanyi et al., 1999; Greer et al., 2006). Importantly, the observation that TRH depolarized inspiratory type-I mouse neurons in the slice model led to the hypothesis that rhythmogenic pre-BötC cells possess yet uncharacterized postsynaptic TRH receptors as a characteristic marker in addition to NK1 and μ receptors (Gray et al., 1999).

The major source of TRH and SP to the preBötC is from serotonergic raphe neurons. The raphe system projects extensively to various respiratory nuclei. Although, TRH and SP are colocalized with serotonergic neurons, no double-labelling of NK1 receptor expressing neurons and tryptophanhydroxylase-immunoreactive neurons has been found (Kachidian et al., 1991; Nattie et al., 2004). This suggests possible differential roles of these neuromodulators on respiratory functions.

1.5.4 Ca^{2+}

In VRC neurons of adult cats, injection of the Ca^{2+} chelator BAPTA increased the steepness and amplitude of excitatory drive potentials (Richter et al., 1993) and prolonged the time period of repetitive action potential discharge due to a decrease in membrane conductance attenuating adaptation (Pierrefiche et al., 1995). It was hypothesised that a prominent excitation-related rise of intracellular Ca^{2+} activates different types of Ca^{2+} -activated K^+ channels, which are involved in the termination of inspiration (Figure 1-5) (Pierrefiche et al., 1995). Indeed, rises in intracellular Ca^{2+} by up to several hundred nanomolar accompanied rhythmic depolarizations of inspiratory neurons in preBötC slices (Frermann et al., 1999; Koshiya & Smith, 1999). Such Ca^{2+} transients were strongly attenuated in voltage-clamp, suggesting that a major component of these responses is caused by Ca^{2+} influx via voltage-activated Ca^{2+} channels (Frermann et al., 1999). Indeed, different classes of VRC neurons in rodents possess a characteristic array of voltage-activated Ca^{2+} channels (Onimaru et al., 1996, 2003; Elsen & Ramirez, 2005). However, termination of the excitatory phase is only followed by a significant (non-synaptically mediated) hyperpolarization in a minority of Pre-I or inspiratory neurons of the neonatal rat en bloc model (Onimaru et al., 1996, Ballanyi et al., 1999).

Besides, oscillatory membrane potential trajectories do not appear to differ when respiratory neurons in the brainstem-spinal cord preparation are whole-cell recorded with electrodes containing either 1 mM (Brockhaus & Ballanyi, 1998) or 10-11 mM of Ca^{2+} chelators BAPTA (Smith et al., 1992; Onimaru et al., 1996) or EGTA (Onimaru & Homma, 1992; Onimaru et al., 1998). These results indicate that this particular second-messenger function of Ca^{2+} , which is important for adaptation of excitability in a variety of neuronal systems, may not be crucial for generation of primary rhythm or respiratory phase transitions in the in vitro respiratory network, at least not in neonatal rats. However, recent studies on the mouse slice model indicated that Ca^{2+} -activated nonselective cation channels play a major role in rhythmogenic preBötC networks (Pace et al., 2007b; Mironov, 2008).

1.5.5 cAMP

Beside Ca^{2+} , cAMP is another crucial second messenger that modulates neuronal functions (Figure 1-5) (Hille, 1992). For example, a nonspecific cAMP-dependent cation conductance has been hypothesized to be involved in bursting of respiratory neurons in vivo (Richter et al., 1992). However, cAMP-elevating drugs such as forskolin, db-cAMP and 8-Br-cAMP had no effects on inspiratory rhythm in the newborn rat brainstem-spinal cord preparation (Smith et al., 1995). In contrast, an acceleration of burst rate due to such drugs was reported by others (Arata et al., 1993). In the latter study, the stimulatory effect of cAMP-elevating drugs was particularly evident in preparations with a rather low control burst rate, whereas no effect or even a slight inhibitory action was revealed in preparations with a high frequency, similar to the actions of SP and TRH (see above). It might well be that under the experimental conditions of the study by Smith et al. (1995) cellular cAMP levels were already high enough to produce maximal respiratory network stimulation. Arata et al. (1993) also showed that forskolin reversed the frequency depression of the in vitro respiratory rhythm elicited by clonidine which lowers cAMP via α_2 adrenoceptors (Uhlén & Wikberg, 1988). The assumption of a stimulatory action of cAMP on the respiratory network gains further support by the finding that cAMP-elevating drugs also antagonize the respiratory depression (and even in vitro apnea), evoked by opiates, nociceptin or prostaglandins (Figure 1-5) (Ballanyi et al., 1997;

Ruangkittisakul & Ballanyi, 2006). cAMP-elevating agents also have a direct excitatory effect on the intrinsic burst rate of Pre-I neurons (Arata et al., 1993). Elevation of cAMP also increases the excitability of expiratory neurons in vivo through stimulation of protein kinase A, likely via phosphorylation of a multitude of possible targets, resulting in inhibition of different types of K⁺ channels, depression of GABAergic and glycinergic conductances, and enhancement of glutamate-mediated excitability (Lalley et al., 1997). Regardless of which mechanism will turn out to be primarily responsible for the overall increase in excitability of VRC neurons upon cAMP elevation (and also for the block of respiratory rhythm when cAMP levels fall below a critical level), regulation of cellular cAMP does play a critical role in respiratory rhythm generation (Arata et al., 1993; Ballanyi et al., 1997, 1999; Richter et al., 1997). This may have potential therapeutic importance for the treatment of pathological disturbances of breathing.

1.6 Respiratory Network Visualization

The most commonly used approach to characterize neurons from the proposed preBötC and pFRG respiratory centers is to record their rhythmic activity extracellularly (Guyenet et al., 2004), or preferentially intracellularly with whole-cell or perforated patch-clamp recording techniques (Ballanyi et al., 1997). In the case of hypothesized preBötC neurons, it may be tested during such intracellular recording whether these cells are capable of intrinsic bursting and also show postsynaptic responses to TRH, NK1 agonist, and opioids prior to addressing a specific (pharmacological) question. However, this is technically challenging because of a limited long term stability of intracellular recording, and thus is rarely done (Lorier et al., 2008). Alternatively, the recorded cells may be tested for these receptors afterward using antibodies for NK1 receptors, μ receptors, and/or glutamate transporter VGLUT1 and VGLUT2 to identify them as excitatory neurons (Guyenet et al., 2004). A novel technique aimed at visualizing NK1 receptors of rhythmogenic preBötC neurons uses fluorescent dye-labelled SP prior to intracellular recording in rhythmic slices (Pagliardini et al., 2005). However, this approach is limited by the fact that various respiratory neuron classes within and outside the preBötC express

NK1 receptors (Hayes & Del Negro, 2007). Accordingly, the identification of rhythmogenic preBötC neurons until now relies on rather vague criteria that are difficult to test on a routine basis. Until highly specific and easily testable markers of preBötC neurons are available, it is at least desirable to use recording techniques that allow the assessment of the activity of visually-identified neurons in the hypothesized preBötC region. Ca^{2+} imaging is suited for this purpose because rhythmic respiratory neuronal activity results in oscillations of the free cytosolic Ca^{2+} which can be measured both at the cellular and network levels (Frermann et al., 1999; Koshiya & Smith, 1999; Thoby-Brisson et al., 2005; Ballanyi et al., 2008).

Ca^{2+} imaging of inspiratory-related neuronal population activity was originally done with charged-coupled device (CCD) video cameras in preBötC slices that were labelled “overnight” (>10 hours) with the membrane-permeant acetoxymethyl (AM) form of the Ca^{2+} -sensitive dye calcium green-1-AM (Koshiya & Smith, 1999). Specifically, this study showed that the rhythmic Ca^{2+} oscillations persisted in approximately 70% of labelled inspiratory neurons after XII nerve motor output was blocked with a blocker of kainate/AMPA-type glutamate receptors (Figure 1-7). Accordingly, that imaging study supported the hypothesis, proposed and confirmed via whole-cell recording by the same group in the report on the discovery of the preBötC neurons, that inspiratory center neurons possess pacemaker properties (Smith et al., 1991). Ca^{2+} imaging also revealed emergent respiratory-like activity in the VRC region of mouse slices starting at embryonic day 15 (Thoby-Brisson et al., 2005). Recently, a novel “tilted sagittal slab” preparation from neonatal rats enabled simultaneous Ca^{2+} imaging from extended lateral portions of the VRC including both the pFRG and preBötC (Barnes et al., 2007). Although these studies provide important information on the rhythmic behaviour of populations of inspiratory neurons in the slice model, such Ca^{2+} imaging has limitations. Firstly, although video camera Ca^{2+} imaging allowed the discrimination of single spots corresponding to individual cells, no morphological details of these neurons were revealed (Figure 1-7). The use of multiphoton confocal microscopes for imaging of respiratory activity may provide better spatial resolution, deeper recording depth, and less photodamage compared to CCD cameras (Ballanyi et al., 2008). Secondly, the time

resolution of sampling (in the study on the tilted sagittal slab) was not adequate to distinguish between pre-inspiratory and inspiratory activity of Pre-I neurons and preBötC cells, respectively. Thirdly, since Ca^{2+} dyes also buffer free cytosolic Ca^{2+} and therefore delay and attenuate its dynamic changes, the duration of cytosolic Ca^{2+} rises can last up to several seconds compared to less than one second cellular inspiratory activity (Ballanyi et al., 1999; Feldman & Del Negro, 2006). This also impedes the differentiation between Pre-I and inspiratory cells based on the presence/absence of post-inspiratory activity.

Alternatively, voltage-sensitive dye-imaging techniques allow for the detection of rhythmic activity at a much higher time resolution compared to Ca^{2+} imaging, although the use of voltage-sensitive dyes itself may change respiratory neuronal properties (Ballanyi et al., 2008). Specifically, the pre-inspiratory but not the post-inspiratory component of Pre-I neuronal bursting is revealed by voltage-sensitive dye-imaging (Onimaru & Homma, 2003). To date, this technique has been used at a spatial resolution that is insufficient to resolve the activities of single respiratory neurons (Figure 1-3) (Onimaru & Homma, 2003; Oku et al., 2007). Nevertheless, voltage-sensitive dye-imaging studies led to the discovery of the pFRG (Onimaru & Homma, 2003). They also provided important information regarding the activity of the pontine and dorsal respiratory groups (Onimaru & Homma, 2005) and the response to opioids in the en bloc model (Oku et al., 2007).

1.7 Open Questions of Respiratory Center Organization

The topics dealt with in this section and also the objectives and hypotheses in section 1.8 are based on knowledge of respiratory center functions in the perinatal rodent en bloc and slice models at the start and during the projects of this thesis. Since this time period spans over several years, progress may have been made by others in some regard. For example, according to my knowledge we were the first to use multiphoton microscopy for Ca^{2+} imaging of preBötC neurons in acute slices. Since our findings were published (Ruangkittisakul et al., 2006), others have also used this imaging technique in the slice model (Hayes & Del Negro, 2007; Mironov, 2008).

The research on the hypothesized preBötC inspiratory and the pFRG expiratory center in the perinatal rodent en bloc and slice models described above has greatly increased the understanding of neural control of breathing. Nevertheless, there are a number of open questions particularly regarding structure-function analyses for both components of the hypothesized dual respiratory center and their interactions in the “respiratory networks in the dish”. Several of these questions refer to the fact that a variety of findings differ notably between research groups. Some of these discrepancies are referred to below. One common feature of these discrepant findings is that the (age-related) anatomical content of the in vitro models and/or the composition of the superfusate for their study vary between these groups.

1.7.1 Rostrocaudal preBötC and pFRG Extension

Until now, functional studies on the inspiratory and expiratory center using both the en bloc and slice model typically did not provide histological proof of their rostrocaudal dimensions. Accordingly, the content of VRC structures in these models may differ between groups. This creates difficulty when trying to compare results between studies, as these preparations may contain different extents of brainstem structures that are capable of modulating respiratory activity. For the en bloc model, it would be beneficial to show the level at which the spinal cord and adjacent brainstem areas are isolated via transection from rostrally neighboring tissue. Moreover, the section level may also be important in en bloc preparations without the pons since such preparations may contain a different content of the preBötC and the pFRG, in addition to the chemosensitive RTN that may partially overlap with or even be identical to the pFRG (Figure 1-1) (Feldman & Del Negro, 2006; Guyenet et al., 2008; Fortuna et al., 2008).

The latter consideration also applies for the slice model. Because the thickness of the rhythmic rodent slices varies between 1100 μm (Rekling et al., 1996) and 200 μm (Koshiya & Smith, 1999), they contain a notably differing content of neighboring VRC structures in addition to the preBötC. It is remarkable that slices as thin as 200 μm generate inspiratory-related rhythm, though in superfusate K^+ above physiological levels

(see below). This suggests that the rostrocaudal thickness of the preBötC that is sufficient for generation of rhythm is smaller than the 225 μm suggested by measurements of the critical rostral and caudal boundary for inspiratory rhythm generation in sectioned caudal and rostral newborn rat brainstem blocks (Figure 1-2) (Smith et al., 1991). Despite the use of 200 μm or slightly thicker slices by several groups, there is yet no information regarding the histological boundaries of slices which contain the minimal content of the preBötC that is sufficient (in a thin slice) for generation of fictive inspiratory rhythm. Similarly, it is not known whether an even smaller fraction of the preBötC is necessary for such rhythm in a thicker slice which presumably provides more tonic drive to rhythmogenic neurons.

Another point that needs to be considered is the age of the animals. In studies on newborn rats, 0-4 days-old animals are used in most cases for the *in vitro* analysis of the preBötC and pFRG. During this time period, various brain regions may show a notable increase in physical dimension (Paxino et al., 2007). If such growth includes the rostrocaudal extension of the brainstem, a 400 μm slice from a 0-day-old rat would probably contain a relatively larger content of the VRC compared to a slice of identical thickness from a 4-days-old rat. Whether that is the case can be estimated by measuring the rostrocaudal extensions of respiratory marker nuclei in the vicinity of the functionally defined VRC. Examples of such respiratory marker nuclei include the VII motor nucleus and different subsections of the inferior olive. According to such information, it may be possible to generate “calibrated” *en bloc* preparations and medullary slices with a histologically defined content of respiratory structures. This histological information may not only be important for determination of preBötC boundaries that are sufficient or necessary for generation of rhythm in the slice model, but may also provide functional information regarding the rostrocaudal extent of the pFRG. Specifically, systematic transection of calibrated newborn rat brainstem-spinal cords in conjunction with recording of the pre/post-inspiratory motor output of lumbar or VII nerve roots may help to identify the boundaries of the functional pFRG.

1.7.2 Endogenous Rhythmogenic Properties of the Isolated preBötC and pFRG

As described above (1.3.2), newborn rat brainstem blocks cut rostral to the preBötC generate presumably pFRG-driven rhythmic VII nerve activity (Onimaru et al., 2006). However, such activity has so far only been recorded in solution with 6.2 mM K^+ , which is more than twice higher than the physiological K^+ concentration (3 mM) in interstitial brain tissues (Somjen, 2002). Furthermore, bath-application of the μ receptor agonist DAMGO enhances the rather weak VII nerve activity and Pre-I neuronal bursting in the rostral brainstem blocks in 6.2 mM K^+ (Onimaru et al., 2006). This indicates that the isolated pFRG needs external stimuli such as elevated K^+ and likely disinhibition by opioids to operate in isolation. A similar external drive is thought to be necessary for the generation of inspiratory rhythm in the slice model (Feldman & Del Negro, 2006). The latter hypothesis is based on an observation stated under “references and notes” in the report on the preBötC discovery (Smith et al., 1991) that “slices thinner than 500 μ m did not generate [XII] motor output at 3 mM K^+ , but generated rhythmic output at K^+ concentrations of 9 to 11 mM”. Since then, elevated superfusate K^+ levels (mostly 8-9 mM) are routinely used to study the rhythmic preBötC slices (Richter & Spyer, 2001; Feldman & Del Negro, 2006). However, elevated superfusate K^+ increases neuronal excitability unspecifically throughout the entire preparation. Such high K^+ may result in different patterns and pharmacological responses of respiratory rhythm in slices compared to the in vivo situation (Richter & Spyer, 2001; St. John et al., 2002). For example, elevated extracellular K^+ causes a positive shift of the equilibrium potential of K^+ currents leading to membrane depolarization. Elevated K^+ also depolarizes the membrane potential of astrocytes (White et al., 1992). Since glial cells may modulate respiratory activity (Hulsmann et al., 2000; Funk et al., 2008), K^+ may indirectly alter respiratory network functions through modulation of glial networks. Additionally, effects of Cl^- current activation on isolated respiratory network functions were reported with contradictory results. On the one hand, GABA mediates respiratory depression in newborn rat brainstem spinal cord preparations in 3 mM K^+ (Brockhaus & Ballanyi 1998; Ren & Greer, 2006). On the other hand, the opposite effect was observed when GABA was applied to neonatal rat slices in 9 mM K^+ (Ren & Greer, 2006) or slices from 0-3

days-old mice in 8 mM K^+ (Ritter & Zhang, 2000). As discussed by Ren & Greer (2006), this discrepancy is possibly due to the use of different superfusate K^+ levels which modulates the activity of Cl^- transporters such as KCC2 (Payne, 1997), resulting in a positive shift of Cl^- equilibrium potential by several tens of millivolt. Consequently, depending on superfusate K^+ , the direction of Cl^- currents can be either inward or outward, leading to membrane potential hyperpolarization or depolarization, respectively.

The finding in the original report (Smith et al., 1991) that preBötC slices thinner than 500 μm did not generate motor output was in apparent conflict with the findings in Figure 1 of that study, in which rhythm seems stable even when the defined 75 μm sections were rather close to the critical boundary of the preBötC (Figure 1-2). While this was not discussed in that initial report or follow-up studies, it is possible that these sectioned newborn rat en bloc preparations remained able to generate rhythm because the partially exposed preBötC still received adequate drive from the remaining caudal or rostral structures as opposed to a possibly smaller drive from neighboring structures in slices <500 μm thick. Furthermore, it was not studied by Smith et al. (1991) whether the apparent lack of rhythmic activity in thinner slices at physiological K^+ was limited to only XII motor output while the preBötC interneuron burstings possibly still remained active (Figure 1-2).

In contrast to the persistence of inspiratory-related cervical nerve bursts in 3 mM K^+ of en bloc brainstems with a rostral boundary close to the preBötC in the latter study, inspiratory rhythm was depressed (McLean & Remmers, 1994) or stopped (Onimaru & Homma, 1987) upon brainstem section between the VII nucleus and the preBötC. These discrepant findings may be explained by the use of superfusate with different Ca^{2+} concentration in these studies. Specifically, preBötC rhythm was unaltered in 1.5 mM Ca^{2+} (Smith et al., 1991), whereas burst rate was slowed after presumable similar transection in the study using 2 mM Ca^{2+} (McLean & Remmers, 1994), while rhythm was blocked after comparable transection in 2.4 mM Ca^{2+} (Onimaru & Homma, 1987). Accordingly, it is possible that the activity of the isolated preBötC is depressed by extracellular Ca^{2+} which is a crucial determinant of neuronal excitability (Hille, 1992;

Somjen, 2002). If that were the case, other discrepant findings in the in vitro models, e.g., regarding the role of pacemaker neurons for generation of rhythm (1.4.2), may at least be partly related to the use of superfusate Ca^{2+} that varies between 0.8 mM and 2.4 mM in these studies (Onimaru & Homma, 1987; Rekling et al., 1996; Brockhaus & Ballanyi, 1998; Gray et al., 1999; Peña & Ramirez, 2004).

1.7.3 Modulation of preBötC Activity Patterns by Neighboring Structures

The adaptation of breathing movements in vivo caused by changes in the environment or emotional processes is sometimes accompanied by a change of inspiratory-related behaviours. For example, a severe fall of the oxygen content of the inhaled air (hypoxia) causing complete oxygen depletion (anoxia) in respiratory brainstem tissues results in gasps that also occur shortly before death (St. John, 1996). On the other hand, sighs are enhanced breathing efforts similar to gasps that are associated with emotional processes such as a “sigh of relief”. Moreover, sighs are also the initial response of full behavioural arousal from sleep in infants and are hypothesized to be associated with sudden infant death syndrome (Thach & Lijowska, 1996; Franco et al., 2003). Findings from mouse slices in 8 mM K^+ indicated that isolated preBötC networks are capable of generating fictive sighs and gasps in addition to “normal” (eupnea) fictive breathing activity (Lieske et al., 2000) (Figure 1-6). In contrast, sighs do not appear to be a typical behaviour seen in newborn rat preBötC slices in 8-9 mM K^+ . However, “sigh-like” inspiratory-related activity, labelled as “biphasic bursts”, comprised of cervical nerve bursts with an initial fast peak followed by a secondary peak that was similar or smaller in amplitude to the first peak was revealed in the newborn rat en bloc model in 6.2 mM K^+ (Shvarev et al., 2003) (Figure 1-6). The frequency of these biphasic bursts increases upon application of SP (Shvarev et al., 2003). It has not been studied whether the lack of occurrence of sighs in rat slices represents a species difference compared to mice or is rather due to differences in the dimensions of brainstem structures in rat and mouse slices (1.7.1). It remains to be elucidated whether specific brainstem structures, superfusate K^+ concentrations, or specific neuromodulators contribute to generation of eupnea, eupnea-sigh, and eupnea-biphasic inspiratory burst patterns.

Another question relates to the origin of fictive eupnea, sighs and gasps in the mouse slices. The group of Ramirez presented evidence that fictive sighs and eupnea are induced in mouse slices via distinct sets of receptors such as ionotropic/metabotropic glutamate receptors, cholinergic receptors, and tachykinin (SP) receptors, in addition to Ca^{2+} channel subtypes (Lieske et al., 2000; Lieske & Ramirez, 2006a,b; Tryba et al., 2008). On the other hand, the generation of fictive gasps involves 5HT_{2A} receptors (Tryba et al., 2006). Ramirez's group also showed that whole-cell recorded inspiratory neurons reconfigure their activity pattern between fictive eupnea, sigh and gasp bursts following pharmacological or metabolic manipulation of the mouse slices (Lieske et al., 2000). This led to the hypothesis that distinct inspiratory behaviours are mediated by a reconfiguring network of rhythmogenic preBötC neurons (Lieske et al., 2000, 2001). In that work, rather thick (550-700 μm) mouse slices were used. It therefore remains to be studied whether reconfiguring activity patterns are an intrinsic property of the small preBötC network in these thick slices. Alternatively, rostrocaudally neighboring structures such as the pFRG or the RTN may provide, possibly via different sets of sigh or eupnea neurotransmitters, a drive that causes the reconfiguration.

1.8 Objectives and Hypotheses

It was the aim of this thesis to study some of the open questions outlined in section 1.7 regarding the neural control of breathing. In summary, these questions referred to the analysis of the relationship of inspiratory-related interneuronal preBötC activity and preBötC-driven motor output with the physical dimensions of the en bloc and the slice model, and the K^+ and Ca^{2+} content of the superfusate used to study these models. Several hypotheses were studied in three distinct projects. Results of Project 1 and 2 have each been published in the Journal of Neuroscience while those of Project 3 have been published in the Journal of Physiology.

I hypothesize for Project 1 that

- (i) The rostrocaudal extent of respiratory brainstem marker nuclei is constant in newborn rats, thus enabling the generation of calibrated preBötC slices.
- (ii) Calibrated slices with the preBötC in the center and 500-600 μm thickness are capable of stable inspiratory rhythm in physiological (3 mM) K^+ .
- (iii) Inspiratory rhythms in 3 mM K^+ of calibrated preBötC slices have a high sensitivity to neuromodulators, in particular to opioids.
- (iv) The morphology of histologically identified preBötC neurons can be visualized with multiphoton Ca^{2+} imaging.

I hypothesize for Project 2 that

- (i) The necessary and sufficient rostrocaudal extension for a functional preBötC in calibrated newborn rat brainstem slices in 3 mM K^+ are $<200 \mu\text{m}$.
- (ii) Structures that rostrocaudally neighbor the preBötC affect its activity and inspiratory patterns, in particular eupnea and eupnea-sigh burst patterns.
- (iii) The rhythmogenic preBötC kernel in thin slices is capable of reconfiguring its activity between eupnea and eupnea-sigh patterns.

I hypothesize for Project 3 that

- (i) “Calibrated” newborn rat brainstem-spinal cord preparations with a reproducible brainstem section level can be generated based on the constancy of the location of ventral brainstem surface markers.
- (ii) The longevities in physiological K^+ and Ca^{2+} (1.2 mM) of inspiratory-related preBötC-driven cervical and XII motor activity in the en bloc model depend on the amount of brainstem tissue rostral to the preBötC.
- (iii) Pre/post-inspiratory bursting in physiological K^+ and Ca^{2+} of pFRG-driven lumbar nerves in the en bloc model also depends on the amount of brainstem tissue rostral to the preBötC.
- (iv) Elevation of superfusate Ca^{2+} above 1.2 mM depresses endogenous preBötC activity in 3 mM K^+ , in both the slice and the en bloc model, and that this depression is antagonized by raised K^+ .

Figures

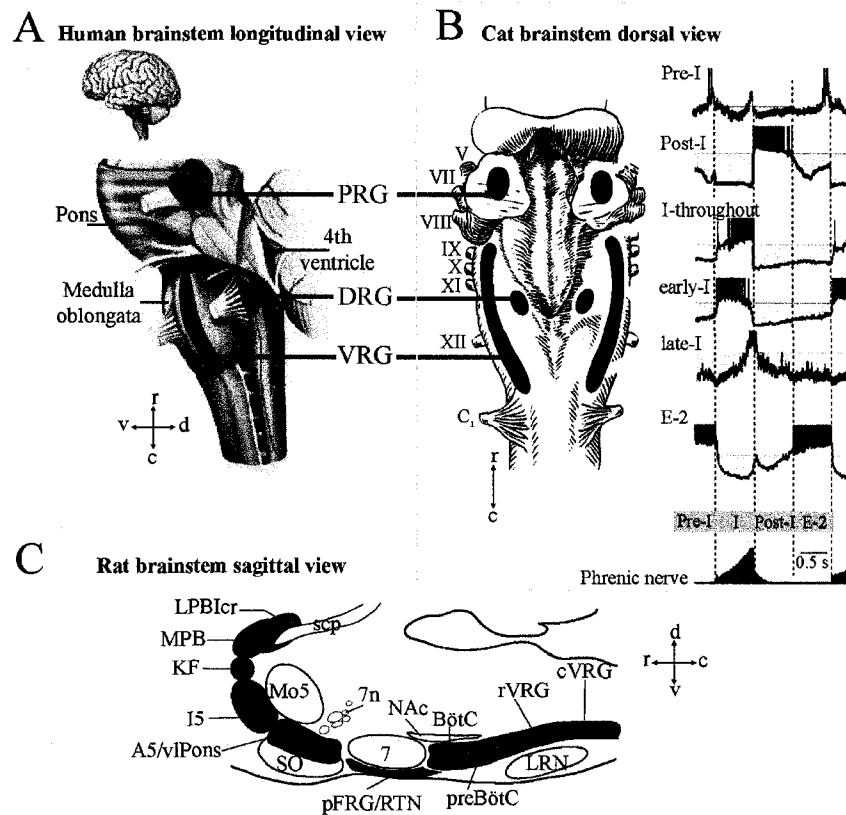


Figure 1-1. Location of respiratory neuronal groups. Three bilaterally-organized respiratory groups are located in the lower brainstem as evident from the longitudinal and dorsal views of the human and cat brainstem in **A** and **B**, respectively. The right panel in **B** shows membrane potential recordings from six classes of respiratory neurons from adult cats in vivo which show excitatory drive potentials and associated action potential discharges that alternate with pronounced hyperpolarizations mediated by γ -aminobutyric acid_A and glycine receptors (gray areas). The membrane potential recordings are referred to the primarily inspiratory (I) discharge of phrenic nerve. Other respiratory phases are the pre-inspiratory (Pre-I), the post-inspiratory (Post-I), and the active expiratory (E-2) phase. **C**, Compartmentalization of respiratory-related pontine (dark green) and VRC (blue) structures including the functionally defined inspiratory center, the pre-Bötzinger complex (preBötC, red), and the hypothesized expiratory center, the parafacial respiratory group (pFRG). Other abbreviations: r, rostral; c, caudal; v, ventral; d, dorsal; V, VII, VIII,

IX, X, XI, XII, cranial nerves; C₁, cervical spinal nerve; 7/7n, facial nucleus/nerve; NAc, compact part of nucleus ambiguus; A5/vlPons, area of A5 noradrenergic neurons and non-catecholamine neurons in ventrolateral pons; BötC, Bötzing complex; cVRG, caudal VRG; I5, intertrigeminal region; KF, Kölliker-Fuse nucleus; LPBlcr, lateral crescent subnucleus of the lateral parabrachial complex; LRN, lateral reticular nucleus; MPB, medial parabrachial nucleus; Mo5, motor nucleus of the trigeminal nerve; RTN, retrotrapezoid nucleus; scp, superior cerebellar peduncle; SO, superior olive. Modified from **A**: Herbrandson, 2005. **B**: Feldman, 1986; Ballanyi & Onimaru, 2008. **C**: Alheid et al., 2004

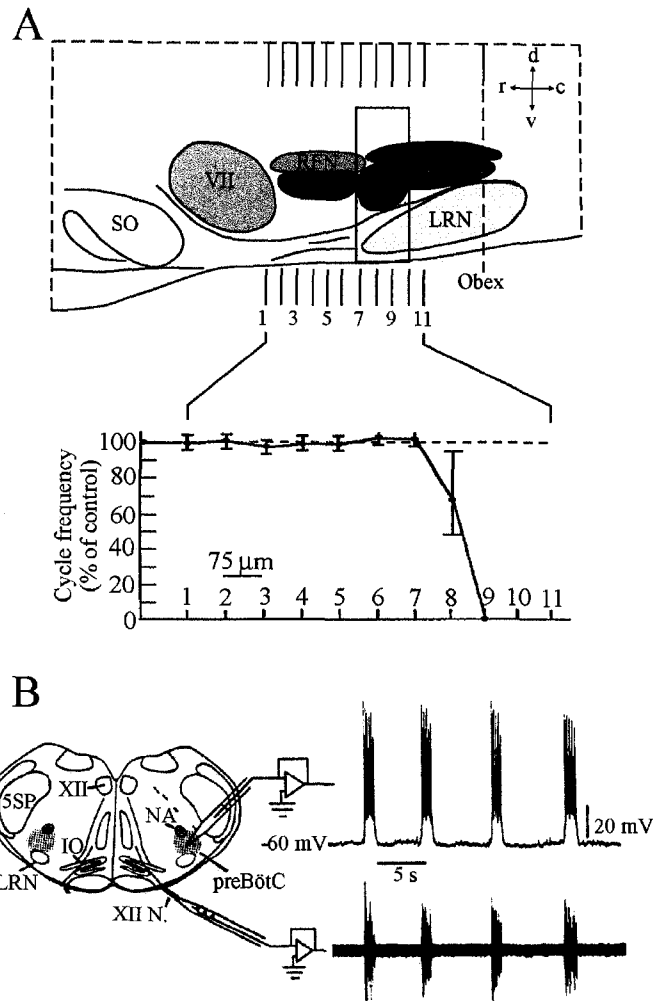


Figure 1-2. Isolation of the preBötC inspiratory center. A, Schematic parasagittal section of the ventral aspect of the newborn rat brainstem. Consecutive 75 μm transverse sections of the brainstem-spinal cord preparation in rostrocaudal or caudorostral direction resulted in irreversible block of inspiratory-related motor nerve output (plotted in cycle frequency as percent of control) when the brainstem was transected between section 9 and 8, respectively. This critical rostrocaudal region for respiratory rhythm generation spans 225 μm (red box) and was termed pre-Bötzinger Complex (preBötC). **B,** Inspiratory neurons in the preBötC remain rhythmically active in 350-600 μm thick brainstem slices and provide drive to XII motoneurons which innervate muscles of the tongue and maintain upper airway patency. Abbreviations not listed in Figure 1-1: 5SP, spinal trigeminal nucleus; NA, semicomcompact division of nucleus ambiguus; RFN, retrofacial nucleus. Modified from Smith et al., 1991.

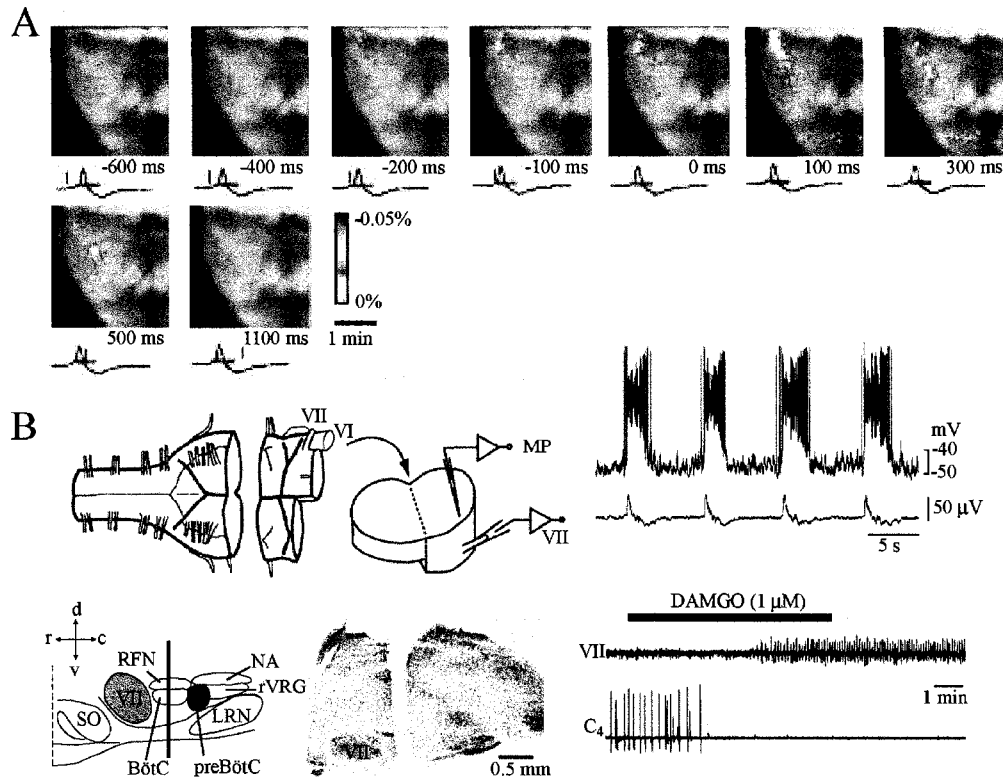


Figure 1-3. Activity of the isolated pFRG. **A**, Voltage-sensitive dye-imaging revealed respiratory neuronal activity in two distinct regions in the ventrolateral medulla of the newborn rat brainstem-spinal cord preparation. The more rostral region, termed the parafacial respiratory group (pFRG), showed activity starting ~400 ms before the onset of the inspiratory-related cervical (C_4) nerve burst. The activity in the caudal region, corresponding approximately to the preBötC, appeared ~100 ms prior to the onset of the C_4 burst. The horizontal blue bars indicate the inspiratory phase and the vertical red bars indicate the time at which the image was obtained. From Onimaru & Homma, 2003. **B**, A newborn rat rostral brainstem block devoid of the preBötC (top left schema) generated rhythmic VII nerve activity that was synchronous with membrane potential oscillations of putative Pre-I neurons (top right panels). Histological reconstruction revealed the transection at the level of the BötC (bottom left and middle panels). The μ -opioid receptor agonist [D-Ala², N-Me-Phe⁴, Gly⁵-ol] Enkephalin (DAMGO) blocked preBötC-driven C_4 bursts in the caudal aspect of the transected brainstem and reactivated rhythmic bursting of VII nerve motor output, which was transiently depressed due to sectioning procedure. Modified from Ballanyi & Onimaru, 2008.

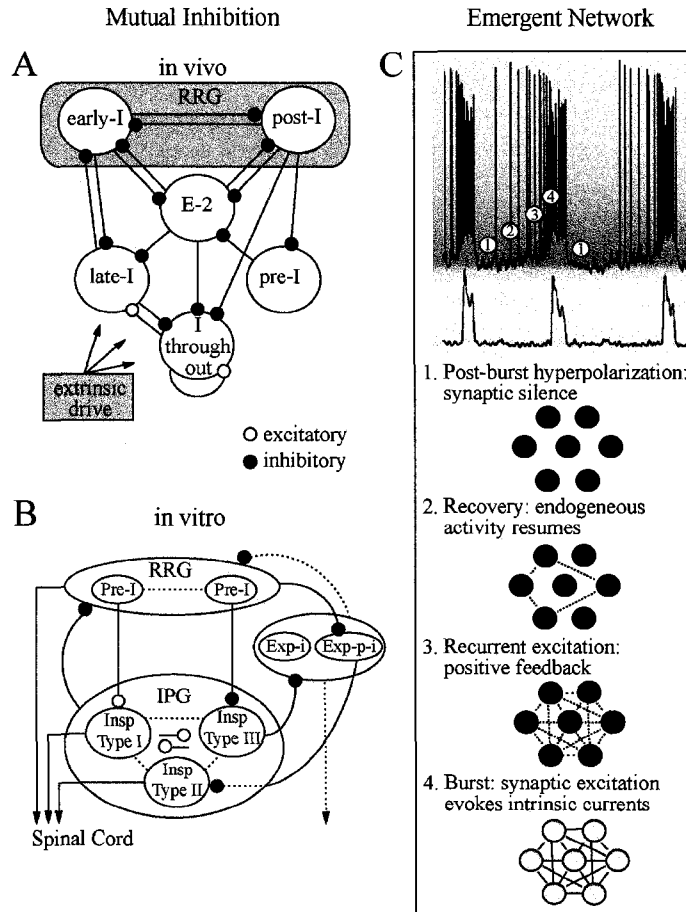


Figure 1-4. Mechanisms of respiratory rhythm generation. **A**, Analysis of discharge profiles and postsynaptic activities of respiratory neurons in adult cats suggest that the respiratory rhythm generator (RRG) is composed of early-inspiratory and post-inspiratory neurons that are connected by mutual inhibition. The RRG is influenced by other classes of respiratory neurons which show inhibitory connectivity (●) except for I-throughout neurons that show glutamatergic excitatory connectivity (○). From Richter et al., 1992. **B**, A different model based on findings in the newborn rat en bloc preparation proposes that the RRG is comprised of pre-inspiratory (Pre-I) neurons that drive an inspiratory pattern generator (IPG) comprised of three types of inspiratory (Insp) neurons. The activity of this network is modulated by two types of expiratory (Exp) neurons. From Onimaru et al., 1997. **C**, The group-pacemaker hypothesis proposes that respiratory rhythm is an emergent behavior generated by recurrent excitation among preBötC neurons. Intrinsic conductances serve to amplify synaptic input resulting in generation of rhythmic bursting. Modified from Del Negro & Feldman, 2006.

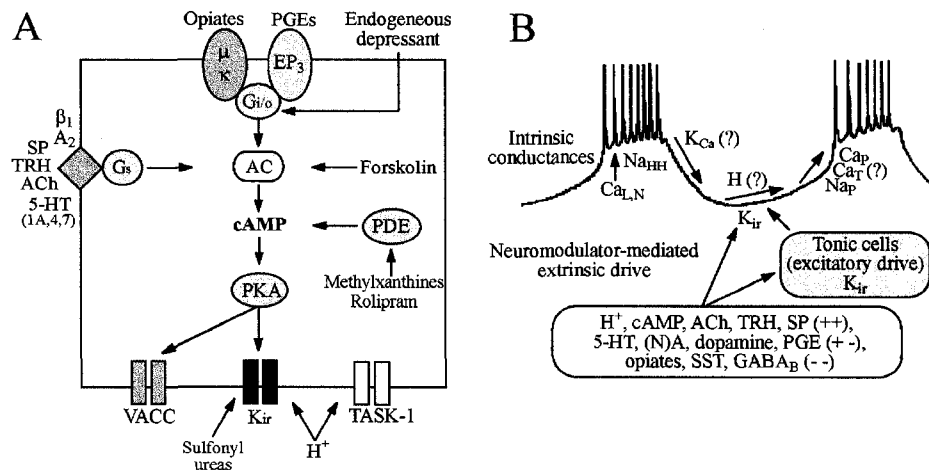


Figure 1-5. Intracellular respiratory signalling pathways and modulation of intrinsic ion conductances. **A**, Endogenous modulators and also opioids or prostaglandins (PGEs) depress respiratory and/or tonic neurons providing excitatory drive to these neurons via $G_{i/o}$ -coupled μ -, κ - or prostanoid (EP_3) receptors that block adenylyl cyclase (AC) activity. The resultant decrease in cellular cyclic adenosine monophosphate (cAMP) reduces protein kinase-A (PKA) activity, which in turn closes voltage-activated Ca^{2+} channels (VACC) and/or opens inwardly-rectifying K^+ (K_{ir}) channels. Such respiratory depression is reversed by AC activation (e.g. by forskolin) or inhibition of cAMP breakdown by phosphodiesterase (PDE) blockers (e.g. methylxanthines and rolipram.) Neuromodulators such as substance-P (SP), thyrotropin-releasing hormone (TRH), serotonin (5-HT), acetylcholine (ACh), adenosine (A_2), or (nor)adrenaline (β_1) stimulate respiratory activity via activation of G_s -coupled receptors. TRH and H^+ may also cause respiratory stimulation via their effects on TASK-1 K^+ channels in addition to K_{ir} . (Red arrows: inhibition. Green arrows: excitation). **B**, The latter and other neuro-modulators exert exclusively stimulatory (++) , inhibitory (--), or biphasic (+-) effects on K^+ conductances, and possibly also non-specific cation (H) channels, important for resting potential. They also contribute to slow depolarization leading to activation of persistent Na^+ channels (Na_p) and P/T-type Ca^{2+} channels ($Ca_{p,T}$) that are involved in burst initiation. Action potentials are mediated by Hodgkin-Huxley-type Na^+ channels (Na_{HH}). The resulting membrane depolarization activates L- and N-type Ca^{2+} channels ($Ca_{L,N}$). Ca^{2+} influx through these channels triggers Ca^{2+} -activated K^+ channels (K_{Ca}) leading to burst termination. Modified from Ballanyi, 2004a (**A**) and Ballanyi et al., 1999 (**B**).

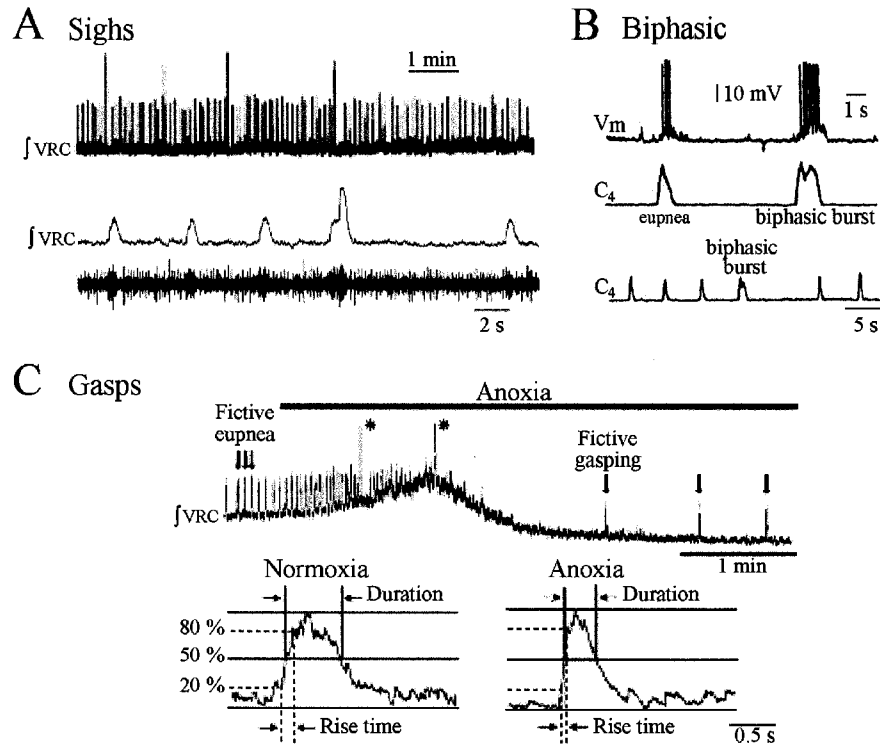


Figure 1-6. In vitro inspiratory patterns. **A**, Integrated VRC population activity shows fictive eupnea and sighs in 550-700 μm thick brainstem slices from 0-2 weeks-old mice in oxygenated solution with 8 mM K^+ . Fictive sigh bursts consist of a eupnea-like burst connected with a distinct higher amplitude phase, followed by post-sigh inhibition. Similarly, bursts resembling sighs, except for the similar or smaller amplitude in the second phase (biphasic bursts), are observed in newborn rat brainstem spinal cords in 6.2 mM K^+ (**B**). **C**, During anoxia evoked by gassing of the superfusate with nitrogen instead of 95% $\text{O}_2/5\%$ CO_2 , eupnea-like inspiratory activity transforms into fictive gasps characterized by a shorter rise time and burst duration. Modified from **A,C**: Lieske et al., 2000; **B**: Shvarev et al., 2003.

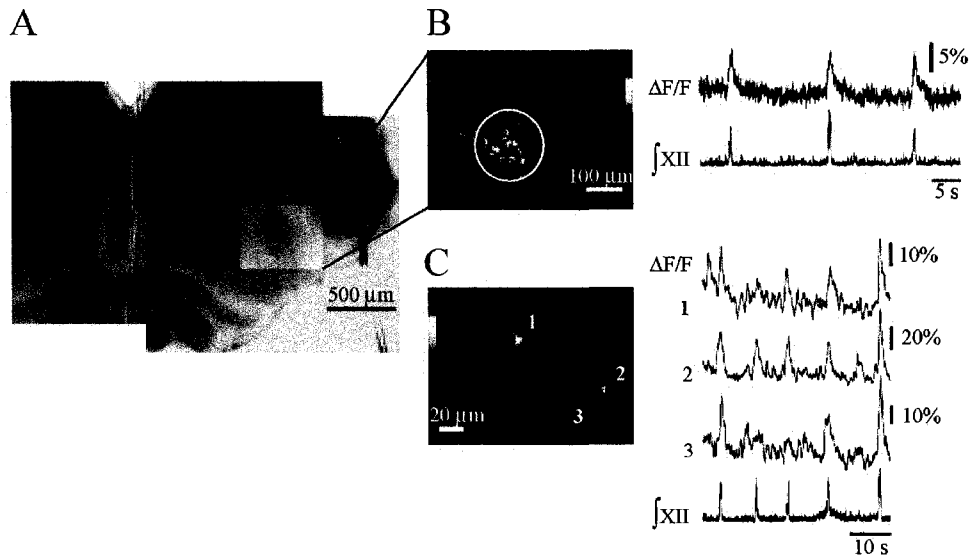


Figure 1-7. Visualization of preBötC neuron activity. A, A newborn rat preBötC-containing slice midline injected with the Ca^{2+} -sensitive fluorescent dye Calcium Green-1-AM shows spreading of intracellular fluorescence signals after 12 hours (in pseudocolour). The area corresponding to the ventrolateral preBötC region (B) and individual inspiratory active neurons (C) show fluorescence intensity increases ($\Delta F/F$) that are synchronous with inspiratory-related XII nerve activity. Modified from Koshiya & Smith, 1999.

1.9 References

- Alheid GF, Milsom WK, McCrimmon DR (2004) Pontine influences on breathing: An overview. *Respir Physiol Neurobiol* 143, 105-114.
- Arata A, Onimaru H, Homma I (1993) Effects of cAMP on respiratory rhythm generation in brainstem-spinal cord preparation from newborn rat. *Brain Res* 605, 193-199.
- Arata A, Onimaru H, Homma I (1990) Respiration-related neurons in the ventral medulla of newborn rats in vitro. *Brain Res Bull* 24, 599-604.
- Ballanyi K, Onimaru H (2008) Respiratory network analysis, isolated respiratory center functions. In: *Encyclopedic reference of neuroscience*. Eds Binder M, Hirsch M, Hirokawa N, Windhorst U. Springer, New York (in press).
- Ballanyi K, Onimaru H, Keller B (2008) Respiratory network analysis, functional imaging. In: *Encyclopedic reference of neuroscience*. Eds Binder M, Hirsch M, Hirokawa N, Windhorst U. Springer, New York (in press).
- Ballanyi K (2004a) Neuromodulation of the perinatal respiratory network. *Curr Neuropharmacol* 2, 221-243.
- Ballanyi K (2004b) Protective role of neuronal KATP channels in brain hypoxia. *J Exp Biol* 207, 3201-3212.
- Ballanyi K, Onimaru H, Homma I (1999) Respiratory network function in the isolated brainstem-spinal cord of newborn rats. *Prog Neurobiol* 59, 583-634.
- Ballanyi K, Lalley PM, Hoch B, Richter DW (1997) cAMP-dependent reversal of opioid- and prostaglandin-mediated depression of the isolated respiratory network in newborn rats. *J Physiol* 504, 127-134.
- Barnes BJ, Tuong CM, Mellen NM (2007) Functional imaging reveals respiratory network activity during hypoxic and opioid challenge in the neonate rat tilted sagittal slab preparation. *J Neurophysiol* 97, 2283-2292.
- Bertrand F, Hugelin A, Vibert JF (1973) Quantitative study of anatomical distribution of respiration related neurons in the pons. *Exp. Brain Res.* 16, 383-399.
- Bianchi AL, Denavit-Saubie M, Champagnat J (1995) Central control of breathing in mammals: Neuronal circuitry, membrane properties, and neurotransmitters. *Physiol Rev* 75, 1-45.

- Bianchi AL, St John WM (1982) Medullary axonal projections of respiratory neurons of pontile pneumotaxic center. *Respir Physiol* 48, 357-373.
- Bodineau L, Frugiere A, Marlot D, Wallois F (2000) Connections between retrotrapezoid nucleus and nucleus tractus solitarii in cat. *Neurosci Lett* 280, 111-114.
- Borday C, Wrobel L, Fortin G, Champagnat J, Thaeron-Antono C, Thoby-Brisson M (2004) Developmental gene control of brainstem function: Views from the embryo. *Prog Biophys Mol Biol* 84, 89-106.
- Brockhaus J, Ballanyi K (2000) Anticonvulsant A(1) receptor-mediated adenosine action on neuronal networks in the brainstem-spinal cord of newborn rats. *Neuroscience* 96, 359-371.
- Brockhaus J, Ballanyi K (1998) Synaptic inhibition in the isolated respiratory network of neonatal rats. *Eur J Neurosci* 10, 3823-3839.
- Busselberg D, Bischoff AM, Richter DW (2003) A combined blockade of glycine and calcium-dependent potassium channels abolishes the respiratory rhythm. *Neuroscience* 122, 831-841.
- Champagnat J, Denavit-Saubie M, Moyanova S, Rondouin G (1982) Involvement of amino acids in periodic inhibitions of bulbar respiratory neurones. *Brain Res* 237, 351-365.
- Del Negro CA, Morgado-Valle C, Hayes JA, Mackay DD, Pace RW, Crowder EA, Feldman JL (2005) Sodium and calcium current-mediated pacemaker neurons and respiratory rhythm generation. *J Neurosci* 25, 446-453.
- Del Negro CA, Koshiya N, Butera RJ, Jr, Smith JC (2002) Persistent sodium current, membrane properties and bursting behavior of pre-botzinger complex inspiratory neurons in vitro. *J Neurophysiol* 88, 2242-2250.
- Dutschmann M, Morschel M, Kron M, Herbert H (2004) Development of adaptive behaviour of the respiratory network: Implications for the pontine kolliker-fuse nucleus. *Respir Physiol Neurobiol* 143, 155-165.
- Ellenberger HH, Feldman JL (1990) Brainstem connections of the rostral ventral respiratory group of the rat. *Brain Res* 513, 35-42.

- Elsen FP, Ramirez JM (2005) Postnatal development differentially affects voltage-activated calcium currents in respiratory rhythmic versus nonrhythmic neurons of the pre-botzinger complex. *J Neurophysiol* 94, 1423-1431.
- Feldman JL, Del Negro CA (2006) Looking for inspiration: New perspectives on respiratory rhythm. *Nat Rev Neurosci* 7, 232-242.
- Feldman JL, Mitchell GS, Nattie EE (2003) Breathing: Rhythmicity, plasticity, chemosensitivity. *Annu Rev Neurosci* 26, 239-266.
- Feldman JL, Smith JC (1989) Cellular mechanisms underlying modulation of breathing pattern in mammals. *Ann N Y Acad Sci* 563, 114-130.
- Feldman JL (1986) Neurophysiology of breathing in mammals. In: *Handbook of physiology. The nervous system. Intrinsic regulatory systems in the brain. Neurophysiology of breathing in mammals.* 463-524. Washington, DC.: Am. Physiol. Soc.
- Finley JC, Katz DM (1992) The central organization of carotid body afferent projections to the brainstem of the rat. *Brain Res* 572, 108-116.
- Flourens P (1858) Nouveaux details sur le noeud vital. *C R Acad Sci (Paris)* 47, 803-806.
- Fortuna MG, West GH, Stornetta RL, Guyenet PG (2008) Botzinger expiratory-augmenting neurons and the parafacial respiratory group. *J Neurosci* 28, 2506-2515.
- Franco P, Verheulpen D, Valente F, Kelmanson I, de Broca A, Scaillet S, Groswasser J, Kahn A (2003) Autonomic responses to sighs in healthy infants and in victims of sudden infant death. *Sleep Medicine* 4, 569-577
- Frermann D, Keller BU, Richter DW (1999) Calcium oscillations in rhythmically active respiratory neurones in the brainstem of the mouse. *J Physiol* 515, 119-131.
- Funk GD, Huxtable AG, Lorier AR (2008) ATP in central respiratory control: A three-part signaling system. *Respir Physiol Neurobiol* (in press).
- Funk GD, Smith JC, Feldman JL (1994) Development of thyrotropin-releasing hormone and norepinephrine potentiation of inspiratory-related hypoglossal motoneuron discharge in neonatal and juvenile mice in vitro. *J Neurophysiol* 72, 2538-2541.
- Funk GD, Smith JC, Feldman JL (1993) Generation and transmission of respiratory oscillations in medullary slices: Role of excitatory amino acids. *J Neurophysiol* 70, 1497-1515.

- Gray PA, Janczewski WA, Mellen N, McCrimmon DR, Feldman JL (2001) Normal breathing requires preBotzinger complex neurokinin-1 receptor-expressing neurons. *Nat Neurosci* 4, 927-930.
- Gray PA, Rekling JC, Bocchiario CM, Feldman JL (1999) Modulation of respiratory frequency by peptidergic input to rhythmogenic neurons in the preBotzinger complex. *Science* 286, 1566-1568.
- Greer JJ, Funk GD, Ballanyi K (2006) Preparing for the first breath: Prenatal maturation of respiratory neural control. *J Physiol* 570, 437-444.
- Greer JJ, Funk GD (2005) Perinatal development of respiratory motoneurons. *Respir Physiol Neurobiol* 149, 43-61.
- Greer JJ, Al-Zubaidy Z, Carter JE (1996) Thyrotropin-releasing hormone stimulates perinatal rat respiration in vitro. *Am J Physiol* 271, R1160-4.
- Greer JJ, Carter JE, Al-Zubaidy Z (1995) Opioid depression of respiration in neonatal rats. *J Physiol* 485, 845-855.
- Greer JJ, Smith JC, Feldman JL (1991) Role of excitatory amino acids in the generation and transmission of respiratory drive in neonatal rat. *J Physiol* 437, 727-749.
- Guyenet PG, Stornetta RL, Bayliss DA (2008) Retrotrapezoid nucleus and central chemoreception. *J Physiol* 586, 2043-2048.
- Guyenet PG, Stornetta RL, Weston MC, McQuiston T, Simmons JR (2004) Detection of amino acid and peptide transmitters in physiologically identified brainstem cardiorespiratory neurons. *Autonomic Neuroscience-Basic & Clinical* 114, 1-10.
- Haji A, Takeda R, Remmers JE (1992) Evidence that glycine and GABA mediate postsynaptic inhibition of bulbar respiratory neurons in the cat. *J Appl Physiol* 73, 2333-2342.
- Hayes JA, Del Negro CA (2007) Neurokinin receptor-expressing pre-botzinger complex neurons in neonatal mice studied in vitro. *J Neurophysiol* 97, 4215-4224.
- Hedner J, Hedner T, Jonason J, Lundberg D (1981) Central respiratory stimulant effect by thyrotropin releasing hormone in the rat. *Neurosci Lett* 25, 317-320.
- Herbrandson C (2005) "Learning the nervous system". *Bio201 Human Anatomy*. Kellogg Community College. 7 June 2008 <http://academic.kellogg.cc.mi.us/herbrandsonc/bio201_McKinley/Nervous%20System.htm>

- Hilaire G, Monteau R, Gauthier P, Rega P, Morin D (1990) Functional significance of the dorsal respiratory group in adult and newborn rats: In vivo and in vitro studies. *Neurosci Lett* 111, 133-138.
- Hilaire G, Monteau R, Errchidi S (1989) Possible modulation of the medullary respiratory rhythm generator by the noradrenergic A5 area: An in vitro study in the newborn rat. *Brain Res* 485, 325-332.
- Hille B (1992) Ionic channels of excitable membranes.
- Homma I, Masaoka Y (2008) Breathing rhythms and emotions. *Exp Physiol* (in press).
- Homma I, Oouchi M, Ichikawa S (1984) Facilitation of inspiration by intracerebroventricular injection of thyrotropin-releasing hormone in rabbits. *Neurosci Lett* 44, 265-269.
- Hulsmann S, Oku Y, Zhang W, Richter DW (2000) Metabolic coupling between glia and neurons is necessary for maintaining respiratory activity in transverse medullary slices of neonatal mouse. *Eur J Neurosci* 12, 856-862.
- Hwang JC, Chien CT, St John WM (1988) Characterization of respiratory-related activity of the facial nerve. *Respir Physiol* 73, 175-187.
- Ireland MF, Lenal FC, Lorier AR, Loomes DE, Adachi T, Alvares TS, Greer JJ, Funk GD (2008) Distinct receptors underlie glutamatergic signalling in inspiratory rhythm-generating networks and motor output pathways in neonatal rat. *J Physiol* 586, 2357-2370.
- Isoe S (1998) Control of abdominal muscles. *Prog Neurobiol* 56, 433-506.
- Janczewski WA, Feldman JL (2006) Distinct rhythm generators for inspiration and expiration in the juvenile rat. *J Physiol* 570, 407-420.
- Janczewski WA, Onimaru H, Homma I, Feldman JL (2002) Opioid-resistant respiratory pathway from the preinspiratory neurones to abdominal muscles: In vivo and in vitro study in the newborn rat. *J Physiol* 545, 1017-1026.
- Jiang C, Lipski J (1990) Extensive monosynaptic inhibition of ventral respiratory group neurons by augmenting neurons in the botzinger complex in the cat. *Exp Brain Res* 81, 639-648.
- Johnson SM (2007) Glutamatergic synaptic inputs and ICAN: The basis for an emergent property underlying respiratory rhythm generation? *J Physiol* 582, 5-6.

- Johnson SM, Smith JC, Feldman JL (1996) Modulation of respiratory rhythm in vitro: Role of Gi/o protein-mediated mechanisms. *J Appl Physiol* 80, 2120-2133.
- Kachidian P, Poulat P, Marlier L, Privat A (1991) Immunohistochemical evidence for the coexistence of substance P, thyrotropin-releasing hormone, GABA, methionine-enkephalin, and leucin-enkephalin in the serotonergic neurons of the caudal raphe nuclei: a dual labelling in the rat. *J Neurosci Res* 30, 521–530.
- Kaila K (1994) Ionic basis of GABAA receptor channel function in the nervous system. *Prog Neurobiol* 42, 489-537.
- Koshiya N, Smith JC (1999) Neuronal pacemaker for breathing visualized in vitro. *Nature* 400, 360-363.
- Kubin L, Alheid GF, Zuperku EJ, McCrimmon DR (2006) Central pathways of pulmonary and lower airway vagal afferents. *J Appl Physiol* 101, 618-27.
- Lalley PM, Pierrefiche O, Bischoff AM, Richter DW (1997) cAMP-dependent protein kinase modulates expiratory neurons in vivo. *J Neurophysiol* 77, 1119-1131.
- Ley R (1999) The modification of breathing behavior. pavlovian and operant control in emotion and cognition. *Behav Modif* 23, 441-479.
- Li YM, Shen L, Peever JH, Duffin J (2003) Connections between respiratory neurones in the neonatal rat transverse medullary slice studied with cross-correlation. *J Physiol* 549, 327-332.
- Lieske SP, Ramirez JM (2006a) Pattern-specific synaptic mechanisms in a multifunctional network. I. Effects of alterations in synapse strength. *J Neurophysiol* 95, 1323-1333.
- Lieske SP, Ramirez JM (2006b) Pattern-specific synaptic mechanisms in a multifunctional network. II. Intrinsic modulation by metabotropic glutamate receptors. *J Neurophysiol* 95, 1334-1344.
- Lieske SP, Thoby-Brisson M, Ramirez JM (2001) Reconfiguration of the central respiratory network under normoxic and hypoxic conditions. *Adv Exp Med Biol* 499, 171-8.
- Lieske SP, Thoby-Brisson M, Telgkamp P, Ramirez JM (2000) Reconfiguration of the neural network controlling multiple breathing patterns: Eupnea, sighs and gasps. *Nat Neurosci* 3, 600-607.

- Lorier AR, Lipski J, Housley GD, Greer JJ, Funk GD (2008) ATP sensitivity of preBotzinger complex neurones in neonatal rat in vitro: Mechanism underlying a P2 receptor-mediated increase in inspiratory frequency. *J Physiol* 586, 1429-1446.
- Lumsden T (1923) Observations on the respiratory centres in the cat. *J Physiol* 57, 153-160.
- McCown TJ, Hedner JA, Towle AC, Breese GR, Mueller RA (1986) Brainstem localization of a thyrotropin-releasing hormone-induced change in respiratory function. *Brain Res* 373, 189-196.
- McLean HE, Remmers JA (1994) Respiratory motor output of the sectioned medulla of the neonatal rat. *Respir Physiol* 96, 49-60
- Mellen NM, Janczewski WA, Bocchiaro CM, Feldman JL (2003) Opioid-induced quantal slowing reveals dual networks for respiratory rhythm generation. *Neuron* 37, 821-826.
- Mironov SL (2008) Metabotropic glutamate receptors activate dendritic calcium waves and TRPM channels which drive rhythmic respiratory patterns in mice. *J Physiol* 586, 2277-91
- Monteau R, Ptak K, Broquere N, Hilaire G (1996) Tachykinins and central respiratory activity: An in vitro study on the newborn rat. *Eur J Pharmacol* 314, 41-50.
- Morgado-Valle C, Feldman JL (2004) Depletion of substance P and glutamate by capsaicin blocks respiratory rhythm in neonatal rat in vitro. *J Physiol* 555, 783-792.
- Morin-Surun MP, Boudinot E, Gacel G, Champagnat J, Roques BP, Denavit-Saubie M (1984) Different effects of mu and delta opiate agonists on respiration. *Eur J Pharmacol* 98, 235-240.
- Mutolo D, Bongianini F, Carfi M, Pantaleo T (1999) Respiratory responses to thyrotropin-releasing hormone microinjected into the rabbit medulla oblongata. *Am J Physiol* 5 (Pt.2), R1331-8.
- Nattie EE, Li A, Richerson G, Lappi DA (2004) Medullary serotonergic neurones and adjacent neurones that express neurokinin-1 receptors are both involved in chemoreception in vivo. *J Physiol* 556, 235-53

- Oku Y, Masumiya H, Okada Y (2007) Postnatal developmental changes in activation profiles of the respiratory neuronal network in the rat ventral medulla. *J Physiol* 585, 175-186.
- Onimaru H, Kumagawa Y, Homma I (2006) Respiration-related rhythmic activity in the rostral medulla of newborn rats. *J Neurophysiol* 96, 55-61.
- Onimaru H, Homma I (2005) Optical imaging of respiratory neuron activity from the dorsal view of the lower brainstem. *Clin Exp Pharmacol Physiol* 32, 297-301.
- Onimaru H, Ballanyi K, Homma I (2003) Contribution of Ca^{2+} -dependent conductances to membrane potential fluctuations of medullary respiratory neurons of newborn rats in vitro. *J Physiol* 552, 727-741.
- Onimaru H, Homma I (2003) A novel functional neuron group for respiratory rhythm generation in the ventral medulla. *J Neurosci* 23, 1478-1486.
- Onimaru H, Shamoto A, Homma I (1998) Modulation of respiratory rhythm by 5-HT in the brainstem-spinal cord preparation from newborn rat. *Pflugers Arch* 435, 485-494.
- Onimaru H, Arata A, Homma I (1997) Neuronal mechanisms of respiratory rhythm generation: An approach using in vitro preparation. *Jpn J Physiol* 47, 385-403.
- Onimaru H, Ballanyi K, Richter DW (1996) Calcium-dependent responses in neurons of the isolated respiratory network of newborn rats. *J Physiol* 491, 677-695.
- Onimaru H, Homma I (1992) Whole cell recordings from respiratory neurons in the medulla of brainstem-spinal cord preparations isolated from newborn rats. *Pflugers Arch* 420, 399-406.
- Onimaru H, Homma I, Iwatsuki K (1992) Excitation of inspiratory neurons by preinspiratory neurons in rat medulla in vitro. *Brain Res Bull* 29, 879-882.
- Onimaru H, Arata A, Homma I (1990) Inhibitory synaptic inputs to the respiratory rhythm generator in the medulla isolated from newborn rats. *Pflugers Arch* 417, 425-432.
- Onimaru H, Arata A, Homma I (1987) Localization of respiratory rhythm-generating neurons in the medulla of brainstem-spinal cord preparations from newborn rats. *Neurosci Lett* 78, 151-155.
- Onimaru H, Homma I (1987) Respiratory rhythm generator neurons in medulla of brainstem-spinal cord preparation from newborn rat. *Brain Res* 403, 380-384.

- Pace RW, Mackay DD, Feldman JL, Del Negro CA (2007a) Role of persistent sodium current in mouse preBotzinger complex neurons and respiratory rhythm generation. *J Physiol* 580, 485-496.
- Pace RW, Mackay DD, Feldman JL, Del Negro CA (2007b) Inspiratory bursts in the preBotzinger complex depend on a calcium-activated non-specific cation current linked to glutamate receptors in neonatal mice. *J Physiol* 582, 113-125.
- Pagliardini S, Adachi T, Ren J, Funk GD, Greer JJ (2005) Fluorescent tagging of rhythmically active respiratory neurons within the pre-botzinger complex of rat medullary slice preparations. *J Neurosci* 25, 2591-2596.
- Pagliardini S, Ren J, Greer JJ (2003) Ontogeny of the pre-Bötzinger complex in perinatal rats. *J Neurosci* 23, 9575-9584.
- Paton JF, St-John WM (2007) Counterpoint: Medullary pacemaker neurons are essential for gasping, but not eupnea, in mammals. *J Appl Physiol* 103, 718-20; discussion 721-2.
- Paxino G, Halliday G, Watson C, Koutcherov Y, Wang H (2007) Atlas of the developing mouse brain, 1st ed., San Diego: Elsevier Academic Press.
- Payne JA (1997) Functional characterization of the neuronal-specific K-Cl cotransporter: Implications for [K⁺]_o regulation. *Am J Physiol* 273, C1516-25.
- Peña F, Parkis MA, Tryba AK, Ramirez JM (2004) Differential contribution of pacemaker properties to the generation of respiratory rhythms during normoxia and hypoxia. *Neuron* 43, 105-117.
- Peña F, Ramirez JM (2004) Substance P-mediated modulation of pacemaker properties in the mammalian respiratory network. *Journal of Neuroscience* 24, 7549-7556.
- Pierrefiche O, Champagnat J, Richter DW (1995) Calcium-dependent conductances control neurones involved in termination of inspiration in cats. *Neurosci Lett* 184, 101-104.
- Ptak K, Zummo GG, Alheid GF, Tkatch T, Surmeier DJ, McCrimmon DR (2005) Sodium currents in medullary neurons isolated from the pre-botzinger complex region. *J Neurosci* 25, 5159-5170.
- Ramirez JM, Garcia A, 3rd (2007) Point: Medullary pacemaker neurons are essential for both eupnea and gasping in mammals. *J Appl Physiol* 103, 717-8; discussion 722.

- Ramirez JM, Schwarzacher SW, Pierrefiche O, Olivera BM, Richter DW (1998) Selective lesioning of the cat pre-botzinger complex in vivo eliminates breathing but not gasping. *J Physiol (Lond)* 507, 895-907.
- Ramirez JM, Telgkamp P, Elsen FP, Quellmalz UJ, Richter DW (1997) Respiratory rhythm generation in mammals: Synaptic and membrane properties. *Respir Physiol* 110, 71-85.
- Rampin O, Pierrefiche O, Denavit-Saubie M (1993) Effects of serotonin and substance P on bulbar respiratory neurons in vivo. *Brain Res* 622, 185-193.
- Rekling JC, Champagnat J, Denavit-Saubie M (1996) Electroresponsive properties and membrane potential trajectories of three types of inspiratory neurons in the newborn mouse brain stem in vitro. *J Neurophysiol* 75, 795-810.
- Ren J, Greer JJ (2006) Modulation of respiratory rhythmogenesis by chloride-mediated conductances during the perinatal period. *J Neurosci* 26, 3721-3730.
- Ren J, Poon BY, Tang Y, Funk GD, Greer JJ (2006) Ampakines alleviate respiratory depression in rats. *Am J Respir Crit Care Med* 174, 1384-1391.
- Richter DW, Spyer KM (2001) Studying rhythmogenesis of breathing: Comparison of in vivo and in vitro models. *Trends Neurosci* 24, 464-472.
- Richter DW, Lalley PM, Pierrefiche O, Haji A, Bischoff AM, Wilken B, Hanefeld F (1997) Intracellular signal pathways controlling respiratory neurons. *Respir Physiol* 110, 113-123.
- Richter DW, Champagnat J, Jacquin T, Benacka R (1993) Calcium currents and calcium-dependent potassium currents in mammalian medullary respiratory neurones. *J Physiol* 470, 23-33.
- Richter DW, Ballanyi K, Schwarzacher S (1992) Mechanisms of respiratory rhythm generation. *Curr Opin Neurobiol* 2, 788-793.
- Ritter B, Zhang W (2000) Early postnatal maturation of GABAA-mediated inhibition in the brainstem respiratory rhythm-generating network of the mouse. *Eur J Neurosci* 12, 2975-2984.
- Ruangkittisakul A, Ballanyi K (2006) Reversal by phosphodiesterase-4 blockers of in vitro apnea in the isolated brainstem-spinal cord preparation from newborn rats. *Neurosci Lett* 401, 194-198.

- Ruangkittisakul A, Schwarzacher SW, Secchia L, Poon BY, Ma Y, Funk GD, Ballanyi K (2006) High sensitivity to neuromodulator-activated signaling pathways at physiological [K⁺] of confocally imaged respiratory center neurons in on-line-calibrated newborn rat brainstem slices. *J Neurosci* 26, 11870-11880.
- Rybak IA, Shevtsova NA, Paton JF, Dick TE, St-John WM, Morschel M, Dutschmann M (2004) Modeling the ponto-medullary respiratory network. *Respir Physiol Neurobiol* 143, 307-319.
- Schwarzacher SW, Wilhelm Z, Anders K, Richter DW (1991) The medullary respiratory network in the rat. *J Physiol* 435, 631-644.
- Segers LS, Shannon R, Lindsey BG (1985) Interactions between rostral pontine and ventral medullary respiratory neurons. *J Neurophysiol* 54, 318-334.
- Shao XM, Feldman JL (1997) Respiratory rhythm generation and synaptic inhibition of expiratory neurons in pre-botzinger complex: Differential roles of glycinergic and GABAergic neural transmission. *J Neurophysiol* 77, 1853-1860.
- Shvarev YN, Lagercrantz H, Yamamoto Y (2003) Two types of rhythm in the respiratory network output in the isolated ventrolateral medulla in the neonatal rats. *Neurosci Lett* 347, 53-56.
- Smith JC, Butera RJ, Koshiya N, Del Negro C, Wilson CG, Johnson SM (2000) Respiratory rhythm generation in neonatal and adult mammals: The hybrid pacemaker-network model. *Respir Physiol* 122, 131-147.
- Smith JC, Funk GD, Johnson SM, Feldman JL (1995) Cellular and synaptic mechanisms generating respiratory rhythm: insights from in vitro and computational studies. In: *Ventral brainstem mechanisms and control of respiration and blood pressure*, pp. 463-496. Eds Trouth CO, Millis RM, Kiwull-Schöne HF, Schläfke ME. M. Dekker, New York, Basel, Hongkong.
- Smith JC, Ballanyi K, Richter DW (1992) Whole-cell patch-clamp recordings from respiratory neurons in neonatal rat brainstem in vitro. *Neurosci Lett* 134, 153-156.
- Smith JC, Ellenberger HH, Ballanyi K, Richter DW, Feldman JL (1991) Pre-botzinger complex: A brainstem region that may generate respiratory rhythm in mammals. *Science* 254, 726-729.

- Smith JC, Greer JJ, Liu GS, Feldman JL (1990) Neural mechanisms generating respiratory pattern in mammalian brain stem-spinal cord in vitro. I. spatiotemporal patterns of motor and medullary neuron activity. *J Neurophysiol* 64, 1149-1169.
- Smith JC, Morrison DE, Ellenberger HH, Otto MR, Feldman JL (1989) Brainstem projections to the major respiratory neuron populations in the medulla of the cat. *J Comp Neurol* 281, 69-96.
- Solomon I (2002) Modulation of gasp frequency by activation of pre-bötzing complex in vivo. *J Neurophysiol* 87, 1664-8.
- Solomon IC, Edelman NH, Neubauer JA (1999) Patterns of phrenic motor output evoked by chemical stimulation of neurons located in the pre-botzinger complex in vivo. *J Neurophysiol* 81, 1150-1161.
- Somjen GG (2002) Ion regulation in the brain: Implications for pathophysiology. *Neuroscientist* 8, 254-267.
- St-John WM, Rybak IA, Paton JF (2002) Potential switch from eupnea to fictive gasping after blockade of glycine transmission and potassium channels. *Am J Physiol Regul Integr Comp Physiol* 283, R721-31.
- St-John WM (1996) Medullary regions for neurogenesis of gasping: noeud vital or noeuds vitaux? *J Appl Physiol* 81, 1865-1877.
- Strohl KP (1985) Respiratory activation of the facial nerve and alar muscles in anaesthetized dogs. *J Physiol* 363, 351-362.
- Sun QJ, Minson J, Llewellyn-Smith IJ, Arnolda L, Chalmers J, Pilowsky P (1997) Botzinger neurons project towards bulbospinal neurons in the rostral ventrolateral medulla of the rat. *J Comp Neurol* 388, 23-31.
- Sun QJ, Llewellyn-Smith I, Minson J, Arnolda L, Chalmers J, Pilowsky P (1996) Thyrotropin-releasing hormone immunoreactive boutons form close appositions with medullary expiratory neurons in the rat. *Brain Res* 715, 136-144.
- Suzue T (1984) Respiratory rhythm generation in the in vitro brain stem-spinal cord preparation of the neonatal rat. *J Physiol (Lond)* 354, 173-183.
- Taccola G, Secchia L, Ballanyi K (2007) Anoxic persistence of lumbar respiratory bursts and block of lumbar locomotion in newborn rat brainstem spinal cords. *J Physiol* 585, 507-524.

- Takeda S, Eriksson LI, Yamamoto Y, Joensen H, Onimaru H, Lindahl SG (2001) Opioid action on respiratory neuron activity of the isolated respiratory network in newborn rats. *Anesthesiology* 95, 740-749.
- Tan W, Janczewski WA, Yang P, Shao XM, Callaway EM, Feldman JL (2008) Silencing preBotzinger complex somatostatin-expressing neurons induces persistent apnea in awake rat. *Nat Neurosci* 11, 538-540.
- Telgkamp P, Cao YQ, Basbaum AI, Ramirez JM (2002) Long-term deprivation of substance P in PPT-A mutant mice alters the anoxic response of the isolated respiratory network. *J Neurophysiol* 88, 206-213.
- Thach BT, Lijowska A (1996) Arousals in infants. *Sleep* 19, S271-273.
- Thoby-Brisson M, Trinh JB, Champagnat J, Fortin G (2005) Emergence of the prebotzinger respiratory rhythm generator in the mouse embryo. *J Neurosci* 25, 4307-4318.
- Thoby-Brisson M, Cauli B, Champagnat J, Fortin G, Katz DM (2003) Expression of functional tyrosine kinase B receptors by rhythmically active respiratory neurons in the pre-botzinger complex of neonatal mice. *J Neurosci* 23, 7685-7689.
- Tryba AK, Peña F, Lieske SP, Viemari JC, Thoby-Brisson M, Ramirez JM (2008) Differential modulation of neural network and pacemaker activity underlying eupnea and sigh breathing activities. *J Neurophysiol* 99, 2114-2125.
- Tryba AK, Peña F, Ramirez JM (2006) Gasping activity in vitro: a rhythm dependent on 5-HT_{2A} receptors. *J Neurosci* 26, 2623-2634.
- Uhlen S, Wikberg JE (1988) Inhibition of cyclic AMP production by alpha 2-adrenoceptor stimulation in the guinea-pig spinal cord slices. *Pharmacol Toxicol* 63, 178-182.
- Wang H, Stornetta RL, Rosin DL, Guyenet PG (2001) Neurokinin-1 receptor-immunoreactive neurons of the ventral respiratory group in the rat. *J Comp Neurol* 434, 128-146.
- White HS, Skeen GA, Edwards JA (1992) Pharmacological regulation of astrocytic calcium channels: Implications for the treatment of seizure disorders. *Prog Brain Res* 94, 77-87.

Xia Y, Haddad GG (1991) Ontogeny and distribution of opioid receptors in the rat brainstem. *Brain Res* 549, 181-193.

Yamamoto Y, Onimaru H, Homma I (1992) Effect of substance P on respiratory rhythm and pre-inspiratory neurons in the ventrolateral structure of rostral medulla oblongata: An in vitro study. *Brain Res* 599, 272-276.

***CHAPTER II**

High Sensitivity to Neuromodulator-Activated Signaling Pathways at Physiological K^+ of Confocally Imaged Respiratory Center Neurons in Online-Calibrated Newborn Rat Brainstem Slices

* Previously published paper:

Ruangkittisakul A[†], Schwarzacher SW[†], Secchia L, Poon BY, Ma Y, Funk GD, Ballanyi K (2006) High sensitivity to neuromodulator-activated signalling pathways at physiological $[K^+]$ of confocally-imaged respiratory centre neurons in online-calibrated newborn rat brainstem slices. *J Neurosci* 26, 11870-11880. Copyright 2006 by the Society for Neuroscience. My contribution to this study consisted in execution of >70% of both electrophysiological and Ca^{2+} imaging experiments and 100% of the corresponding analyses. Importantly, I established both multiphoton/confocal Ca^{2+} imaging techniques and histological procedures for the novel “online histology” in Dr. Ballanyi’s laboratory. Additionally, I performed histological procedure, i.e., fixation, staining, slicing and generation of digital images of >80% of brainstem slices. I also provided the histological data for the reference brainstem atlas. The boundaries of the slices were determined by Dr. S.W. Schwarzacher. [†]Authors contributed equally to the study.

2.1 Introduction

The pre-Bötzinger complex (preBötC) constitutes a pivotal inspiratory center. Through microsection of newborn rat brainstems, it has been identified as a medullary region that extends between 400 and 600 μm caudal to facial (VII) motor nucleus and generates inspiratory rhythm in a transverse slice preparation (Smith et al., 1991). The hypothesized importance of the preBötC for inspiratory rhythm generation has been confirmed in numerous studies combining electrophysiological preBötC recording with microinjection of neuromodulators in both preBötC slices and in vivo (Feldman et al., 2003; Feldman & Del Negro, 2006). Immunohistochemical studies have identified putative markers for preBötC neurons such as μ -opiate and neurokinin-1 (NK1)-type substance-P (SP) receptors (Gray et al., 1999). In turn, targeted lesioning of preBötC neurons with SP-tagged saporin profoundly perturbs breathing (Gray et al., 2001).

Despite agreement on the significance of the preBötC slice model, it is recognized that the in vitro rhythm differs from respiratory activity in vivo (Richter & Spyer, 2001; Feldman & Del Negro, 2006). For example, low nanomolar concentrations of μ -opioid receptor agonists abolish inspiratory rhythm in situ (Manzke et al., 2003), whereas micromolar concentrations are typically necessary to abolish the slice rhythm (Johnson et al., 1994). Such discrepancies may reflect the routine use of superfusates with elevated (8-10 mM) K^+ to study preBötC slices. These high K^+ levels may provide a powerful although nonspecific excitatory stimulus (Somjen, 2002) that may attenuate the sensitivity of the isolated preBötC to neuromodulators. The original report on the preBötC indicated that slices ≥ 500 μm thick generate inspiratory activity in superfusate of physiological K^+ (3 mM), but for brief periods only (Smith et al., 1991). Accordingly, it was a major aim of our study to examine the basic rhythm and responses to neuromodulators of preBötC slices in physiological K^+ .

Furthermore, we exploited the fact that the rhythm would arrest after some time (Smith et al., 1991; Funk et al., 1993) and used this “in vitro apnea” as a tool to study reactivation of rhythm by neuromodulators affecting distinct second-messenger signaling pathways.

Incorporation of two-photon/confocal Ca^{2+} imaging to simultaneously monitor the activity of multiple neurons (Yuste et al., 2006) allowed us to assess whether endogenous and evoked rhythms involve the same or distinct neuronal assemblies. The combined electrophysiological/imaging approach will establish network sensitivity to specific signaling cascades and may possibly reveal the potential involvement of particular neurotransmitter(s), before their putative depletion from the slice, in maintaining network excitability or generating rhythm.

Critical to the success of these experiments was the generation of consistent preBötC slices. For this, we developed “on-line histology” using a reference newborn rat brainstem atlas to generate slices with reproducible and defined rostrocaudal boundaries. The objective was to establish and analyze sustained inspiratory rhythm in “calibrated slices” containing the preBötC in the middle. Our rationale was that failure of previous studies to obtain long-term rhythm in 3 mM K^+ might reflect slice topography. Specifically, slices with the preBötC exposed to one boundary may lack subpopulation(s) of preBötC neurons (or dendrites), such that connectivity and excitatory drive are reduced below levels required for rhythm generation.

2.2 Material and Methods

2.2.1 Preparation and Solutions

Experiments were performed on transverse brainstem slices from Sprague Dawley (SD) and Wistar (W) rats between postnatal day 0 (P0) and P4. Procedures were approved by the ethics committee of the University of Alberta. Animals were anesthetized with 2-3% isoflurane until the paw withdrawal reflex disappeared. They were then decerebrated and the neuraxis isolated at 18-20°C in saline containing the following (in mM): 120 NaCl, 3 KCl, 1 CaCl_2 , 2 MgSO_4 , 26 NaHCO_3 , 1.25 NaH_2PO_4 , and 20 D-glucose (pH adjusted to 7.4 by gassing with 95% O_2 , 5% CO_2). After removal of the cerebellum and transverse sectioning at the pontomedullary junction and just rostral to the C_1 cervical segment, the brainstem was glued rostral side down to a metal plate. Serial transverse sections were

made with a vibratome (Leica VT1000S; Leica Microsystems, Richmond Hill, Ontario, Canada) in caudal-to-rostral direction starting near the pyramidal decussation (Schwarzacher et al., 2002). Sectioning was stopped based on appearance of landmarks identified by on-line histology (see Results). One preBötC-containing slice with rostrocaudal thickness of 500 or 600 μm was cut and fixed (caudal surface up) with insect pins on the silicone layer covering the bottom of the recording chamber (volume, 1.5 ml). Superfusate was administered at a flow rate of 5 ml/min via a peristaltic pump (Watson-Marlow Alitea-AB; Sin-Can, Calgary, Alberta, Canada). Superfusate temperature in the recording chamber was kept at 25-27°C (TC-324B; Harvard Apparatus, Saint-Laurent, Quebec, Canada).

2.2.2 Agents

Agents were as follows: [D-Ala², N-Me-Phe⁴, Gly⁵-ol] Enkephalin (DAMGO) (10-25 nM; stock 100 μM in superfusate), 3,5-dihydroxy-phenylglycine (DHPG) (0.1-10 μM ; stock 10 mM in superfusate), thyrotropin-releasing hormone (TRH) (0.1-100 nM; stocks 1 μM and 1 mM in superfusate), rolipram (0.25, 1, and 5 μM ; stocks 1 and 10 mM in dimethyl sulfoxide), theophylline (0.25 and 2.5 mM; added to superfusate), glutamate (1 mM; stock 1 M in superfusate), fluo-4 acetoxymethyl (fluo-4-AM) (0.5 mM; stock 5 mM in pluronic acid, 20% in dimethyl sulfoxide), agar-agar (6% in H₂O), fixation solution [4% paraformaldehyde in phosphate buffer (i.e., 1:2 mixture of 0.1 M NaH₂PO₄ plus 0.1 M Na₂HPO₄ in H₂O, pH 7.2)], and staining solution (1% thionin acetate in 0.1 M sodium acetate trihydrate plus 0.1 M acetic acid). Agents were obtained from Sigma (Oakville, Ontario, Canada) except salts for superfusate, sodium acetate trihydrate, acetic acid (Fisher Scientific, Ottawa, Ontario, Canada), DHPG (Tocris Biosciences, Ellisville, MO), theophylline, naloxone, glutamate (ICN Biomedicals, Costa Mesa, CA), and fluo-4-AM (TEF Labs, Austin, TX).

2.2.3 Electrophysiological Recording

Discharge of ventral respiratory column (VRC) (Alheid et al., 2004) was recorded extracellularly with a differential amplifier (DAM 50; WPI, Sarasota, FL) via suction electrodes (outer diameter, 80-250 μm) filled with superfusate, positioned on the caudal

slice surface. Signals were amplified ($\times 10k$), bandpass filtered (0.3-1 kHz), integrated, and recorded digitally (Powerlab/8SP; ADInstruments, Colorado Springs, CO).

2.2.4 Two-Photon/Confocal Ca^{2+} Imaging

Rhythmic activity of newborn rat VRC neurons that express specific sets of voltage-activated Ca^{2+} channels (Onimaru et al., 1996, 2003) was visualized with cytosolic [Ca^{2+}] imaging (Yuste et al., 2006). The membrane-permeable Ca^{2+} sensitive dye fluo-4-AM (0.5 mM in superfusate) was backfilled into a broken patch pipette (outer diameter, 5-10 μm) and pressure-injected (0.7-1.0 psi) for 10 min (Stosiek et al., 2003) into the VRC/preBötC from the caudal surface while inspiratory activity was electrophysiologically monitored from the contralateral VRC/preBötC. Fluorescence signals were measured using either a confocal microscope and software (20X XLUMPlanF1, numerical aperture, 0.95, objective; Olympus FV300; Carsen group, Markham, Ontario, Canada) or a FV300 connected with a Ti:Sa laser (10 W Mira/Verdi; Coherent, Santa Clara, CA) for two-photon imaging (Nikolenko et al., 2003). Within 10-20 min after injection, labelling revealed basic neuronal morphology and changes in fluorescence intensity that oscillated in phase with electrophysiological VRC/preBötC activity. Stained areas were 200-300 μm in diameter. Ca^{2+} oscillations, cell bodies, and primary dendrites could be resolved at tissue depths up to 60 μm for confocal and 90 μm for 2-photon microscopy. Respiratory neurons were typically imaged at tissue depths between 30 and 60 μm . Rhythmic Ca^{2+} rises were visualized in up to 10 cells (typically 3-6) in a single xy-image plane. The stained region was monitored using a 2-3 \times digital zoom at reduced settings for y-axis scanning. Compared with full-frame acquisition (512 x 512 pixels), such “clipped mode” imaging sampled an area of 512 x 100-220 pixels and provided scan rates of 1.25-1.43 scans/s sufficient to detect 70-100% of peak respiratory Ca^{2+} rises as established empirically. The morphology of cell bodies and primary dendrites was revealed by combining “z-stack” imaging (single z-steps, 0.5 μm) with three-dimensional (3D) animation using Fluoview software. Fluo-4 fluorescence emission is weak at low cytosolic [Ca^{2+}] (Stosiek et al., 2003; Yuste et al., 2006). Therefore, to improve morphological reconstruction, slices were exposed to glutamate (0.25-1 mM; 5-10 min) after the experiments and z-stack image series acquired. Glutamate-induced

fluorescence signals were 3-10 times larger than those associated with spontaneous or drug-induced inspiratory activity.

2.2.5 Histological Procedures

Respiratory marker nuclei were mapped in 50 and 100 μm serial brainstem sections. Brainstems and brainstem slices were kept for >1 h in fixation solution (see above, Agents). For staining, slices were incubated in phosphate buffer for 2 min and immersed for 45-60 s in thionin staining solution (see above, Agents). Slices were consecutively washed with 50% ethanol (2 min), 70% ethanol (1 min), 50% ethanol (2 min), and phosphate buffer (2 min). One hundred micrometer sections caudal and rostral to a prospective rhythmic slice were fixed for at least 15 min and stained for 30-40 s with the above solutions. Sections were transferred on a “hanging drop” glass slide (Fisher Scientific) to a microscope (Standard 16; magnification, 32x; Carl Zeiss, Jena, Germany) and photographed (PL-A642, 1.3 megapixel; PixeLINK, Ottawa, Ontario, Canada). preBötC slices were stained after experiments using an identical method, except they were immersed in thionin for 90 s. Stained preBötC slices were transferred in phosphate buffer to a Petri dish and photographed (PL-A686, 6.6 megapixel; PixeLINK) under a stereo microscope (Zeiss SR15; magnification, 32x).

2.2.6 Data Analysis

Inspiratory activity of preBötC slices in 3 mM $[\text{K}^+]$ solution was continuously recorded at a sampling rate of 1 kHz. Burst rate was averaged every 20 min over 2 min time windows. “Longevity” of rhythm was defined as the time from start of recording until the time when the period between consecutive bursts exceeded 5 min. Burst duration was defined using ClampFit software (Molecular Devices, Chicago, IL) as the time interval from when the signal increased above and decreased below a threshold set at 10% of the peak amplitude for that burst. Pharmacologically reactivated rhythms were described by averaging burst rates over a 2 min time period at steady state. Values are means \pm SEM except for histological analyses (means \pm SD). Significance ($p < 0.05$) was assessed by one-sample t test using Sigmaplot (Systat Software, Point Richmond, CA).

2.3 Results

2.3.1 Anatomical Relationship between Neonatal Rat Brainstem Nuclei and preBötC

Inspiratory active medullary slices are most commonly obtained from rats between P0 and P4. They are generated either in approximate reference to gross anatomical features, such as the position of hypoglossal nerve roots or obex, or in more precise reference to brainstem marker nuclei visualized in transilluminated, transverse brain sections produced during cutting. The latter approach is more precise, but assumes a constant anatomical relationship between the functionally defined preBötC and the marker nuclei (Schwarzacher et al., 1995) (Figures 2-1, 2-2). We tested this assumption by comparing the rostrocaudal extensions of marker nuclei in P0, P2, and P4 SD and W rats. Convenient ventral marker nuclei include the VII motor nucleus, the lateral reticular nucleus, and in particular different subnuclei of the inferior olive (Li et al., 2001). Less valuable information is obtained from dorsal structures such as the hypoglossal motor nucleus or obex as their association with ventral structures is sensitive to the cutting angle (“tilt”) (Figure 2-2A). Ambigular motor neurons do not aggregate to a detectable nucleus in transverse 50-100 μm sections.

The marker nuclei were first studied in thionin-stained transverse serial sections (50 μm) from 15 agar-embedded fixed brainstems (Figure 2-1). The position of each section was defined by its distance (in millimeters) from the caudal end of VII nucleus (VII_c) (Figure 2-1A, left) (regions caudal to VII_c were assigned negative values). Living tissue from 11 brainstems was then sectioned serially (100 μm) in superfusate, photographed (Figure 2-1A, middle), fixed, and stained with thionin, and then rephotographed (Figure 2-1A, right). In these sets of serial sections, the rostrocaudal extensions of marker nuclei (Figure 2-1B), as well as the distance from the rostral margin of the VII nucleus (VII_r) to the caudal margin of the medial inferior olivary nucleus (IOM_c) (Figure 2-1C) was the same whether compared between rat strains (W vs SD), age groups (P0 vs P2 and P4), or live versus fixed sections. The anatomical relation of the marker nuclei with respiratory brainstem regions, specifically the parafacial respiratory group/retrotrapezoid nucleus

complex and the VRC including the preBötC and Bötzing complex (BötC), are shown in Figure 2-2A and B. The consistency of marker nuclei, both in absolute dimension and position relative to each other, allowed construction from one P2 W rat brainstem of a “reference atlas” comprising serial transverse 50 μm sections through the neonatal rat medulla that was applicable to SD and W rats between P0 and P4 (Figure 2-1C; see also Appendix I).

2.3.2 On-line Histology for Generating Calibrated preBötC Slices

Based on the constancy of brainstem anatomy for P0-P4 rats, we developed on-line histology, a method for generation and rapid documentation of preBötC slices with defined boundaries. Brainstem sections were cut with a vibratome in the caudal-to-rostral direction starting at the caudal end of the inferior olive (Figure 2-3). Section thickness was reduced to 100 μm when approaching the desired level for generating a rhythmic slice. Pre-rhythmic live sections were inspected on-line and photographed. Varying the focus or condensor aperture revealed medullary marker nuclei, especially subnuclei of the inferior olive (Figure 2-3A). Sections were compared with the reference atlas (Figure 2-3B) to evaluate, on-line, the rostrocaudal position. For defining the rostral border of the rhythmic slice, “post-rhythmic” sections were cut and photographed (Figure 2-3C). For more detailed “off-line” analysis of slice boundaries, pre-rhythmic and post-rhythmic “frame” sections were fixed and stained with thionin (Figure 2-3A,C).

2.3.3 Generation of Calibrated 500 μm Thick preBötC Slices

We next tested whether on-line histology facilitates generation of rhythmic slices with predetermined and consistent rostrocaudal borders. We compared the actual versus desired rostrocaudal boundaries of 21 slices (500 μm thick) that were cut to have the caudal and rostral boundaries at -0.70 and -0.20 mm caudal to VII_c, respectively. This should place the center of the preBötC (located at about -0.50 mm) (Smith et al., 1991) near the middle of such slices (Figures 2-2, 2-3, 2-4), denoted as m-preBötC [500/-0.70]SD/W-P0/4 (m-preBötC, preBötC in the middle; 500 indicates thickness in micrometers; -0.70 refers to caudal boundary relative to VII_c; SD/W-P0/4, 0- to 4-d-old SD or W rats). Slice thickness was determined by sectioning a horizontal strip at the level

of the VRC/preBötC (Figure 2-3D). Values were similar in freshly cut ($560 \pm 12 \mu\text{m}$; $n = 3$) and fixed slices ($518 \pm 38 \mu\text{m}$; $n = 7$) (Figure 2-4A), indicating minimal shrinkage during fixation. Sectioning for physical thickness also revealed that the dye penetrated $<50 \mu\text{m}$ into the translucent brainstem tissue (Figure 2-3D). Thus, identification of transection level based on analysis of stained surface structures in rhythmic and frame slices should be accurate within $50 \mu\text{m}$. Caudal and rostral slice boundaries determined by analyzing surface structures in the rhythmic slices (Figure 2-3D) averaged -0.70 ± 0.05 and -0.20 ± 0.09 ($n = 21$), respectively (Figure 2-4A). Because these values were very close to the targeted values, we propose that rostrocaudal boundaries of preBötC slices can be accurately quantified off-line by comparing their surface structures with those in the atlas.

Comparison of rhythmic slice boundaries with the position of the last pre-rhythmic and first post-rhythmic slice revealed a rostrocaudal gap between surface structures in the rhythmic slice (“slice image”) and the adjacent pre-rhythmic or post-rhythmic frame sections of 89 ± 24 and $86 \pm 58 \mu\text{m}$ ($n = 21$), respectively (Figure 2-4A). This gap likely reflects tissue transparency, dye entry into rhythmic and frame slices, and possibly disintegration of a thin layer of tissue during slicing procedures. This gap has to be taken into account for generation of a rhythmic slice using on-line histology.

2.3.4 Rhythm in Calibrated preBötC Slices at 3 mM K⁺

Our next objective was to assess the activity of defined m-preBötC slices in solution of physiological K⁺. Fifteen m-preBötC[500/-0.70]SD/W-P0/4 slices generated regular inspiratory VRC rhythm for 142 ± 13 min (range, 53-221 min) (Figure 2-5). Despite our original premise that rhythmic activity in 3 mM K⁺ might be limited in slices with the preBötC close to the surface, there was no obvious correlation between slice boundaries and longevity of rhythm (Figure 2-4B). In fact, slices with the preBötC near their rostral or caudal surfaces were among those with the greatest longevity. Whether longevity is reduced in slices with the preBötC at the slice surface, however, requires additional investigation.

We then characterized whether longevity of rhythm depends on slice thickness. For this, we generated slices extending an additional 50 μm in rostral and caudal directions ($n = 11$). These m-preBötC[600/-0.76]SD/W-P0/4 slices showed rhythm for 240 ± 25 min ($n = 8$; range, 126-322 min) thus for a notably longer time period than the above 500 μm slices. In the 500 and 600 μm thick slices, mean inspiratory frequencies were 8.8 ± 0.8 ($n = 15$) and 8.1 ± 0.5 ($n = 8$) bursts/min at 20 min of recording. Burst rate typically remained rather constant until 10-20 min before arrest of rhythm (Figure 2-6A,B). In 80% of m-preBötC [500/-0.70] slices, 1-15 single bursts (“S-bursts”) of relatively uniform duration (0.61 ± 0.03 s; $n = 4$) alternated with bursts of similar amplitude that were of longer duration (0.80 ± 0.05 s; $n = 4$) and appeared to comprise two partially overlapping single, “intermingled” bursts (“I-bursts”) (Figure 2-5). In 60% of those 500 μm slices, the duration of the I- and S-bursts began to decline after >1 h and >20 min, respectively (Figure 2-6C). The duration of both types of bursts typically remained stable for >2 h in m-preBötC[600/-0.76] slices.

Three of 11 m-preBötC[600/-0.76] and 6 of 21 m-preBötC[500/-0.70] slices developed “sigh-like” activity (Figure 2-7A) (Lieske et al., 2000). Sigh-like bursts, which were larger in amplitude because of the occurrence of a second burst during the decaying phase of the initial burst, occurred at a rate of 2.1 ± 0.4 bursts/min ($n = 5$; at 20 min of recording) (Figure 2-7B). They were often followed by a period of reduced activity during which burst amplitude decreased markedly (sometimes disappearing for brief periods) and then increased gradually during the next 3-12 consecutive intersigh bursts, which occurred with an average frequency of 8.7 ± 1.1 bursts/min at 20 min of recording ($n = 5$) (Figure 2-7B). Longevity of sigh-like rhythm in 500 μm slices was 108 ± 12 min ($n = 6$).

2.3.5 Neuromodulation of preBötC Inspiratory Networks

2.3.5.1 Inhibition by opiates

Bath application of DAMGO (10 nM), which decreases cellular cAMP via μ -opioid receptors (Ballanyi et al., 1997; Richter et al., 1997), lowered burst frequency to <20% of control (i.e., to 0-2 bursts/min in four m-preBötC[500/-0.70] slices), whereas 25 nM

DAMGO abolished rhythm in m-preBötC[500/-0.70] (n = 3) and m-preBötC[600/-0.76] (n = 3) slices (Figure 2-8). In the 600 μm slices, rhythm was effectively reactivated after combining washout of the drug with application of the μ -receptor antagonist naloxone (1 μM) (Figure 2-8).

2.3.5.2 Neurostimulants

Our above data show that longevity of rhythm in 3 mM K^+ superfusate increases with slice thickness consistent with the hypothesis that rundown of bursting reflects depletion of endogenous excitatory neuromodulator(s). Given this observation, we assessed in the m-preBötC[500/-0.70] slices the ability to reactivate rhythm of neurostimulants acting on different signaling pathways.

Glutamate and Metabotropic Receptors

Bath application of 1 μM DHPG, a group-I metabotropic glutamate receptor agonist (Conn & Pin, 1997), reactivated rhythm with a pattern and frequency very similar to control (Figure 2-9A,B,D). At threshold concentration (0.25 μM), rhythm returned at very low frequencies (<1 burst/min), whereas 10 μM DHPG evoked 17.1 ± 1.4 bursts/min (n = 6; maximum, 24) (Figure 2-9D). In >50% of cases, 2.5-10 μM DHPG elicited tonic VRC activity initially (Figure 2-9B). Rhythm persisted throughout drug administration periods of 15-20 min and typically disappeared within <15 min of starting washout of DHPG (Figure 2-9A).

Thyrotropin-Releasing Hormone

Very similar results were obtained with TRH (Figure 2-9A,C,E), which blocks K^+ channels via G_q proteins (Chen et al., 2006). At 0.5 nM, TRH reactivated rhythm almost indiscernible from control. At threshold concentration (0.1 nM), TRH evoked <1 bursts/min, whereas frequency reached 17.2 ± 1.1 bursts/min (n = 8; maximum, 21) at 100 nM TRH (Figure 2-9E). In three slices, 10-100 nM TRH induced tonic activity initially (Figure 2-9C) and also decreased burst strength to 20-70% of the value of uniform bursting at lower concentrations in two cases. At all concentrations, the frequency of

TRH-induced rhythm remained stable throughout the application period (15-20 min). In two slices, rhythm persisted for >1 h after start of washout (Figure 2-9A).

Elevation of cAMP Levels

We tested next effects of receptor-independent elevation of cellular cAMP induced by the phosphodiesterase-4 blocker rolipram and the less specific blocker theophylline (O'Donnell & Zhang, 2004). Inspiratory rhythm was reactivated to frequencies of 1.6 ± 0.7 (n = 5) and 5.4 ± 0.8 (n = 8) bursts/min by 0.25 and 2.5 mM theophylline, respectively (Figure 2-10A,C). Rolipram, at 1 and 5 μ M, also reactivated the arrested preBötC network in the 500 μ m slices, causing burst rate to increase to 6.1 ± 0.9 (n = 11) and 6.8 ± 2.3 bursts/min (n = 3), respectively (Figure 2-10B,C). In six m-preBötC [600/-0.76] slices, 0.25 and 5 μ M rolipram were comparably effective (6.3 ± 0.3 vs 6.9 ± 0.6 bursts/min) (Figure 2-10D). At 1-5 μ M, the action of rolipram persisted between 30 and 120 min after washout of the agent (Figure 2-10B). Theophylline and rolipram did not typically induce tonic activity. Although lower in frequency, these drugs often elicited more robust and regular bursting than DHPG and TRH. All neurostimulators also evoked regular rhythm in four slices with sigh pattern (Figure 2-7).

2.3.6 Ca²⁺ Imaging of Neuromodulator-Induced Rhythmic Activities in Assemblies of VRC/preBötC Neurons

Our electrophysiological VRC approach was not suited to study whether rhythmic behaviors elicited by the above agents stimulate the same VRC/preBötC neurons. Consequently, we combined electrophysiological recording with Ca²⁺ imaging for assessment within the contralateral VRC/preBötC of activity and morphology of groups of individual neurons. In eight m-preBötC [500/-0.69] slices, recordings were done from 17 preBötC cells located between -0.60 and -0.58, thus within the caudal preBötC boundary and 34 non-preBötC VRC cells located between -0.78 and -0.69 (compare Figure 2-2A). Somata of these cells showed Ca²⁺ rises in phase with VRC/preBötC rhythm (Figures 2-11, 2-12). In <15% of cells, Ca²⁺ oscillations were also apparent in proximal dendrites. Neurons with higher resting fluorescence intensity typically showed larger inspiratory-related Ca²⁺ oscillations. The vast majority of neurons initially active in

3 mM $[K^+]$ showed very similar Ca^{2+} rises when rhythm was reactivated with DHPG (87.8%; n = 41), TRH (70.6%; n = 34), rolipram (84.2%; n = 19), or theophylline (94.1%; n = 17) (Figures 2-11, 2-12). Z-stack image series enabled 3D-animated movies which revealed basic morphological features of VRC (Figure 2-11) and preBötC neurons (Figure 2-12) such as soma shape and number of primary dendrites.

2.4 Discussion

We have analyzed for the first time endogenous inspiratory rhythm at physiological extracellular K^+ in brainstem slices containing the preBötC inspiratory center. These slices with well defined rostrocaudal boundaries were highly sensitive to neuromodulators. Activity of localized and functionally identified preBötC neurons and reactivation of their rhythmic discharge via distinct second-messenger pathways after spontaneous in vitro apnea was assessed with two-photon/confocal Ca^{2+} imaging.

2.4.1 Calibrated preBötC Slices

We found that the rostrocaudal extensions of respiratory marker nuclei (i.e., VII nucleus, lateral reticular nucleus, inferior olive) are remarkably constant in newborn rats. This enabled use of a reference rat brainstem atlas for generation of preBötC slices with predictable and reproducible boundaries. Our on-line histological approach is a valuable step toward standardizing slicing procedures and provides a reference for comparison of results between laboratories. It will also form a reference for exploring the modification of preBötC function by surrounding brainstem structures such as the parafacial respiratory group and the retrotrapezoid nucleus, which both overlap with the VII motor nucleus (Figure 2-2A) and contain chemosensitive neurons that presumably drive the preBötC (Onimaru & Homma, 2003; Mulkey et al., 2004; Kawai et al., 2006). Here, we showed that the preBötC is capable to generate rhythm at physiological K^+ without drive from these areas which were not included in m-preBötC[500/-0.70] slices.

2.4.2 High Sensitivity to Neuromodulators of Rhythm in 3 mM K⁺

The original report on the preBötC stated briefly that slices thicker than 500 μm can be active at physiological extracellular K⁺ (Smith et al., 1991; Funk et al., 1993). Here, 600- and 500 μm thick slices with the preBötC in the center generated inspiratory rhythm for 4 and >2 h, respectively, at frequencies comparable with those of slices in elevated K⁺. Similar to the in situ perfused brainstem preparation (Manzke et al., 2003), the rhythm was blocked by low nanomolar concentrations of μ -agonist, whereas micromolar concentrations are typically necessary to abolish slice rhythms in high K⁺ superfusate (Johnson et al., 1994). This indicates that K⁺ counteracts depressant effects of inhibitory neuromodulators in preBötC slices by unspecifically increasing neuronal excitability (Somjen, 2002).

The preBötC network in the calibrated slices is also very sensitive to excitatory neuromodulators. TRH is often used at high nanomolar to micromolar concentrations to reveal stimulatory effects on (respiratory) brainstem slices (Funk et al., 1994; Rekling et al., 1996; Browning & Travagli, 2001). Here, picomolar TRH concentrations could already reactivate regular rhythm after spontaneous arrest, whereas 0.5 nM TRH mimicked rhythm in preBötC slices before arrest. Regarding the mechanism of action, TRH targets G_q-protein-linked receptors that may directly block two-pore-domain K⁺ channels (Töpert et al., 1998; Chen et al., 2006) that are proposed to contribute to respiratory rhythm generation (Ballanyi et al., 1999; Smith et al., 2000). While the respiratory stimulatory action of TRH is established (Hedner et al., 1983; Bennet et al., 1988), we report for the first time that DHPG-mediated activation of metabotropic glutamate receptors induces preBötC rhythm. Locomotor networks in neonatal rats (Nistri et al., 2006) and respiratory networks in lampreys (Bongianni et al., 2002) are similarly sensitive to the agent. Furthermore, DHPG augments L-type Ca²⁺ channel currents in unidentified VRC/preBötC neurons (Mironov & Richter, 1998) and enhances the excitability of respiratory motoneurons (Dong & Feldman, 1999; Nistri et al., 2006). Our data suggest that glutamate may act endogenously through group-I metabotropic receptors coupled to phospholipase-C inositol-1,4,5-triphosphate signaling (Conn & Pin, 1997) to stimulate breathing.

The increased longevity of rhythm in thicker slices is consistent with the hypothesis that in vitro apnea reflects depletion of excitatory agents. However, our findings do not allow the conclusion that the rhythm arrests because of depletion of glutamate and/or TRH from the slices. Also, depletion of SP from presynaptic terminals abolishes the slice rhythm (Morgado-Valle & Feldman, 2004), whereas SP reactivates bursting following its arrest after lowering superfusate K^+ from 8 to 3 mM (Pena & Ramirez, 2004). Neuromodulator(s) acting through the cAMP-protein kinase A pathway, such as norepinephrine or serotonin (Richter et al., 1997; Manzke et al., 2003), may also be among the excitatory agent(s) that appear to be depleted from the slices. This is indicated by the stimulatory effects on the slice rhythm of theophylline and rolipram, which both inhibit cAMP-specific phosphodiesterase-4, resulting in a rise of cellular cAMP (Nikulina et al., 2004; O'Donnell & Zhang, 2004). While theophylline is commonly used clinically to reverse apneas in (preterm) infants, the antidepressant rolipram (O'Donnell & Zhang, 2004) antagonizes in vitro respiratory depression in perinatal rats (Ballanyi, 2004; Ruangkittisakul & Ballanyi, 2006). Here, theophylline stimulated the preBötC network at low millimolar concentrations, whereas 250 nM rolipram already reactivated rhythm with rates only slightly lower than in controls. This rolipram concentration may be similar to or lower than those exerting beneficial effects on age-related memory deficits (Barad, 2003) and depression (O'Donnell & Zhang, 2004). Because rolipram-evoked rhythm was regular and robust, this or more recent phosphodiesterase-4 inhibitors with fewer side effects (Dal Piaz & Giovannoni, 2000; O'Donnell & Zhang, 2004) may effectively stimulate breathing in intact animals or humans.

The observation that all agents were comparably effective suggests that rhythmogenic preBötC neurons and/or neurons providing tonic excitatory drive to these cells (Richter et al., 1992; Feldman et al., 2003) are targeted by multiple signaling pathways (Richter et al., 1997). This shows that run down of rhythm from preBötC slices in 3 mM K^+ is not necessarily an obstacle to study the neural control of breathing. Rather, it enables both the identification of second-messenger pathways that can promote rhythm generation and the analysis of how these signaling cascades interact to modulate the rhythm. In that regard, the sigh-like inspiratory pattern (Lieske et al., 2000) in vitro may be associated with the

hormonal status of pups resulting in an imbalance of endogenous neuromodulators. Interstitial levels of TRH, which facilitates regular rhythm in preBötC slices, may be lower in poorly lactated animals (Nillni et al., 2001), resulting in a relative dominance of endogenous neuromodulator(s) promoting sighs, probably involving SP (Shvarev et al., 2003).

2.4.3 Imaging of VRC/preBötC Neurons

Similar to a current lack of knowledge on anatomical slice boundaries, the rostrocaudal location of electrophysiologically recorded respiratory neurons has not been reconstructed so far in most studies on rodent preBötC slices. Accordingly, a significant portion of cells referred to as preBötC neurons possibly comes from regions outside the preBötC. In our study, all active cells at identified rostrocaudal levels showed Ca^{2+} rises during inspiratory VRC bursting with no indication of activity associated with other respiratory phases. Because no ratiometric Ca^{2+} dye was used here, no attempt was made to quantify the Ca^{2+} rises. Since glutamate evoked notably larger Ca^{2+} signals, the inspiratory Ca^{2+} transients may be rather modest (100-200 nM) as estimated by fura-2 Ca^{2+} measurements in unidentified VRC/preBötC neurons (Fermann et al., 1999). Dialysis via the patch electrode with Ca^{2+} dye as in the latter study is one potent approach to reveal structural features of respiratory neurons. A unique advantage of our approach is that populations of neurons can be imaged after pressure injection of dye (Stosiek et al., 2003) into the VRC/preBötC. A similar approach has been used previously (Koshiya & Smith, 1999), whereas another study loaded preBötC slices from mice after bath application of membrane-permeable Ca^{2+} dye (Thoby-Brisson et al., 2005). Confocal imaging in our study afforded high spatial resolution and 3D images of neuronal networks within the VRC/preBötC (Figures 2-11, 2-12) as prerequisites for analysis of a structure-function relationship of the preBötC.

2.5 Summary

A most important finding is that the same population of neurons that showed rhythmic Ca^{2+} rises in 3 mM K^+ solution was reactivated by the neurostimulants. This suggests that either the agents (1) reactivate rhythm through a common population of rhythmogenic preBötC neurons, (2) activate distinct pools of neurons that drive a common set of rhythmogenic preBötC neurons that we imaged, or (3) activate distinct pools of rhythmogenic preBötC neurons that converge on a common set of follower neurons that we imaged. We were unable to distinguish between these possibilities because optical recording in this study was restricted to tissue depths $<70 \mu\text{m}$ for confocal imaging and $<100 \mu\text{m}$ for two-photon imaging. The critical rostrocaudal boundaries of the newborn rat preBötC have not yet been determined in slices but its center is hypothesized (Smith et al., 1991) to be close to -0.50 following the terminology introduced here (Figure 2-2, 2-3) and extend $100 \mu\text{m}$ in rostral and caudal directions. Accordingly, only a subpopulation of cells studied here represents “real” preBötC neurons, which did not show major differences in gross morphology (i.e., soma shape and size or array of primary dendrites) among each other or compared with VRC cells. Recording from cells in slices with the preBötC more exposed to the caudal or rostral surface may reveal a morphology feature specific to rhythmogenic neurons. Additional criteria such as (fluorescent) tagging for preBötC neuronal markers such as characteristic neurotransmitter receptors and transporters (Gray et al., 1999; Guyenet et al., 2004; Pagliardini et al., 2005) may facilitate the identification and analysis of the cellular rhythm generator.

Figures

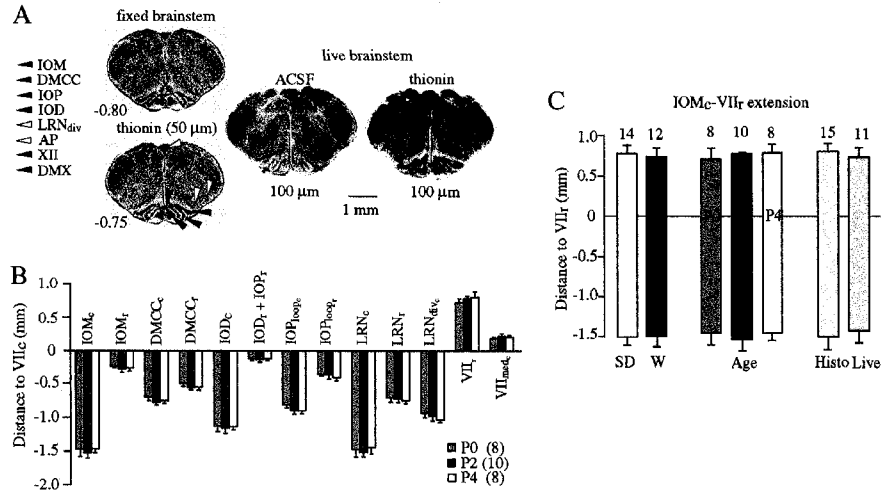


Figure 2-1 Constancy of rostrocaudal extensions of “respiratory marker nuclei” in the ventral brainstem of newborn SD and W rats between P0 and P4. **A**, The left panel shows two serial, transverse sections (50 μ m thin) of fixed, thionin-stained brainstem tissue from P2 W rat, which are part of a reference atlas (Appendix I). The middle panel shows a 100 μ m section of living tissue taken at the rostrocaudal level encompassed by the two fixed sections in the left panel. The right panel is an image of the section in the middle panel taken after fixation and thionin staining. **B**, Distances from the caudal end of VII motor nucleus (VII_c) to the caudal (c) and rostral (r) boundaries of specific marker nuclei (negative value indicating location caudal to VII_c). **C**, Location, relative to VII_c, of the boundaries of the most rostral (VII_r) and caudal (IOM_c) brainstem marker nuclei. Extensions are very similar when data are analyzed either from W versus SD rats, animals from both strains at different ages, or initially fixed (Histo) versus live preparations. The bars in **B** and **C** represent means \pm SD; values above bars and in parentheses in **B** represent the number of preparations. The histology of some marker structures is shown in **A**. Additional images of marker nuclei are in Figures 2-2C, 2-3, and the Appendix I. DMCC, Dorsomedial cell column of inferior olive (IO); IOM, medial IO; IOD, dorsal IO; IOP, principal IO; IOP_{loop}, lateral loop of IOP; LRN, lateral reticular nucleus; LRN_{div}, LRN divided in medial and lateral subnucleus; VII, facial motor nucleus; VII_{med}, medial subnucleus of VII; AP, area postrema; XII, hypoglossal motor nucleus; DMX, dorsal vagal motor nucleus.

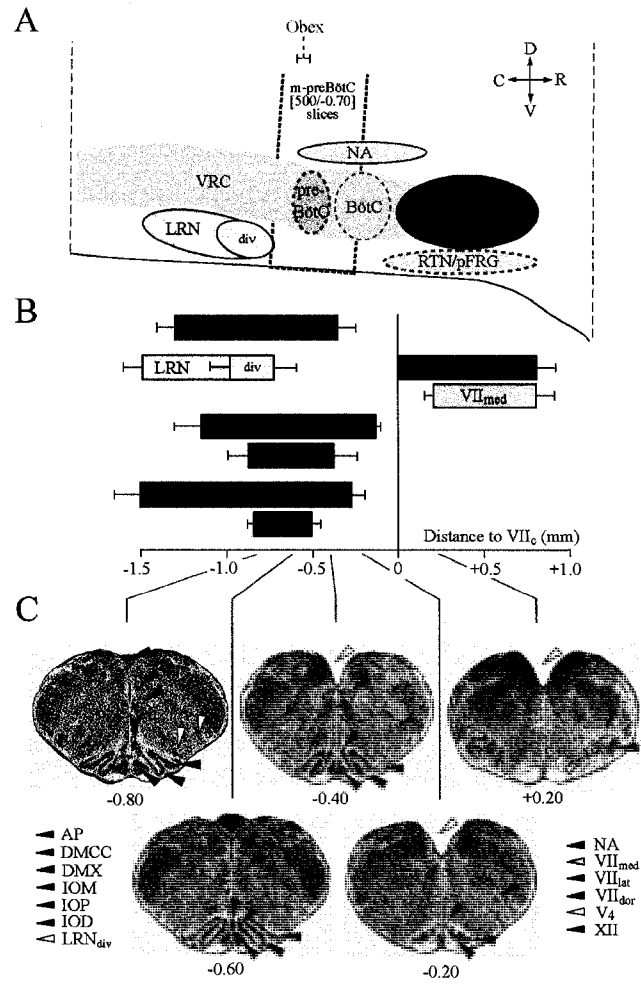


Figure 2-2 Ventral respiratory regions and respiratory marker nuclei. **A**, Schematic sagittal section showing ventral respiratory regions [modified from Smith et al. (1991); Alheid et al. (2004)] and marker nuclei of Figure 2-1B. The dotted box indicates the mean position of 500 μ m thick slices with the preBötC in the middle (“m-preBötC”) and mean boundaries at -0.70 and -0.20 mm, respectively (compare Figures 2-3, 2-4). The position of obex (-0.55 VII_c) relative to preBötC in transverse sections depends on sectioning angle (Figure 2-3). The horizontal scale is the same as for **B** showing means (\pm SD) of rostral-caudal boundaries of marker nuclei from 15 fixed brainstems. **C**, Sample transverse sections from W-P2 reference atlas (Appendix I) showing marker nuclei in **A** and **B** and additional structures. Abbreviations not used in Figure 2-1: VRC, ventral respiratory column; BötC, Bötzing complex; RTN, retrotrapezoid nucleus; pFRG, parafacial respiratory group; NA, nucleus ambiguus; VII_{dor}, dorsal subnucleus of VII; VII_{lat}, lateral subnucleus of VII; V₄, fourth ventricle.

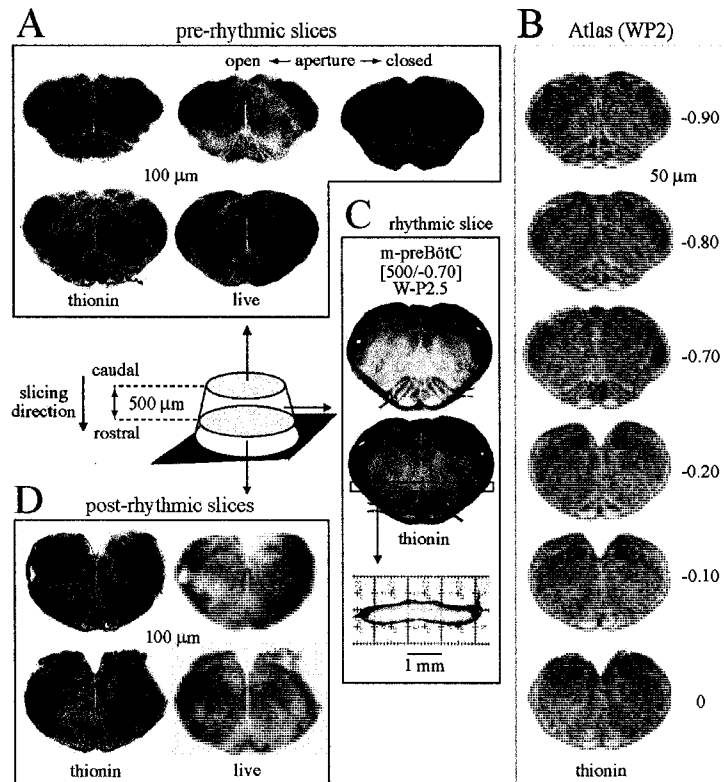


Figure 2-3 On-line histology for generating calibrated preBötC slices. The diagram shows newborn rat brainstem glued with rostral side to metal plate attached to vibratome stage. Serial sectioning in caudorostral direction provides 100- μ m-thin pre-rhythmic sections (A), which are compared with a W-P2 rat atlas (B) (Appendix I) to determine cutting level and caudal boundary of the rhythmic slice, in this case -0.70 mm relative to VII_c. As shown for the second-to-last pre-rhythmic slice (top row), resolution can be enhanced by adjusting the condenser aperture or focus. Sections are photographed, fixed for thionin staining, and rephotographed for higher resolution off-line analysis. C, Post-rhythmic slices taken after cutting the rhythmic slice are used for on- and off-line analysis of rostral slice boundary. D, Fixed rhythmic slice stained with thionin to define caudal (top image) and rostral (bottom image) surfaces. The thickness of the rhythmic slice, here 500 μ m, is determined by sectioning the horizontal strip at level of VRC/preBötC. Combined on-line/off-line analysis revealed caudal and rostral slice boundaries at -0.70 and -0.20, respectively, and that the preBötC is close to the middle of the slice (Figure 2-2A). Sections in A, C, and D are from one individual WP2.5 brainstem. Thus, this calibrated preBötC slice is described as “m-preBötC[500/-0.70]W-P2.5.”

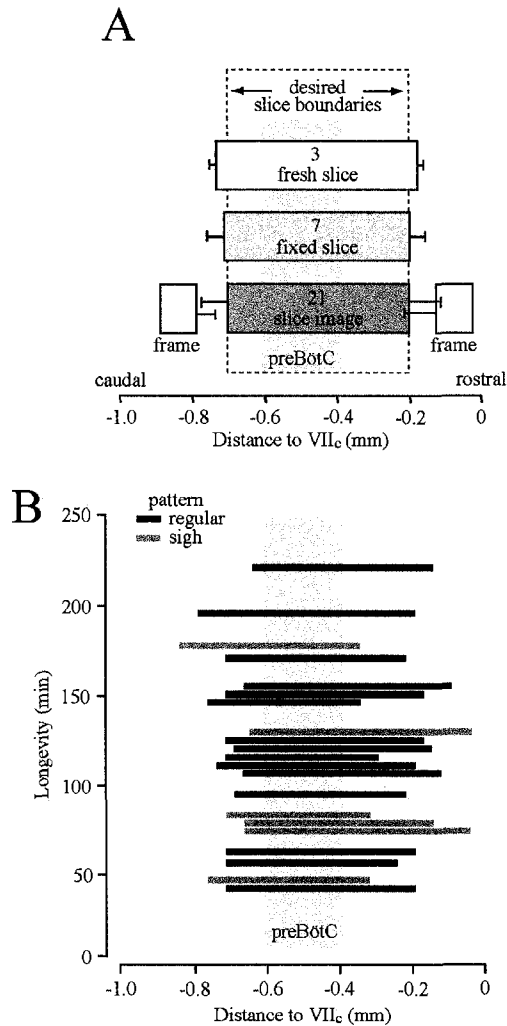


Figure 2-4 Boundaries and dimensions of m-preBötC[500/-0.70]SD/W-P0/4 slices versus longevity of rhythm in 3 mM [K⁺] solution. A, Means (\pm SD) of rostral and caudal slice boundaries (slice image) determined in 21 slices in relation to atlas (Appendix I). Caudal and rostral frame values were similarly obtained from last pre-rhythmic and first post-rhythmic slices, respectively (for details, see Figure 2-3). The location and physical thickness of seven fixed, thionin-stained slices (“fixed slice”) are compared with three unfixed, unstained slices (“fresh slice”) measured in standard superfusate within 20 min of preparation. Note gaps between slice boundaries determined from analysis of rhythmic slices compared with frame sections. B, Plot of rostrocaudal boundaries of slices versus longevity of rhythm (Figure 2-5). Most slices showed a regular inspiratory pattern (dark bars) (Figures 2-5, 2-6), whereas some showed sigh-like activity (gray bars) (Figure 2-7).

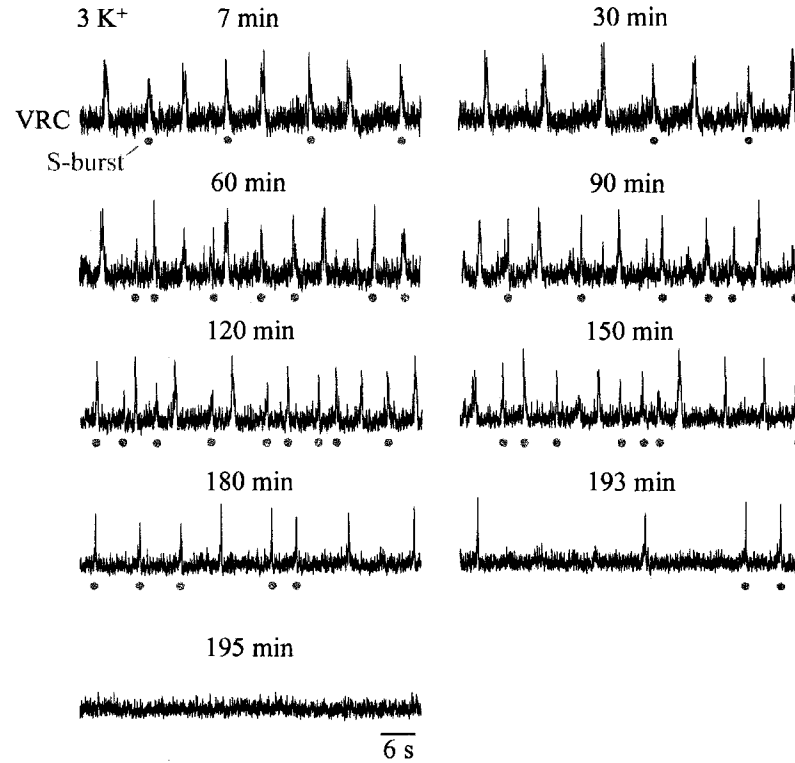


Figure 2-5 Inspiratory rhythm in 3 mM [K⁺] superfusate. Suction electrode recording of VRC activity in a m-preBötC[500/-0.78]W-P0 slice producing regular rhythm. The frequency of VRC population activity varied between 8 and 13 bursts/min for a time period of 180 min, before rhythm slowed after 193 min and then stopped after 195 min. The gray circles indicate single bursts (S-bursts). Nonlabelled bursts are intermingled bursts (I-bursts) comprising two partially overlapping S-bursts.

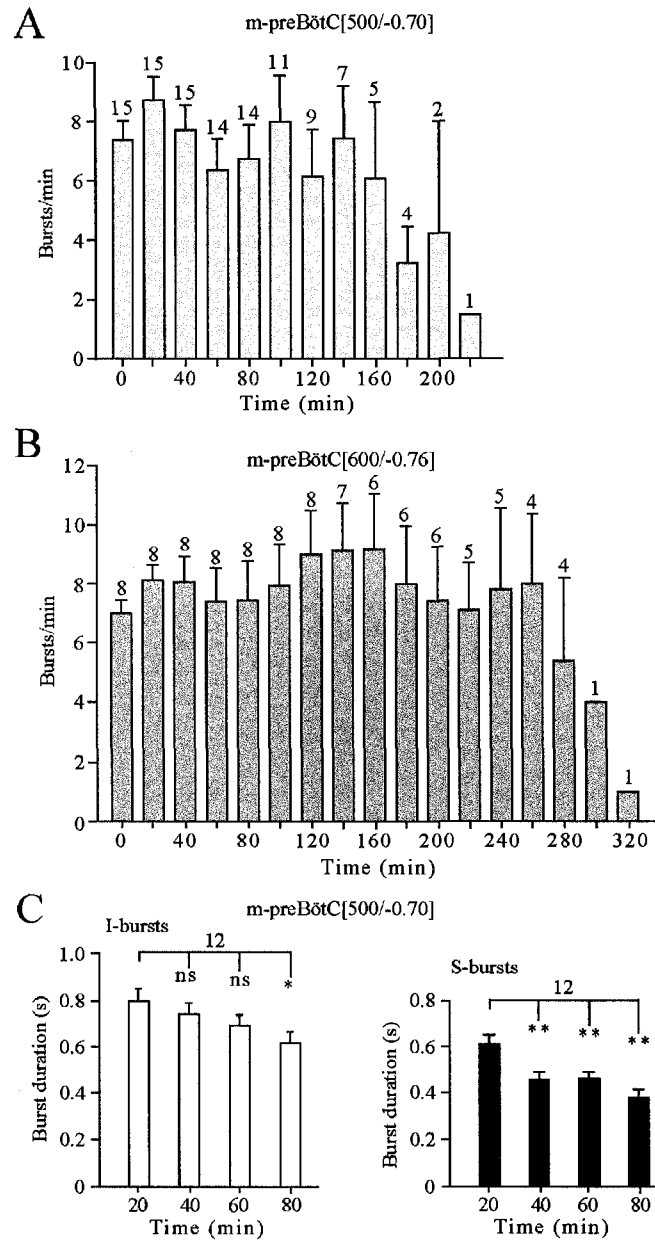


Figure 2-6 Time dependence of inspiratory burst frequency and duration. **A**, **B**, Burst rates in m-preBötC[500/-0.70] (**A**) and m-preBötC[600/-0.76] (**B**) slices. The digits indicate the number of slices [out of 15 (**A**) and 8 (**B**)] active at indicated time periods. **C**, Duration of intermingled bursts (I-bursts, left) and single bursts (S-burst, right). Three consecutive bursts were analyzed for each time period in each slice. The bars represent means \pm SEM; digits indicate the number of slices. * $p < 0.05$; ** $p < 0.01$.

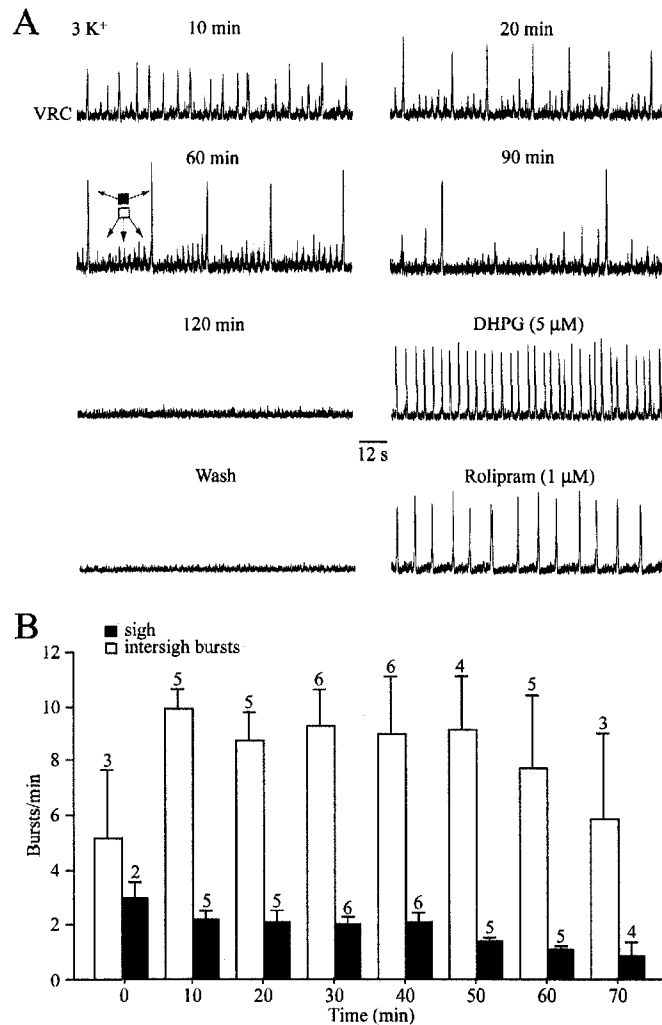


Figure 2-7. Sigh-like inspiratory activity. **A**, In an m-preBötC[500/-0.73]W-P0 slice, an initially regular rhythm of small amplitude bursts transformed within 10 min into a pattern of single augmenting, sigh-like bursts followed by a period in which the burst amplitude cycled from a low-amplitude burst followed by four to eight bursts of progressively greater amplitude and one very large amplitude sigh-like burst that seemed to restart the cycle. After spontaneous arrest of rhythm after 120 min, regular inspiratory bursting was evoked by bath application of the group-I metabotropic glutamate receptor agonist DHPG and, after washout of DHPG, the inhibitor of cAMP-specific phosphodiesterase-4 rolipram. **B**, Time dependence of mean sigh-like (■) and intersigh (□) burst frequencies in m-preBötC[500/-0.70] slices. The bars represent means \pm SEM; values indicate the number of slices.

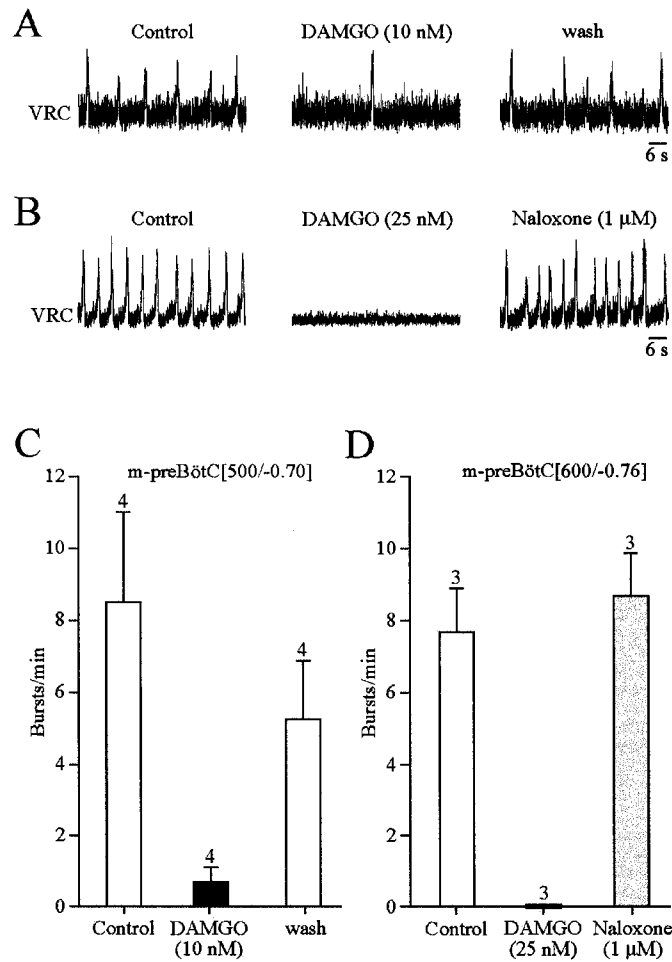


Figure 2-8 Opioid-induced depression of inspiratory rhythm. **A**, In an m-preBötC[500/-0.77] W-P2 slice, bath application of the μ -opioid receptor agonist DAMGO depressed frequency, but not amplitude of inspiratory VRC bursting. Rhythm recovered partially after 25 min of washout. **B**, In an m-preBötC[600/-0.80] W-P3 slice, DAMGO abolished rhythm, which was reactivated within 5 min of simultaneously washing out DAMGO while washing in (bath application) of the opioid receptor antagonist naloxone. **C**, **D**, Bar graphs show effects of DAMGO on frequency and the recovery of rhythm after washout of DAMGO alone (**C**) and in the presence of naloxone (**D**). The bars represent means \pm SEM; values indicate the number of slices tested.

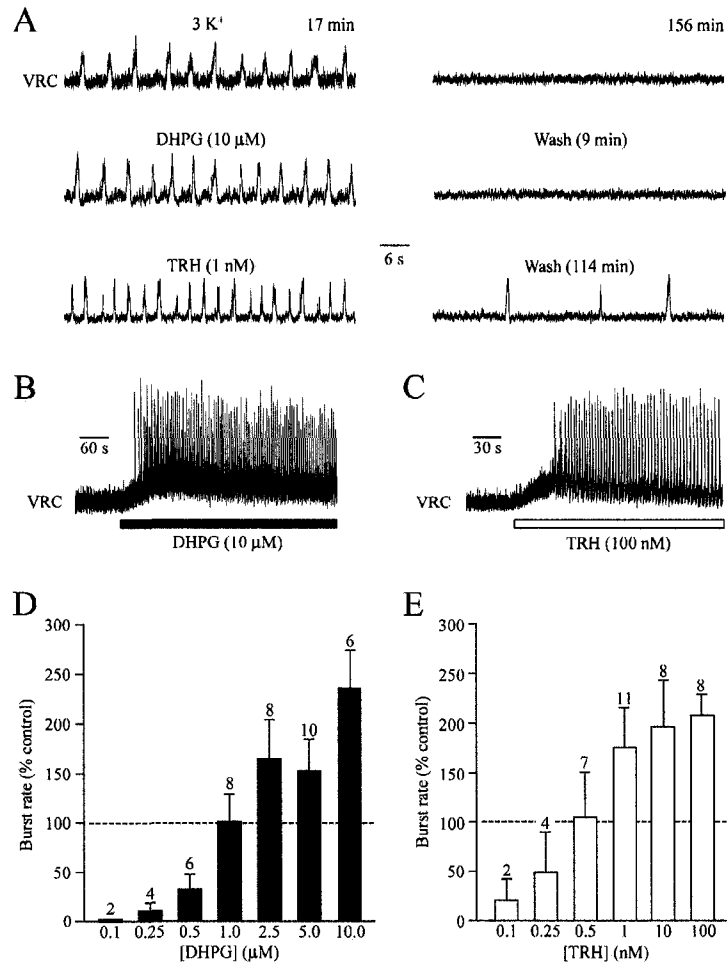


Figure 2-9 Neurotransmitter-evoked reversal of in vitro apnea. **A**, Control activity in 3 mM K^+ (left, top trace) spontaneously arrested after 156 min in an m-preBötC [500/-0.70]SD-P1.5 slice (right). Bath application of DHPG reactivated bursting activity very similar to control, which again stopped within 9 min of wash. A comparable rhythm was also elicited by TRH. Note that, in contrast to DHPG, bursting continued for almost 2 h after TRH washout. **B**, **C**, In the initial phases of bath application, DHPG (**B**) (10 μ M; m-preBötC[500/-0.70]SD-P1.5) or TRH (**C**) (100 nM; m-preBötC[500/-0.70]W-P2) evoked tonic activity, as evidenced by a shift and increased thickness in the baseline of the integrated VRC signals. **D**, **E**, Bar graphs show that the efficacy of DHPG (**D**) and TRH (**E**) in reactivating inspiratory rhythm is strongly dose dependent. Note that 1 μ M DHPG and 0.5 nM TRH evoke a rhythm similar to that observed in control solution. The bars represent means \pm SEM; values indicate the number of preparations tested.

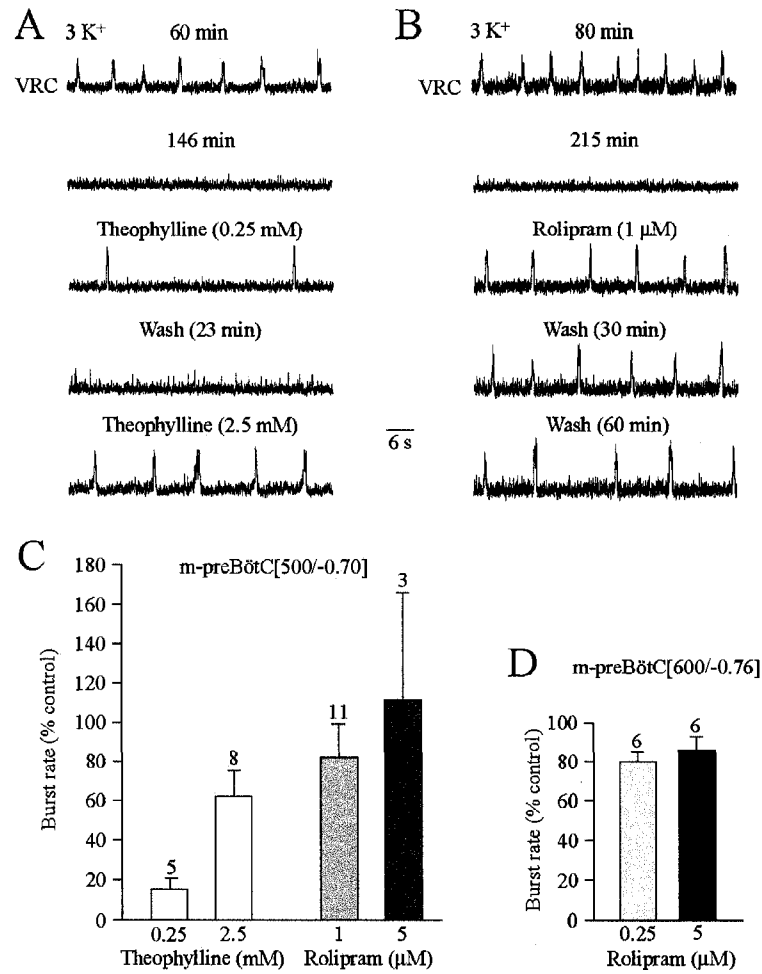


Figure 2-10 Reversal of in vitro apnea by cAMP-elevating phosphodiesterase-4 blockers. **A**, After spontaneous arrest of inspiratory bursting in an m-preBötC[500/-0.68]SD-P0.5 slice after 146 min, a low-frequency rhythm was evoked by the nonspecific blocker of cAMP-specific phosphodiesterase-4, theophylline. A 10-fold increase in theophylline concentration to 2.5 mM raised frequency ~2.5-fold. **B**, The specific phosphodiesterase-4 blocker rolipram reactivated rhythm in an m-preBötC [500/-0.63]W-P2 slice. The stimulating action of rolipram persisted for >1 h after washout. **C**, Histograms summarizing the dose-dependent stimulatory effects of theophylline and rolipram on quiescent m-preBötC[500/-0.70] slices. **D**, Histogram summarizing effects of rolipram on quiescent m-preBötC[600/-0.76] slices. Note that nanomolar concentrations of rolipram reactivate rhythm at rates similar to controls. The bars represent means ± SEM; values indicate the number of slices.

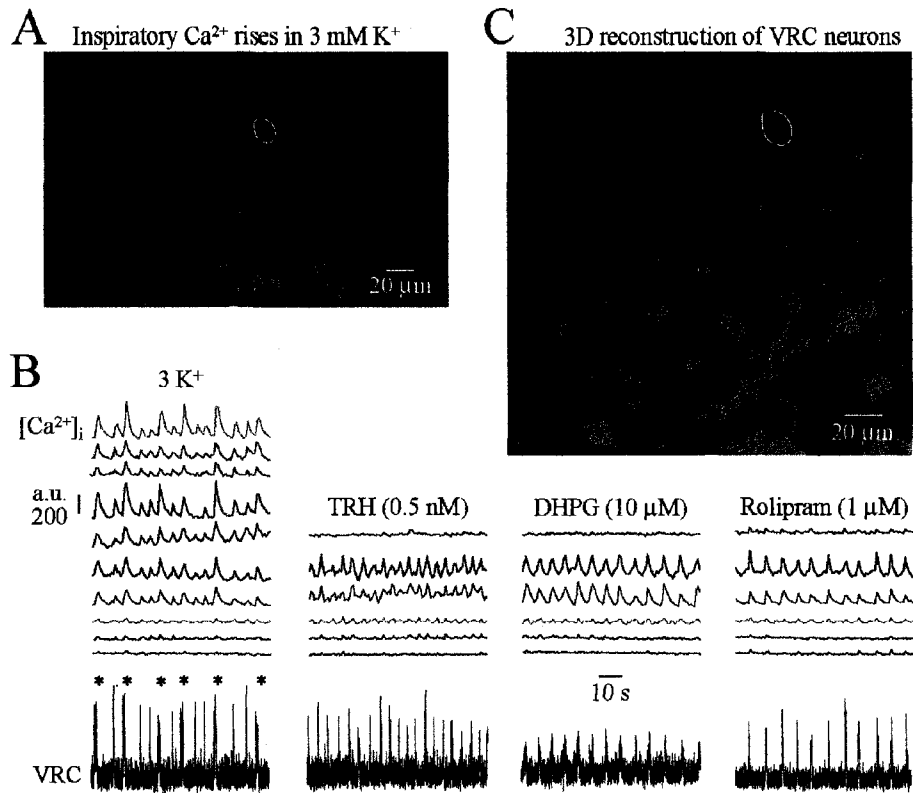


Figure 2-11 Confocal imaging of activity and morphology of inspiratory VRC neurons. **A**, Cells in the VRC region of m-preBötC[500/-0.75] W-P3 slice stained after pressure injection with the Ca^{2+} -sensitive dye fluo-4-AM. Cells showing inspiratory-related increases of fluo-4 fluorescence, outlined as regions of interest, were located at a depth of 30 μm (i.e., -0.72 mm caudal to VII_c). **B**, Eighty second simultaneous recordings in 3 mM K^{+} of rhythmic Ca^{2+} oscillations plotted as fluorescence intensity in arbitrary units (a.u.) in identified VRC neurons in **A** and electrophysiological population activity in the contralateral VRC (bottom trace). Note that fluorescence increases were consistently larger during intermingled (I-bursts; asterisk) compared with single (S)-bursts; compare Figures 2-5, 2-6). After washout of rhythm in 3 mM K^{+} , VRC bursting and Ca^{2+} oscillations were consecutively reactivated by TRH, DHPG, or rolipram. Note that cells represented by the top four traces in the left panel were not monitored during drug application because of a minor shift in focal plane over time. **C**, 3D reconstruction showing gross morphology of VRC inspiratory neurons and nonrhythmic cells obtained from z-stack (0.5 μm single step) image series encompassing areas starting 7.5 μm above to 7.5 μm below the image plane of **A**.

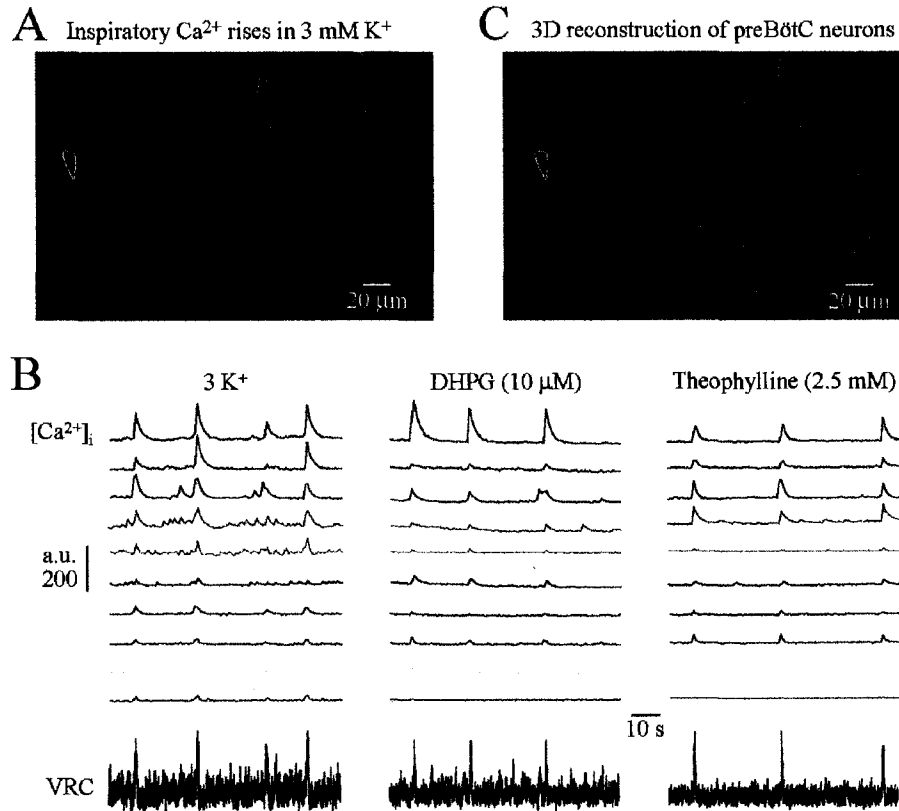


Figure 2-12 Confocal imaging of activity and morphology of inspiratory preBötC neurons. **A**, Fluo-4-AM-stained preBötC neurons outlined by regions of interest at -0.59 in an m-preBötC[500/-0.64] W-P1.5 slice. **B**, Fluo-4-AM fluorescence intensity is plotted in arbitrary units (a.u.) against time. After washout of rhythm in 3 mM K^+ , preBötC bursting and Ca^{2+} oscillations were reactivated by DHPG and theophylline. **C**, 3D reconstruction showing gross morphology of preBötC neurons and neighboring nonrhythmic cells obtained from z-stack image series (0.5 μm single step) encompassing areas starting 7.5 μm above to 7.5 μm below image plane of **A**.

2.6 References

- Alheid GF, Milsom WK, McCrimmon DR (2004) Pontine influences on breathing: an overview. *Respir Physiol Neurobiol* 143, 105-114.
- Ballanyi K (2004) Neuromodulation of the perinatal respiratory network. *Curr Neuropharmacol* 2, 221-243.
- Ballanyi K, Onimaru H, Homma I (1999) Respiratory network function in the isolated brainstem-spinal cord of newborn rats. *Prog Neurobiol* 59, 583-634.
- Ballanyi K, Lalley PM, Hoch B, Richter DW (1997) cAMP-dependent reversal of opioid- and prostaglandin-mediated depression of the isolated respiratory network in newborn rats. *J Physiol (Lond)* 504, 127-134.
- Barad M (2003) Later developments: molecular keys to age-related memory impairment. *Alzheimer Dis Assoc Disord* 17, 168-176.
- Bennet L, Gluckman PD, Johnston BM (1988) The central effects of thyrotropin-releasing hormone on the breathing movements and electrocortical activity of the fetal sheep. *Pediatr Res* 23, 72-75.
- Bongianni F, Mutolo D, Carfi M, Pantaleo T (2002) Group I and II metabotropic glutamate receptors modulate respiratory activity in the lamprey. *Eur J Neurosci* 16, 454-460.
- Browning KN, Travagli RA (2001) The peptide TRH uncovers the presence of presynaptic 5-HT_{1A} receptors via activation of a second messenger pathway in the rat dorsal vagal complex. *J Physiol (Lond)* 531, 425-435.
- Chen X, Talley EM, Patel N, Gomis A, McIntire WE, Dong B, Viana F, Garrison JC, Bayliss DA (2006) Inhibition of a background potassium channel by G_q protein alpha-subunits. *Proc Natl Acad Sci USA* 103, 3422-3427.
- Conn PJ, Pin JP (1997) Pharmacology and functions of metabotropic glutamate receptors. *Annu Rev Pharmacol Toxicol* 37, 205-237.
- Dal Piaz V, Giovannoni MP (2000) Phosphodiesterase 4 inhibitors, structurally unrelated to rolipram, as promising agents for the treatment of asthma and other pathologies. *Eur J Med Chem* 35, 463-480.

- Dong XW, Feldman JL (1999) Distinct subtypes of metabotropic glutamate receptors mediate differential actions on excitability of spinal respiratory motoneurons. *J Neurosci* 19, 5173-5184.
- Feldman JL, Del Negro CA (2006) Looking for inspiration: new perspectives on respiratory rhythm. *Nat Rev Neurosci* 7, 232-242.
- Feldman JL, Mitchell GS, Nattie EE (2003) Breathing: rhythmicity, plasticity, chemosensitivity. *Annu Rev Neurosci* 26, 239-266.
- Frermann D, Keller BU, Richter DW (1999) Calcium oscillations in rhythmically active respiratory neurones in the brainstem of the mouse. *J Physiol (Lond)* 515, 119-131.
- Funk GD, Smith JC, Feldman JL (1994) Development of thyrotropin-releasing hormone and norepinephrine potentiation of inspiratory-related hypoglossal motoneuron discharge in neonatal and juvenile mice in vitro. *J Neurophysiol* 72, 2538-2541.
- Funk GD, Smith JC, Feldman JL (1993) Generation and transmission of respiratory oscillations in medullary slices: role of excitatory amino acids. *J Neurophysiol* 70, 1497-1515.
- Gray PA, Janczewski WA, Mellen N, McCrimmon DR, Feldman JL (2001) Normal breathing requires preBotzinger complex neurokinin-1 receptor-expressing neurons. *Nat Neurosci* 4, 927-930.
- Gray PA, Rekling JC, Bocchiaro CM, Feldman JL (1999) Modulation of respiratory frequency by peptidergic input to rhythmogenic neurons in the preBotzinger complex. *Science* 286, 1566-1568.
- Guyenet PG, Stornetta RL, Weston MC, McQuiston T, Simmons JR (2004) Detection of amino acid and peptide transmitters in physiologically identified brainstem cardiorespiratory neurons. *Auton Neurosci* 114, 1-10.
- Hedner J, Hedner T, Wessberg P, Lundberg D, Jonason J (1983) Effects of TRH and TRH analogues on the central regulation of breathing in the rat. *Acta Physiol Scand* 117, 427-437.
- Johnson SM, Smith JC, Funk GD, Feldman JL (1994) Pacemaker behavior of respiratory neurons in medullary slices from neonatal rat. *J Neurophysiol* 72, 2598-2608.

- Kawai A, Onimaru H, Homma I (2006) Mechanisms of CO₂/H⁺ chemoreception by respiratory rhythm generator neurons in the medulla from newborn rats in vitro. *J Physiol (Lond)* 572, 525-537.
- Koshiya N, Smith JC (1999) Neuronal pacemaker for breathing visualized in vitro. *Nature* 400, 360-363.
- Li YX, Tokuyama W, Okuno H, Miyashita Y, Hashimoto T (2001) Differential induction of brain-derived neurotrophic factor mRNA in rat inferior olive subregions following unilateral labyrinthectomy. *Neuroscience* 106, 385-394.
- Lieske SP, Thoby-Brisson M, Telgkamp P, Ramirez JM (2000) Reconfiguration of the neural network controlling multiple breathing patterns: eupnea, sighs and gasps. *Nat Neurosci* 3, 600-607.
- Manzke T, Guenther U, Ponimaskin EG, Haller M, Dutschmann M, Schwarzacher S, Richter DW (2003) 5-HT_{4(a)} receptors avert opioid-induced breathing depression without loss of analgesia. *Science* 301, 226-229.
- Mironov SL, Richter DW (1998) L-type Ca²⁺ channels in inspiratory neurones of mice and their modulation by hypoxia. *J Physiol (Lond)* 512, 75-87.
- Morgado-Valle C, Feldman JL (2004) Depletion of SP and glutamate by capsaicin blocks respiratory rhythm in neonatal rat in vitro. *J Physiol (Lond)* 555, 783-792.
- Mulkey DK, Stornetta RL, Weston MC, Simmons JR, Parker A, Bayliss DA, Guyenet PG (2004) Respiratory control by ventral surface chemoreceptor neurons in rats. *Nat Neurosci* 7, 1360-1369.
- Nikolenko V, Nemet B, Yuste R (2003) A two-photon and second-harmonic microscope. *Methods* 30, 3-15.
- Nikulina E, Tidwell JL, Dai HN, Bregman BS, Filbin MT (2004) The phosphodiesterase inhibitor rolipram delivered after a spinal cord lesion promotes axonal regeneration and functional recovery. *Proc Natl Acad Sci USA* 101, 8786-8790.
- Nilni EA, Aird F, Seidah NG, Todd RB, Koenig JI (2001) PreproTRH(178-199) and two novel peptides (pFQ7 and pSE14) derived from its processing, which are produced in the paraventricular nucleus of the rat hypothalamus, are regulated during suckling. *Endocrinology* 142, 896-906.

- Nistri A, Ostroumov K, Sharifullina E, Taccola G (2006) Tuning and playing a motor rhythm: how metabotropic glutamate receptors orchestrate generation of motor patterns in the mammalian central nervous system. *J Physiol (Lond)* 572, 323-334.
- O'Donnell JM, Zhang HT (2004) Antidepressant effects of inhibitors of cAMP phosphodiesterase (PDE4). *Trends Pharmacol Sci* 25, 158-163.
- Onimaru H, Ballanyi K, Homma I (2003) Contribution of Ca²⁺-dependent conductances to membrane potential fluctuations of medullary respiratory neurons of newborn rats in vitro. *J Physiol (Lond)* 552, 727-741.
- Onimaru H, Homma I (2003) A novel functional neuron group for respiratory rhythm generation in the ventral medulla. *J Neurosci* 23, 1478-1486.
- Onimaru H, Ballanyi K, Richter DW (1996) Calcium-dependent responses in neurons of the isolated respiratory network of newborn rats. *J Physiol (Lond)* 491, 677-695.
- Pagliardini S, Adachi T, Ren J, Funk GD, Greer JJ (2005) Fluorescent tagging of rhythmically active respiratory neurons within the pre-Botzinger complex of rat medullary slice preparations. *J Neurosci* 25, 2591-2596.
- Pena F, Ramirez JM (2004) SP-mediated modulation of pacemaker properties in the mammalian respiratory network. *J Neurosci* 24, 7549-7556.
- Rekling JC, Champagnat J, Denavit-Saubie M (1996) Thyrotropin-releasing hormone (TRH) depolarizes a subset of inspiratory neurons in the newborn mouse brain stem in vitro. *J Neurophysiol* 75, 811-819.
- Richter DW, Spyer KM (2001) Studying rhythmogenesis of breathing: comparison of in vivo and in vitro models. *Trends Neurosci* 24, 464-472.
- Richter DW, Lalley PM, Pierrefiche O, Haji A, Bischoff AM, Wilken B, Hanefeld V (1997) Intracellular signal pathways controlling respiratory neurons. *Respir Physiol* 110, 113-123.
- Richter DW, Ballanyi K, Schwarzacher S (1992) Mechanisms of respiratory rhythm generation. *Curr Opin Neurobiol* 2, 788-793.
- Ruangkittisakul A, Ballanyi K (2006) Reversal by phosphodiesterase-4 blockers of in vitro apnea in the isolated brainstem-spinal cord preparation from newborn rats. *Neurosci Lett* 401, 194-198.

- Schwarzacher SW, Pestean A, Gunther S, Ballanyi K (2002) Serotonergic modulation of respiratory motoneurons and interneurons in brainstem slices of perinatal rats. *Neuroscience* 115, 1247-1259.
- Schwarzacher SW, Smith JC, Richter DW (1995) Pre-Botzinger complex in the cat. *J Neurophysiol* 73, 1452-1461.
- Shvarev YN, Lagercrantz H, Yamamoto Y (2003) Two types of rhythm in the respiratory network output in the isolated ventrolateral medulla in the neonatal rats. *Neurosci Lett* 347, 53-56.
- Smith JC, Butera RJ, Koshiya N, Del Negro C, Wilson CG, Johnson SM (2000) Respiratory rhythm generation in neonatal and adult mammals: the hybrid pacemaker-network model. *Respir Physiol* 122, 131-147.
- Smith JC, Ellenberger HH, Ballanyi K, Richter DW, Feldman JL (1991) Pre-Bötzing complex: a brainstem region that may generate respiratory rhythm in mammals. *Science* 254, 726-729.
- Somjen GG (2002) Ion regulation in the brain: implications for pathophysiology. *Neuroscientist* 8, 254-267.
- Stosiek C, Garaschuk O, Holthoff K, Konnerth A (2003) In vivo two-photon calcium imaging of neuronal networks. *Proc Natl Acad Sci USA* 100, 7319-7324.
- Thoby-Brisson M, Trinh JB, Champagnat J, Fortin G (2005) Emergence of the pre-Botzinger respiratory rhythm generator in the mouse embryo. *J Neurosci* 25, 4307-4318.
- Töpert C, Doring F, Wischmeyer E, Karschin C, Brockhaus J, Ballanyi K, Derst C, Karschin A (1998) Kir2.4: a novel K⁺ inward rectifier channel associated with motoneurons of cranial nerve nuclei. *J Neurosci* 18, 4096-4105.
- Yuste R, Konnerth A, Masters BR (2006) Imaging in neuroscience and development, a laboratory manual. *J Biomed Opt* 11, 19902.

***CHAPTER III**

Generation of Eupnea and Sighs by a Spatiochemically Organized Inspiratory Network

* Previously published paper:

Ruangkittisakul A, Schwarzacher SW, Secchia L, Ma Y, Boboccea N, Poon BY, Funk GD, Ballanyi K (2008) Generation of eupnea and sighs by a spatiochemically organized inspiratory network. *J Neurosci* 28, 2447-2458. Copyright 2008 by the Society for Neuroscience. My contribution to this study consisted in the execution of >70% of both the electrophysiological and Ca²⁺ imaging experiments and 100% of the corresponding analyses. In addition, I performed histological treatment, i.e., fixation, staining, slicing and generation of digital images of >80% of brainstem slices. Lastly, I did ~50% of the histological analysis of slice boundaries.

3.1 Introduction

The pre-Bötzinger complex (preBötC) contains neurons that are necessary for generating inspiratory-related rhythm and remain active in a transverse brainstem slice from perinatal rodents (Smith et al., 1991). Since its first description, numerous *in vitro* and *in vivo* reports support the hypothesis that the preBötC is a pivotal rhythmogenic inspiratory network (Ramirez et al., 2002; Feldman & Del Negro, 2006). Despite the importance of the preBötC discovery for the understanding of neural respiratory control, fundamental questions remain unanswered. For example, the rostrocaudal boundaries of regions necessary and sufficient for generation of inspiratory-related behaviors in preBötC slices have not been defined. Furthermore, it is proposed that the preBötC can reconfigure between distinct inspiratory-related patterns, including fictive eupnea- or sigh-like activities, in slices >500 μm thick (Lieske & Ramirez, 2006a,b; Tryba et al., 2006). It is not known whether the preBötC retains its capacity for reconfiguration when isolated in a thinner slice. Alternatively, the reconfiguration may be driven by more rostral or caudal structures. Specifically, the preBötC is neighbored and presumably influenced by other respiratory groups, such as the parafacial respiratory group/retrotrapezoid nucleus complex (Onimaru & Homma, 2003; Mulkey et al., 2004) and nonrespiratory modulatory areas such as the raphe (Richerson, 2004; Feldman & Del Negro, 2006). If the presumptive capability of the preBötC to generate different inspiratory-related behaviors depends on input from rostrocaudally neighboring structures, it is possible that slices lacking these structures cannot produce such activities. Here, we tested this hypothesis and also assessed basic features of inspiratory-related activity such as burst rates and longevity of rhythm in solution of physiological (3 mM) K^+ in slices with systematically varied boundaries and thickness using “on-line histology” (Ruangkittisakul et al., 2006).

We found that the minimal preBötC slice thickness that is sufficient for generation of inspiratory rhythm is 175 μm , whereas a kernel of rhythmogenic tissue <100 μm appears to be necessary for bursting in 700 μm slices with the preBötC exposed to one surface. The latter slices generated fictive eupnea bursts with regular amplitude and frequency when the preBötC was isolated with caudal tissue. Conversely, fictive sighs intermingled

with rhythmic activity of variable amplitude, but burst duration typical for eupnea, were generated in 700 μm slices containing the preBötC plus rostral tissue. In these preparations, and in 250-500 μm slices with the preBötC in the center, thyrotropin-releasing hormone (TRH) and cAMP-dependent phosphodiesterase-4 blockers induced the eupnea burst pattern after spontaneous arrest of rhythm (“in vitro apnea”), whereas substance-P (SP) and neurokinin-1 (NK1) receptor agonist evoked the eupnea-sigh burst pattern. Multicellular Ca^{2+} imaging revealed that preBötC neurons active during eupnea are active also during the eupnea-sigh burst pattern. This supports the previous hypothesis that these behaviors derive from preBötC reconfiguration (Lieske et al., 2000).

We hypothesize that a small rhythmogenic preBötC kernel can reconfigure to produce either a eupnea or a eupnea-sigh inspiratory-related burst pattern in physiological $[\text{K}^+]$. The former emerges when the influence of caudal structures or TRH-like transmitters is dominant, whereas the latter emerges when the influence of rostral structures or SP-like transmitters is dominant.

3.2 Material and Methods

3.2.1 Preparation and Solutions

Experiments were performed on brainstem slices from Sprague Dawley (SD) and Wistar (W) rats between postnatal day 0 (P0) and P4. All procedures were performed in compliance with the guidelines of the Canadian Council for Animal Care and with the approval of the University of Alberta Health Animal Care and Use Committee for Health Sciences. Rats were anesthetized with isoflurane until the paw withdrawal reflex disappeared. They were then decerebrated, and the neuraxis was isolated at 19-22°C in superfusate containing (in mM) 120 NaCl, 3 KCl, 1 CaCl_2 , 2 MgSO_4 , 26 NaHCO_3 , 1.25 NaH_2PO_4 , and 20 D-glucose, pH adjusted to 7.4 by gassing with 95% O_2 , 5% CO_2 . For some experiments, superfusate K^+ was increased by the addition of KCl. After removal of the cerebellum and transection slightly rostral to the caudal cerebellar artery and just rostral to the C_1 spinal segment (Figure 3-1A), the brainstem was glued rostral side down to a metal plate, and preBötC slices with defined boundaries were generated using on-line

histology (Ruangkittisakul et al., 2006) (Figure 3-1B). Serial sections were made with a Vibratome (VT1000S; Leica, Richmond Hill, Ontario, Canada) in the caudorostral direction starting at the caudal end of the inferior olive. Section thickness was reduced to 100 μm when approaching the level for generating a rhythmic slice as evidenced by respiratory marker structures, in particular the subnuclei of the inferior olive. These structures in the prerhythmic slices were compared with a newborn rat brainstem atlas to predetermine, on-line, the rostrocaudal position of the prospective rhythmic slice (Ruangkittisakul et al., 2006). When necessary, the thickness of the last prerhythmic slice was $<100 \mu\text{m}$ to produce a rhythmic slice with a specific boundary. For “off-line” analysis of slice boundaries, prerhythmic and postrhythmic “frame” sections were fixed (see below, Agents) and stained with thionin (Figure 3-1B).

Boundaries determined previously via surface values in 500 μm thick slices with the preBötC in the middle (m-preBötC[500] slices) were very similar to targeted values, although a 50-100 μm gap between the rhythmic slices and the adjacent frame sections had to be taken into account (Ruangkittisakul et al., 2006). Here, boundaries of $<300\text{-}\mu\text{m}$ -thin m-preBötC slices according to the determination of surface structures were 25-50% smaller than tissue thickness. The physical thickness of 200- μm -thin sectioned agar blocks or living slices cut in superfusate indicated that the error of vibratome cutting was $<8\%$. Thus, the mean values between slice surface and frame were used instead of the slice surface value alone to identify the boundaries in $<300 \mu\text{m}$ thick slices. In addition to m-preBötC slices of 175-700 μm thickness, 700 μm thick slices containing either “rostral” brainstem tissue plus the preBötC (r+preBötC slices) or “caudal” tissue plus the preBötC (c+preBötC slices) were used. The complete label for slices included two numbers; the first indicates their thickness, and the second indicates the individual or mean distance from the caudal margin of the facial (VII) motor nucleus (VII_c). A negative sign represents the location caudal to VII_c of the caudal slice boundary. However, for c+preBötC slices, the value reported is the distance from their rostral boundary to VII_c (Figure 3-1). The final components of the label refer to rat strain and age. Thus, a 500 μm thick slice from a P3 W rat with the preBötC in the middle and a caudal surface 0.71 mm caudal to VII_c was labeled m-preBötC[500/-0.71]W-P3. Rhythmic slices were

immediately fixed caudal side up (except c+preBötC slices) with insect pins on the silicone layer covering the bottom of the recording chamber (volume, 1.5 ml). Superfusate was administered at a flow rate of 5 ml/min via a peristaltic pump (Watson-Marlow Alitea-AB; Sin-Can, Calgary, Alberta, Canada). Superfusate temperature in the recording chamber was 25-27°C (TC-324B; Harvard Apparatus, Saint-Laurent, Quebec, Canada).

3.2.2 Agents

Drugs and solutions included the following: TRH (0.5-100 nM; stocks, 1 µM and 1 mM in H₂O), GR82334 (2.5 µM; stock, 1 mM in H₂O), GR73632 (2.5-10 nM; stock, 1 mM in H₂O), SP (25-100 nM; stock, 1 mM in dimethylsulfoxide), rolipram (1 µM; stock, 1 mM in dimethylsulfoxide), theophylline (2.5 mM; added to superfusate), fluo-4-AM (0.5 mM; stock, 5 mM in dimethylsulfoxide with 20% pluronic acid), agar-agar (6% in H₂O), 4% paraformaldehyde fixation solution in phosphate buffer (1:2 mixture of 0.1 M NaH₂PO₄ plus 0.1 M Na₂HPO₄ in H₂O, pH 7.2), and staining solution (1% thionin acetate in 0.1 M sodium acetate trihydrate plus 0.1 M acetic acid). Agents were obtained from Sigma-Aldrich (Oakville, Ontario, Canada), except salts for the superfusate, sodium acetate trihydrate, and acetic acid (Fisher Scientific, Ottawa, Ontario, Canada); theophylline and glutamate (ICN Biomedicals, Costa Mesa, CA); fluo-4-AM (TEFLabs, Austin, TX); and GR82334 and GR73632 (Tocris Biosciences, Ellisville, MO).

3.2.3 Histological Procedures

For staining, frame sections were sequentially incubated (after >15 min of fixation) in phosphate buffer (2 min), thionin solution (45 s), phosphate buffer (2 min), 50% ethanol (4 min), and finally, phosphate buffer (2 min). Sections were then transferred on a hanging drop glass slide (Fisher Scientific) to a microscope (Standard 16; magnification, 32x; Zeiss, Jena, Germany) and photographed (PL-A642-1.3 Megapixel; PixelINK, Ottawa, Ontario, Canada). After the experiments, rhythmic slices were fixed overnight and stained using the same procedure, except these thicker slices were immersed in thionin for 90 s. Stained rhythmic slices were photographed (PL-A686-6.6 Megapixel; PixelINK) in phosphate buffer under a stereo microscope (Zeiss SR15; magnification, 32x) (Figure 3-1B).

3.2.4 Electrophysiological Recording

Neuronal population activities were differentially recorded (DAM 50; WPI, Sarasota, FL) via suction electrodes (outer diameter, 80-250 μm) filled with superfusate. Electrodes were positioned in the ventrolateral regions of the slices (Appendix II, Figures A2-1, A2-2) for (simultaneous) monitoring of bursting within the bilaterally organized ventral respiratory column that includes the preBötC (Alheid et al., 2004). Signals were amplified (10,000 times), bandpass filtered (0.3-3 kHz), integrated, and digitally recorded at a sampling rate of 1-4 kHz (Powerlab/8SP; ADInstruments, Colorado Springs, CO).

3.2.5 Multiphoton/Confocal Ca²⁺ Imaging

The activity of multiple preBötC neurons was simultaneously assessed with Ca²⁺ imaging (Ruangkittisakul et al., 2006). The membrane-permeant, Ca²⁺-sensitive dye fluo-4-AM was backfilled into a broken (5-10 μm outer diameter) patch pipette and pressure injected (0.7-1.0 psi, 10 min) into the preBötC while inspiratory rhythm was monitored electrophysiologically from the contralateral preBötC. Fluorescence signals were assessed with a confocal microscope (Olympus FV300, Fluoview software; Carsten Group, Markham, Ontario, Canada) or a FV300 connected to a Ti:Sa laser (Coherent, Santa Clara, CA) for multiphoton imaging. Ca²⁺ oscillations, cell bodies, and primary dendrites could be resolved in areas of 200-300 μm diameter at tissue depths up to 60 μm for confocal and 90 μm for multiphoton microscopy. Rhythmic Ca²⁺ rises were visualized as increases in fluo-4-AM fluorescence intensity in up to 15 cells (typically 3-8 cells) per single xy-image plane. Stained regions were monitored using a 2-3 \times digital zoom at reduced settings for y-axis scanning. Compared with full-frame acquisition (512 \times 512 pixels), such “clipped mode” imaging sampled an area of 512 \times 100-220 pixels and provided scan rates of 1.25-1.43 scans/s, sufficient to detect 70-100% of the peak of inspiratory-related Ca²⁺ rises, as determined empirically.

3.2.6 Data Analysis

The inspiratory burst rate was averaged every 20 min over 2 min time windows. The “longevity” of inspiratory rhythms was defined as the time from start of the continuous recording until the time when the period between consecutive bursts exceeded 5 min. The

rise time of bursts was defined using ClampFit software (Molecular Devices, Chicago, IL) as the time interval from when the signal increased above a threshold set at 10-100% of the peak amplitude for that burst. Burst duration, defined as the time period from when the signal exceeded to the point when it fell below the 50% value of the peak amplitude (“half-width”), and rate were analyzed at both 20 and 80 min after the start of recording (see above) by averaging >10 consecutive bursts (except for sighs, in which at least three events were averaged). Irregularity scores for burst amplitudes were determined for each cycle using the formula $S_n = 100 \times \text{ABS}(X_n - X_{n-1})/X_{n-1}$, where S_n is the irregularity score for the n^{th} cycle, ABS is the absolute value, and X_n and X_{n-1} are peak amplitude of the n^{th} cycle and the previous cycle, respectively. Frequency irregularity scores were assessed by the same formula with X representing the time interval between bursts. For the determination of signal-to-noise ratios, the peak amplitude of an inspiratory burst was normalized to the thickness of the trace of suction electrode recording in the absence of rhythmic bursting. Pharmacologically reactivated rhythms were described by averaging burst rates over a 2 min time period at steady state (i.e., when drug had evoked a maximal and stable effect). Values are means \pm SEM, except for histology (means \pm SD). Significance (*p <0.05; **p <0.01) was determined with Student’s t tests using SigmaPlot (Systat Software, Point Richmond, CA).

3.2.7 Anatomical Preconditions for Determination of Necessary and Sufficient preBötC Boundaries.

The original report on the discovery of the preBötC estimated that its rostrocaudal extension necessary for the generation of inspiratory rhythm spans 225 μm (Smith et al., 1991). This value was derived based on regions necessary for the generation of inspiratory-related nerve bursts that were common to rhythmic newborn rat brainstem-spinal cord preparations serially sectioned in either rostrocaudal or caudorostral directions (Smith et al., 1991). Based on the analysis of 15 fixed brainstems, we have recently produced a brainstem atlas for neonatal P0-P4 SD and W rats (Ruangkittisakul et al., 2006), thereby covering the age range most commonly used for preBötC slices from this species (Smith et al., 1991; Funk et al., 1993; Reklings & Feldman, 1998). In our previous study, the relative positions of respiratory brainstem marker nuclei were plotted in a

sagittal plane in relation to the preBötC, the center of which was hypothesized to be located 0.5 mm caudal to VII_c. Here, we analyzed an additional 11 unfixed brainstems kept during slicing (100 μ m sections) in the same type of saline used to study preBötC slice functions. The mean values \pm SD of the extensions of respiratory marker nuclei in these preparations were identical to those of the fixed brainstems showing that fixation artifacts were minimal for the generation of the reference atlas. The mean values \pm SD of the rostrocaudal extensions of marker nuclei in all 26 preparations were reported in relation to VII_c and projected on the ventral brainstem surface to show the anatomical content and borders, referred to VII_c, of the different types of preBötC slices with systematically varied boundaries and/or thicknesses (Figure 3-1A). Specifically, these were 175- to 700 μ m thick m-preBötC, r+preBötC[700], and c+preBötC[700] slices. These slices were generated with on-line histology, and their boundaries were determined after fixation and thionin staining after the experiments (Figure 3-1B).

3.2.8 Criteria for Identification and Classification of Inspiratory-Related Bursting.

In the present study, we determined the rostrocaudal preBötC boundaries that are necessary and sufficient for the generation of inspiratory-related behaviors in 3 mM K⁺ solution in brainstem slices with systematically varied boundaries and/or thickness (Figure 3-1). We also tested the hypothesis that the capability of the preBötC to generate distinct inspiratory-related behaviors is differentially influenced by input from rostrocaudally neighboring structures. Before this, the baseline inspiratory burst behavior (e.g., duration, rise time) of “reference” slices with an undisturbed preBötC was established to facilitate comparison of burst parameters with those generated by the novel slices with exposed (and reduced) preBötC. These 500 and 700 μ m thick m-preBötC slices generated three types of inspiratory activities in oxygenated 3 mM K⁺ solution [(1) “eupnea (bursts),” (2) “sigh (bursts),” and (3) “biphasic bursts”, as reported for newborn mouse or rat slices (Lieske et al., 2000; Ruangkittisakul et al., 2006) or newborn rat brainstem-spinal cords (Shvarev et al., 2003). The burst patterns comprised either a uniform eupnea burst pattern or a pattern in which eupneic bursts were intermingled with either sighs (“eupnea-sigh burst pattern”) or biphasic bursts (“eupnea-biphasic burst pattern”).

Properties that discriminate these different burst patterns are described in the Appendix II. In brief, a burst was counted as a sigh compared with eupneic bursts in the same slice if it had (1) a greater amplitude, (2) a longer duration, (3) a longer rise time, and (4) postsigh inhibition (of burst rate and/or amplitude). Conversely, a burst was counted as a biphasic burst if, compared with eupneic bursts in the same slice, it had (1) a longer duration and (2) a secondary peak that was similar in amplitude to the first peak.

3.3 Results

The rostrocaudal preBötC boundaries that are sufficient and necessary for the generation of inspiratory-related behaviors in 3 mM K^+ were determined in preBötC slices by systematically varying their boundaries and/or thickness (Figure 3-1). This approach included the analysis of whether distinct inspiratory-related burst patterns including fictive eupnea and sighs depend on slice dimensions. In addition, multiphoton/confocal Ca^{2+} imaging was used to test the previous hypothesis that the preBötC reconfigures between distinct inspiratory-related burst patterns.

3.3.1 Slice Thickness Sufficient for Inspiratory-Related Rhythm in 3 mM K^+

First, we tested whether 250 μm or thinner m-preBötC slices generate inspiratory rhythm in 3 mM K^+ . In eight m-preBötC[250/-0.65] slices, rhythmic bursts had maximal amplitudes in the typical ventrolateral respiratory surface region (Figure A2-2), and rhythm lasted 99 ± 14 min (Figure 3-2A). In contrast, rhythmic bursting was seen neither in this “hot spot” nor surrounding regions in six other 250 μm slices with borders deviating ≥ 100 μm from the mean margin of the rhythmic slices (Figure 3-2A). Similar bursting was seen for 103 ± 13 min exclusively in the same respiratory region of six m-preBötC[200/-0.63] slices (Figures 3-2A, A2-2). Also, two m-preBötC[175] slices showed rhythmic bursting in the respiratory hot spot, in contrast to lack of rhythmic bursting in this or surrounding regions in five other 175 μm slices with similar boundaries (Figures 3-2A). The most typical bursts in the m-preBötC[250] slices had a rather uniform amplitude with a good signal-to-noise ratio (4.2 ± 0.5 ; $n = 4$) (Figures 3-2B,C,D, A2-4).

In >50% of these slices, the maximal amplitude and rate of such bursts developed over a time period of 20 min after the start of recording. At this time, the rate of these bursts was 4.3 ± 0.7 bursts/min ($n = 4$) and remained constant for the next hour (2.7 ± 0.8 bursts/min at 80 min) (Figures 3-2B, A2-5). In six of the eight m-preBötC[250] slices, 2-15 bursts with a smaller and variable amplitude occurred in the interval between the robust bursts at a rate of 8.0 ± 2.2 bursts/min ($n = 4$) at 20 min of recording (Figures 3-2C,D). Compared with the large-amplitude bursts, the bursts with variable amplitude were significantly smaller at 20 min (Figure A2-5). At 80 min, a quantitative comparison of both burst types was not possible because of a progressive attenuation of the smaller bursts that started after >40 min and was followed by their disappearance (Figure 3-2C). The latter features resembled the eupnea-sigh burst pattern in a subgroup of 500 or 600 μm thick m-preBötC slices (Figures A2-3, A2-4). The large bursts in the m-preBötC[250] slices had a shape similar to sighs in thicker m-preBöt slices and also a significantly longer duration and rise time than the smaller bursts (Figures A2-4, A2-5). Thus, we propose that this burst pattern is a eupnea-sigh pattern. Also, the burst pattern in four of the six rhythmic m-preBötC[200] slices was characterized by sigh-like bursts with a signal-to-noise ratio of 2.7 ± 0.4 ($n = 4$) that were intermingled with 2-15 eupneic bursts of significantly smaller amplitude and duration (Figure 3-2E, A2-4). As in the 250 μm thin slices, it took up to 20 min until the amplitude and rate of the sighs were maximal, whereas the eupneic bursts started to decrease progressively in amplitude after time periods >40 min. The rate of eupneic bursts at 20 min was 7.4 ± 2.6 bursts/min ($n = 4$) compared with a sigh rate of 3.6 ± 0.8 bursts/min ($n = 4$) that did not change in the next hour (5.6 ± 2.0 bursts/min) (Figure A2-5). The other two m-preBötC[200] slices and two of the eight m-preBötC[250] slices showed rhythmic activity consisting primarily of sighs (Figure 3-2B,E). In all eight m-preBötC[250] and 50% of m-preBötC[200] slices, all sighs and most eupneic bursts were bilaterally synchronous, at least at 20-50 min (Figure 3-2B-E). Asynchronous bilateral activity was seen in the remaining m-preBötC[200] slices.

After onset of in vitro apnea, 6 mM K^+ restored in all m-preBötC[250] slices bilaterally synchronous bursting resembling the original pattern (Figure 3-2B,C). In three of these slices, the addition to 3 mM K^+ solution of the clinical respiratory stimulant theophylline

(2.5 mM) (Bhatia, 2000) resulted in a eupnea burst pattern. Application of TRH (1-100 nM) and rolipram (1 μ M) in 3 mM K^+ during in vitro apnea also evoked a eupnea burst pattern, whereas SP (25-100 nM) or the NK1 receptor agonist GR73632 (2.5-10 nM) elicited bursting with a eupnea-sigh pattern similar to m-preBötC[500] slices (Figures 3-2B,C,D, 3-3). Also, in all m-preBötC[200] slices, 6 mM K^+ restored bilaterally synchronous rhythm, the burst amplitude and rate of which were further enhanced and transformed into a eupnea pattern by 2.5 mM theophylline (Figure 3-2E). TRH, rolipram, or SP was not tested, because the capability of 200 μ m slices to generate rhythm appeared to deteriorate after >3 h (i.e., after the test for longevity, 6 mM K^+ , and theophylline). Burst parameters were not quantified in the two active m-preBötC[175] slices because the signal-to-noise ratio was too low (<1.5) and bursting was quite irregular in 3 mM K^+ . These slices showed rhythmic activity for 33 and 38 min with a maximal rate of 4.0 and 2.8 bursts/min, respectively. One slice showed bilaterally nonsynchronous bursts, whereas the other generated only unilateral activity. During in vitro apnea, 6 mM K^+ (plus 2.5 mM theophylline) increased the signal-to-noise ratio to >2 and elicited synchronous bursts in these slices.

These results showed that slices as thin as 175 μ m can generate inspiratory-related rhythm in 3 mM K^+ . The area between 0.42 and 0.59 mm caudal to VII_c, contained in these slices, is also common to rhythmic 200-250 μ m slices (Figure 3-2A). The typical burst pattern in most 200 to 250 μ m thin slices resembles the eupnea-sigh pattern in some 500 or 600 μ m thick m-preBötC slices.

3.3.2 Necessary preBötC Boundaries in 700 μ m Slices with Exposed preBötC

Next, inspiratory-related bursting in 3 mM K^+ was assessed in 700 μ m thick slices in which the preBötC was exposed, more or less, at either their rostral or caudal surface. Ten c+preBötC[700/-0.42] slices generated rhythmic bursts for 121 ± 22 min, whereas rhythm lasted 137 ± 14 min in 12 r+preBötC[700/-0.58] slices (Figure 3-4A). In both types of slices, burst amplitudes were maximal, with a good signal-to-noise ratio (>4), in the typical respiratory hot spot, even when slice boundaries were <100 μ m distant to the proposed location of the preBötC center (i.e., 0.5 mm caudal to VII_c) (Figures 3-1A, A2-

2, A2-4). In contrast, nonrhythmic slices did not show any type of phasic bursting in the ventrolateral hot spot or surrounding regions. The rostrocaudal brainstem region common to rhythmic slices of both types was $<100\ \mu\text{m}$, centered at 0.5 mm caudal to VII_c, and corresponds to the preBötC extent necessary for generation of inspiratory-related rhythm in 700 μm thick slices (Figure 3-4A).

3.3.3 Distinct Inspiratory Patterns in 700 μm Slices with Exposed preBötC

Despite similar longevities of rhythms in both types of 700 μm slices with the preBötC at one surface, their inspiratory patterns differed notably. These distinct burst patterns were analyzed in 33 r+preBötC[700] and 20 c+preBötC[700] slices with boundaries $<150\ \mu\text{m}$ distant to the center of the preBötC. Fifteen of the c+preBötC[700] slices showed a eupnea burst pattern, whereas a eupnea-biphasic burst pattern was seen in the other five slices (Figures 3-4A,B, 3-5A). In contrast, only 4 of the 33 r+preBötC[700] slices (12%) generated rhythm with either a eupnea or eupnea-biphasic burst pattern (two cases each), whereas the burst pattern included sighs in the other 29 slices (88%) (Figure 3-5A). In the latter group of slices, a stable eupnea-sigh burst pattern was seen in 21 cases (72%), whereas the rhythm consisted in the other 8 cases (28%) of a eupnea-sigh pattern with eupneic bursts of very small amplitude that disappeared in 3 cases after 30-45 min of recording (Figures 3-4A,C, 3-5A).

In six c+preBötC[700] slices with a eupnea burst pattern, the burst rate fell significantly between 20 and 80 min of recording, from 9.5 to 6.0 bursts/min, whereas amplitude increased during that time but duration and rise time did not change (Figures A2-4, A2-5). In six r+preBötC[700] slices with a eupnea-sigh burst pattern, the amplitude of eupneic bursts increased significantly between 20 and 80 min, whereas sigh amplitude remained stable (Figure A2-4). Sigh rate decreased significantly from 1.9 to 0.7 bursts/min during that time period, whereas the eupneic burst rate (5.1 bursts/min at 20 min) did not change (Figure A2-5). Both, the duration and rise time of eupneic bursts (0.36 and 0.62 s at 20 min) decreased significantly (0.18 and 0.44 s) between 20 and 80 min (Figure A2-5). Neither the duration nor rise time of sighs changed during that time period (0.56 and 0.96 s at 20 min, respectively) (Figure A2-5). Further analysis of the dependence of burst

patterns on the location of the preBötC in 700 μm thick slices revealed that r+preBötC[700] slices typically showed a major difference between the amplitudes of sighs and eupneic bursts and among eupneic bursts (Figures 3-4C, 3-5A). This difference was reflected by an irregularity score of sigh burst amplitudes that was significantly (2 times) higher between 0 and 80 min ($n = 8$) than for eupneic bursts of uniform amplitude in the c+preBötC[700] slices ($n = 8$) (Figure 3-5B). Similarly, burst rate was significantly more irregular in the r+preBötC[700] slices than in the c+preBötC[700] slices (Figure 3-5C). Also the rise time of sighs was significantly (approximately two times) longer than that of the eupneic bursts in the c+preBötC[700] slices (Figure 3-5D). After onset of in vitro apnea, TRH (0.5-100 nM) or rolipram (1 μM) evoked the eupnea burst pattern, whereas SP (25-100 nM) or NK1 receptor agonist (2.5-10 nM) elicited rhythm with the eupnea-sigh burst pattern in both slice types (Figures 3-3, 3-4B,C).

3.3.4 Effects of NK1 Receptor Antagonism on preBötC Activity

We found that NK1 receptor activation in vitro induces the eupnea-sigh burst pattern in preBötC-containing medullary slices after onset of in vitro apnea. We thus tested whether NK1 receptors contribute to the generation of endogenous rhythm in 3 mM K^+ . Bath application of the NK1 receptor antagonist GR82334 (2.5 μM) for 5-15 min abolished the endogenous rhythm within 3-12 min in three of four m-preBötC[350] slices (Figure 3-6A,B) and reduced the burst rate to 21% of control in the fourth case. Within 15-25 min after starting the washout of the antagonist, the mean burst rate recovered to 37% of control (Figure 3-6A,B). Because recording periods for this protocol lasted >1 h, the incomplete reversibility may reflect, at least in part, a time-dependent reduction in endogenous burst rate.

Also, in five of nine m-preBötC[500] slices, GR82334 blocked the 3 mM K^+ rhythm within 5-25 min after the start of the bath application. In two of these nine slices, the NK1 receptor antagonist decreased burst rates to 38 and 31% of control, whereas it had no effect in the remaining two cases. Recovery was maximal within 12-40 min after the start of washout of GR82334 but reached only 35% of control, similar to the incomplete recovery in 350 μm slices (Figure 3-6B). We thus tested whether this reflects an

incomplete reversibility of GR82334. For this purpose, rhythm with a eupnea-sigh burst pattern was induced by bath application of GR73632 (5 nM) after onset of in vitro apnea in two m-preBötC[350] and two m-preBötC[500] slices (Figure 3-6C,D). In all these slices, GR82334 (2.5 μ M) abolished bursting within 3-14 min, but burst rate recovered very close to its initial rate of 14 ± 1.2 bursts/min within 6-22 min after the washout of GR82334 in the presence of the NK1 receptor agonist (Figure 3-6D,E).

3.3.5 Ca^{2+} Imaging of Reconfiguring preBötC Neurons

Finally, we assessed with multiphoton/confocal Ca^{2+} imaging (Ruangkittisakul et al., 2006) whether both eupneic and eupnea-sigh burst patterns derive from separate or rather one reconfiguring preBötC network. In 16 r+preBötC[700] slices with the mean border 110 μ m caudal to the preBötC center, multineuronal activity was monitored during transitions from the eupnea-sigh burst pattern in 3 mM K^+ to a eupnea pattern induced during in vitro apnea by TRH (1-100 nM), rolipram (1 μ M), or theophylline (2.5 mM). Transitions in burst amplitude and rate, recorded electrophysiologically in one preBötC area, were correlated with Ca^{2+} transients in all inspiratory preBötC neurons imaged in the contralateral area 40-70 μ m below the caudal slice surface. Specifically, 88% (TRH, n = 68), 86% (rolipram, n = 36), and 86% (theophylline, n = 32) of preBötC neurons active during the endogenous eupnea-sigh burst pattern reconfigured to a eupnea pattern in response to the three agents (Figure 3-7A). The other cells did not show rhythmic Ca^{2+} rises in response to the drugs, or to subsequent application of 6 or 9 mM K^+ , indicating phototoxic cell damage (Yuste et al., 2006).

In four different r+preBötC[700] slices with their surface 50 μ m caudal to the preBötC center, GR73632 was used to reactivate a eupnea-sigh burst pattern of preBötC activity after onset of in vitro apnea. The NK1 receptor agonist induced inspiratory-related Ca^{2+} oscillations corresponding to a eupnea-sigh burst pattern in 33 of 44 preBötC neurons that showed a similar pattern of Ca^{2+} rises before in vitro apnea. The other 11 cells also did not respond subsequently to 6-9 mM K^+ , again suggesting photodamage. Importantly, after the washout of GR73632 and activation of eupnea with rolipram, Ca^{2+} oscillations of

uniform amplitude and frequency were evoked in the same 33 neurons that were active during the eupnea-sigh activity induced by GR73632 (Figure 3-7B).

The rostrocaudal extents of neuronal networks sufficient and necessary for generation of inspiratory-related behaviors were identified in newborn rat brainstem slices in 3 mM K⁺. The findings suggest that a small kernel of inspiratory preBötC neurons reconfigures in favor of a eupnea-sigh pattern via regions rostral to the preBötC or transmitters acting like SP, whereas it reconfigures in favor of a eupnea pattern via caudal regions or transmitters acting like TRH.

3.4 Discussion

3.4.1 A Closer Look at the preBötC

The original report indicated that the preBötC extends 225 μm rostrocaudally in newborn rats (Smith et al., 1991). Most studies since then used slices 500 μm thick in elevated K⁺ to facilitate motor output via hypoglossal nerve roots (Richter & Spyer, 2001; Ramirez et al., 2002). Slice boundaries that are necessary or sufficient for generating inspiratory rhythm have not been defined precisely. The original report in rats (Smith et al., 1991) and subsequent work in mice (Tryba et al., 2003) demonstrated that slices >500 μm thick generate inspiratory-related bursts in 3 mM K⁺, but only recently has it been shown that this behavior is stable for several hours (Ruangkittisakul et al., 2006). Here, we show that 250 μm and 50% of 200 μm thin slices, containing a common (170 μm) portion of the preBötC, also generate robust bilaterally synchronized, inspiratory-related rhythm for >1.5 h in 3 mM K⁺. The other 50% of 200 μm slices produced bilaterally asynchronous rhythm. Furthermore, two of seven slices with 175 μm thickness slices generated either bilaterally asynchronous or unilateral activity. The lack of bilateral (synchronous) bursting in the thinnest slices could reflect uneven ipsilateral and contralateral sectioning or tissue impairment by the suction electrode, which both would weaken neuronal connectivity unilaterally and between the bilaterally distributed preBötC. This would reduce recurrent excitation within this network below the threshold for synchronized

burst generation (Del Negro et al., 2002a,b). As slice thickness is reduced, rhythmic burst amplitude decreases, presumably reflecting that fewer neurons are discharging in synchrony. Therefore, unilateral or no activity in slices $<200\ \mu\text{m}$ may indicate a limited sensitivity of suction electrode recording. Nevertheless, we can conclude that the preBötC core sufficient for the generation of inspiratory rhythm is, at most, $175\ \mu\text{m}$ in neonatal rats (Figure 3-8). The preBötC kernel necessary for rhythm generation is notably smaller ($<100\ \mu\text{m}$, centered at $0.5\ \text{mm}$ caudal to VII_c) when included with neighboring tissue (Figure 3-8). A more exact determination of this region is limited by the resolution of on-line histology, possibly in conjunction with variation between rats in the extension of respiratory marker nuclei. Important to note, drive from neighboring tissue in $700\text{-}\mu\text{m}$ -thick slices results in a robust burst amplitude, even when one of their boundaries is $<100\ \mu\text{m}$ distant to the center of the preBötC. That these rhythms in $3\ \text{mM}\ \text{K}^+$ are inspiratory related, whether recorded unilaterally or bilaterally, is based on the observation that they disappear if the recording suction electrode is moved by a few hundred micrometers from the hot spot that is colocated with the preBötC in the ventrolateral aspect of the slice surface (Figure A2-2).

3.4.2 A Reconfiguring preBötC Kernel

All (except photodamaged) inspiratory preBötC neurons were active during Ca^{2+} imaging of both eupnea and eupnea-sigh burst patterns, supporting the hypothesis of Lieske et al. (2000) that multiple inspiratory behaviors derive from one reconfiguring network. In extension of their findings in $>500\ \mu\text{m}$ mouse slices, we show that inspiratory networks as thin as $250\ \mu\text{m}$ reconfigure under influence of specific neuromodulators (see below), indicating that this may be an intrinsic capacity of the preBötC kernel.

3.4.3 Origin of Sighs versus Biphasic Bursts

The analysis of m-preBötC[500] slices showed that sighs and biphasic bursts can be distinguished by criteria such as amplitude, rise time, and the presence or absence of a second peak (Appendix II). However, they also share several features because their durations and rise times are both longer compared with eupneic bursts. Discrimination between these events is even more difficult in thin m-preBötC slices. On the one hand,

the fact that the primary burst type in both m-preBötC[250] and m-preBötC[200] slices is substantially larger and longer than intermittent eupnea-like bursts suggests that it is a sigh-like event. On the other hand, the shape of the larger-amplitude burst in the 250- μm -thin slices resembles that of a sigh, whereas in the 200 μm slices the shape is more consistent with a biphasic burst. It is possible that sighs and biphasic bursts constitute variations of one type of “augmented in vitro breath.” Some yet unknown factors may determine whether the onset of the secondary event is earlier and its amplitude more pronounced (in the case of sighs), or whether its onset is delayed and of smaller amplitude (in the case of biphasic bursts). In line with this view, an initial eupnea-biphasic burst pattern could spontaneously transform into a eupnea-sigh pattern (Figure A2-3B). It remains to be determined whether the occurrence of sighs versus biphasic bursts depends, for example, on (recurrent) mechanisms intrinsic to the emerging network of the preBötC kernel (Del Negro et al., 2002a,b).

3.4.4 Spatiochemical Organization of Inspiratory Networks

A eupnea or a eupnea-sigh burst pattern was typical in 3 mM K^+ for 700 μm slices lacking either tissue rostral or caudal to the preBötC, respectively. We hypothesize that these distinct inspiratory-related patterns reflect a spatial organization of the medullary inspiratory network. Structures caudal to the preBötC kernel appear to promote eupnea, whereas areas rostral to the kernel appear to promote sighs (Figure 3-8). These influences could derive from particular patterns of synaptic input including tonic drive, or specific neuromodulatory inputs as suggested by the differing effects of SP and TRH. Several brainstem structures neighboring the preBötC could account for this slice-type-specific behavior. For example, c+preBötC[700] and r+preBötC[700] slices may differ in the content of raphe obscurus versus raphe pallidus (Jacobs & Azmitia, 1992) that provide inputs to the ventral respiratory column (Holtman & Speck, 1994). In raphe neurons, SP and TRH colocalize with other modulators, but not with each other (Kachidian et al., 1991). Thus, their inputs to the preBötC may be organized in a rostrocaudal SP-TRH gradient. The ventral respiratory column is also organized asymmetrically with regard to the preBötC, with the Bötzing complex and the parafacial respiratory group/retrotrapezoid nucleus complex located rostrally and the rostral ventral respiratory group located

caudally (Alheid et al., 2004). These or others structures, or neuromodulators, may reconfigure the preBötC kernel to favor one type of burst pattern (Richerson, 2004; Feldman & Del Negro, 2006; Pace et al., 2007). Although the mechanisms remain unknown, the hypothesized input from rostrally neighboring structures increases the probability at which the preBötC kernel produces sighs, which are typically followed by an inhibitory period as in mouse slices (Lieske et al., 2000; Telgkamp et al., 2002).

The importance of endogenous neuromodulatory drive in generating the typical pattern of sigh-like bursts and smaller eupnea bursts in the 200-250 μm slices is not known. Possible sources are axotomized synaptic terminals or raphe cells. That a modulator can specifically influence slice activity is clear because both SP and NK1 agonist induced, after in vitro apnea, the eupnea-sigh burst pattern in all slices 250 μm thick. More significant is that NK1 receptor antagonist depressed endogenous activity in 3 mM K^+ . We therefore hypothesize that SP is the transmitter of the rostral structures that promote a eupnea-sigh burst pattern. This view is consistent with previous findings in mouse slices in 8 mM K^+ that a NK1 receptor antagonist depressed inspiratory rhythm (Telgkamp et al. 2002), whereas SP increased the probability of sighs more than that of eupneic bursts (Lieske et al., 2000) and also restored rhythm during in vitro apnea (Peña & Ramirez, 2004). This supports the proposed importance of NK1 receptors for modulation of inspiratory rhythm (Murakoshi & Otsuka, 1985; Rampin et al., 1993; Gray et al., 1999, 2001; Morgado-Valle & Feldman, 2004).

In contrast to NK1 receptor activation, TRH (Hedner et al., 1983; Funk et al., 1994) reactivated a eupnea burst pattern in slices 250 μm thick during in vitro apnea. A direct involvement of TRH in rhythm generation was not tested because of lack of antagonists. Eupnea was also induced by the clinical phosphodiesterase-4 blockers rolipram and theophylline (Fredholm et al., 1999; O'Donnell & Zhang, 2004; Ruangkittisakul & Ballanyi, 2006), supporting the idea that cAMP stimulates the preBötC (Ballanyi et al., 1997, 1999; Richter et al., 1997; Ballanyi, 2004). This also indicates that neurotransmitters that raise cellular cAMP such as serotonin via 5-HT_{4(a)} receptors (Richter et al., 1997; Manzke et al., 2003), configure the network in favor of eupnea.

However, the mechanisms may be more complex because a membrane-permeant cAMP analog stimulated both eupneic and sigh bursts in mouse slices (Lieske & Ramirez, 2006b). Pharmacological tools such as strychnine or modulators of metabotropic glutamate receptors that target either sighs or eupnea in mouse slices (Lieske et al., 2000; Lieske & Ramirez, 2006a,b) may be useful for dissecting the inspiratory patterns in the 3 mM K^+ newborn rat preBötC slices.

3.5 Summary

Multineuronal Ca^{2+} imaging revealed that preBötC neurons reconfigure between eupnea and eupnea-sigh burst patterns, as modulated by the hypothesized (gradient-like) spatiochemical organization of regions adjacent to the preBötC. The preBötC kernel, <100 μm thick, generates eupnea under the dominant influence of caudal structures or TRH-like transmitters but eupnea-sigh activity when the influence of rostral structures or substance-P-like transmitters predominates.

Figures

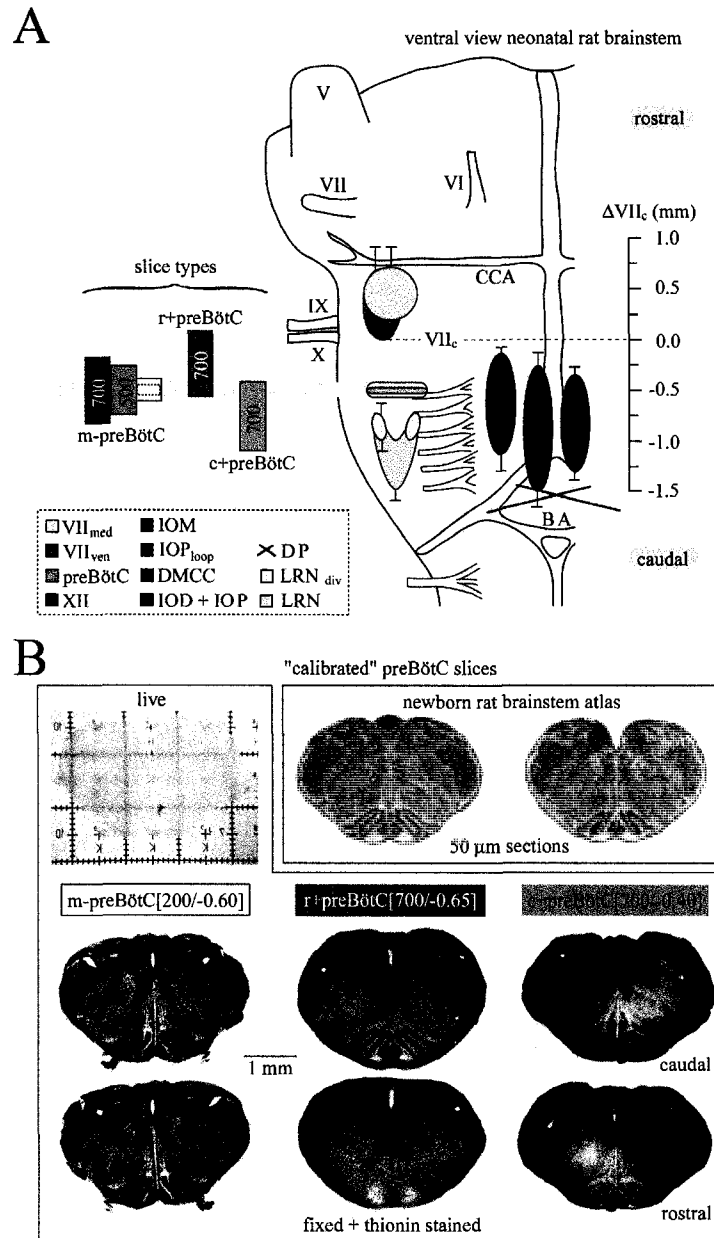


Figure 3-1 On-line histology for the determination of structure-function relationships in physiological (3 mM) $[K^+]$ of the isolated inspiratory preBötC neuronal network. A, Rostrocaudal extensions in postnatal day P0-P4 S-D or W rats of brainstem marker nuclei for generating rhythmic preBötC slices. The data stem from 15 fixed brainstems plus 11 brainstems sectioned in saline used for studying slice functions. The small SDs indicate a high constancy of these nuclei during early postnatal development. The boundaries of preBötC slices are identified by the distance (in

millimeters, negative sign indicating caudal location) from the caudal end of the facial (VII) motor nucleus (VII_c) by comparing structures in the pre/post rhythmic slices with those in a newborn rat brainstem atlas (Ruangkittisakul et al., 2006) (see **B**). DMCC, Dorsomedial cell column of inferior olive; IO, inferior olive; IOM, medial inferior olive; IOD, dorsal inferior olive; IOP, principal inferior olive; IOP_{loop}, lateral loop of IOP; LRN, lateral reticular nucleus; LRN_{div}, LRN divided into medial and lateral subnuclei; VII_{med}, medial subnucleus of VII; VII_{ven}, ventral subnucleus of VII; XII, hypoglossal nucleus; DP, pyramidal decussation; BA, basilar artery; CCA, caudal cerebellar artery; V, VI, IX, and X, trigeminal, abducens, glossopharyngeal, and vagal nerves, respectively. **B**, For the determination of regions that are sufficient or necessary for the generation of inspiratory-related rhythm, slices were generated of different thickness with the preBötC in the middle (m-preBötC slices), or containing either caudal or rostral tissue plus the preBötC (c+preBötC and r+preBötC slices) (values in brackets indicate slice thickness in micrometers and boundary in millimeters; see also left panel of **A**). The calibration bar is identical for all slices in **B**. The left slice in the top right box shows the -0.65 section from the atlas corresponding to the caudal surface of the r+preBötC[700/-0.65] slice. The right slice shows the -0.40 section from the atlas corresponding to the rostral boundary of the c+preBötC[700/-0.40] slice.

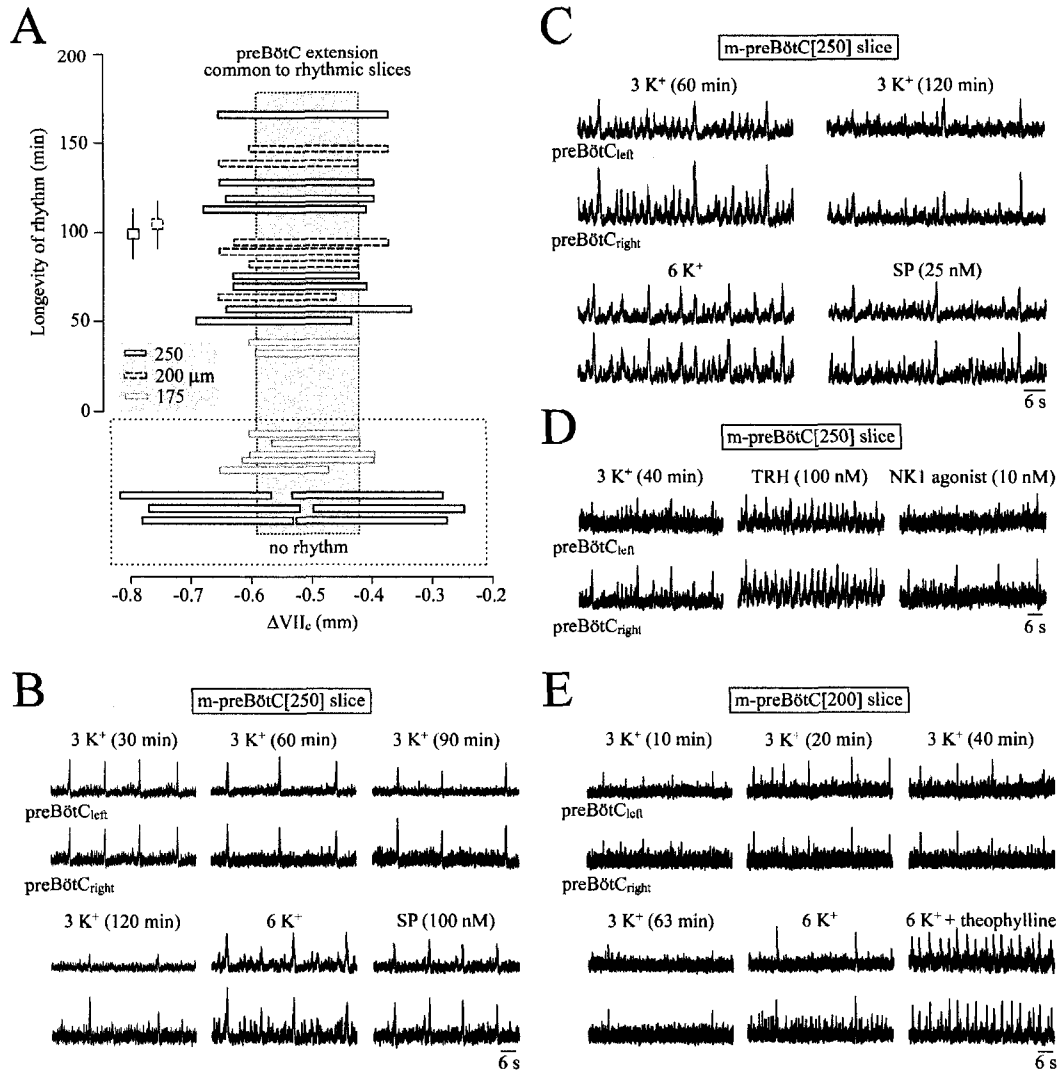


Figure 3-2 Boundaries and burst properties in 3 mM K^+ of thin m-preBötC slices. A, Plot of the rostrocaudal boundaries of eight m-preBötC[250/-0.65]W-P0/1 slices, six m-preBötC[200/-0.63]W-P0 slices, and seven m-preBötC[175/-0.63]W-P0 slices versus the longevity of inspiratory-related bursting. The mean (\pm SEM) of the longevities of rhythms in the 250 and 200 μ m thin slices are indicated by the squares. The gray box represents the region common to the rhythmic slices. Note that five of seven m-preBötC[175] slices with boundaries similar to those of the two rhythmic slices did not show rhythm. In contrast, the boundaries of six nonrhythmic m-preBötC[250] slices deviated notably from those of the rhythmic slices of this type. **B,** A m-preBötC[250/-0.65]W-P1 slice showed bilaterally synchronous robust bursts with a pattern resembling the eupnea-sigh pattern (although with very small amplitude eupneic bursts) in thicker slices (compare Figure

A2-1). This rhythm was stable for >90 min, before it stopped spontaneously (in vitro apnea) shortly after 120 min. Sighs and smaller-amplitude eupneic bursts were activated by 6 mM K⁺, whereas SP, after return to 3 mM K⁺ solution, evoked primarily sighs. **C**, An m-preBötC[250/-0.65]W-P1 slice generated bilaterally synchronous bursts resembling the eupnea-sigh pattern in thicker slices (Figures A2-1, A2-3). The burst pattern became more irregular after >60 min, partly because of disappearance of the eupneic bursts, but rhythm persisted for an additional 106 min, before rhythm stopped. A 6 mM K⁺ solution reactivated both sighs and eupneic bursts, whereas SP elicited sighs and intermittent very-small-amplitude eupneic bursts. **D**, After in vitro apnea after 113 min in a m-preBötC[250/-0.68]W-P1 slice, TRH evoked a regular pattern of eupneic bursts, whereas subsequent application after washout of TRH of the NK1 receptor agonist GR73632 evoked sighs at rather low-rate and intermittent very-small-amplitude eupneic bursts. **E**, Twenty minutes after the start of the recording, bilaterally synchronous bursting in the m-preBötC[200/-0.60]W-P0 slice of Figure 3-1B reached a maximal amplitude. Burst amplitude decreased, and rate slowed after 63 min to 2 bursts/min and remained at that level for an additional 80 min before rhythm stopped. Synchronous bursting of sighs and unilateral eupneic bursts were reactivated by 6 mM K⁺, whereas the addition of 2.5 mM theophylline to 6 mM K⁺ solution resulted in a faster rhythm with a eupnea pattern.

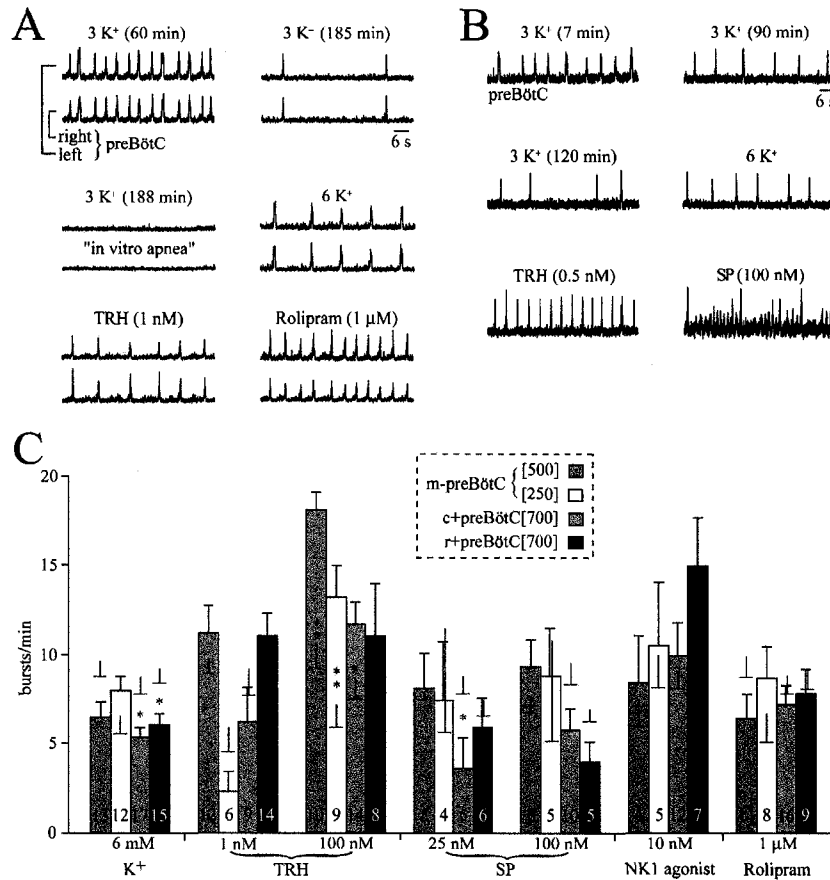


Figure 3-3 Pharmacological reactivation of 3 mM K⁺ rhythms in preBötC slices after onset of in vitro apnea. **A**, In a m-preBötC[500/-0.70]W-P3 slice, the inspiratory rate slowed to 2 bursts/min after 185 min of recording, and rhythm stopped 3 min later. Such in vitro apnea was reversed by bath application of 6 mM K⁺ solution or the more specific respiratory stimulants TRH and rolipram. **B**, In a m-preBötC[500/-0.75]W-P2 slice, rhythm stopped 6 min after burst rate had dropped to 4 bursts/min after 2 h of recording. Eupneic bursts were activated by either 6 mM K⁺ or TRH, whereas SP induced bursting with a eupnea-sigh pattern. **C**, Burst rates of pharmacologically restored inspiratory rhythms in different preBötC slice types. After the onset of in vitro apnea, bursting was reactivated by 6 mM K⁺, TRH, SP, the NK1 receptor agonist GR73632, and rolipram in the slice types shown in the dashed box. Bars show means ± SEM; digits in bars indicate the number of slices. Additional horizontal plus vertical lines indicate the means ± SEM of the control burst rate for those slices tested for a specific agent. Note that the values correspond to the combined average burst rate of slices that showed a dual burst patterns (i.e., a eupnea-biphasic or a eupnea-sigh pattern).

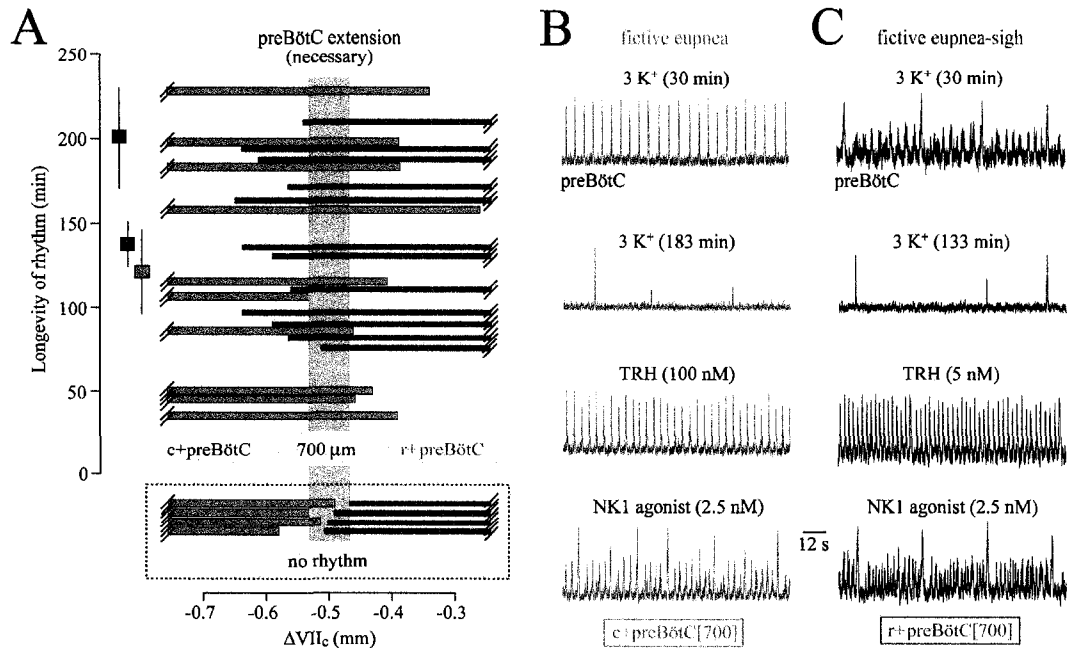


Figure 3-4 Boundaries necessary for rhythm and activity patterns in 3 mM [K⁺] of 700 μm thick slices with unilaterally exposed preBötC. **A**, Plot of the longevity of rhythms versus boundaries of 10 c+preBötC[700/-0.42]W-P1/4 slices and 12 r+preBötC[700/-0.58]S-D/W-P0/4 slices. The preBötC extension necessary for rhythm is possibly <100 μm as indicated by the pink box framing brainstem tissue common to the rhythmic slices of both types. The dashed box underneath **A** indicates the boundaries of nonrhythmic slices. The squares next to the longevity scale bar show the mean longevity (\pm SEM) of rhythms in the 10 c+preBötC[700] (blue square) and the 12 r+preBötC[700] (purple square) slices, whereas the black square shows the longevity of rhythm in 7 m-preBötC[700/-0.89]W-P1/3 slices (see Appendix II). **B**, The top panel shows eupneic bursts of regular rate and amplitude in the c+preBötC[700/-0.40]W-P2 slice of Figure 3-1B. After the occurrence of in vitro apnea 2 min after the recording in the second panel from the top, consecutive bath application of TRH (third panel) and (after washout of TRH) NK1 receptor agonist GR73632 (bottom panel) reactivated a eupnea and a eupnea-sigh burst pattern, respectively. **C**, The top panel shows large sigh bursts and eupneic bursts of smaller and variable amplitude in the r+preBötC[700/-0.65]W-P1 slice of Figure 3-1B. After in vitro apnea, occurring 3 min after the recording in second panel from the top, TRH induced a eupnea burst pattern (third panel), whereas GR73632 initiated a eupnea-sigh pattern very similar to that in control (bottom panel).

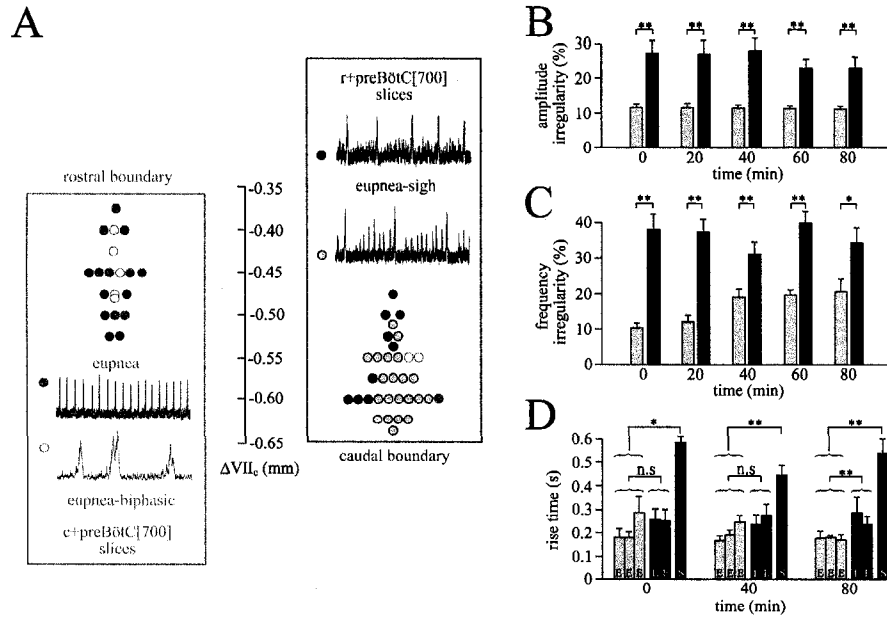


Figure 3-5 Rostrocaudal distribution and properties of inspiratory-related burst patterns in 3 mM K^+ of 700 μ m slices with unilaterally exposed preBötC. **A**, Plot of inspiratory-related patterns, specifically eupnea, eupnea-biphasic, and eupnea-sigh versus the rostral boundaries of 20 c+preBötC [700/-0.44]S-D/W-P1/4 (blue box) and the caudal boundaries of 33 r+preBötC[700/-0.60]S-D/W-P0/3 slices (purple box), respectively. Note that eupnea bursts had a rather small amplitude in some slices with a eupnea-sigh burst pattern (see example in top panel). Note also that the time scale for the example of a eupnea-biphasic burst pattern is expanded approximately threefold compared with the examples of rhythms with a solely eupnea or a eupnea-sigh pattern. **B**, Irregularity score plots show that the burst amplitude of eupneic bursts (E) in c+preBötC[700] (blue panel; $n = 8$) slices was more uniform than that of sighs plus eupneic bursts (S) in the r+preBötC[700] slices (purple panel; $n = 8$). **C**, Also the frequency of eupneic bursts (E) in the c+preBötC[700] slices of **B** was significantly more regular than that of the eupnea-sigh bursts (S) in the r+preBötC[700] slices. In **B** and **C**, significances were determined between mean values for each group at a given time period between 0 and 80 min of recording. **D**, Plots show that the rise times of means of three consecutive eupneic bursts (E) in the c+preBötC[700] slices do not differ from the means of two consecutive E bursts in the r+preBötC[700] slices (except at 80 min) but are significantly shorter than the mean rise times of sighs (S) in the latter slices. Significance values are as follows: * $p < 0.05$; ** $p < 0.01$; n.s., nonsignificant difference.

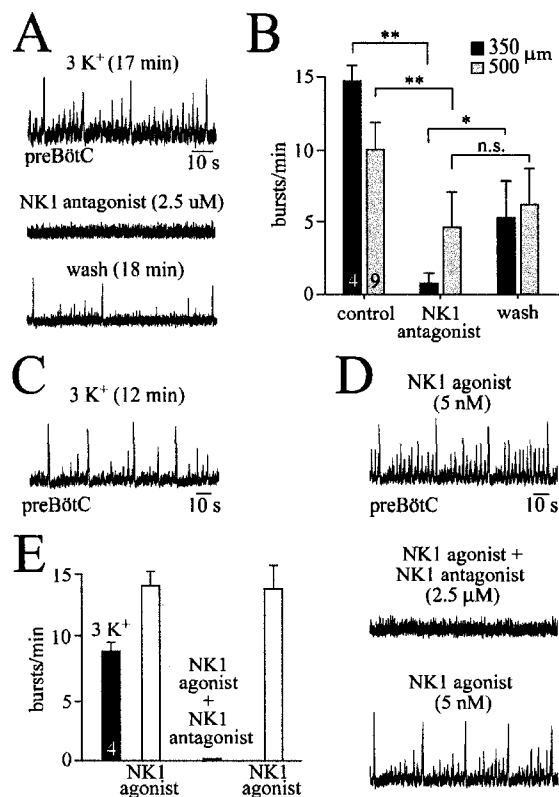


Figure 3-6 Depression of preBötC rhythms by block of NK1 receptors. **A**, Rhythm in 3 mM K⁺ with a eupnea-sigh burst pattern in a m-preBötC[350/-0.69]W-P1 slice was abolished 12 min after the start of bath application of the NK1 receptor antagonist GR82334. Recovery of the rhythm was incomplete within 18 min after the start of the washout of GR82334. **B**, Statistical analysis of the effects of the NK1 antagonist (2.5 μM) on nine m-preBötC[500/-0.75]W-P1/4 slices (gray bars) and four m-preBötC [350/-0.70]W-P1/2 slices (black bars). Note that the block was more pronounced in the thinner slices. **C**, In 3 mM K⁺, a m-preBötC[500/-0.68]W-P0 slice generated rhythm with a eupnea-sigh burst pattern. **D**, After onset of in vitro apnea in the slice of **C**, bath application of the NK1 receptor agonist GR73632 restored a very similar eupnea-sigh burst pattern. GR82334 abolished the agonist-evoked rhythm within 4 min, whereas the rhythm was fully restored 10 min after washout of the NK1 antagonist. **E**, Statistical analysis of the depressing effects of GR82334 (2.5 μM) on the rhythms evoked by GR73632 (5 nM) in a group consisting of two m-preBötC[350/-0.70]W-P0 and two m-preBötC[500/-0.74]W-P2 slices. In **B** and **E**, digits in bars indicate the number of slices.

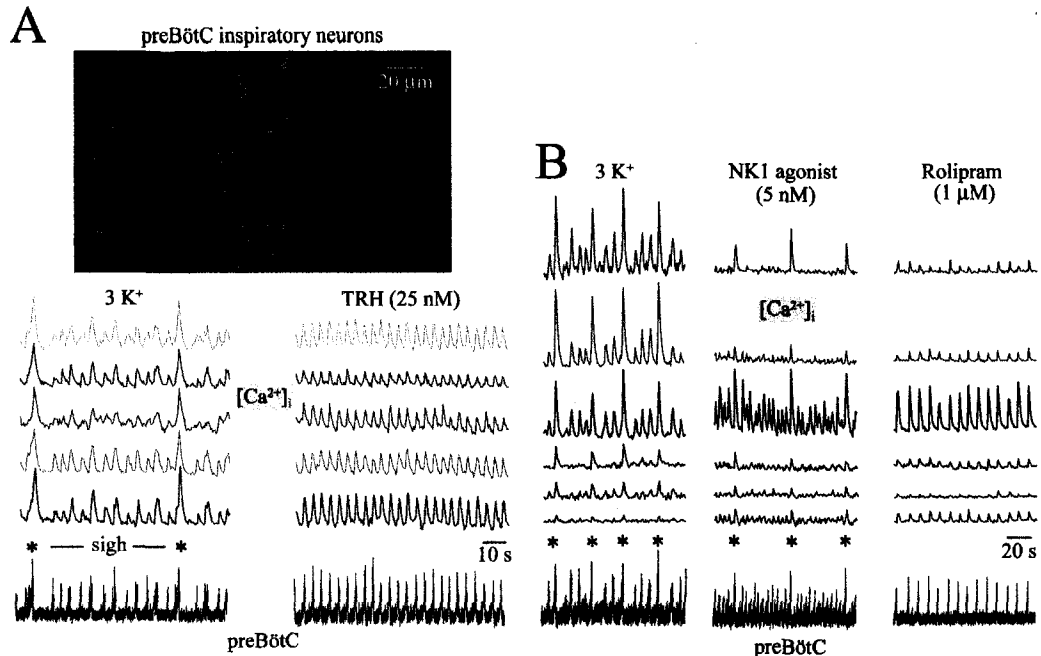


Figure 3-7 Reconfiguring burst patterns of inspiratory preBötC neurons visualized with multiphoton imaging of cytosolic $[\text{Ca}^{2+}]_i$ rises. Cells were loaded with the membrane-permeant, Ca^{2+} -sensitive dye fluo-4-AM by unilateral pressure injection into the preBötC (Ruangkittisakul et al., 2006). **A**, $[\text{Ca}^{2+}]_i$ rises in preBötC neurons located 25 μm caudal to the preBötC center occurred simultaneously with contralateral preBötC neuronal population activity recorded electrophysiologically from a r+preBötC[700/-0.58]W-P1 slice. Bath-applied TRH transformed both the inspiratory optical and electrophysiological pattern with two major sighs (asterisks) and various eupneic bursts into a more regular eupnea burst pattern without sighs. **B**, The size of larger amplitude sigh (asterisks) and smaller-amplitude eupneic bursts recorded electrophysiologically from a r+preBötC[700/-0.60]W-P1 slice was reflected in the amplitude of Ca^{2+} oscillations in preBötC neurons located 60 μm caudal to the preBötC center. After in vitro apnea, more irregular activities associated with a eupnea-sigh burst pattern were reactivated by the NK1 receptor agonist GR73632, whereas the cAMP-elevating blocker of phosphodiesterase-4 rolipram activated transients associated with eupneic bursts after washout of NK1 agonist.

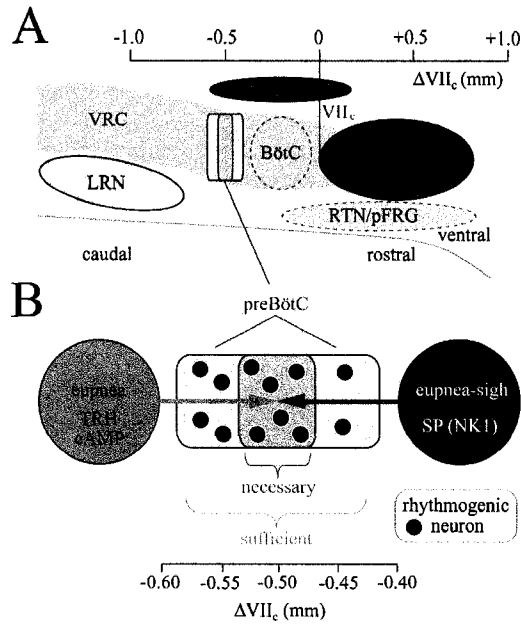


Figure 3-8 Organization of the rhythmogenic preBötC inspiratory network isolated in 3 mM K⁺. **A**, Respiratory (marker) regions in a schematic sagittal section of a newborn rat brainstem. The scale is referred to VII_c. Modified from Ruangkittisakul et al. (2006). For abbreviations, see Figure 3-1B. A summary of the main findings is as follows (see **B**). The rostrocaudal extension of the rhythmogenic preBötC kernel sufficient for generation of inspiratory rhythm in thin brainstem slices is, at most, 175 μm, corresponding to the minimal thickness of slices with rhythmic activity in physiological (3 mM) K⁺ solution. In contrast, the extension that is necessary for rhythm in 3 mM K⁺ is possibly <100 μm in 700 μm thick slices with the preBötC exposed at one boundary. The latter type of slices with the preBötC exposed to the rostral boundary generate rhythm resembling eupnea in vivo when receiving modulatory drive from caudal structures via a neurotransmitter(s) that acts like TRH and/or acts via increasing cAMP. Conversely, 700 μm slices with the preBötC at the caudal surface generate an inspiratory pattern with a eupnea-sigh burst pattern provided by drive from structures rostral to the preBötC via a neurotransmitter(s) acting like SP on NK1 receptors. The rhythmogenic neurons of the preBötC kernel reconfigure their activity pattern after changes in the dominance of either drive.

3.6 References

- Alheid GF, Milsom WK, McCrimmon DR (2004) Pontine influences on breathing: an overview. *Respir Physiol Neurobiol* 143, 105-114.
- Ballanyi K (2004) Neuromodulation of the perinatal respiratory network. *Curr Neuropharmacol* 2, 221-243.
- Ballanyi K, Onimaru H, Homma I (1999) Respiratory network function in the isolated brainstem-spinal cord of newborn rats. *Prog Neurobiol* 59, 583-634.
- Ballanyi K, Lalley PM, Hoch B, Richter DW (1997) cAMP-dependent reversal of opioid- and prostaglandin-mediated depression of the isolated respiratory network in newborn rats. *J Physiol (Lond)* 504, 127-134.
- Bhatia J (2000) Current options in the management of apnea of prematurity. *Clin Pediatr (Phila)* 39, 327-336.
- Del Negro CA, Wilson CG, Butera RJ, Rigatto H, Smith JC (2002a) Periodicity, mixed-mode oscillations, and quasiperiodicity in a rhythm-generating neural network. *Biophys J* 82, 206-214.
- Del Negro CA, Morgado-Valle C, Feldman JL (2002b) Respiratory rhythm: an emergent network property? *Neuron* 34, 821-830.
- Feldman JL, Del Negro CA (2006) Looking for inspiration: new perspectives on respiratory rhythm. *Nat Rev Neurosci* 7, 232-242.
- Fredholm BB, Battig K, Holmen J, Nehlig A, Zvartau EE (1999) Actions of caffeine in the brain with special reference to factors that contribute to its widespread use. *Pharmacol Rev* 51, 83-133.
- Funk GD, Smith JC, Feldman JL (1994) Development of thyrotropin-releasing hormone and norepinephrine potentiation of inspiratory-related hypoglossal motoneuron discharge in neonatal and juvenile mice in vitro. *J Neurophysiol* 72, 2538-2541.
- Funk GD, Smith JC, Feldman JL (1993) Generation and transmission of respiratory oscillations in medullary slices: role of excitatory amino acids. *J Neurophysiol* 70, 1497-1515.

- Gray PA, Janczewski WA, Mellen N, McCrimmon DR, Feldman JL (2001) Normal breathing requires preBötzing complex neurokinin-1 receptor-expressing neurons. *Nat Neurosci* 4, 927-930.
- Gray PA, Reikling JC, Bocchiaro CM, Feldman JL (1999) Modulation of respiratory frequency by peptidergic input to rhythmogenic neurons in the preBötzing complex. *Science* 286, 1566-1568.
- Hedner J, Hedner T, Wessberg P, Lundberg D, Jonason J (1983) Effects of TRH and TRH analogues on the central regulation of breathing in the rat. *Acta Physiol Scand* 117, 427-437.
- Holtman JR Jr, Speck DF (1994) Substance P immunoreactive projections to the ventral respiratory group in the rat. *Peptides* 15, 803-808.
- Jacobs BL, Azmitia EC (1992) Structure and function of the brain serotonin system. *Physiol Rev* 72, 165-229.
- Kachidian P, Poulat P, Marlier L, Privat A (1991) Immunohistochemical evidence for the coexistence of substance P, thyrotropin-releasing hormone, GABA, methionine-enkephalin, and leucin-enkephalin in the serotonergic neurons of the caudal raphe nuclei: a dual labeling in the rat. *J Neurosci Res* 30, 521-530.
- Lieske SP, Ramirez JM (2006a) Pattern-specific synaptic mechanisms in a multifunctional network. I. Effects of alterations in synapse strength. *J Neurophysiol* 95, 1323-1333.
- Lieske SP, Ramirez JM (2006b) Pattern-specific synaptic mechanisms in a multifunctional network. II. Intrinsic modulation by metabotropic glutamate receptors. *J Neurophysiol* 95, 1334-1344.
- Lieske SP, Thoby-Brisson M, Telgkamp P, Ramirez JM (2000) Reconfiguration of the neural network controlling multiple breathing patterns: eupnea, sighs and gasps. *Nat Neurosci* 3, 600-607.
- Manzke T, Guenther U, Ponimaskin EG, Haller M, Dutschmann M, Schwarzacher S, Richter DW (2003) 5-HT_{4(a)} receptors avert opioid-induced breathing depression without loss of analgesia. *Science* 301, 226-229.

- Morgado-Valle C, Feldman JL (2004) Depletion of substance P and glutamate by capsaicin blocks respiratory rhythm in neonatal rat in vitro. *J Physiol (Lond)* 555, 783-792.
- Mulkey DK, Stornetta RL, Weston MC, Simmons JR, Parker A, Bayliss DA, Guyenet PG (2004) Respiratory control by ventral surface chemoreceptor neurons in rats. *Nat Neurosci* 7, 1360-1369.
- Murakoshi T, Otsuka M (1985) Respiratory reflexes in an isolated brainstem-lung preparation of the newborn rat: possible involvement of γ -aminobutyric acid and glycine. *Neurosci Lett* 62, 63-68.
- O'Donnell JM, Zhang HT (2004) Antidepressant effects of inhibitors of cAMP phosphodiesterase (PDE4). *Trends Pharmacol Sci* 25, 158-163.
- Onimaru H, Homma I (2003) A novel functional neuron group for respiratory rhythm generation in the ventral medulla. *J Neurosci* 23, 1478-1486.
- Pace RW, Mackay DD, Feldman JL, Del Negro CA (2007) Inspiratory bursts in the preBötzinger complex depend on a calcium-activated nonspecific cationic current linked to glutamate receptors. *J Physiol (Lond)* 582, 113-125.
- Peña F, Ramirez JM (2004) Substance P-mediated modulation of pacemaker properties in the mammalian respiratory network. *J Neurosci* 24, 7549-7556.
- Ramirez JM, Zuperku EJ, Alheid GF, Lieske SP, Ptak K, McCrimmon DR (2002) Respiratory rhythm generation: converging concepts from in vitro and in vivo approaches? *Respir Physiol Neurobiol* 131, 43-56.
- Rampin O, Pierrefiche O, Denavit-Saubie M (1993) Effects of serotonin and substance P on bulbar respiratory neurons in vivo. *Brain Res* 622, 185-193.
- Rekling JC, Feldman JL (1998) PreBötzinger complex and pacemaker neurons: hypothesized site and kernel for respiratory rhythm generation. *Annu Rev Physiol* 60, 385-405.
- Richerson GB (2004) Serotonergic neurons as carbon dioxide sensors that maintain pH homeostasis. *Nat Rev Neurosci* 5, 449-461.
- Richter DW, Spyer KM (2001) Studying rhythmogenesis of breathing: comparison of in vivo and in vitro models. *Trends Neurosci* 24, 464-472.

- Richter DW, Lalley PM, Pierrefiche O, Haji A, Bischoff AM, Wilken B, Hanefeld V (1997) Intracellular signal pathways controlling respiratory neurons. *Respir Physiol Neurobiol* 110, 113-123.
- Ruangkittisakul A, Ballanyi K (2006) Reversal by phosphodiesterase-4 blockers of in vitro apnea in the isolated brainstem-spinal cord preparation from newborn rats. *Neurosci Lett* 401, 194-198.
- Ruangkittisakul A, Schwarzacher SW, Secchia L, Poon BY, Ma Y, Funk GD, Ballanyi K (2006) High sensitivity to neuromodulator-activated signaling pathways at physiological $[K^+]$ of confocally imaged respiratory center neurons in on-line-calibrated newborn rat brainstem slices. *J Neurosci* 26, 11870-11880.
- Shvarev YN, Lagercrantz H, Yamamoto Y (2003) Two types of rhythm in the respiratory network output in the isolated ventrolateral medulla in the neonatal rats. *Neurosci Lett* 347, 53-56.
- Smith JC, Ellenberger HH, Ballanyi K, Richter DW, Feldman JL (1991) Pre-Bötzinger complex: a brainstem region that may generate respiratory rhythm in mammals. *Science* 254, 726-729.
- Telgkamp P, Cao YQ, Basbaum AI, Ramirez JM (2002) Long-term deprivation of substance P in PPT-A mutant mice alters the anoxic response of the isolated respiratory network. *J Neurophysiol* 88, 206-213.
- Tryba AK, Peña F, Ramirez JM (2006) Gasping activity in vitro: a rhythm dependent on 5-HT_{2A} receptors. *J Neurosci* 26, 2623-2634.
- Tryba AK, Peña F, Ramirez JM (2003) Stabilization of bursting in respiratory pacemaker neurons. *J Neurosci* 23, 3538-3546.
- Yuste R, Konnerth A, Masters BR (2006) Imaging in neuroscience and development, a laboratory manual. *J Biomed Opt* 11, 19902.

***CHAPTER IV**

Dependence on Extracellular $\text{Ca}^{2+}/\text{K}^{+}$ Antagonism of Inspiratory Centre Rhythms in Slices and En Bloc Preparations of Newborn Rat Brainstem

* Previously published paper:

Ruangkittisakul A[†], Secchia L[†], Bornes TD, Palathinkal DM, Ballanyi K (2007) Dependence on extracellular $\text{Ca}^{2+}/\text{K}^{+}$ antagonism of inspiratory centre rhythms in slices and en bloc preparations of newborn rat brainstem. *J Physiol* 584, 489-508. Copyright 2007 by the Journal of Physiology. My contribution to this study consisted in the execution of >60% of electrophysiological experiments and corresponding analyses, and >60% of histological analyses. [†] Authors contributed equally to the study.

4.1 Introduction

The neural control of breathing is studied in reduced preparations such as isolated newborn rat brainstem-spinal cords (Smith et al., 1990; Ballanyi et al., 1999). Microsectioning of this *in vitro* model showed that neurons of the pre-Bötzinger Complex (preBötC) inspiratory centre remain active in a transverse brainstem slice (Smith et al., 1991). In both, slice and *en bloc* models, rhythmogenic preBötC networks and preBötC-driven motor circuits are studied under quite divergent experimental conditions. preBötC slice thickness ranges from 200 to 1000 μm , and rostrocaudal boundaries of slices and brainstem-spinal cords vary notably (Rekling et al., 1996; Ballanyi et al., 1999; Koshiya & Smith, 1999; Ruangkittisakul et al., 2006). This may affect fictive inspiratory rhythms as the preBötC is neighboured by other ventral respiratory column structures such as the more rostral Bötzing complex (BötC) and the parafacial respiratory group (pFRG), which is presumably closely associated with the retrotrapezoid nucleus (RTN) (Monnier et al., 2003; Feldman & Del Negro, 2006). While differences in the content of ventral respiratory column structures may modulate preBötC rhythms specifically, unspecific modulation may arise from interstitial accumulation or, conversely, depletion of neuromodulator(s), which both depend on physical dimensions of isolated preparations (Ballanyi, 1999; Ruangkittisakul et al., 2006). PreBötC activity may also be affected by superfusate constituents such as Ca^{2+} and K^+ that modulate excitability in other neuronal systems (Hille, 2001; Somjen, 2002). The most common values of interstitial $[\text{Ca}^{2+}]$ and $[\text{K}^+]$ in diverse mammalian brain regions *in vivo* are 1.2 mM and 3 mM, respectively (Somjen, 2002). This contrasts with a wide range of superfusate Ca^{2+} (0.8-2.4 mM) and K^+ (3-11 mM) in studies on isolated respiratory networks (Suzue, 1984; Smith et al., 1991; Johnson et al., 1996; Rekling et al., 1996; Ruangkittisakul et al., 2006).

Differences in dimensions of preparations and/or superfusate composition may be responsible for discrepant findings, e.g. regarding the capability of the isolated preBötC to generate rhythm. The above transection study (Smith et al., 1991) showed that the rate of inspiratory-related cervical nerve bursting is not affected by transection between preBötC and facial motonucleus (VII) in 1.5 mM Ca^{2+} solution. Other studies on this

model showed that such transection depressed inspiratory burst rate in 2 mM Ca^{2+} (McLean & Remmers, 1994), whereas cervical rhythm was abolished following transection in “Suzue-type” solution with 2.4 mM Ca^{2+} (Onimaru & Homma, 1987). We hypothesize that effects of brainstem transection on inspiratory-related rhythms depend critically on superfusate Ca^{2+} . The constancy of extensions of respiratory brainstem marker nuclei in early postnatal rats enables “online” histology for generation of preBötC slices with defined boundaries that are capable of stable rhythm in 3 mM K^+ (Ruangkittisakul et al., 2006). Our finding here that cranial nerves and blood vessels are ventral brainstem surface landmarks with a constant anatomical relation to the marker nuclei allowed generation of brainstem-spinal cords with defined rostral boundary. As one major aim of our study, we quantified in these en bloc preparations in physiological (1.2/3 mM) $\text{Ca}^{2+}/\text{K}^+$ the relation of their boundaries to the rate and duration of inspiratory cervical/hypoglossal nerve bursts and longevity of these rhythms, and compared the findings with those in the above slices. We then studied the Ca^{2+} dependence of preBötC (related) rhythms in both models. Finally, we elucidated the dependence on the rostral brainstem boundary of pre-/post-inspiratory lumbar nerve activity driving expiratory muscles (Janczewski et al., 2002; Janczewski & Feldman, 2006).

We found that preBötC (related) rhythms in 1.2 mM Ca^{2+} and 3 mM K^+ were basically similar in slices and en bloc preparations. Hypoglossal rhythm was stable and 1:1-coupled to preBötC population activity in slices and to cervical bursting in brainstems without VII. In contrast, hypoglossal rhythm was depressed in en bloc preparations with more rostral boundaries, while pre-/post-inspiratory lumbar nerve bursting was only present in brainstems with a major portion of VII. Most importantly, preBötC bursting and associated motor rhythms in slices and en bloc medullas without VII were greatly depressed upon Ca^{2+} elevation by only 0.5 and 0.6 mM, respectively, and were reactivated by 8-10 mM K^+ . Conversely, in 1 mM instead of 1.2 mM Ca^{2+} solution, slice rhythms had a substantially greater longevity (>3.5 h vs. 1.5 h) and higher long-term burst rate. After spontaneous arrest of rhythm in 3 mM K^+ and 1-1.2 mM Ca^{2+} in (slice) preparations with exposed preBötC, similar rhythm was reevoked by 6-7 mM K^+ and cAMP elevation by rolipram.

We discuss whether lack of pre-/post-inspiratory activity in preparations with <79% VII is due to impairment of the pathway from pre-inspiratory (pFRG) interneurons to abdominal expiratory muscles. We hypothesize that depression of hypoglossal rhythm and attenuated Ca^{2+} sensitivity of preBötC rhythm in less-reduced en bloc medullas is probably not related to increased content of rostral respiratory structures, but rather due to larger dimensions creating interstitial gradients for inhibitory neuromodulator(s) and K^+ . The strong dependence of inspiratory rhythms on an extracellular $\text{Ca}^{2+}/\text{K}^+$ antagonism suggests use of 1 mM Ca^{2+} for analyzing isolated preBötC functions in 3 mM K^+ .

4.2 Material and Methods

4.2.1 Preparations and Solutions

Brainstem-spinal cord preparations were generated from 57 Sprague-Dawley (SD) and 54 Wistar (W) rats between postnatal day 0 (P0) and P4. The University of Alberta Animal Care and Ethics Committee approved all procedures and provided governance for the animal care. Animals were anaesthetized with 2-3% isoflurane and rapidly decerebrated after the paw withdrawal reflex disappeared. The neuraxis was isolated at 19-22°C in superfusate (for composition, see below) (Brockhaus & Ballanyi, 1998, 2000). The brainstem was transected rostral to the trigeminal nerve (Figure 4-1), and the spinal cord cut at the cervical level (C_{6-8}), except for one series of experiments in which the entire spinal cord was isolated for recording from ventral lumbar (L_{1-2}) nerve roots. To obtain preparations with a defined boundary, rostral brainstem tissue including the pons was manually sectioned with a razor blade based on the constancy of ventral surface anatomical landmarks that we have revealed here (Figure 4-1; see also Appendix III Figure A3-1). The desired rostrocaudal sectioning level was histologically verified after the electrophysiological experiments (Figure A3-1,2,3). Preparations were fixed with the ventral side up at the spinal cord to the bottom silicone layer of the superfusion chamber with insect pins (volume 1.5 ml). Further stabilization was achieved by suction electrodes used to record nerve activities (see below). Superfusate was administered at a flow rate of

5 ml min⁻¹ via a peristaltic pump (Watson-Marlow Alitea-AB, Sin-Can, Calgary, Alberta, Canada). Temperature in the recording chamber was kept at 25-27°C (TC-324B, Harvard Apparatus, Saint-Laurent, Quebec, Canada).

Superfusate with [Ca²⁺] (Heinemann et al., 1977; Nicholson et al., 1978; Hansen, 1985; Richter & Acker, 1989; Trippenbach et al., 1990; Nilsson et al., 1993; Puka-Sundvall et al., 1994; Somjen, 2002; Brown et al., 2004) and [K⁺] (Leusen, 1972; Hansen, 1985; Somjen, 2002; Brown et al., 2004) resembling most common values in the extracellular space of brain tissue in vivo, i.e. 1.2 mM and 3 mM, respectively, contained (mM): 120 NaCl, 3 KCl, 1.2 CaCl₂, 1 MgCl₂, 1.25 NaH₂PO₄, 26 NaHCO₃ and 30 D-glucose (pH adjusted to 7.4 by gassing with 95% O₂, 5% CO₂).

preBötC-related rhythms in brainstem-spinal cords in standard solution were compared with those in solution of elevated Ca²⁺, K⁺ and Mg²⁺ (2.4, 6.2 and 1.3 mM, respectively), very similar to that in the first study (Suzue, 1984) and numerous follow-up reports on this and other isolated respiratory networks (e.g. Oshima et al., 2000; Herlenius et al., 2002; Iizuka, 2004; St. John et al., 2005; Kuwana et al., 2006; Onimaru et al., 2006). This “Suzue-type” solution contained (mM): 120 NaCl, 6.2 KCl, 2.4 CaCl₂, 1.3 MgCl₂, 1.25 NaH₂PO₄, 26 NaHCO₃ and 30 D-glucose (pH adjusted to 7.4 by gassing with 95% O₂, 5% CO₂). In a related series of experiments, Ca²⁺ and K⁺ in the standard solution were varied between 1.2 and 6 mM, and 3 and 10 mM, respectively.

PreBötC-related rhythms were also studied in 600 µm thick “m-preBötC slices” with the preBötC in the middle (Ruangkittisakul et al., 2006). After removal of the cerebellum and sectioning close to the caudal cerebellar artery (De Araujo & Campos, 2005) (Figure 4-1), the brainstem of P0-4 SD (n = 8) or W rats (n = 28) was glued rostral side down to a metal plate and transferred to a vibrating microtome (Leica VT1000S, Leica Microsystems, Richmond Hill, Ontario, Canada). Serial transverse sectioning (100 µm) was stopped, and one “rhythmic” slice was cut, when specific landmarks were reached, in particular subregions of the inferior olive (Figure 4-1 and Appendix III Figure S1). Slices were fixed caudal side up with insect pins in the recording chamber and superfused with

standard saline in which Ca^{2+} and K^{+} were varied between 1 and 1.8 mM and 3 and 10 mM, respectively, at either 1 or 2 mM Mg^{2+} (Ruangkittisakul et al., 2006).

Rolipram (Sigma-Aldrich, Canada), a phosphodiesterase-4 blocker (O'Donnell & Zhang, 2004) stimulating inspiratory rhythm (Ruangkittisakul & Ballanyi, 2006; Ruangkittisakul et al., 2006), was kept frozen in stock solution (1 mM in dimethyl sulfoxide). Chemicals for salines were purchased from Fisher Scientific (Oakville, Ottawa, Ontario, Canada).

4.2.2 Electrophysiological Recording

Discharge of preBötC-driven motoneurons providing inspiratory motor output in brainstem-spinal cord preparations (Smith et al., 1990; Ballanyi et al., 1999) was recorded from ventral spinal (C_{3-4}) and cranial (hypoglossal) nerve roots with suction electrodes (outer diameter 80-250 μm) filled with standard superfusate. In brainstem preparations with a complete spinal cord, activity was recorded simultaneously from C_{3-4} and ventral L_{1-2} roots, the latter containing axons of pre-/post-inspiratory active motoneurons that appear to be driven by the pFRG and innervate expiratory abdominal muscles (Janczewski et al., 2002; Iizuka, 2004). Neuronal population activity was recorded with a differential amplifier ($\times 10000$, DAM 50, World Precision Instruments, Sarasota, FL, USA), bandpass-filtered (0.3-3 kHz) and integrated. In the slices, suction electrode recording was done at the caudal surface from the ventral respiratory column containing the preBötC (Alheid et al., 2004), in most cases combined with recording from one hypoglossal nerve root. Signals were fed into a computer (sampling rate 1 kHz) via a digital recording system (Powerlab/8SP, ADInstruments, Colorado Springs, CO, USA).

4.2.3 Data Analysis

Respiratory-related activity of brainstem-spinal cord preparations and slices was continuously recorded and quantified by measuring every 20 min over 2 min time periods the frequency of rhythm and single burst duration. Longevity of rhythms was defined as the time from start of recording until the time when the interval between consecutive bursts exceeded 1 min. Burst duration was defined, using Clampfit software (Molecular Devices, Union City, CA, USA), as the time interval from when the signal increased

above and decreased below a threshold set at 10% of the peak amplitude value for that burst. Rhythms modified by changing superfusate cation composition or adding rolipram were analyzed over a time period of 2 min at steady-state. Values are reported as means \pm S.E.M. except for histological analyses where means \pm S.D. were determined. Significance of values was determined by Student's one-sample t test using SigmaPlot (Systat software, Point Richmond, CA, USA). Significance was defined as *p <0.05 and **p <0.01.

4.2.4 Histology

For histological analysis after the experiments, both aspects of transected brainstem-spinal cords were fixed in phosphate buffer (1:2 mixture of 0.1 M NaH₂PO₄ + 0.1 M Na₂HPO₄ in H₂O, pH 7.2) containing 4% paraformaldehyde (all agents from Sigma). For staining after >15 min of fixation, preparations were incubated in phosphate buffer for at least 2 min and subsequently immersed 90 s for en bloc brainstems and slices and 45 s for 200-250 μ m thick sagittal brainstem-pons slices in a solution consisting of 1% thionin acetate (Sigma) in a mixture of 0.1 M sodium acetate trihydrate and 0.1 M acetic acid (Fisher). After staining, preparations were first "washed" with phosphate buffer (2 min) and then with 50% ethanol (4 min) before returning to phosphate buffer for 2 min. Subsequently, preparations were transferred to a Petri dish and photographed (PL-A686 6.6 megapixel camera, Capture-SE software, PixeLINK, Ottawa, Ontario, Canada) in phosphate buffer under a stereo microscope (Zeiss-SR15, magnification x32; Carl Zeiss, Jena, Germany).

4.2.5 Defined Sectioning of Brainstem-Spinal Cords

Brainstem-spinal cords with defined rostral boundary were generated using ventral brainstem surface landmarks (Figure 4-1, A3-1). Specifically, we found that the vagal nerve is located 0.06 ± 0.05 mm (n = 5) caudal to the caudal end of VII (VII_c) used as reference, whereas the location of the caudal cerebellar artery matches well with the rostral border of VII, i.e. 0.74 ± 0.16 mm (n = 14) vs. 0.76 ± 0.07 mm (n = 16) rostral to VII_c, respectively. The area covered by the most rostral hypoglossal nerve root spans the proposed (Smith et al., 1991; Ruangkittisakul et al., 2006) extension of the preBötC

between 0.4 and 0.6 mm caudal to VII_c, with its rostral end located 0.41 ± 0.13 mm ($n = 5$) caudal to VII_c (Figure 4-1, A3-1).

preBötC slice boundaries can be determined “online” by comparing respiratory marker nuclei in (pre)rhythmic slices with those in a reference brainstem atlas (Ruangkittisakul et al., 2006). The rostrocaudal locations of the marker structures, and thus slice boundaries, are referred to their distance from VII_c. Here, we used the atlas to identify the rostral boundary of transected brainstem-spinal cords (Figure 4-1, A3-1,2,3). This method was not suited to determine the boundary of preparations transected between VII_c and the inferior olive due to lack of marker structures. In these cases, the boundary was determined by measuring the distance in sagittal slices between VII_c and the caudal surface of the rostral aspects of the sectioned preparations (Figures A3-2, A3-3). Analysis of the sagittal sections revealed a distance between inferior olive and VII_c of 0.16 ± 0.03 mm ($n = 5$), similar to our previous value (0.13 ± 0.03 mm, $n = 26$) based on 50 μ m transverse serial sections (Ruangkittisakul et al., 2006).

4.2.6 Ventral Respiratory Column Structures in Newborn Rat Brainstem-Spinal Cords

As one major aim, we investigated the dependence of fictive respiratory rhythms in brainstem-spinal cords on their rostral boundary. We restricted our analysis to preparations without pons as influences of this structure on respiratory activity in this model were previously studied (Monteau et al., 1989; Errchidi et al., 1991; see also Alheid et al., 2004).

In the original voltage-sensitive dye imaging study on newborn rat brainstem-spinal cords, the pFRG was defined as a pre-/post-inspiratory active neuronal group, located ventrolateral to VII and close to the ventral surface (Onimaru & Homma, 2003). More recently, Onimaru et al., (2006) proposed that the pFRG may include regions up to 0.2 mm caudal to VII_c (Figure 4-1). Moreover, cells with pFRG-like activity pattern are also distributed caudal to that area (Arata et al., 1990; Smith et al., 1990; Ballanyi et al., 1999; Onimaru et al., 2003).

Compared to the RTN/pFRG, the preBötC was proposed to have a more defined rostrocaudal extension of 0.2 mm, centred 0.5 mm caudal to VII_c (Smith et al., 1991; Ruangkittisakul et al., 2006) (Figure 4-1). Inspiratory neurons seem to be by far the major respiratory neuron class in thin preBötC slices. However, in less-reduced brainstem preparations a variety of respiratory neuron classes including pFRG-like cells are active within the region spanned by the preBötC (Arata et al., 1990; Smith et al., 1990; Schwarzacher et al., 1995; Sun et al., 1998; Onimaru et al., 2003; Paton et al., 2006). The area between preBötC and VII_c contains the BötC (Figure 4-1) with a large number of expiratory neurons in addition to other types of respiratory cells (Feldman, 1986; Sun et al., 1998). Due to this overlap in the distribution of distinct respiratory neuron classes within the rostral ventrolateral respiratory column and other reasons, results from transection experiments should be interpreted with caution (Wilson et al., 2006).

4.3 Results

First, we studied inspiratory cervical nerve rhythms in three groups of brainstem-spinal cords with the boundary (i) slightly rostral to VII (thus including the BötC and RTN/pFRG), (ii) between VII and preBötC, and (iii) at or into the rostral preBötC border (Figure 4-1).

4.3.1 Inspiratory Cervical Rhythm in Transected Brainstem-Spinal Cords

The mean boundary of six preparations with VII was 0.83 ± 0.08 mm rostral to VII_c (Figure 4-2). In standard 1.2 mM Ca²⁺, 3 mM K⁺ solution, these brainstems generated cervical rhythm with an initial frequency of 6.9 ± 0.8 bursts min⁻¹ and a burst duration of 0.60 ± 0.05 s (Figure 4-2). After 3 h of recording, burst rate did not change (7.1 ± 0.35 bursts min⁻¹), whereas burst duration decreased to 0.40 ± 0.02 s. Raising superfusate K⁺ from 3 to 6.2 mM (as in “Suzue-type” solution) after the 5 h recording period reactivated rhythm, which stopped after 298 min in one preparation lacking 10% of VII, and

increased mean burst rate above control (8.7 ± 1.2 bursts min^{-1} , $n = 6$) with no stimulating effect on burst duration (Figure 4-2).

The mean boundary of seven medullas cut between VII and preBötC was 0.25 ± 0.04 mm caudal to VII_c (Figure 4-3). The initial burst rate of 9.4 ± 0.7 bursts min^{-1} decreased to 8.1 ± 0.6 bursts min^{-1} within 20 min and remained rather stable for >2 h in five cases. Burst duration decreased from initially 0.47 ± 0.02 s to 0.24 ± 0.06 s within 2 h, but remained stable thereafter (Figure 4-3). In three preparations, rhythm stopped after 2-3 h, whereas four preparations showed rhythm for >4 h (mean longevity 236 ± 26 min, $n = 7$). 6.2 mM K⁺ reactivated rhythms with rate 6.7 ± 0.6 and duration 0.45 ± 0.04 s while cAMP-elevating agent rolipram (1 μM) reactivated rhythms with rate 6.9 ± 0.9 bursts min^{-1} and duration 0.36 ± 0.08 s (Figure 4-3).

The mean boundary of six preparations with rostrally exposed preBötC was 0.39 ± 0.04 mm caudal to VII_c (Figure 4-4). Initial burst rate was 9.3 ± 1.7 bursts min^{-1} , but decreased monotonically until rhythm stopped spontaneously (mean longevity 71.5 ± 14.1 min, $n = 6$). In three preparations still active after 80 min of recording, burst rate at that time was 3.3 ± 0.3 bursts min^{-1} and burst duration was 0.17 ± 0 s (Figure 4-4). K⁺ at 6.2 mM and rolipram (1 μM) reactivated rhythms with rates slightly lower than (7.5 ± 1.2 vs. 8.3 ± 0.5 bursts min^{-1}) and durations similar to (0.32 ± 0.07 vs. 0.30 ± 0.08 s) the initial value (Figure 4-4). Four preparations with the rostral boundary 0.45 mm caudal to VII_c, and thus likely to be very close to the preBötC centre (Figure 4-1), did not generate respiratory rhythm in either 3 mM or 6.2 mM K⁺. In three of these cases, elevated K⁺ induced <0.3 s irregular cervical nerve bursts with >15 events min^{-1} and a distinct activity consisting of a >1 min massive discharge (Figure A3-4).

Analysis of pooled data from the above groups of brainstem-spinal cord preparations revealed a significant correlation between rostral boundary and longevity of rhythm, but not between boundary and burst rate, or initial frequency and longevity (Figure 4-5).

4.3.2 Pre-/post-inspiratory Lumbar Rhythm in Transected Brainstem-Spinal Cords

In a further approach, we studied the dependence of pre-/post-inspiratory lumbar nerve bursting (Janczewski et al., 2002) on the rostral boundary of en bloc brainstems with complete spinal cord. Ten preparations with boundaries <0.6 mm rostral to VII_c, thus containing <79% of VII, did not show pre-/post-inspiratory lumbar bursting, but generated regular cervical inspiratory rhythm (Figure 4-6). On the contrary, seven preparations with boundaries >0.6 mm rostral to VII_c showed both pre-/post-inspiratory lumbar and inspiratory cervical nerve bursting (Figure 4-6).

4.3.3 Hypoglossal Nerve Activity in Transected Brainstem-Spinal Cords

Next, we assessed whether inspiratory hypoglossal rhythms in en bloc preparations also depend on the transection level. In five preparations cut between preBötC and VII_c (mean boundary 0.20 ± 0.04 mm caudal to VII_c), burst rates in 3 mM K⁺ of synchronous rhythms in cervical and most rostral hypoglossal nerve roots were identical. After an initial time period of 8.7 ± 1.1 bursts min⁻¹, burst rate stabilized at 7.1 and 7.7 bursts min⁻¹ between 20 and 120 min, but decreased to 4.8 ± 1.0 and 4.8 ± 1.3 bursts min⁻¹ at 180 and 240 min, respectively (Figure 4-7). The amplitude of rostral hypoglossal root bursts was stable during recording periods >4 h in some cases (Figures 4-7, 4-8). Also their duration remained stable at 0.4 s, whereas cervical burst duration decreased from 0.4 s to <0.3 s after 1 h of recording (Figure 4-7). Hypoglossal burst duration was also similar to control when rhythm was reactivated after spontaneous arrest by elevated K⁺ (6.2, 7, 9 mM) or rolipram (1 μM), all of which restored cervical burst duration to control values (Figure 4-7). Only 9 mM K⁺ increased the burst rate of re-evoked rhythms above initial control values. Under all these conditions, hypoglossal and cervical rhythms showed 1:1-coupling (Figure 4-7). Neither K⁺ nor rolipram affected the amplitude of hypoglossal or cervical bursting. In 12 additional preparations with similar boundaries caudal to VII_c, the amplitude of bursting of rostral hypoglossal roots remained constant or increased during the first hour of recording (Figure 4-8).

In contrast, burst amplitude, but not duration, decreased within 20-90 min after start of recording in caudal hypoglossal roots of brainstem-spinal cords without VII (Figure 4-8).

Bursting disappeared in 1 of 4 preparations and stabilized after 1 h in the other cases at $17 \pm 6.9\%$ of the initial value. In four preparations with VII (mean boundary 0.11 ± 0.07 mm rostral to VII_c), amplitude of rostral hypoglossal root bursts fell to $23 \pm 4.7\%$ of initial values after 20-50 min of recording. Furthermore, the depression was more pronounced ($6.8 \pm 2.8\%$) after similar time periods in four preparations with complete VII (Figure 4-8).

4.3.4 Rhythm in preBötC Slices

Next, we compared inspiratory-related rhythms in 1.2 mM Ca^{2+} and 3 mM K^+ between en bloc medullas and 600 μm m-preBötC slices with a mean rostral boundary 0.24 ± 0.11 mm ($n = 5$) caudal to VII_c. The initial rate of bursting in the region of the ventral respiratory column containing the preBötC was 7.2 ± 1.0 bursts min^{-1} , but decreased within 20 min to 5.2 ± 0.8 bursts min^{-1} . Burst rate remained approximately at that value until rhythm stopped after 60-140 min (mean longevity 87.8 ± 16.8 min, $n = 5$) (Figure 4-9). preBötC burst duration fluctuated between 0.5 and 0.8 s within the first 80 min of recording. As with cervical bursts in en bloc medullas, the rate of hypoglossal bursts was 1:1-coupled to preBötC activity, while their duration was shorter and decreased from an initial value of 0.39 ± 0.07 to 0.30 ± 0.14 after 1 h (Figure 4-9). After spontaneous arrest, preBötC and hypoglossal rhythms were restored by 6.2 mM K^+ or rolipram (1 μM) with rates comparable to those in 3 mM K^+ 20-40 min after start of recording. While the duration of K^+ -induced preBötC and hypoglossal bursts was also similar to control, rolipram-induced bursts were shorter (Figure 4-9).

The limited longevity of slice rhythms in standard 1.2 mM Ca^{2+} and 3 mM K^+ solution contrasted with 4 h longevity of rhythm in m-preBötC slices with similar boundaries in our previous study (Ruangkittisakul et al., 2006). Thus, we tested next whether this difference may be due to use of 1 mM instead of 1.2 mM Ca^{2+} in that report. Indeed, rhythm in five slices with the rostral boundary 0.21 ± 0.08 mm caudal to VII_c lasted >2 h and even >3 h in three of these cases in 1 mM Ca^{2+} . Thus, longevity was significantly greater (211.4 ± 39.2 min, $P < 0.05$) in 1 mM Ca^{2+} compared to slices in 1.2 mM Ca^{2+} (Figure 4-10). Also in 1 mM Ca^{2+} , hypoglossal bursts showed 1:1-coupling to preBötC

bursting, but their amplitude fluctuated by 40% with a period of 20-40 min in two slices. Rhythm was effectively restored after spontaneous arrest by both K^+ (6-9 mM) and rolipram (1 μ M) (Figure 4-10).

Next, we studied whether slice rhythms are modified by raising Mg^{2+} from 1 to 2 mM as was used by Ruangkittisakul et al., (2006). In four slices with mean rostral boundary 0.10 ± 0.07 mm caudal to VII_c, longevity of rhythm (216 ± 37 min, $n = 4$) was very similar in 1 mM Ca^{2+} , 2 mM Mg^{2+} to that in 1 mM Ca^{2+} , 1 mM Mg^{2+} slices and significantly ($P < 0.05$) greater than in 1.2 mM Ca^{2+} , 1 mM Mg^{2+} slices. Also two of these slices showed fluctuations in hypoglossal burst amplitude (Figure 4-10). In three slices, synchronous preBötC and hypoglossal rhythms were stable for >3 h, in two cases for >4 h (Figures 4-10, 4-11). Burst rates during these time periods ranged from 7 to 9.4 bursts min^{-1} , which was higher than in 1.2 mM Ca^{2+} (after 40-60 min). The duration of preBötC and hypoglossal bursts decreased from initially 0.75 ± 0.06 s to 0.49 ± 0.03 s and 0.45 ± 0.06 s to 0.21 ± 0.08 s after 3 h, respectively (Figure 4-11). After spontaneous arrest, rhythm of similar burst duration was restored by K^+ (6.2, 7, 9 mM) or rolipram (1 μ M). K^+ at 6.2 mM and 7 mM as well as rolipram restored bursting at rates similar to control, whereas 9 mM K^+ induced a faster rhythm at 15 bursts min^{-1} (Figure 4-11).

4.3.5 Ca^{2+} Sensitivity of Inspiratory Rhythms in Transected Brainstem-Spinal Cords

As one major finding, inspiratory-related rhythms in en bloc medullas with distinct rostral boundaries shared various features with those in preBötC slices. These features included a similar limited longevity of rhythms in brainstem-spinal cords with exposed preBötC and m-preBötC slices. In the slices, longevity and burst rate were greatly enhanced by lowering superfusate Ca^{2+} from 1.2 mM to 1 mM. This suggests that, conversely, raising Ca^{2+} above 1.2 mM may depress preBötC-related (motor) rhythms. In the Introduction, we hypothesized that raised Ca^{2+} may be responsible for block of cervical rhythms in transected brainstem-spinal cords. The studies reporting such block (Onimaru & Homma, 1987; Onimaru et al., 2006) used “Suzue-type” solution containing 2.4 mM Ca^{2+} and also higher K^+ (6.2 mM) and Mg^{2+} (1.3 mM) compared to the standard solution used here.

We tested the effects of this solution on five brainstem-spinal cord preparations that were transected between preBötC and VII. Raising first K^+ from 3 to 6.2 mM changed neither the rate nor the duration of cervical bursts, whereas subsequent elevation of Ca^{2+} (from 1.2 to 2.4 mM) and Mg^{2+} (from 1 to 1.3 mM) blocked rhythm within <10 min (Figure 4-12). Rhythm with a rate and burst duration similar to control was reactivated in that solution by 10 mM K^+ , whereas 8 mM K^+ was less effective (Figure 4-12). Six preparations cut more caudally (at the rostral preBötC border) responded similarly. However, 10 mM K^+ reactivated rhythm with a burst duration similar to controls, but at a lower rate, and 8 mM K^+ did not restore bursting (Figure 4-12). This high Ca^{2+}/K^+ (Mg^{2+}) solution also modified non-respiratory activity in three preparations with boundaries 0.45 mm caudal to VII_c that did not generate respiratory rhythm (Figure A3-4).

The fact that Ca^{2+} was doubled, whereas Mg^{2+} was raised by only 30%, suggests that Ca^{2+} is responsible for depression of cervical rhythm. To test this, eight preparations with exposed preBötC were kept in 6.2 mM K^+ to maintain stable rhythm and were superfused with 1.8 mM Ca^{2+} at constant Mg^{2+} (1 mM). This modest Ca^{2+} rise by 0.6 mM decreased burst rate within <10 min from 5.5 ± 0.9 to 1.1 ± 0.4 bursts min^{-1} ($P < 0.01$; block of rhythm in 3 cases) (Figure 4-13). The inhibition by Ca^{2+} of cervical rhythm was accompanied in >50% of cases by non-respiratory bursting that was absent or less pronounced, in hypoglossal recordings (Figure 4-13). Thus, Ca^{2+} effects were quantified by analyzing only synchronous cervical and hypoglossal bursts, which were 1:1-coupled during both control and raised Ca^{2+} (Figure 4-13). In four of the preparations exposed to 1.8 mM Ca^{2+} , a subsequent Ca^{2+} rise to 2 mM depressed rhythm further to 0.3 ± 0.3 bursts min^{-1} ($p < 0.01$; block of rhythm in 3 cases) (Figure 4-14). Rhythm reappeared at 4.8 ± 0.5 bursts min^{-1} with burst duration similar to control in 10 mM K^+ after block by 2 mM Ca^{2+} , whereas 8 mM K^+ was less effective (2.4 ± 1.1 bursts min^{-1}). In contrast to preparations transected between VII and preBötC, cervical rhythm in 6.2 mM K^+ was not blocked by 1.8-2.4 mM Ca^{2+} in preparations with (portions of) VII (Figures 4-13, 4-14). The $[Ca^{2+}]$ to effectively depress or abolish rhythm increased significantly with increasing amount of tissue rostral to the preBötC (Figure 4-14).

4.3.6 Ca²⁺ Block of preBötC Slice Rhythm

The latter results in brainstem-spinal cord preparations suggested that the capability of the preBötC to generate rhythm in moderately elevated K⁺ is substantially impaired by raising Ca²⁺ by only 0.6 mM. In a final approach, we investigated whether preBötC bursting and inspiratory motor rhythm in slices with robust longevity in 1 mM Ca²⁺ and 3 mM K⁺ have a similarly high sensitivity to acutely elevated superfusate Ca²⁺.

In 10 slices with a mean rostral boundary 0.19 ± 0.10 caudal to VII_c, raising Ca²⁺ from 1 to 1.5 mM depressed within 10-15 min the rate of 1:1-coupled preBötC and hypoglossal bursting from 8.1 ± 0.8 to 1.2 ± 0.4 bursts min⁻¹ ($p < 0.01$; block of rhythm in 4 cases) (Figure 4-15). Both rhythms started to recover within 10-20 min after return to 1 mM Ca²⁺, but mean recovery was <50% of control even after 30 min of washout of 1.5 mM Ca²⁺. The incomplete recovery of burst rates was not caused by time-dependent spontaneous slowing of rhythm in 3 mM K⁺ as inspiratory frequency was stable during comparable time periods in seven control slices with a mean rostral boundary 0.18 ± 0.11 mm caudal to VII_c (Figure 4-15).

For comparison with our findings in brainstem-spinal cords, the effects of 1.8 mM Ca²⁺ in 6.2 mM K⁺ were tested in six m-preBötC slices with a mean rostral boundary 0.26 ± 0.12 mm caudal to VII_c. Synchronous preBötC and hypoglossal burst rates were depressed by 1.8 mM Ca²⁺ from 6.1 ± 0.8 to 0.2 ± 0.2 bursts min⁻¹ ($p < 0.01$; block of rhythm in 5 cases). Elevating K⁺ to 8 mM and 10 mM reactivated both types of rhythms at 3.2 ± 0.7 and 10.1 ± 1.9 bursts min⁻¹, respectively, with burst durations similar to control (Figure 4-15).

4.4 Discussion

Inspiratory-related rhythms in newborn rat brainstem-spinal cords containing the preBötC inspiratory centre (plus more rostral respiratory regions) and preBötC slices were similar in physiological $\text{Ca}^{2+}/\text{K}^{+}$ solution. The reduced longevity of inspiratory rhythms in en bloc preparations with exposed preBötC and slices is caused by a strong extracellular $\text{Ca}^{2+}/\text{K}^{+}$ antagonism. We discuss whether the absence of pre-/post-inspiratory rhythms in brainstems lacking a major portion of VII may be due to reduction of the RTN/pFRG, whereas block of hypoglossal bursting in preparations with (portions of) VII may possibly result from interstitial accumulation of inhibitory neuromodulator(s).

4.4.1 Implications from Defined Sectioning of Isolated Brainstem-Spinal Cords

In early postnatal rats, the constancy of rostrocaudal extensions of marker brainstem nuclei enables the generation of preBötC slices with defined boundaries (Ruangkittisakul et al., 2006). Based on a similar constancy of ventral brainstem surface landmarks, we generated here brainstem-spinal cords with a defined rostral boundary. Such preparations with rostrally exposed preBötC allow the study of how the preBötC drives hypoglossal and spinal motor networks with as little as possible interference from the more rostral BötC and RTN/pFRG. Also preBötC interactions with the RTN/pFRG and/or BötC should be studied in defined preparations where the extension of the rostral ventral respiratory column can be determined within a few tens of micrometres. The finding of stable cervical rhythm in en bloc preparations cut between VII and preBötC is very similar to our previous report (Smith et al., 1991). As discussed below, use of 2-2.4 mM Ca^{2+} (instead of 1.5 mM Ca^{2+} in the latter study) explains depression/block of rhythm observed by others upon similar transection (Onimaru & Homma, 1987; McLean & Remmers, 1994; Onimaru et al., 2006).

Despite caveats (Wilson et al., 2006), sectioning experiments can increase understanding of structure-function relationships of respiratory networks. For example, the RTN/pFRG in the rostral aspect of transected newborn rat medullas remained functional without the preBötC (Onimaru et al., 2006). Furthermore, transection close to VII_c abolished

expiration in juvenile rats in vivo (Janczewski & Feldman, 2006). Those authors hypothesized that breathing is generated by anatomically separate rhythm generators; one generating active expiration located close to VII in the region of the RTN/pFRG, the other generating inspiration located more caudally in the preBötC. The latter study supported the conclusion from a previous combined in vivo/in vitro report that the pFRG ultimately drives expiratory abdominal muscles in vivo via ipsilateral medullary premotoneurons located caudal to the preBötC that project to contralateral pre-/post-inspiratory lumbar motoneurons (Janczewski et al., 2002). The findings of Janczewski & Feldman (2006) also support the hypothesis, based on a differential sensitivity in vivo and in vitro of preBötC- and pFRG-related rhythms to opioids, that these rhythmogenic respiratory groups form a functionally coupled dual respiratory centre (Mellen et al., 2003). We found that the brainstem level critical for pre-/post-inspiratory lumbar bursting is close to the rostral and not caudal end of VII, at least in isolated neonatal rat brainstems. It cannot be concluded however that pFRG networks, which presumably generate this expiratory motor behaviour, are only located rostral to that sectioning level. For example, if the axons of caudal RTN/pFRG interneurons or premotoneurons project rostrally first, cutting would affect this pathway.

4.4.2 Modulation of preBötC Rhythms by Neighboring Brainstem Regions

Burst rates of cervical rhythm in physiological $\text{Ca}^{2+}/\text{K}^{+}$ did not substantially differ between en bloc medullas with VII and those cut close to the rostral preBötC boundary. This suggests that rhythmogenic preBötC networks are not subjected to a major specific frequency modulation by rostrally neighbouring portions of the BötC or RTN/pFRG, in line with our findings in en bloc medullas (Smith et al., 1991) and, more recently, in preBötC slices (Ruangkittisakul et al., 2006). In extension of these studies, we show that the longevity of cervical and hypoglossal rhythms is limited to <1.5 h, when the transection is at, or removes some portion of, the rostral preBötC. As one explanation, long-term preBötC rhythm in en bloc medullas may depend on drive from more rostral respiratory networks (Feldman & Janczewski, 2006; Onimaru & Homma, 2006). However, rhythm in 1.2 mM Ca^{2+} and 3 mM K^{+} lasted for considerably shorter time periods in 600 μm m-preBötC slices (1.5 h) than in en bloc medullas (4 h) with similar

rostral boundaries between preBötC and VII_c. This would suggest that caudal structures also drive the preBötC. But, since longevity of rhythms is greater in 600 μm compared to 500 μm -preBötC slices (Ruangkittisakul et al., 2006), it is more likely that the amount of neighbouring tissue, rather than a specific rostral or caudal (respiratory) structure, determines the strength of drive to the preBötC. In that regard, one of several possible explanations for spontaneous arrest of rhythm in 3 mM K^+ is a depletion of excitatory neuromodulator(s), which would occur more rapidly in preparations with exposed preBötC (Ruangkittisakul et al., 2006).

Sectioning at the preBötC border removes distal dendrites of preBötC neurons that extend 0.3-0.4 mm rostrocaudally (S. W. Schwarzacher & K. Ballanyi, unpublished observations). Sectioning thus reduces the connectivity and recurrent excitation within and between the bilaterally organized preBötC regions, which is presumably pivotal for rhythm generation at physiological K^+ (Ramirez et al., 2002; Del Negro et al., 2005). This would explain why rhythm stops after shorter time periods in highly reduced en bloc preparations. Inspiratory rhythms were reactivated by raised K^+ or the blocker of cAMP-specific phosphodiesterase-4 rolipram. The stimulatory action of rolipram supports previous assumptions of the pivotal role of cAMP for maintaining respiratory rhythm (Ballanyi et al., 1997, 1999; Richter et al., 1997; Ruangkittisakul et al., 2006). In addition to the spontaneous arrest of preBötC rhythm in physiological $\text{Ca}^{2+}/\text{K}^+$ solution, we showed a time-dependent decrease in the duration of preBötC and cervical/hypoglossal nerve bursts. Such “rundown” of burst duration (which was moderate for hypoglossal rhythm in en bloc preparations) was reversed by raised K^+ (and in most cases by rolipram) as a further indication of a proposed depletion of endogenous excitatory neurostimulator(s). This phenomenon has to be taken into account for studies analyzing neuromodulator effects on the strength of inspiratory activities in slice and en bloc models. Elevating superfusate K^+ for a stable burst duration may not be adequate as this would eventually decrease the sensitivity of preBötC networks to neuroactive agents such as opioids (Onimaru et al., 2006; Ruangkittisakul et al., 2006).

4.4.3 $\text{Ca}^{2+}/\text{K}^+$ Antagonism of preBötC Rhythms

One major finding of this study explains the limited longevity in physiological $\text{Ca}^{2+}/\text{K}^+$ of rhythms generated by the preBötC after rostral exposure (brainstem-spinal cords) or isolation (slices). In highly reduced en bloc medullas, raising Ca^{2+} by only 0.6 mM from 1.2 mM greatly depressed cervical and hypoglossal rhythms. This Ca^{2+} sensitivity of preBötC-driven motor systems is likely to be even higher as these preparations were kept at 6.2 mM instead of 3 mM K^+ for stabilization of rhythm, while further elevation of K^+ to 8-10 mM reversed the Ca^{2+} block. In line with that view, both the longevity and long-term burst rate of preBötC slice rhythms in 3 mM K^+ were substantially augmented in 1 mM instead 1.2 mM Ca^{2+} , whereas raising Ca^{2+} from 1 to 1.5 mM in 3 mM K^+ depressed burst rate to <20% of control. This supports our hypothesis that raised superfusate Ca^{2+} is responsible for depressed cervical rhythms in transected brainstem-spinal cords (Onimaru & Homma, 1987; McLean & Remmers, 1994; Onimaru et al., 2006). First, our findings suggest that preBötC slices are not active in 2.4 mM Ca^{2+} “Suzue-type” superfusate used by numerous groups (see Methods for references). Also, we propose that robust slice rhythm in 3 mM K^+ in our recent study (Ruangkittisakul et al., 2006) is, at least partly, related to use of 1 mM superfusate Ca^{2+} . As a third implication, longevity of rhythms in en bloc preparations with exposed preBötC will likely be substantially greater in 1 mM instead of 1.2 mM Ca^{2+} .

The finding that the Ca^{2+} block of rhythm is also revealed in preBötC recordings in the slices excludes the possibility that raised Ca^{2+} primarily affects (pre)motor circuits. The Ca^{2+} block of primary preBötC rhythm can, nevertheless, be indirect as suggested by the finding that block of slice rhythm by bath-application of persistent Na^+ channel blockers is mimicked by local injection of the agents into the raphe, but not the preBötC (Pace et al., 2007). Performing a similar test was beyond the scope of this study, as was to elaborate the mechanism of Ca^{2+} block. As one possibility, Ca^{2+} may inhibit preBötC cells or tonic neurons driving the preBötC via a more pronounced stimulatory effect on (tonic) inhibitory than on excitatory synapses (Jefferys, 1995). In fact, GABA_A and glycine receptors depress inspiratory bursting in newborn rat brainstem-spinal cords (Onimaru et al., 1990; Brockhaus & Ballanyi, 1998, 2000). Ca^{2+} -induced block of rhythm could also

be caused by Ca^{2+} screening of negative membrane surface charges (Hille, 2001; Somjen, 2002). However, if this was the main mechanism, raising Mg^{2+} from 1 to 2 mM should have a similar blocking effect on slice rhythms, while returning to normal Ca^{2+} should have reversed the depression. Alternatively, raised Ca^{2+} may have long-term effects on Ca^{2+} homeostasis in respiratory (drive) neurons with low Ca^{2+} buffering capacity (Alheid et al., 2002).

In line with our findings, early *in vivo* studies showed that Ca^{2+} injection into the ventriculo-cisternal space depresses breathing (Berndt et al., 1969; Leusen, 1972; Berkenbosch & Adan, 1974). In that regard, a $\text{Ca}^{2+}/\text{K}^+$ antagonism was proposed to compensate for respiratory depression by Ca^{2+} when K^+ was simultaneously injected (Leusen, 1972). Moreover, our results show that isolated preBötC rhythms at physiological K^+ are stimulated by decreasing superfusate Ca^{2+} . We chose 1.2 mM for our standard solution as a major number of *in vivo* studies reported values of 1.1-1.3 mM for interstitial Ca^{2+} in diverse brain tissue, including the ventral respiratory column (Heinemann et al., 1977; Nicholson et al., 1978; Richter & Acker, 1989; Trippenbach et al., 1990; Nilsson et al., 1993; Puka-Sundvall et al., 1994; Somjen, 2002). Respiratory rhythm was also revealed in 0.8 mM Ca^{2+} and 6.2 mM K^+ superfusate in 1 mm thick mouse brainstem slices (Rekling et al., 1996), while hypothalamic slices generate *in vivo*-like spontaneous activity in 0.75 mM, but not >1 mM Ca^{2+} (Pittman et al., 1981). Accordingly, “real” *in vivo* extracellular Ca^{2+} levels may be close to, or slightly less than, 1 mM. However, there may be a critical minimal Ca^{2+} level as 0.5 mM superfusate Ca^{2+} is a common epilepsy model (Konnerth et al., 1986; Jefferys, 1995). We propose that 1 mM Ca^{2+} is best suited to study isolated preBötC functions in 3 mM K^+ .

4.4.4 Relation of Hypoglossal Bursting with Cervical and preBötC Rhythms

Simultaneous recordings revealed 1:1-coupling of hypoglossal bursting with either cervical nerve activity (in *en bloc* medullas) or preBötC population activity (in slices). This argues against concerns that hypoglossal recordings may not necessarily be indicative of respiratory activity *in vitro*, in particular at hypothermia (St-John et al., 2004). However, the amplitude of hypoglossal bursts fluctuated periodically in 3 mM K^+ ,

1 mM Ca^{2+} and 1-2 mM Mg^{2+} in some slices. Elevating K^+ to 6.2-9 mM stabilized, and sometimes increased, the amplitude of hypoglossal (and preBötC) bursts and restored their durations to, or even beyond, the values during the initial phase of recordings. In contrast to a stable hypoglossal rhythm in the slices and (in rostral roots of) en bloc preparations transected close to or into the preBötC, rhythm was greatly depressed in all hypoglossal roots within 1 h in preparations containing (portions of) VII (for reasons, see below). This finding is important for studies devoted to the analysis of the function of hypoglossal neurons in en bloc medullas. For example, it was proposed that serotonin depresses hypoglossal, but not phrenic, motor output in brainstem-spinal cords (Monteau et al., 1990). In such studies, it is pivotal to test first for stable control hypoglossal nerve amplitudes.

4.4.5 Influence of Restricted Diffusion on Respiratory Activities in En Bloc

Medullas

Notably higher superfusate Ca^{2+} levels were necessary to block rhythm in less-reduced en bloc preparations, e.g. 3.6 mM in brainstems with complete VII. This is in line with the observation that 4 mM Ca^{2+} depressed cervical bursting in such preparations (Kuwana et al., 1998). As one explanation for this phenomenon, (respiratory) structures in the rostral medulla may be less sensitive to Ca^{2+} , thus being capable of driving the preBötC in high Ca^{2+} . Alternatively, the decreased Ca^{2+} sensitivity of inspiratory rhythms may result from the larger dimension of en bloc preparations, constituting a diffusion barrier for build-up, e.g. of a modest interstitial K^+ gradient (and a pH gradient) by an anoxic core that does not, however, appear to contain pivotal O_2 - or pH-sensitive inspiratory structures (Ballanyi et al., 1992, 1999; Brockhaus et al., 1993; Ballanyi, 2004). It may, though, be argued that the pre-/post-inspiratory activity pattern of newborn rat pFRG neurons in vitro results from hypoxia/anoxia in en bloc preparations with more rostral tissue as evoked hypoxia activated pre-inspiratory bursting in post-inspiratory ventral respiratory column neurons of adult rats (Schwarzacher et al., 1991). It may further be speculated that transection 0.6 mm or less rostral to VII_c reduces the anoxic core, inactivates these neurons and, consequently, silences lumbar pre-/post-inspiratory bursting. However, several findings argue against this hypothetical scenario. First, pre-inspiratory activity

was also induced in post-inspiratory neurons of the latter in vivo study by prolonged lung inflation or deflation during normoxia. Second, pre-/post-inspiratory abdominal muscle activity is seen in normoxic juvenile rats in vivo (Janczewski & Feldman, 2006). Furthermore, experimentally induced anoxia blocks the pre-inspiratory and greatly augments the post-inspiratory component of pFRG-related activities (Ballanyi, 2004), opposite to the above in vivo findings by Schwarzacher et al., (1991). Finally, rostral pFRG neurons are located within <300 μm from the ventral brainstem surface (Onimaru & Homma, 2003), whereas the anoxic core is restricted to tissue depths >700 μm (Brockhaus et al., 1993).

In preparations with a major amount of rostral tissue, extracellular $[\text{K}^+]$ is several millimolar higher in the vicinity of preBötC neurons than in the superfusate, due to the modest K^+ gradient (Brockhaus et al., 1993; Okada et al., 2005). These elevated interstitial K^+ levels may antagonize the depressing action of elevated superfusate Ca^{2+} as suggested by the finding that preBötC rhythm persisted in “Suzue-type” solution after transection of brainstem-spinal cords between the preBötC and VII, but was abolished upon subsequent removal of the transected rostral aspect of the preparation (Onimaru et al., 2006). Consequently, lower K^+ (e.g. 2 mM), may be used instead of 3 mM in en bloc preparations with more rostral tissue to compensate for changes in the interstitial $\text{Ca}^{2+}/\text{K}^+$ ratio. Hampered diffusion of raised Ca^{2+} into the tissue could also explain the attenuated blocking effect. However, this is not likely as millimolar superfusate Ca^{2+} concentrations equilibrate within minutes in this en bloc preparation, which does not show an interstitial Ca^{2+} gradient in control (Völker et al., 1995; Ballanyi et al., 1996; Kuwana et al., 1998). Also the longevity of hypoglossal rhythms depended on the rostrocaudal extension of en bloc medullas. We hypothesize that arrest of hypoglossal bursting in preparations with VII is caused by accumulation of inhibitory neuromodulator(s) and/or metabolite(s) depressing hypoglossal (pre)motoneurons, but not preBötC interneurons and cervical premotoneurons.

4.5 Summary

The isolated inspiratory centre generates robust rhythm in physiological cation solution. PreBötC rhythms are blocked by minor extracellular Ca^{2+} rises, but can be restored by elevation of extracellular K^+ . The dependence of inspiratory-related rhythms on this strong $\text{Ca}^{2+}/\text{K}^+$ antagonism decreases in en bloc preparations with increasing amount of tissue rostral to the preBötC. Based on these findings, we recommend the use of superfusate Ca^{2+} levels at the lower end of the physiological spectrum, i.e. 1 mM, for the study of functions of the isolated preBötC in physiological K^+ . In addition, one may consider the use of reduced superfusate K^+ (e.g. 2 mM) for studies of respiratory rhythms in en bloc preparations with extended rostral tissue. It should be considered further that hypoglossal rhythm is blocked in such less-reduced brainstem-spinal cords, whereas pre-/post-inspiratory lumbar bursting is absent in more reduced en bloc medullas. Our findings suggest that discrepant results using en bloc preparations with varying rostral boundaries may be partly explained by different dimensions, affecting diffusion of endogenous neuromodulators, rather than changes in specific structures present in more rostral respiratory regions. We hypothesize that the preBötC is more sensitive in such solutions to CO_2/H^+ , hypoxia/anoxia or neuromodulators such as (endogenous) opiates or substance P, all of which determine respiratory rhythm in vivo.

Figures

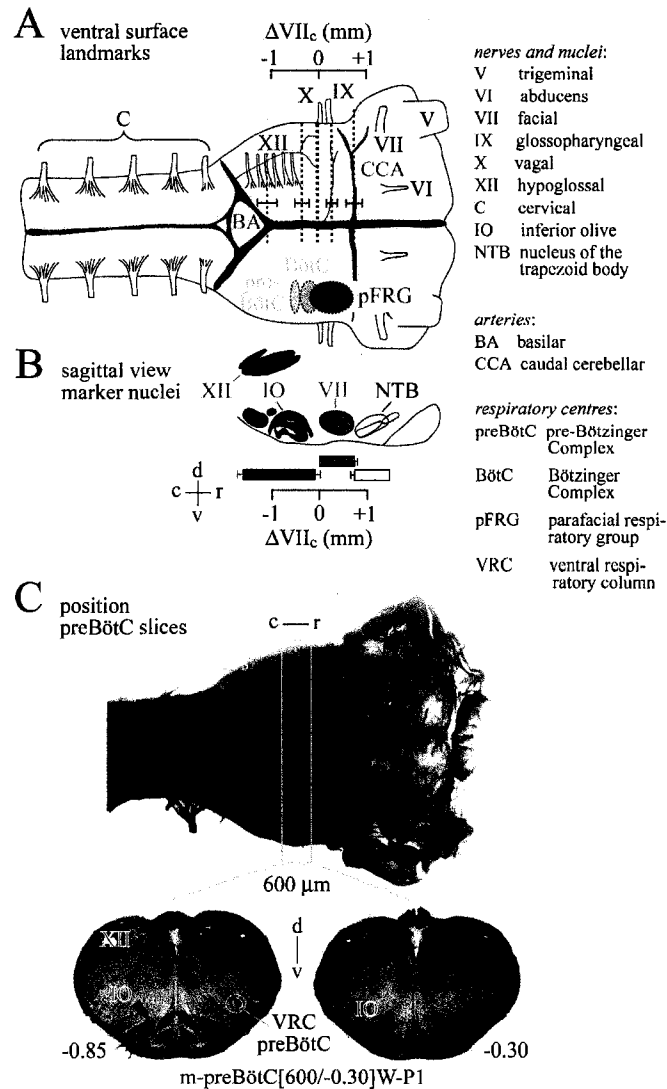


Figure 4-1 Regions of the ventral respiratory column and their ventral brainstem surface/nuclei landmarks in newborn rat brainstem-spinal cords. A, schematic drawing of ventral brainstem surface indicating the proposed locations of the pre-Bötzinger complex (preBötC), the Bötzingler complex (BötC) and the parafacial respiratory group (pFRG) of the ventral respiratory column (Alheid et al., 2004; Feldman & Del Negro, 2006). Vertical dotted lines and attached horizontal bars show means \pm S.D. of the positions of surface structures in Sprague-Dawley (SD) and Wistar (W) rats of postnatal days (P) 0-4, specifically cranial nerves (IX, X, XII) and arteries (BA, CCA). The positions of BA, CCA, IX and XII were quantified (in mm) in reference to dotted

line at X. The centre of the ~0.2 mm spanning preBötC is presumably located 0.5 mm caudal to the caudal end of VII nucleus (VII_c) (+ and - signs indicating the location of structures rostral or caudal to VII_c, respectively), and the VII nucleus extends 0.76 mm rostrocaudally (Smith et al., 1991; Ruangkittisakul et al., 2006; Figures A3-1, A3-2). The pFRG extends presumably from the rostral boundary of VII to ~0.2 mm caudal to VII_c (Onimaru & Homma, 2003, 2006; Onimaru et al., 2006). We found here that the caudal boundary of X nerve is located at VII_c, whereas the position of the CCA, at -0.74, matches well with the rostral end of VII. Furthermore, the proximal rostral boundary of the most rostral XII root coincides with the rostral preBötC border. The ΔVII_c scale in **A** is positioned based on findings from cuts at levels including the BA, XII and X lines (Figure A3-1). **B**, position projected onto a sagittal brainstem view of the respiratory marker nuclei IO, VII, XII (Ruangkittisakul et al., 2006) and NTB (Figure A3-2). Scales in **A** and **B** have identical dimensions and positions, thus allowing comparison of respiratory structures relative to VII, XII, IO and NTB. **C**, most surface structures of **A** are seen in a fixed and thionin-stained SD-P2 brainstem. The pink box indicates the mean position of 600 μm thick “m-preBötC slices” with the preBötC in the middle. The slice was labelled “m-preBötC[600/-0.30]W-P1” (m, middle; 600, slice thickness in μm; -0.30, rostral boundary in mm; W-P1, rat strain and age). Here, we classified slices according to their rostral instead of caudal boundary in contrast to Ruangkittisakul et al., (2006) to allow for comparison with rostral boundaries of brainstem-spinal cord preparations. Other abbreviations: r, rostral; c, caudal; d, dorsal; v, ventral.

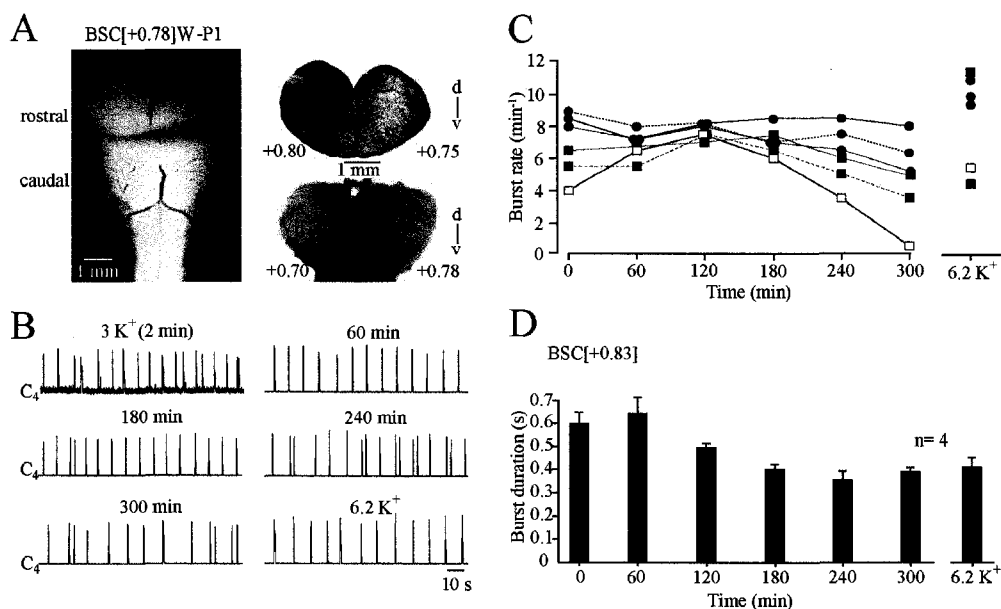


Figure 4-2 Cervical rhythm in 1.2 mM Ca²⁺, 3 mM K⁺ solution in brainstem-spinal cords with VII. **A**, left panel, transected brainstem-spinal cord (BSC) preparation from a P1 W rat with the rostral boundary 0.78 mm rostral to VII_c, thus a “BSC[+0.78]W-P1”, in standard saline after manual transection with a razor blade. Right panels, photographs of fixed and thionin-stained cut surfaces of corresponding rostral and caudal brainstem blocks after experiment. Numbers indicate transection level referred to VII_c (compare Figures 4-1, A3-1). The differing numbers on the left and right side of transection indicate a lateral tilt of the section plane. **B**, in the preparation of **A**, regular band-pass-filtered and integrated inspiratory-related bursting of the 4th ventral cervical (C₄) nerve rootlet was monitored for 5 h before superfusate K⁺ level was raised to 6.2 mM. **C**, burst rates of 6 BSC with a mean boundary 0.83 rostral to VII_c (BSC[+0.83]). Note that rhythms slowed down slightly during the 4th hour of recording and stopped in one preparation shortly before 5 h (after 298 min). Raising K⁺ to 6.2 mM after 5 h recording increased burst rates in all but one brainstems. **D**, burst duration in 4 preparations of **C**. Bars represent means and S.E.M. Numbers in the left part of the abscissa indicate the time period after start of recording.

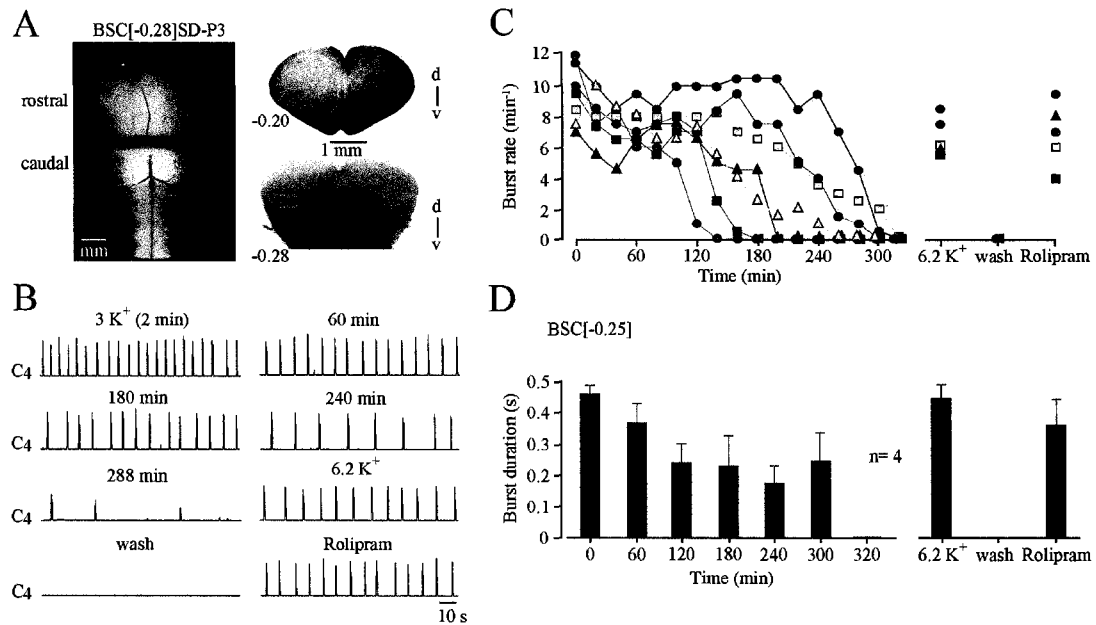


Figure 4-3 Cervical rhythm in brainstem-spinal cords cut between preBötC and VII. **A**, left panel, transected BSC[-0.28]SD-P3 preparation. Right panels, fixed and thionin-stained cut surfaces of corresponding rostral and caudal brainstem blocks. **B**, between 3 and 4 h of recording, inspiratory C₄ nerve bursting slowed down notably before rhythm stopped spontaneously after 288 min (last bursts shown). Very similar rhythm was reactivated by raising superfusate K⁺ to 6.2 mM and, after return to 3 mM K⁺ saline, by bath-application of the cAMP-elevating agent rolipram (1 μM). **C**, burst rates of 7 BSC[-0.25]. Note that rhythm persisted in 5 preparations for >3 h. **D**, burst duration in 4 preparations of **C** with very similar mean rostral boundary (BSC[-0.26]). Bars represent means and S.E.M. Numbers in the left part of the abscissa indicate the time period after start of recording.

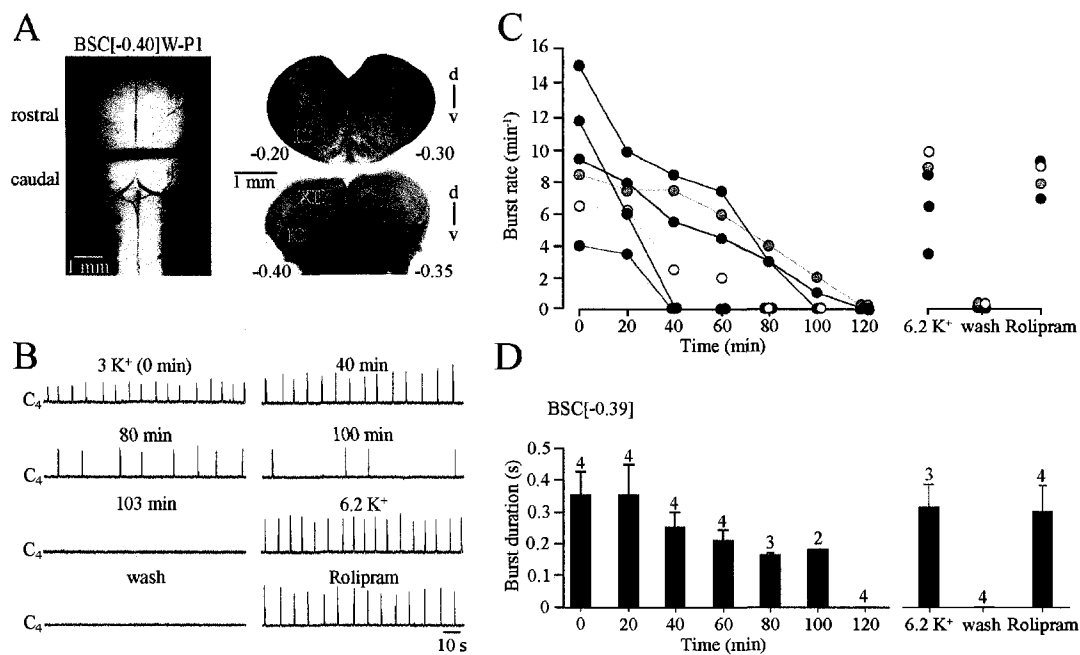


Figure 4-4 Cervical rhythm of brainstem-spinal cords with boundaries at or into the rostral preBötC border. **A**, left panel, transected BSC[-0.40]W-P1 preparation. Right panels, fixed and thionin-stained cut surfaces of corresponding brainstem blocks. **B**, C₄ bursting was revealed for >1 h before rhythm stopped after 103 min. Very similar rhythm was reactivated by 6.2 mM K⁺ and, after return to 3 mM K⁺, bath-application of rolipram (1 μM). **C**, burst rates of 6 BSC[-0.39]. Note that rhythm stopped spontaneously after time periods of 40-120 min. **D**, burst duration in 4 preparations of **C**. Bars represent means and S.E.M. Digits above bars indicate number of (still active) preparations tested. Numbers in the left part of the abscissa indicate the time period after start of recording.

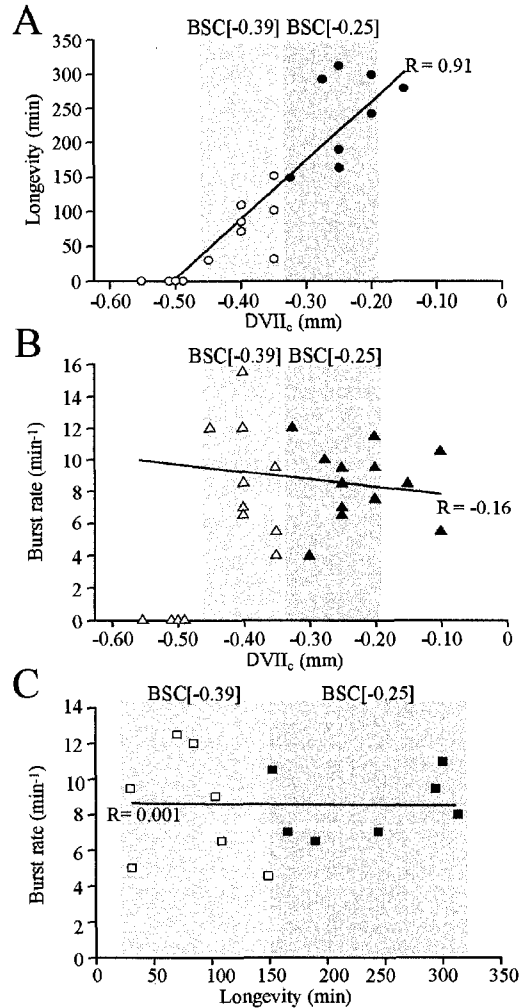


Figure 4-5 Correlation between rostral boundary, longevity and burst rate of cervical rhythm in brainstem-spinal cords. **A**, significant ($p < 0.01$) correlation between the longevity of cervical inspiratory rhythm and rostral boundary (R is correlation coefficient). In contrast, no significant correlations were revealed between burst rates (determined after 10 min of recording) and rostral boundaries (**B**) or longevity of rhythm (**C**). Grey areas indicate the two groups of preparations used for the analyses in Figures 4-3 and 4-4. Note that preparations with the rostral boundary at -0.50 or more caudal (thus caudal to the proposed preBötC centre) did not show respiratory rhythm (compare Figure A3-4). **A** and **C** contain less data points compared to **B** as longevity was not tested in all preparations.

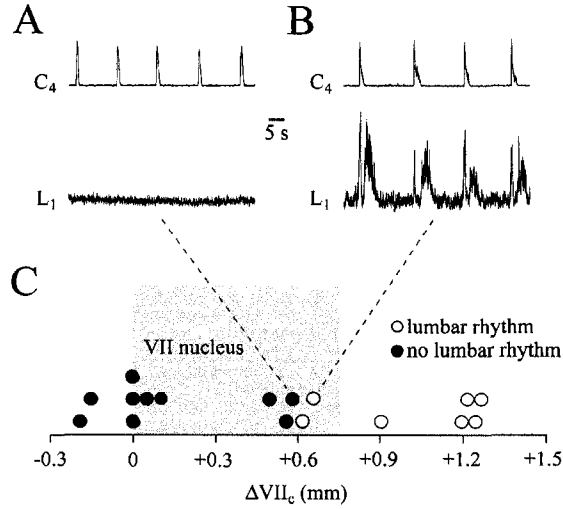


Figure 4-6 Dependence of pre-/post-inspiratory lumbar nerve bursting on rostral boundary of brainstem-spinal cords. **A**, a BSC[+0.58]W-P1 preparation generated stable inspiratory C₄ bursting, but did not show respiratory-related activity in the first ventral lumbar (L₁) root. **B**, pre-/post-inspiratory L₁ bursting was revealed in a BSC[+0.67]W-P0. **C**, plot of the occurrence (○) or absence (●) of lumbar pre-/post-inspiratory rhythm vs. the rostral boundary. Grey area indicates the rostrocaudal extension of VII (compare Figure 4-1).

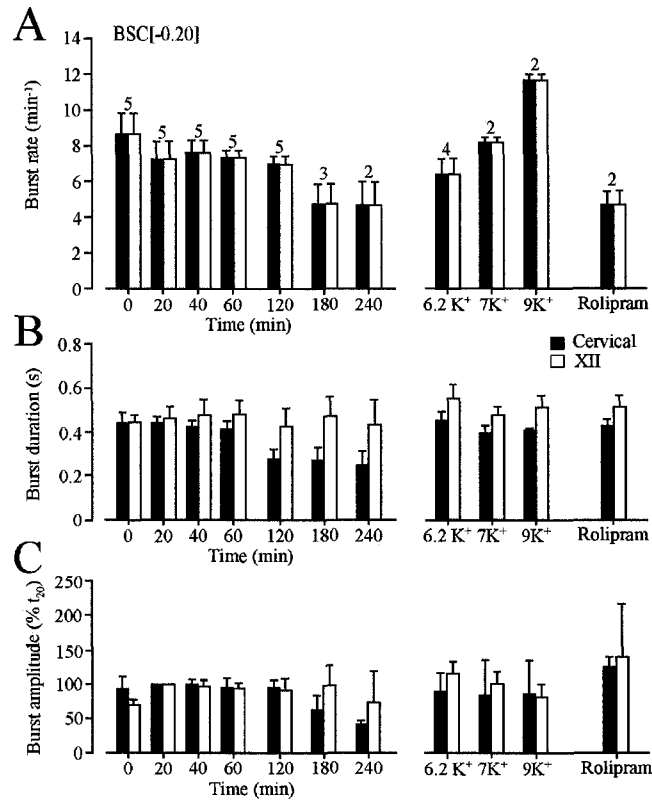


Figure 4-7 Statistical analysis of cervical and hypoglossal rhythms in brainstem-spinal cords without VII. **A**, in 5 BSC[-0.20] preparations, rhythms in cervical roots (□) and most rostral hypoglossal (XII) roots (■) had identical burst rates indicating a 1:1 coupling ratio. As evident from numbers above bars, rhythm stopped in 2 and 3 preparations before 3 and 4 h of recording, respectively. Identical cervical and XII burst rates were also revealed upon reactivation of rhythm with elevated K⁺ or rolipram (1 μM). **B**, XII burst duration was similar during both long-term recording and re-stimulation of rhythm. In contrast, cervical burst duration decreased during the first hour of recording, but was restored by raised K⁺ and rolipram. **C**, cervical burst amplitude decreased after 2 h of recording, but was re-increased by the stimulatory procedures. XII burst amplitude referred to the value at 20 min (t₂₀) was stable under all conditions. Numbers of preparations above bars in **A** are identical to those in **B** and **C**.

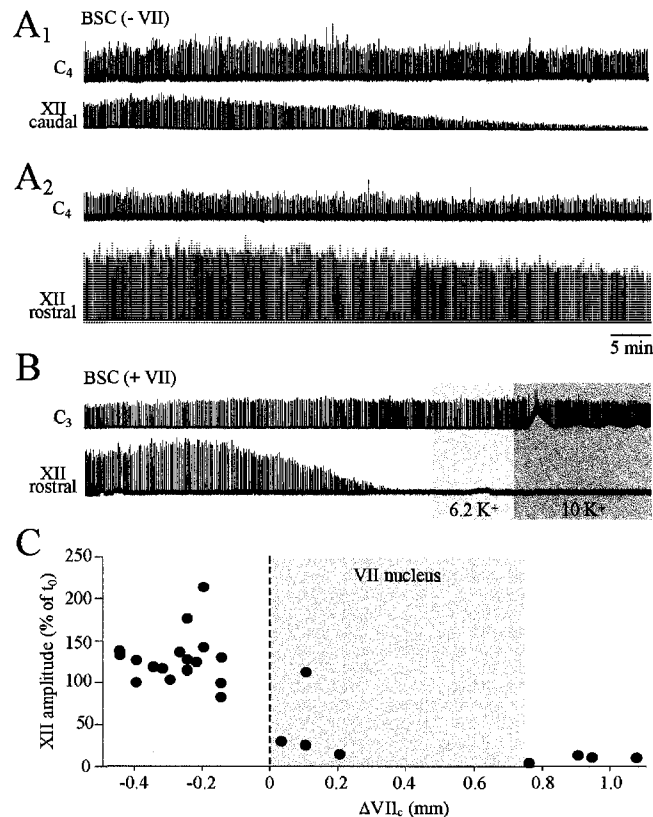


Figure 4-8 Dependence of XII rhythm on rostral boundary of brainstem-spinal cords. **A**, in a BSC[-0.15]SD-P2 preparation, cervical rhythm monitored within <2 min after transfer to the experimental chamber (**A**₁) was stable for >1 h. In contrast, the amplitude of synchronous bursting in a caudal XII root started to decrease after ~17 min and reached <10% of the initial amplitude after 1 h. **A**₂, changing the suction electrode from the caudal to the most rostral XII root within <5 min after end of the recording in **A**₁ revealed robust bursting. The amplitude of most rostral XII root bursts remained at >70% of the initial value for the illustrated time period and continued for >2 h at similar levels afterwards. **B**, in a BSC[+1.1]SD-P1 preparation, cervical rhythm monitored within <2 min after transfer to the experimental chamber was stable for >1 h, whereas bursting of the most rostral XII root started to decrease in amplitude ~17 min after start of the recording and disappeared after ~35 min. XII rhythm could not be reactivated by raising superfusate K⁺ from 3 mM to 6.2 or 10 mM. Same time scale in **A** and **B**. **C**, plot of XII nerve burst amplitude after 1 h, referred to the value at the start of recording (t_0) vs. rostral boundary. Grey area indicates the rostrocaudal extension of VII nucleus (compare Figures 4-1, 4-6).

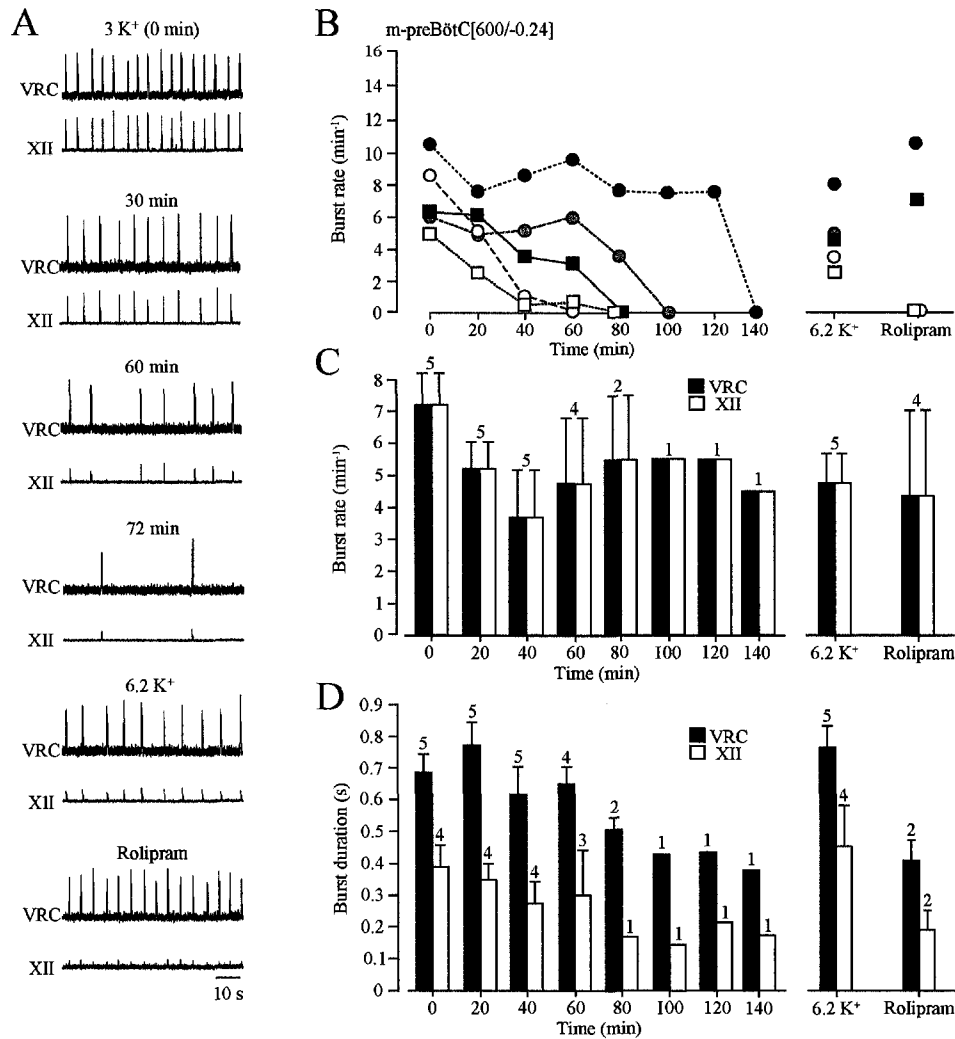


Figure 4-9 preBötC and XII rhythms in preBötC slices in 1.2 mM Ca²⁺ and 3 mM K⁺. **A**, bursting within the ventral respiratory column (VRC), neighbouring the preBötC and reflecting its activity, showed 1:1-coupling to XII nerve bursting in a m-preBötC[600/-0.10]W-P2 slice in standard solution. Following spontaneous arrest of rhythm after 72 min (last bursts shown), 1:1-coupled bursting was reactivated by raised K⁺ and, after return to 3 mM K⁺ solution, rolipram (1 μM). **B**, burst rates in 5 m-preBötC[600/-0.24] slices with mean rostral/caudal boundaries 0.24 ± 0.11/0.86 ± 0.05 mm caudal to VII_c show that rhythm lasted for >80 min in only 2 slices. Rhythm was effectively reactivated in all slices by 6.2 mM K⁺, whereas rolipram (1 μM) was only effective in 2 of 4 slices tested. **C**, mean values of burst rates in **B** show 1:1-coupling between XII and VRC/preBötC bursts under all conditions. **D**, mean burst durations reveal that VRC/preBötC bursts are longer than XII bursts.

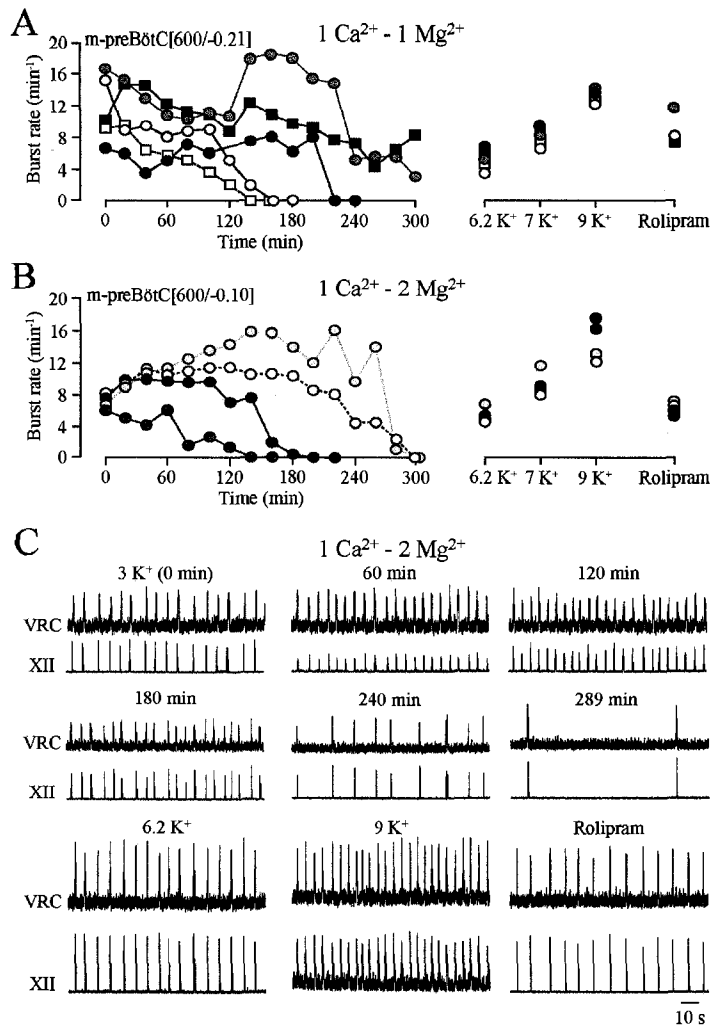


Figure 4-10 preBötC and XII bursting in preBötC slices in 1 mM Ca²⁺ and 3 mM K⁺. **A**, rhythm in 5 m-preBötC[600/-0.21] slices with mean rostral/caudal boundaries $0.21 \pm 0.08/0.82 \pm 0.04$ mm caudal to VII_c kept in superfusate with 3 mM K⁺, 1 mM Ca²⁺ and 1 mM Mg²⁺ persisted for extended time periods, in 2 cases >4 h. **B**, rhythm with similar burst rate and longevity was seen in 4 m-preBötC[600/-0.10] slices with mean rostral/caudal boundaries $0.10 \pm 0.07/0.71 \pm 0.06$ mm caudal to VII_c in superfusate with 3 mM K⁺, 1 mM Ca²⁺ and 2 mM Mg²⁺. Rhythm was effectively reactivated after spontaneous arrest by 6.2, 7 and 9 mM K⁺ and rolipram (1 μM). **C**, the recording from a m-preBötC[600/-0.05]W-P2 slice included in **B** shows a 1:1-coupling of VRC/ preBötC and XII rhythms during spontaneous and re-evoked activity. Note that the recording in rolipram was done 8 h after start of recording and that the amplitude of XII bursting fluctuated during the first 120 min after start of recording.

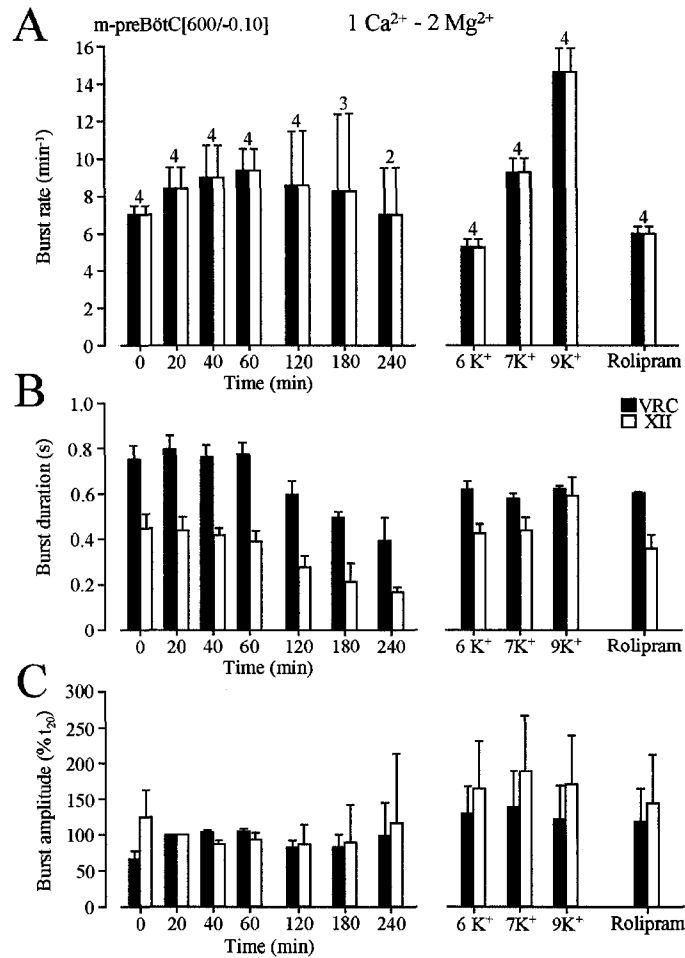


Figure 4-11 Statistical analysis of preBötC and XII rhythms in preBötC slices in 1 mM Ca²⁺ and 3 mM K⁺. **A**, the 4 m-preBötC[600/-0.10] slices of Figure 4-10B showed a 1:1-coupling of VRC/preBötC and XII nerve bursting. Note that burst rate slightly increased during the first hour of recording and that 9 mM K⁺ restored rhythm of ~50% higher burst rate than the initial rhythm in 3 mM K⁺. **B**, the durations of both VRC/preBötC and XII bursts decreased following the first hour of recording. Both, K⁺ and rolipram (1 μM) re-stimulated burst durations. **C**, the amplitude of VRC/preBötC and XII bursts, referred to the value at 20 min (t₂₀), was stable in control solution, whereas elevated K⁺ and rolipram had an augmenting effect. Numbers of slices shown above bars in **A** are identical to those in **B** and **C**.

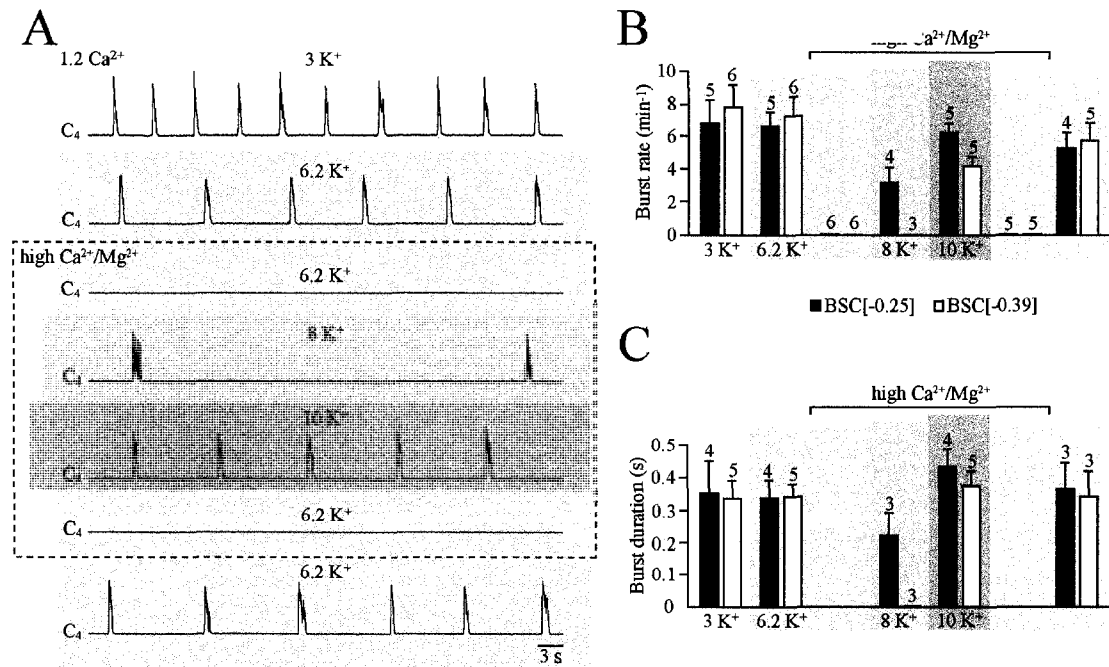


Figure 4-12 Block by high Ca²⁺/K⁺ (Mg²⁺) solution of cervical rhythm in brainstem-spinal cords without VII. A, in a BSC[-0.28]SD-P3, elevating superfusate Ca²⁺ from 1.2 to 2.4 mM and Mg²⁺ from 1.0 to 1.3 mM (3rd trace from top) abolished the inspiratory rhythm which was previously stable in both 3 mM (top trace) and 6.2 mM K⁺ (2nd trace from top). Rhythm very similar to control was reactivated in 2.4 mM Ca²⁺ and 1.3 mM Mg²⁺ by raising K⁺ further, to 10 mM (5th trace from top), whereas 8 mM K⁺ was less effective (4th trace from top). Rhythm was blocked again after return to 6.2 mM K⁺, 2.4 mM Ca²⁺ and 1.3 mM Mg²⁺ solution (2nd trace from bottom) and recovered effectively in 6.2 mM K⁺, 1.2 mM Ca²⁺ and 1 mM Mg²⁺ (bottom trace). B and C, mean rates (B) and durations (C) of cervical bursts in two sets of preparations with different mean rostral boundaries, specifically BSC[-0.25] and BSC[-0.39]. Digits above bars indicate the number of preparations tested. Only a subset of preparations in B was used for the analysis in C. Bars represent means and S.E.M.

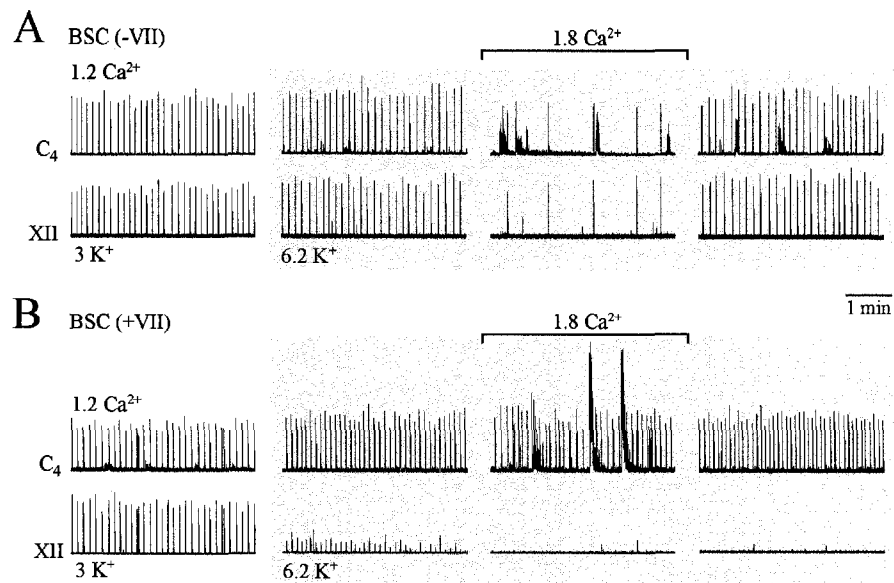


Figure 4-13 Different sensitivity to raised superfusate Ca^{2+} of inspiratory rhythms in brainstem-spinal cords without or with VII. **A**, in a BSC[-0.25]SD-P3 without VII, raising Ca^{2+} from 1.2 to 1.8 mM after changing from 3 to 6.2 mM K^+ reversibly depressed both cervical and XII inspiratory rhythms. Note the occurrence of pronounced non-respiratory activity in the cervical, but not the XII recording during 1.8 mM Ca^{2+} . **B**, 1.8 mM Ca^{2+} did not depress cervical rhythm in a BSC[+0.75]W-P1 preparation with complete VII, but induced large amplitude non-respiratory activity. Note that XII rhythm was stable in **A**, whereas it disappeared in **B** during the time period of raising K^+ . Same time scale in **A** and **B**.

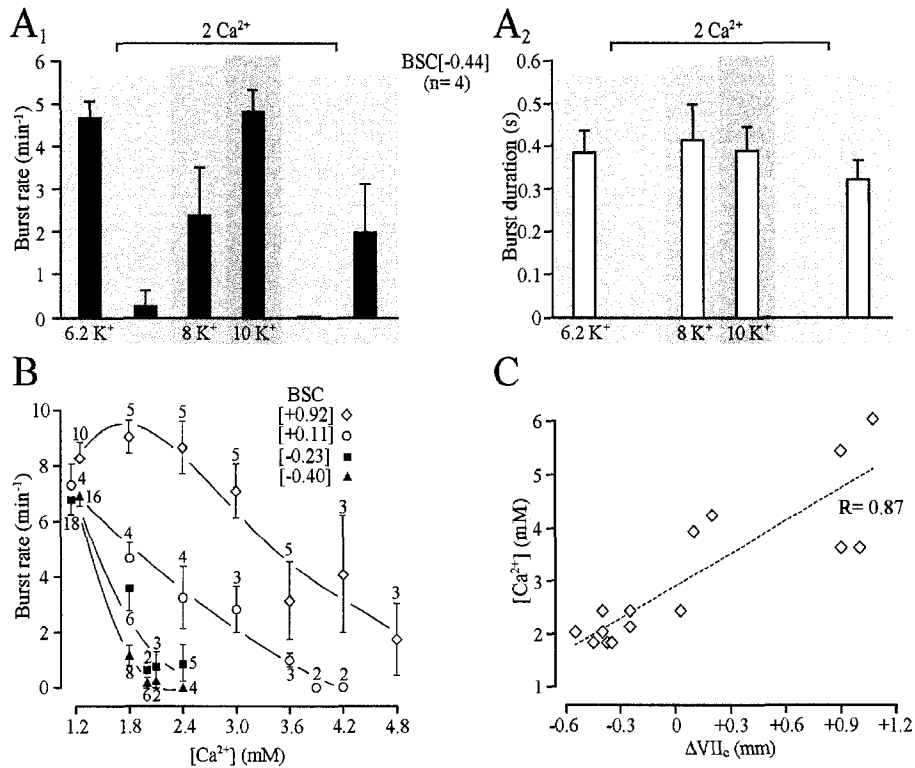


Figure 4-14 Dependence of Ca^{2+} -induced depression of cervical rhythm on rostral boundary in brainstem-spinal cords. **A**, effects of raising Ca^{2+} from 1.2 to 2 mM on mean rate (**Aa**) and duration (**Ab**) of cervical bursts in 4 BSC[-0.44] without VII. **B**, effects of increased Ca^{2+} on cervical burst rates in 4 groups of brainstem-spinal cords with different mean rostral boundaries referred to VIIc indicated in brackets, specifically $+0.92 \pm 0.15$ ($n = 10$), $+0.11 \pm 0.07$ ($n = 4$), -0.23 ± 0.07 ($n = 18$) and -0.40 ± 0.05 ($n = 16$). Note that 1.8-2 mM Ca^{2+} had a major depressing effect on rhythm in preparations without VII (filled symbols), whereas >3 mM Ca^{2+} was necessary for a notable depression of burst rate in preparations with (portions of) VII (open symbols). Digits next to symbols indicate the number of preparations tested. **C**, significant ($P < 0.01$) relation between superfusate Ca^{2+} necessary to abolish preBötC rhythm and the rostral boundary of brainstem-spinal cords referred to their distance from VIIc (ΔVII_c). Note that considerably higher Ca^{2+} levels were necessary to block rhythm in preparations with complete VII. Values represent means and S.E.M.

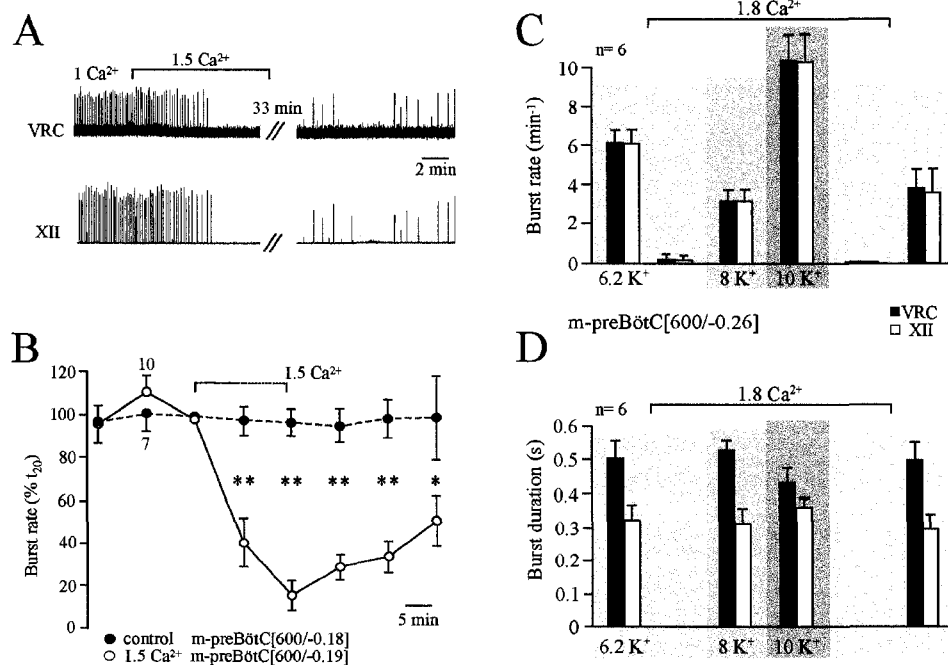


Figure 4-15 Block by Ca²⁺ of preBötC and XII rhythm in preBötC slices. **A**, synchronous inspiratory bursting of XII nerve and VRC/preBötC in a m-preBötC[600/-0.30]W-P1 slice was abolished by raising superfusate Ca²⁺ from 1 to 1.5 mM (in 3 mM K⁺ and 2 mM Mg²⁺). Note that rhythm did not fully recover within >40 min after return to 1 mM Ca²⁺. **B**, plot of burst rate of 10 m-preBötC[600/-0.19] slices with mean boundaries 0.19 ± 0.10/0.82 ± 0.05 mm caudal to VII_c (○) in response to 1.5 mM Ca²⁺ (in 3 mM K⁺ and 2 mM Mg²⁺). The dotted line in bracket indicating the application of elevated [Ca²⁺] symbolizes that administration periods varied between 10 and 20 min depending on when the inhibitory effect reached steady-state. Filled circles indicate burst rates in 7 control m-preBötC[600/-0.18] slices with mean boundaries 0.18 ± 0.11/0.78 ± 0.10 mm caudal to VII_c in 1 mM Ca²⁺, 3 mM K⁺ and 2 mM Mg²⁺ solution. Asterisks show significant (*p < 0.05; **p < 0.01) difference between controls and the group treated with 1.5 mM Ca²⁺. **C** and **D**, mean rate (**C**) and duration (**D**) of VRC/preBötC (■) and XII bursts (□) in 6 m-preBötC[600/-0.26] slices with mean boundaries 0.26 ± 0.12/0.86 ± 0.03 mm caudal to VII_c during variation of superfusate Ca²⁺ and K⁺. In control, slices were kept in 6.2 mM K⁺, 1 mM Ca²⁺ and 2 mM Mg²⁺. Subsequently, rhythm was blocked upon elevation of Ca²⁺ to 1.8 mM and reactivated by raising K⁺, first to 8 mM, then to 10 mM. Rhythm was blocked again upon return to 1.8 mM Ca²⁺ in 6.2 mM K⁺ and recovered to values close to control following lowering of Ca²⁺ to 1 mM.

4.6 References

- Alheid GF, Milsom WK & McCrimmon DR (2004) Pontine influences on breathing: an overview. *Respir Physiol Neurobiol* 143, 105-114.
- Alheid GF, Gray PA, Jiang MC, Feldman JL & McCrimmon DR (2002) Parvalbumin in respiratory neurons of the ventrolateral medulla of the adult rat. *J Neurocytol* 31, 693-717.
- Arata A, Onimaru H & Homma I (1990) Respiration-related neurons in the ventral medulla of newborn rats in vitro. *Brain Res Bull* 24, 599-604.
- Ballanyi K (2004) Neuromodulation of the perinatal respiratory network. *Curr Neuropharmacol* 2, 221-243.
- Ballanyi K (1999) Isolated tissues. In vitro preparations. In *Modern Techniques in Neuroscience Research*, ed. Windhorst U & Johansson H, pp. 307-326. Springer, Heidelberg.
- Ballanyi K, Onimaru H & Homma I (1999) Respiratory network function in the isolated brainstem-spinal cord of newborn rats. *Progr Neurobiol* 59, 583-634.
- Ballanyi K, Lalley PM, Hoch B & Richter DW (1997) cAMP-dependent reversal of opioid- and prostaglandin-mediated depression of the isolated respiratory network in newborn rats. *J Physiol* 504, 127-134.
- Ballanyi K, Völker A & Richter DW (1996) Functional relevance of anaerobic metabolism in the isolated respiratory network of newborn rats. *Pflugers Arch* 432, 741-748.
- Ballanyi K, Kuwana S, Völker A, Morawietz G & Richter DW (1992) Developmental changes in the hypoxia tolerance of the in vitro respiratory network of rats. *Neurosci Lett* 148, 141-144.
- Berkenbosch A & Adan AJ (1974) Influence of CSF calcium concentration on the ventilatory response to CO₂ and O₂. *Pflugers Arch* 348, 33-50.
- Berndt J, Fenner A & Berger K (1969) Influence of calcium and magnesium on the respiratory response to changes in CSF pH. *Respir Physiol* 7, 216-229.

- Brockhaus J & Ballanyi K (2000) Anticonvulsant adenosine A₁ receptor-mediated adenosine action on neuronal networks in the brainstem-spinal cord of newborn rats. *Neuroscience* 96, 359-371.
- Brockhaus J & Ballanyi K (1998) Synaptic inhibition in the isolated respiratory network of neonatal rats. *Eur J Neurosci* 10, 3823-3839.
- Brockhaus J, Ballanyi K, Smith JC & Richter DW (1993) Microenvironment of respiratory neurons in the in vitro brainstem-spinal cord of neonatal rats. *J Physiol* 462, 421-445.
- Brown PD, Davies SL, Speake T & Millar ID (2004) Molecular mechanisms of cerebrospinal fluid production. *Neuroscience* 129, 957-970.
- De Araujo AC & Campos R (2005) A systematic study of the brain base arteries and their blood supply sources in the chinchilla (*Chinchilla lanigeria* - Molina 1782) *Braz J Morph Sci* 22, 221-232.
- Del Negro CA, Morgado-Valle C, Hayes JA, Mackay DD, Pace RW, Crowder EA & Feldman JL (2005) Sodium and calcium current-mediated pacemaker neurons and respiratory rhythm generation. *J Neurosci* 25, 446-453.
- Errchidi S, Monteau R & Hilaire G (1991) Noradrenergic modulation of the medullary respiratory rhythm generator in the newborn rat: an in vitro study. *J Physiol* 443, 477-498.
- Feldman JL & Del Negro CA (2006) Looking for inspiration: new perspectives on respiratory rhythm. *Nat Rev Neurosci* 7, 232-242.
- Feldman JL & Janczewski WA (2006) Point:Counterpoint: The parafacial respiratory group (pFRG)/pre-Botzinger complex (preBotC) is the primary site of respiratory rhythm generation in the mammal. Counterpoint: the preBotC is the primary site of respiratory rhythm generation in the mammal. *J Appl Physiol* 100, 2096-2097; Discussion 2097-2098, 2103-2108.
- Feldman JL (1986) Neurophysiology of breathing in mammals. In *Handbook of Physiology*, section 1, The Nervous System, vol. IV, Intrinsic Regulatory Systems in the Brain, Chap 9. Ed, Mountcastle VB, pp. 463-524. American Physiological Society, Bethesda.

- Hansen AJ (1985) Effect of anoxia on ion distribution in the brain. *Physiol Rev* 65, 101-148.
- Heinemann U, Lux HD & Gutnick MJ (1977) Extracellular free calcium and potassium during paroxysmal activity in the cerebral cortex of the cat. *Exp Brain Res* 27, 237-243.
- Herlenius E, Aden U, Tang LQ & Lagercrantz H (2002) Perinatal respiratory control and its modulation by adenosine and caffeine in the rat. *Pediatr Res* 51, 4-12.
- Hille B (2001) *Ion Channels of Excitable Membranes*. Sinauer Associates, Sunderland, MA, USA.
- Iizuka M (2004) Rostrocaudal distribution of spinal respiratory motor activity in an in vitro neonatal rat preparation. *Neurosci Res* 50, 263-269.
- Janczewski WA & Feldman JL (2006) Distinct rhythm generators for inspiration and expiration in the juvenile rat. *J Physiol* 570, 407-420.
- Janczewski WA, Onimaru H, Homma I & Feldman JL (2002) Opioid-resistant respiratory pathway from the pre-inspiratory neurones to abdominal muscles: in vivo and in vitro study in the newborn rat. *J Physiol* 545, 1017-1026.
- Jefferys JG (1995) Nonsynaptic modulation of neuronal activity in the brain: electric currents and extracellular ions. *Physiol Rev* 75, 689-723.
- Johnson SM, Smith JC & Feldman JL (1996) Modulation of respiratory rhythm in vitro: role of $G_{i/o}$ protein-mediated mechanisms. *J Appl Physiol* 80, 2120-2133.
- Konnerth A, Heinemann U & Yaari Y (1986) Nonsynaptic epileptogenesis in the mammalian hippocampus in vitro. I. Development of seizurelike activity in low extracellular calcium. *J Neurophysiol* 56, 409-423.
- Koshiya N & Smith JC (1999) Neuronal pacemaker for breathing visualized in vitro. *Nature* 400, 360-363.
- Kuwana S, Tsunekawa N, Yanagawa Y, Okada Y, Kuribayashi J & Obata K (2006) Electrophysiological and morphological characteristics of GABAergic respiratory neurons in the mouse pre-Botzinger complex. *Eur J Neurosci* 23, 667-674.
- Kuwana S, Okada Y & Natsui T (1998) Effects of extracellular calcium and magnesium on central respiratory control in the brainstem-spinal cord of neonatal rat. *Brain Res* 786, 194-204.

- Leusen I (1972) Regulation of cerebrospinal fluid composition with reference to breathing. *Physiol Rev* 52, 1-56.
- McLean HA & Remmers JE (1994) Respiratory motor output of the sectioned medulla of the neonatal rat. *Respir Physiol* 96, 49-60.
- Mellen NM, Janczewski WA, Bocchiaro CM & Feldman JL (2003) Opioid-induced quantal slowing reveals dual networks for respiratory rhythm generation. *Neuron* 37, 821-826.
- Monnier A, Alheid GF & McCrimmon DR (2003) Defining ventral medullary respiratory compartments with a glutamate receptor agonist in the rat. *J Physiol* 548, 859-874.
- Monteau R, Morin D, Hennequin S & Hilaire G (1990) Differential effects of serotonin on respiratory activity of hypoglossal and cervical motoneurons: an in vitro study on the newborn rat. *Neurosci Lett* 111, 127-132.
- Monteau R, Errchidi S, Gauthier P, Hilaire G & Rega P (1989) Pneumotaxic centre and apneustic breathing: interspecies differences between rat and cat. *Neurosci Lett* 99, 311-316.
- Nicholson C, ten Bruggencate G, Stockle H & Steinberg R (1978) Calcium and potassium changes in extracellular microenvironment of cat cerebellar cortex. *J Neurophysiol* 41, 1026-1039.
- Nilsson P, Hillered L, Olsson Y, Sheardown MJ & Hansen AJ (1993) Regional changes in interstitial K⁺ and Ca²⁺ levels following cortical compression contusion trauma in rats. *J Cereb Blood Flow Metab* 13, 183-192.
- O'Donnell JM & Zhang HT (2004) Antidepressant effects of inhibitors of cAMP phosphodiesterase (PDE4) *Trends Pharmacol Sci* 25, 158-163.
- Okada Y, Kuwana S, Kawai A, Muckenhoff K & Scheid P (2005) Significance of extracellular potassium in central respiratory control studied in the isolated brainstem-spinal cord preparation of the neonatal rat. *Respir Physiol Neurobiol* 146, 21-32.
- Onimaru H & Homma I (2006) Point:Counterpoint: The parafacial respiratory group (pFRG)/pre-Botzinger complex (preBotC) is the primary site of respiratory rhythm generation in the mammal. Point: The pFRG is the primary site of respiratory rhythm generation in the mammal. *J Appl Physiol* 100, 2094-2095; Discussion 2097-2098, 2103-2108.

- Onimaru H, Kumagawa Y & Homma I (2006) Respiration-related rhythmic activity in the rostral medulla of newborn rats. *J Neurophysiol* 96, 55-61.
- Onimaru H & Homma I (2003) A novel functional neuron group for respiratory rhythm generation in the ventral medulla. *J Neurosci* 23, 1478-1486.
- Onimaru H, Ballanyi K & Homma I (2003) Contribution of Ca^{2+} -dependent conductances to membrane potential fluctuations of medullary respiratory neurons of newborn rats in vitro. *J Physiol* 552, 727-741.
- Onimaru H, Arata A & Homma I (1990) Inhibitory synaptic inputs to the respiratory rhythm generator in the medulla isolated from newborn rats. *Pflugers Arch* 417, 425-432.
- Onimaru H & Homma I (1987) Respiratory rhythm generator neurons in medulla of brainstem-spinal cord preparation from newborn rat. *Brain Res* 403, 380-384.
- Oshima N, Kumagai H, Kawai A, Sakata K, Matsuura T & Saruta T (2000) Three types of putative presympathetic neurons in the rostral ventrolateral medulla studied with rat brainstem-spinal cord preparation. *Auton Neurosci* 84, 40-49.
- Pace RW, Mackay DD, Feldman JL & Del Negro CA (2007) Role of persistent sodium current in mouse preBotzinger complex neurons and respiratory rhythm generation. *J Physiol* 580, 485-496.
- Paton JF, Abdala AP, Koizumi H, Smith JC & St-John WM (2006) Respiratory rhythm generation during gasping depends on persistent sodium current. *Nat Neurosci* 9, 311-313.
- Pittman QJ, Hatton JD & Bloom FE (1981) Spontaneous activity in perfused hypothalamic slices: dependence on calcium content of perfusate. *Exp Brain Res* 42, 49-52.
- Puka-Sundvall M, Hagberg H & Andine P (1994) Changes in extracellular calcium concentration in the immature rat cerebral cortex during anoxia are not influenced by MK-801. *Brain Res Dev Brain Res* 77, 146-150.
- Ramirez JM, Zuperku EJ, Alheid GF, Lieske SP, Ptak K & McCrimmon DR (2002) Respiratory rhythm generation: converging concepts from in vitro and in vivo approaches? *Respir Physiol Neurobiol* 131, 43-56.

- Rekling JC, Champagnat J & Denavit-Saubie M (1996) Electroresponsive properties and membrane potential trajectories of three types of inspiratory neurons in the newborn mouse brain stem in vitro. *J Neurophysiol* 75, 795-810.
- Richter DW, Lalley PM, Pierrefiche O, Haji A, Bischoff AM, Wilken B & Hanefeld V (1997) Intracellular signal pathways controlling respiratory neurons. *Respir Physiol* 110, 113-123.
- Richter DW & Acker H (1989) Respiratory neuron behaviour during medullary hypoxia. In *Chemoreceptors and Reflexes in Breathing: Cellular and Molecular Aspects*, ed. Lahiri S, pp. 267-274. Oxford University Press, Oxford.
- Ruangkittisakul A & Ballanyi K (2006) Reversal by phosphodiesterase-4 blockers of in vitro apnea in the isolated brainstem-spinal cord preparation from newborn rats. *Neurosci Lett* 401, 194-198.
- Ruangkittisakul A, Schwarzacher SW, Ma Y, Poon B, Secchia L, Funk GD & Ballanyi K (2006) High sensitivity to neuromodulator-activated signalling pathways at physiological $[K^+]$ of confocally-imaged respiratory centre neurons in online-calibrated newborn rat brainstem slices. *J Neurosci* 26, 11870-11880.
- Schwarzacher SW, Smith JC & Richter DW (1995) Pre-Bötzinger complex in the cat. *J Neurophysiol* 73, 1452-1461.
- Schwarzacher SW, Wilhelm Z, Anders K & Richter DW (1991) The medullary respiratory network in the rat. *J Physiol* 435, 631-644.
- Smith JC, Ellenberger HH, Ballanyi K, Richter DW & Feldman JL (1991) Pre-Bötzinger complex: a brainstem region that may generate respiratory rhythm in mammals. *Science* 254, 726-729.
- Smith JC, Greer JJ, Liu GS & Feldman JL (1990) Neural mechanisms generating respiratory pattern in mammalian brain stem-spinal cord in vitro. I. Spatiotemporal patterns of motor and medullary neuron activity. *J Neurophysiol* 64, 1149-1169.
- Somjen GG (2002) Ion regulation in the brain: implications for pathophysiology. *Neuroscientist* 8, 254-267.
- St-John WM, Rudkin AH, Harris MR, Leiter JC & Paton JF (2005) Maintenance of eupnea and gasping following alterations in potassium ion concentration of perfusates of in situ rat preparation. *J Neurosci Methods* 142, 125-129.

- St-John WM, Paton JF & Leiter JC (2004) Uncoupling of rhythmic hypoglossal from phrenic activity in the rat. *Exp Physiol* 89, 727-737.
- Sun QJ, Goodchild AK, Chalmers JP & Pilowsky PM (1998) The pre-Botzinger complex and phase-spanning neurons in the adult rat. *Brain Res* 809, 204-213.
- Suzue T (1984) Respiratory rhythm generation in the in vitro brain stem-spinal cord preparation of the neonatal rat. *J Physiol* 354, 173-183.
- Trippenbach T, Richter DW & Acker H (1990) Hypoxia and ion activities within the brain stem of newborn rabbits. *J Appl Physiol* 68, 2494-2503.
- Völker A, Ballanyi K & Richter DW (1995) Anoxic disturbance of the isolated respiratory network of neonatal rats. *Exp Brain Res* 103, 9-19.
- Wilson RJ, Vasilakos K & Remmers JE (2006) Phylogeny of vertebrate respiratory rhythm generators: the oscillator homology hypothesis. *Respir Physiol Neurobiol* 154, 47-60.

CHAPTER V

General Discussion & Conclusions

5.1 Summary of Findings

This work examined the relationship between inspiratory-related interneuronal preBötC activity and preBötC-driven motor output and (i) the physical dimensions of newborn rat brainstem-spinal cord preparations and brainstem slices, and (ii) the K^+ and Ca^{2+} content of the superfusate used to study these models. Three projects revealed the following major findings which all supported the proposed hypotheses.

Project 1: The rostrocaudal extensions of respiratory brainstem marker nuclei, in particular the inferior olive, the lateral reticular nucleus, and the VII nucleus, are constant in 0-4 days-old rats. This constancy of marker nuclei enabled the generation of “calibrated” preBötC slices via a novel “online histology” using a newborn rat brainstem atlas. Calibrated 500 or 600 μm thick slices with the preBötC in the center generate in physiological (3 mM) K^+ a stable inspiratory-related rhythm with a high sensitivity to neuromodulators, in particular opioids. Spontaneous arrest of inspiratory bursting in 3 mM K^+ after several hours (“in vitro apnea”) is an important tool to study the interaction of signalling pathways modulating the preBötC rhythm. The basic morphology of preBötC neurons, i.e., their soma shape and diameter, as well as the number and array of primary dendrites and their activity were visualized by multiphoton Ca^{2+} imaging.

Project 2: The sufficient and necessary histological boundaries for a functional preBötC in newborn rat slices extend $<200 \mu\text{m}$ and $<100 \mu\text{m}$, respectively. The probability for the occurrence of either a fictive eupnea burst pattern or a mixed fictive eupnea-sigh pattern depends on structures that neighbor the $<100 \mu\text{m}$ thin preBötC kernel, centered 0.5 mm caudal to the VII motor nucleus. Specifically, slices containing the preBötC kernel plus caudal structures produced eupneic bursts of regular amplitude and rate, whereas this kernel plus rostral tissue generated sighs that intermingled with eupneic bursts of smaller and variable amplitude. Upon in vitro apnea, SP or a NK1 receptor agonist induced the eupnea-sigh burst pattern in $\geq 250 \mu\text{m}$ thick slices, whereas TRH or the phosphodiesterase-4 blockers rolipram and theophylline evoked the eupnea burst pattern.

Multineuronal Ca^{2+} imaging revealed that preBötC neurons reconfigure between these activity patterns.

Project 3: Calibrated and reproducible newborn rat brainstem-spinal cord preparations can be generated based on the finding that the locations of ventral brainstem surface landmarks, particularly the caudal cerebellar artery and the X and XII nerve rootlets, are constant and provide reference to respiratory nuclei locations. The longevity of inspiratory preBötC-driven cervical and XII nerve motor activity in the en bloc model in 3 mM K^+ and physiological Ca^{2+} (1.2 mM) depends on the amount of brainstem tissue rostral to the preBötC. Elevation of superfusate Ca^{2+} above 1.2 mM depresses the endogenous activity in 3 mM K^+ of the exposed preBötC in the slice and the en bloc model, and this depression is antagonized by raised K^+ . XII nerve rhythm was depressed in en bloc preparations containing (portions of) the VII nucleus, whereas pre-/post-inspiratory lumbar nerve bursting was present only in preparations with >79 % of VII nucleus.

5.2 Necessity for Calibrated in vitro Brainstem Preparations

The preBötC is embedded in a network of respiratory-related nuclei that interact with this hypothesized inspiratory center (Bianchi et al., 1995; Feldman et al., 2003; Feldman & Del Negro, 2006). Examples for (respiratory) modulatory structures rostral to the preBötC are the hypothesized pFRG expiratory center, the chemosensitive RTN that may overlap with or even be identical to the pFRG in newborn mammals, and other chemosensitive neuronal groups in the same area (Feldman & Del Negro, 2006; Voituron et al., 2006; Fortuna et al., 2008; Guyenet et al., 2008). Such neighboring structures presumably modulate preBötC activity in the respiratory active in vitro preparations used for the present work, i.e., the brainstem spinal cord preparation and brainstem slices from newborn rats. In the en bloc model, modulation of the preBötC by the pFRG (Onimaru et al., 1997; Mellen et al., 2003; Taccola et al., 2007) is mediated via both excitatory and inhibitory synaptic connections (Onimaru et al., 1990, 1992; Kashiwagi et al., 1993). In

this model, the extent of interactions between the pFRG and the preBötC is likely determined by the amount of tissue containing the pFRG. The paper on the discovery of the pFRG has reported that this rhythmogenic respiratory group overlaps with the ventrolateral aspect of the VII nucleus (Onimaru & Homma, 2003). This means that en bloc preparations containing a major portion of the VII nucleus may contain a major portion of the pFRG (and the RTN).

In addition to the dependence of in vitro preBötC functions on specific neighboring structures, unidentified neurons that are diffusely distributed within the reticular formation may exert an unspecific tonic drive to the inspiratory center (Richter et al., 1992; Bianchi et al., 1995). Furthermore, preBötC activity is likely modulated by factors that are related with the physical dimensions of the preparations. Specifically, metabolites such as adenosine and CO₂ (and thus H⁺) accumulate in the non-perfused interstitial brainstem tissues, whereas O₂ levels decrease toward the center of these models, resulting in an anoxic core in the en bloc model (Brockhaus et al., 1993; Ballanyi, 1999; Okada et al., 2005; Ballanyi & Ruangkittisakul, 2008). Similarly, non-metabolic neuromodulators such as SP or TRH may accumulate in the en bloc medulla (and thicker slices) and provide a long-term drive to the preBötC (Ballanyi, 1999; Ruangkittisakul et al., 2006, 2008; Ballanyi & Ruangkittisakul, 2008). For these reasons, it is obvious that there is a need for verification of the rostral border of en bloc preparations, and the rostral plus caudal borders of slices, to enable a comparison of findings by different groups using these models.

The constancy of respiratory marker nuclei in the brainstem allowed the construction of a reference newborn rat brainstem atlas and (by comparison with the atlas during the slicing procedure) the generation of preBötC slices with predictable and reproducible boundaries with a precision of about $\pm 50 \mu\text{m}$ (Ruangkittisakul et al., 2006). Similarly, the finding that ventral brainstem surface landmarks are constant in 0-4 days-old rats allowed the generation of brainstem-spinal cords with predictable and reproducible boundaries (Ruangkittisakul et al., 2007). Online histology reduces the variability of the dimensions of preparations and therefore minimizes variations between results. For example, it has

been reported that serotonin irreversibly blocks XII nerve rhythm in the newborn rat en bloc model (Monteau et al., 1990). However, it is not clear whether this block is rather due to the finding revealed here that XII rhythm is spontaneously depressed within <1 h in preparations containing rostral brainstem tissue with a notable portion of the VII nucleus as anatomical reference (Ruangkittisakul et al., 2007).

In contrast to the disappearance of XII nerve bursts in en bloc preparations with a notable portion of tissue rostral to the preBötC, we found that pre-/post-inspiratory lumbar nerve activity is absent in preparations that contain brainstem tissue with <79 % of the VII nucleus (Ruangkittisakul et al., 2007). First, the latter findings showed that the brainstem level critical for the generation of expiratory motor output by the pFRG is located more rostral than indicated by other studies. These other reports showed that section between the VII nucleus and the preBötC does not affect inspiratory activity, but abolishes pre-/post-inspiratory activity of expiratory abdominal muscles in vivo (Janczewski & Feldman, 2006) or lumbar nerves driving these muscles in the en bloc model (Taccola et al., 2007). The present finding of a more rostral critical level for lumbar pFRG-driven activity suggests that the pFRG may be located more rostrally than currently assumed. However, findings from transection studies do not provide direct evidence that rhythmogenic pFRG neurons that are essential for expiratory motor behaviour are located rostral to the section level. This is because axons of pFRG neurons may first project rostrally before projecting back caudally. In which case, the section may cut this connection. Regardless, these studies showed that an important component of the pFRG network mediating this behaviour is located more rostrally than previously thought.

In vitro models with identified boundaries are also important for the determination of sites within respiratory or modulatory brainstem regions that are either lesioned or monitored with imaging techniques. As discussed in detail by Ellenberger (1999), imprecise lesion sites resulted in the misconception that the preBötC may constitute a gasping center activated by hypoxia/anoxia as proposed by Huang et al. (1997). A recent voltage-sensitive dye-imaging study assigned a region of interest presumably representing the preBötC area (Oku et al., 2007). However, that area extended from the

most rostral XII nerve root to the X nerve and thus included not only (the rostral aspect of) the preBötC, but also the BötC and portions of the pFRG according to the findings in the present study.

Finally, an increasing number of studies uses recordings from visually-identified inspiratory neurons located up to 100 μm deep in preBötC slices, e.g., for assessment of biophysical membrane properties with patch-clamp (Ballanyi & Onimaru, 2008) or analysis of intracellular processes such as oscillations of Ca^{2+} or mitochondrial potential with fluorescence imaging techniques (Ballanyi et al., 2008). Unless it is histologically verified that the slice surface is indeed $<100 \mu\text{m}$ distant from the (sufficient) preBötC boundaries, i.e., between $\sim 0.4\text{-}0.6 \text{ mm}$ caudal to VII_c for newborn rats, these cells should be labeled as inspiratory VRC neurons instead of preBötC neurons.

5.3 preBötC Rhythm in Physiological Ion Solution

The original report on the preBötC discovery stated that $\geq 500 \mu\text{m}$ thick newborn rat brainstem slices generate XII motor output in 3 mM K^+ (Smith et al., 1991). Despite that notion, most studies on preBötC slices since then used elevated K^+ (mostly 8-9 mM) for long term stability of respiratory rhythm. Here, it was found that preBötC-containing slices with defined boundaries generate rhythm in 3 mM K^+ for several hours before the occurrence of in vitro apnea. The longevity of rhythms in the novel slices depends on their thickness. Specifically, thicker slices (500-700 μm) remained active in 3 mM K^+ for longer time periods than slices thinner than 500 μm , suggesting a higher level of endogenous excitatory drive to the preBötC and/or slower wash-out of excitatory neuromodulators in the thicker slices (Ruangkittisakul et al., 2006, 2008). Also the location of the preBötC within the slice plays a role in the longevity of inspiratory rhythm in 3 mM K^+ . Rhythms in slices with the preBötC exposed to one surface had a shorter longevity than those with the preBötC in the center. This suggests that exposing the preBötC may have damaged some portion of the dendritic trees of its cellular constituents,

thus reducing its excitability and possibly limiting its ability to respond to neuromodulators (Ruangkittisakul et al., 2008).

In the less reduced en bloc model, the longevity of preBötC-related cervical motor output was also dependent on the rostral boundary (Ruangkittisakul et al., 2007). Systematic variation of the brainstem section level revealed that inspiratory rhythm lasted >6 h in medullas with complete VII nucleus, whereas the longevity was progressively reduced when the rostral boundary approached the preBötC. Moreover, en bloc preparations with the preBötC exposed to the rostral surface, and hence were devoid of (major portions of) the pFRG, remained active for ~1.5 h, similar to 700 μm thick slices with rostrally exposed preBötC. Conversely, newborn rat rostral brainstem blocks sectioned between the preBötC and the VII nucleus generated presumably pFRG-driven VII nerve rhythm (Onimaru et al., 2006). These findings are consistent with those in the report by Smith et al. (1991) showing that sectioned newborn rat en bloc preparations principally generate inspiratory motor output in 3 mM K^+ , unless the sections level is very close to the center of the preBötC. Compared with that report, the findings in the present study add novel information regarding the dependence of the longevity of the inspiratory rhythm and inspiratory motor output in 3 mM K^+ in the transected en bloc preparations on the rostral boundary. The finding that inspiratory rhythms are generated in both slices and en bloc preparations with the rostral boundary at the rostral border of the preBötC supports the hypothesis based on brainstem section in juvenile rats in vivo that the preBötC is capable of functioning without the expiratory component of the dual respiratory center constituted by the pFRG (Janczewski & Feldman, 2006). As discussed in more detail below (5.5), previous findings of depressed (McLean & Remmers, 1994) or abolished (Onimaru & Homma, 1987) preBötC activity upon removal of more rostral tissue are likely due to the use of unphysiologically high superfusate Ca^{2+} levels.

The above hypothesis that spontaneous in vitro apnea in 3 mM K^+ is due to wash-out of neurotransmitters is supported by the finding that inspiratory rhythm could be restored by bath-application of various neurotransmitters, such as DHPG, TRH, SP, and the phosphodiesterase-4 blocker rolipram, which affect distinct second-messenger pathways

(Ruangkittisakul et al., 2008). Analysis of inspiratory rhythms in solution with physiological K^+ and Ca^{2+} revealed a high sensitivity of the novel preBötC slices to these neuromodulators, and in particular to the μ -receptor agonist DAMGO (Ruangkittisakul et al., 2006). Specifically, the rhythm was blocked by low nanomolar concentrations of DAMGO, whereas the drug is typically applied in close to micromolar concentrations to preBötC slices studied in elevated superfusate K^+ (Johnson et al., 1994). Accordingly, it remains to be studied as to which extent elevated K^+ changes endogenous inspiratory network behaviours, e.g., the occurrence of a eupnea-sigh burst pattern versus a solely eupneic inspiratory pattern, and preBötC responses to (metabolic) respiratory modulators such as GABA, glycine, opioids or anoxia.

5.4 Generation of Eupnea versus Eupnea-Sigh Burst Pattern

The study on the discovery of the preBötC (Smith et al., 1991) estimated a $\sim 225 \mu\text{m}$ rostrocaudal extension of the hypothesized inspiratory center based on the effect of removal of rostral or caudal brainstem tissue on inspiratory-related motor output in the newborn rat en bloc model. However, the minimal preBötC extension had not been identified in histologically-identified brainstem slices. The present study showed that preBötC slices as thin as $175 \mu\text{m}$ are able to generate inspiratory rhythm in $3 \text{ mM } K^+$. The extension of the preBötC could even be $<100 \mu\text{m}$ when either rostral or caudal tissue with a thickness of several hundred micrometers was attached to this minimal necessary kernel of rhythmogenic preBötC tissue. This discrepancy possibly reflects a stronger drive to the preBötC provided by (tonic) neurons in the reticular formation (Richter et al., 1992). Similar to thicker preBötC slices, $250 \mu\text{m}$ thin slices are responsive to respiratory neuromodulators such as SP, TRH, and theophylline. Application of SP or activation of NK1 receptors following in vitro apnea in $250 \mu\text{m}$ or thicker preBötC slices revealed a eupnea-sigh inspiratory pattern. Conversely, a solely eupneic burst pattern was induced by TRH or the cAMP-elevating agents theophylline and rolipram. The finding that inspiratory pattern reconfigures in such thin slices suggests that these modulators exert direct action on the preBötC neurons.

In 3 mM K⁺ solution prior to in vitro apnea, a spontaneous eupnea-sigh burst pattern was the predominant inspiratory activity in r+preBötC[700] slices, i.e., 700 μm thick slices with the preBötC plus rostral brainstem tissue. In contrast, the eupnea burst pattern was the predominant activity in c+preBötC slices, i.e., 700 μm slices with the preBötC plus caudal tissue. This suggests that rostral and caudal brainstem structures provide a distinct drive to the preBötC kernel. Regarding the nature of these structures, raphe obscurus and pallidus are the major source of SP and TRH in the caudal brainstem (Jacobs & Azmitia, 1992). Thus, the dependence of inspiratory patterns on structures neighboring the preBötC may be due to a differing content of these raphe nuclei in the r+preBötC and c+preBötC slices. An immunohistochemical study showed colocalization of SP and TRH with other transmitters in nerve terminals of raphe neurons, whereas colocalization of SP and TRH was not found (Kachidian et al., 1991; Nattie et al., 2004). This suggests that these neurotransmitters may serve a distinctive function in the control of respiration.

Another neurotransmitter implicated in promoting sigh bursts is acetylcholine, acting on muscarinic receptors (Tryba et al., 2008) that are present in various (respiratory) brainstem regions, including the RTN (Mallios et al., 1995). A possible involvement of the RTN, a major portion of which is included in r+preBötC[700] slices, is in line with the observed predominant eupnea-sigh burst pattern. Moreover, the RTN receives afferent sensory input which is presumably important for sigh generation (Cherniack et al., 1981). The finding that 600-650 μm islands of the mouse VRC are capable of producing a eupnea-sigh burst pattern in 8 mM K⁺ solution (Tryba et al., 2008) suggests that endogeneous drive for such pattern may reside within the VRC (e.g. the RTN and/or pFRG). Nevertheless, other structures may also be involved in the generation of distinct inspiratory patterns in more intact preparations.

Inspiratory patterns are not necessarily a dichotomy of either eupnea-sigh or eupnea burst patterns, but may rather represent a gradient-like spatiochemical organization of these distinct drives to rhythmogenic preBötC neurons. While r+preBötC[700] and c+preBötC[700] slices generate eupnea-sigh and eupnea burst patterns, respectively, a

biphasic burst pattern is observed in m-preBötC[500-600] slices (Ruangkittisakul et al., 2006, 2008). Such inspiratory pattern may be considered as an intermediate between the two inspiratory patterns.

The findings from multiphoton Ca^{2+} imaging in the present study indicate that all (except photodamaged) inspiratory preBötC neurons are capable of reconfiguring between eupnea-sigh and eupnea patterns (Ruangkittisakul et al., 2008). Specifically, inspiratory preBötC neurons in the present study showed small amplitude Ca^{2+} rises intermingled with large amplitude Ca^{2+} rises in response to SP or a NK1 receptor agonist after onset of in vitro apnea. In contrast, Ca^{2+} oscillations of rather uniform amplitude were revealed in the same cells in response to TRH or the blockers of phosphodiesterase-4 theophylline and rolipram. This supports the previous hypothesis by Ramirez's group based on intracellular recording of eupnea and sigh bursts in single inspiratory neurons in mouse slices that multiple inspiratory behaviours derive from one reconfiguring network (Lieske et al., 2000; Tryba et al., 2008).

Although the present Ca^{2+} imaging results suggest that a single preBötC network reconfigures its activity patterns under the influence of SP and TRH, the possibility can not be excluded that these neuromodulators activate distinct population of neurons that subsequently drive a set of follower preBötC neurons. In line with this view, a population of neurons that are active only during sigh bursts was recently found in mouse slices (Tryba et al., 2008).

In summary, this study provides evidence supporting the hypothesis that the preBötC reconfigures under the influence of (respiratory) brainstem structures providing a possible gradient-like spatiochemical organization of SP- and TRH-like neurotransmitters. The combined effects of these transmitters ultimately determine the burst pattern of single preBötC neurons and of the entire rhythmogenic inspiratory network.

5.5 Determination of preBötC Excitability by $\text{Ca}^{2+}/\text{K}^+$ Antagonism

In addition to the modulatory influences of (respiratory) brainstem structures and superfusate K^+ on the isolated preBötC discussed above, its activity is also modulated by the Ca^{2+} concentration in the superfusate. Ca^{2+} is a major determinant of neuronal network excitability (Hille, 2001; Somjen, 2002). On the one hand, exposure of neuronal tissues to low (<0.5 mM) extracellular Ca^{2+} is a common model for epilepsy (Konnerth et al., 1986; Jefferys, 1995). Moreover, hypocalcemia and associated seizures can also occur in intact animals as a result of vitamin D deficiency, hypothyroidism or renal failure (Riggs, 2002; Castilla-Guerra et al., 2006). In contrast, abnormally high levels of Ca^{2+} in the interstitial space cause a general depression of brain functions (Riggs, 2002). In that regard, malignant neoplasms and hyperparathyroidism can lead to hypercalcemia that may be associated with occurrence of centrally induced apnea in children (Riggs, 2002; Castilla-Guerra et al., 2006). Correspondingly, injection of high Ca^{2+} solution into the ventriculo-cisternal space in vivo results in respiratory depression (Berndt et al., 1969; Leusen, 1972; Berkenbosch & Adan, 1974), whereas such depression is not observed when K^+ is injected simultaneously with Ca^{2+} (Leusen, 1972).

Here, Ca^{2+} effects were studied on preBötC rhythms in both the newborn rat slice and en bloc model. A slight increase of superfusate Ca^{2+} from 1 to 1.2 mM reduced the longevity of inspiratory rhythm in 600 μm thick slices, whereas 1.5 mM Ca^{2+} induced in vitro apnea (Ruangkittisakul et al., 2007), although both concentrations were within the presumable physiological Ca^{2+} range of 1-1.5 mM (Somjen, 2002). In contrast, raising extracellular Mg^{2+} from 1 to 2 mM did not significantly affect the longevity of rhythm in these slices. This finding argues against the role of surface charges in the inhibitory effect of Ca^{2+} on the respiratory rhythm (Hille, 2001; Somjen, 2002).

Similar to the inhibitory effect of Ca^{2+} on inspiratory slice rhythms, raised Ca^{2+} also blocked cervical nerve bursts in the en bloc model. The effective Ca^{2+} concentration to block the rhythm correlated with the rostral boundary of the en bloc model, i.e., more Ca^{2+} was necessary to block the rhythm in preparations with more rostral tissue. This may

indicate that (respiratory) structures in the rostral brainstem such as the pFRG have a higher tolerance to elevated Ca^{2+} , and are therefore capable of driving the preBötC in such preparations. Alternatively, metabolism-related accumulation of interstitial K^+ and H^+ (Brockhaus et al., 1993; Okada et al., 2005) is likely more prominent in en bloc medullas with a complete VII nucleus compared to those whose rostral boundaries were cut more caudally. Such build-up of interstitial K^+ (and H^+) may counteract the inhibitory Ca^{2+} effect in the larger preparations. This is supported by the finding that Ca^{2+} -induced respiratory depression in both the slice and en bloc model is reversed by elevated K^+ , a result consistent with previous in vivo findings (Leusen, 1972). This strong Ca^{2+} dependence of activity of the isolated preBötC explains the need for elevated K^+ in other preBötC slice studies.

One possible target of the inhibitory central respiratory effects of extracellular Ca^{2+} is a class of G-protein coupled Ca^{2+} sensing receptors (Hebert & Brown, 1995; Bouschet & Henley, 2005). These receptors were discovered in kidney tissue and presumably play an important role in Ca^{2+} and Mg^{2+} homeostasis (Hebert, 1996). They are also expressed in central neurons and astrocytes (Bouschet & Henley, 2005), but little is known about their distribution in brainstem regions associated with respiration. Other receptors such as GABA_B and metabotropic glutamate receptors sharing close homology to the Ca^{2+} sensing receptor are also sensitive to changes of extracellular Ca^{2+} in physiological range (Kubo et al., 1998; Wise et al., 1999).

5.6 Conclusions and Future Perspectives

It was first shown that novel online histology enables the generation of calibrated newborn rat preBötC slices with histologically-identified and reproducible rostral and caudal boundaries. A detailed analysis of the structure-function relationship of the preBötC was performed for the first time here using systematically-varied brainstem slices. The findings indicate that the rostrocaudal extension of the hypothesized inspiratory center sufficient for generation of rhythm in thin slices is $<200 \mu\text{m}$, whereas

the preBötC extension necessary for rhythm in thicker slices is $<100\ \mu\text{m}$. A corresponding analysis should also be done on slices from mice, which would facilitate the analysis of the effects of genetical manipulation on the neural control of breathing. Since the brainstem of newborn mice is smaller than that of rats, it is possible that the extension of the mouse preBötC is also smaller. In that case, slices from mice of a particular thickness contain more non-preBötC (respiratory) tissue compared to slices of the same thickness from rat pups of the same early postnatal age. This would make a comparison of findings on preBötC slices between these species difficult. Furthermore, the results from transection experiments of the newborn rat en bloc model in the present work suggest that the pFRG is located more rostrally than previously thought. Future studies may apply combined caudal and rostral transection of the en bloc model for identification of the rostrocaudal extent of the pFRG.

Another interesting question refers to the fact that the activity of the isolated preBötC is strongly depressed by extracellular Ca^{2+} levels close to the upper end of the presumable physiological spectrum of 1-1.5 mM. Accordingly, it would be important to study the Ca^{2+} dependence of the activity of the isolated pFRG. This should in particular be studied in calibrated rostral brainstem blocks without the preBötC that generate presumably pFRG-driven rhythmic VII nerve activity. Besides, the mechanism for the depressing effect of extracellular Ca^{2+} on the preBötC and (possibly also the pFRG) should be identified. Initial targets for such research could be Ca^{2+} sensitive receptors.

Based on the present findings, another important aspect of future research would be devoted to the central chemosensitivity in the novel slices that generate rhythm in 3 mM K^+ solution. It is possible that the sensitivity of these slices to CO_2 and H^+ is higher than that of slices studied in artificially-elevated superfusate K^+ , similar to their increased sensitivity to neuromodulators such as opioids. In that regard, a thorough analysis of the modulating effect of K^+ on the activities of isolated preBötC and pFRG networks would also be important. For example, sighs have not been described in preBötC slices from newborn rats in elevated K^+ . This suggests that K^+ may change the fictive inspiratory patterns in rat preBötC slices.

It was furthermore revealed that the blockers of the cAMP-regulating phosphodiesterase-4 theophylline (at concentrations >1 mM) and rolipram greatly stimulate the interneuronal preBötC networks in both the en bloc and slice model. The more specific agent rolipram has been tested successfully in the clinics for the treatment of neurological disorders such as depression and also asthma-related lung diseases (e.g. chronic obstructive pulmonary disease). However, rolipram does have adverse effects. Therefore, currently-developed more specific phosphodiesterase blockers may be tested in the calibrated en bloc and slice model for a potential future use for the treatment of respiratory-related disturbances such as apneas of prematurity or central congenital hypoventilation syndrome.

A further area of future research could be devoted to the question of the identity of the structures rostral to the preBötC that promote the generation of eupnea and eupnea-sigh patterns. One candidate is the caudal brainstem raphe nuclei whose neurons may show a gradient-like rostrocaudal organization of their transmitters, possibly including TRH for boosting of eupnea-like bursts and SP for the activation of sighs.

The novel use of multiphoton Ca^{2+} imaging in this report provided results that support the previous hypothesis that the preBötC has an intrinsic capability to reconfigure its activity patterns. However, in contrast to studies on other (isolated) neuronal tissues, neither the morphology nor the activity of preBötC neurons were resolved sufficiently well in recording depths >100 μm into the slices. Modification of the currently used multiphoton imaging system, e.g., by positioning the photomultipliers closer to the objective or optimization of the pathway and properties of the titan-sapphire laser beam may notably improve the fluorescence signals in greater tissue depths. Furthermore, the Ca^{2+} sensitive dye fluo-4-AM, used for the present study, is not optimal to reveal the morphology of the loaded preBötC neurons. Additional loading of these cells with “morphological” dyes, e.g., of the “Alexis” family, may provide more details on the structure-function relationship of these cells.

In conclusion, standardization of the dimensions of the respiratory active newborn rat en bloc and slice models, and novel routine use of solution with physiological ion content resulted in important new findings regarding the structure-function relationship and (pharmacological) functional properties of the preBötC (and the pFRG). These findings may stimulate research in other laboratories to use these preparations under similar experimental conditions for a better comparability of findings. Future research will likely establish that (pharmacological) treatment of these defined preparations modifies the activity of the isolated centers more directly than that of less-reduced or intact models for the neural control of breathing. This may result in a more effective approach to test novel therapeutic pharmacology for the treatment of respiratory-related disturbances.

5.7 References

- Ballanyi K, Onimaru H (2008) Respiratory network analysis, isolated respiratory center functions. In: Encyclopedic reference of neuroscience. Eds Binder M, Hirsch M, Hirokawa N, Windhorst U. Springer, New York (in press).
- Ballanyi K, Onimaru H, Keller B (2008) Respiratory network analysis, functional imaging. In: Encyclopedic reference of neuroscience. Eds Binder M, Hirsch M, Hirokawa N, Windhorst U. Springer, New York (in press).
- Ballanyi K, Ruangkittisakul A (2008) Brain slices. In: Encyclopedic reference of neuroscience. Eds Windhorst U, Binder M, Hirokawa. Springer, New York (in press).
- Ballanyi K, Onimaru H, Homma I (1999) Respiratory network function in the isolated brainstem-spinal cord of newborn rats. *Prog Neurobiol* 59, 583-634.
- Berkenbosch A, Adan AJ (1974) Influence of CSF calcium concentration on the ventilatory response to CO₂ and O₂. *Pflugers Arch* 348, 33-50.
- Berndt J, Fenner A, Berger K (1969) Influence of calcium and magnesium on the respiratory response to changes in CSF pH. *Respir Physiol* 7, 216-229.
- Bianchi AL, Denavit-Saubie M, Champagnat J (1995) Central control of breathing in mammals: Neuronal circuitry, membrane properties, and neurotransmitters. *Physiol Rev* 75, 1-45.
- Bouschet T, Henley JM (2005) Calcium as an extracellular signalling molecule: Perspectives on the calcium sensing receptor in the brain. *C R Biol* 328, 691-700.
- Brockhaus J, Ballanyi K, Smith JC, Richter DW (1993) Microenvironment of respiratory neurons in the in vitro brainstem-spinal cord of neonatal rats. *J Physiol* 462, 421-445.
- Castilla-Guerra L, del Carmen Fernandez-Moreno M, Lopez-Chozas JM, Fernandez-Bolanos R (2006) Electrolytes disturbances and seizures. *Epilepsia* 47, 1990-1998.
- Cherniack NS, von Euler C, Glogowska M, Homma I (1981) Characteristics and rate of occurrence of spontaneous and provoked augmented breaths. *Acta Physiol Scand* 111, 349-360.
- Ellenberger HH (1999) Nucleus ambiguus and bulbospinal ventral respiratory group neurons in the neonatal rat. *Brain Res Bull* 50, 1-13.

- Feldman JL, Del Negro CA (2006) Looking for inspiration: New perspectives on respiratory rhythm. *Nat Rev Neurosci* 7, 232-242.
- Feldman JL, Mitchell GS, Nattie EE (2003) Breathing: Rhythmicity, plasticity, chemosensitivity. *Annu Rev Neurosci* 26, 239-266.
- Fortuna MG, West GH, Stornetta RL, Guyenet PG (2008) Botzinger expiratory-augmenting neurons and the parafacial respiratory group. *J Neurosci* 28, 2506-2515.
- Guyenet PG, Stornetta RL, Bayliss DA (2008) Retrotrapezoid nucleus and central chemoreception. *J Physiol* 586, 2043-2048.
- Hebert SC (1996) Extracellular calcium-sensing receptor: Implications for calcium and magnesium handling in the kidney. *Kidney Int* 50, 2129-2139.
- Hebert SC, Brown EM (1995) The extracellular calcium receptor. *Curr Opin Cell Biol* 7, 484-492.
- Hille B (1992) Ionic channels of excitable membranes.
- Huang Q, Zhou D, St John WM (1997) Lesions of regions for in vitro ventilatory genesis eliminate gasping but not eupnea. *Respir Physiol* 107, 111-123.
- Jacobs BL, Azmitia EC (1992) Structure and function of the brain serotonin system. *Physiol Rev* 72, 165-229.
- Janczewski WA, Feldman JL (2006) Distinct rhythm generators for inspiration and expiration in the juvenile rat. *J Physiol* 570, 407-420.
- Jefferys JG, Borck C, Mellanby J (1995) Chronic focal epilepsy induced by intracerebral tetanus toxin. *Ital J Neurol Sci* 16, 27-32.
- Johnson SM, Smith JC, Funk GD, Feldman JL (1994) Pacemaker behavior of respiratory neurons in medullary slices from neonatal rat. *J Neurophysiol* 72, 2598-2608.
- Kachidian P, Poulat P, Marlier L, Privat A (1991) Immunohistochemical evidence for the coexistence of substance P, thyrotropin-releasing hormone, GABA, methionine-enkephalin, and leucin-enkephalin in the serotonergic neurons of the caudal raphe nuclei: A dual labeling in the rat. *J Neurosci Res* 30, 521-530.
- Kashiwagi M, Onimaru H, Homma I (1993) Correlation analysis of respiratory neuron activity in ventrolateral medulla of brainstem-spinal cord preparation isolated from newborn rat. *Exp Brain Res* 95, 277-290.

- Konnerth A, Heinemann U, Yaari Y (1986) Nonsynaptic epileptogenesis in the mammalian hippocampus in vitro. I. development of seizurelike activity in low extracellular calcium. *J Neurophysiol* 56, 409-423.
- Kubo Y, Miyashita T, Murata Y (1998) Structural basis for a Ca^{2+} -sensing function of the metabotropic glutamate receptors. *Science* 279, 1722-1725.
- Leusen I (1972) Regulation of cerebrospinal fluid composition with reference to breathing. *Physiol Rev* 52, 1-56.
- Lieske SP, Thoby-Brisson M, Telgkamp P, Ramirez JM (2000) Reconfiguration of the neural network controlling multiple breathing patterns: Eupnea, sighs and gasps. *Nat Neurosci* 3, 600-607.
- Mallios VJ, Lydic R, Baghdoyan HA (1995) Muscarinic receptor subtypes are differentially distributed across brain stem respiratory nuclei. *Am J Physiol* 268, L941-9.
- McLean HA, Remmers JE (1994) Respiratory motor output of the sectioned medulla of the neonatal rat. *Respir Physiol* 96, 49-60.
- Mellen NM, Janczewski WA, Bocchiaro CM, Feldman JL (2003) Opioid-induced quantal slowing reveals dual networks for respiratory rhythm generation. *Neuron* 37, 821-826.
- Monteau R, Morin D, Hennequin S, Hilaire G (1990) Differential effects of serotonin on respiratory activity of hypoglossal and cervical motoneurons: An in vitro study on the newborn rat. *Neurosci Lett* 111, 127-132.
- Nattie EE, Li A, Richerson G, Lappi DA (2004) Medullary serotonergic neurones and adjacent neurones that express neurokinin-1 receptors are both involved in chemoreception in vivo. *J Physiol* 556, 235-253.
- Okada Y, Kuwana S, Kawai A, Muckenhoff K, Scheid P (2005) Significance of extracellular potassium in central respiratory control studied in the isolated brainstem-spinal cord preparation of the neonatal rat. *Respir Physiol Neurobiol* 146, 21-32.
- Oku Y, Masumiya H, Okada Y (2007) Postnatal developmental changes in activation profiles of the respiratory neuronal network in the rat ventral medulla. *J Physiol* 585, 175-186.

- Onimaru H, Kumagawa Y, Homma I (2006) Respiration-related rhythmic activity in the rostral medulla of newborn rats. *J Neurophysiol* 96, 55-61.
- Onimaru H, Homma I (2003) A novel functional neuron group for respiratory rhythm generation in the ventral medulla. *J Neurosci* 23, 1478-1486.
- Onimaru H, Arata A, Homma I (1997) Neuronal mechanisms of respiratory rhythm generation: An approach using in vitro preparation. *Jpn J Physiol* 47, 385-403.
- Onimaru H, Homma I, Iwatsuki K (1992) Excitation of inspiratory neurons by preinspiratory neurons in rat medulla in vitro. *Brain Res Bull* 29, 879-882.
- Onimaru H, Arata A, Homma I (1990) Inhibitory synaptic inputs to the respiratory rhythm generator in the medulla isolated from newborn rats. *Pflugers Arch* 417, 425-432.
- Onimaru H, Homma I (1987) Respiratory rhythm generator neurons in medulla of brainstem-spinal cord preparation from newborn rat. *Brain Res* 403, 380-384.
- Richter DW, Ballanyi K, Schwarzacher S (1992) Mechanisms of respiratory rhythm generation. *Curr Opin Neurobiol* 2, 788-793.
- Riggs JE (2002) Neurologic manifestations of electrolyte disturbances. *Neurol Clin* 20, 227-39.
- Ruangkittisakul A, Schwarzacher SW, Secchia L, Ma Y, Bobocea N, Poon BY, Funk GD, Ballanyi K (2008) Generation of eupnea and sighs by a spatiochemically organized inspiratory network. *J Neurosci* 28, 2447-2458.
- Ruangkittisakul A, Secchia L, Bornes TD, Palathinkal DM, Ballanyi K (2007) Dependence on extracellular Ca^{2+}/K^{+} antagonism of inspiratory centre rhythms in slices and en bloc preparations of newborn rat brainstem. *J Physiol* 584, 489-508.
- Ruangkittisakul A, Schwarzacher SW, Secchia L, Poon BY, Ma Y, Funk GD, Ballanyi K (2006) High sensitivity to neuromodulator-activated signaling pathways at physiological $[K^{+}]$ of confocally imaged respiratory center neurons in on-line-calibrated newborn rat brainstem slices. *J Neurosci* 26, 11870-11880.
- Smith JC, Ellenberger HH, Ballanyi K, Richter DW, Feldman JL (1991) Pre-botzinger complex: A brainstem region that may generate respiratory rhythm in mammals. *Science* 254, 726-729.

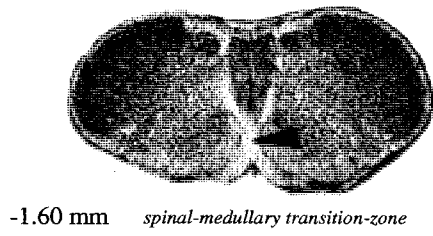
- Somjen GG (2002) Ion regulation in the brain: Implications for pathophysiology. *Neuroscientist* 8, 254-267.
- Taccola G, Secchia L, Ballanyi K (2007) Anoxic persistence of lumbar respiratory bursts and block of lumbar locomotion in newborn rat brainstem spinal cords. *J Physiol* 585, 507-524.
- Tryba AK, Pena F, Lieske SP, Viemari JC, Thoby-Brisson M, Ramirez JM (2008) Differential modulation of neural network and pacemaker activity underlying eupnea and sigh breathing activities. *J Neurophysiol.* (in press)
- Voituron N, Frugiere A, Champagnat J, Bodineau L (2006) Hypoxia-sensing properties of the newborn rat ventral medullary surface in vitro. *J Physiol* 577, 55-68.
- Wise A, Green A, Main MJ, Wilson R, Fraser N, Marshall FH (1999) Calcium sensing properties of the GABA_(B) receptor. *Neuropharmacology* 38, 1647-1656.

Appendix I

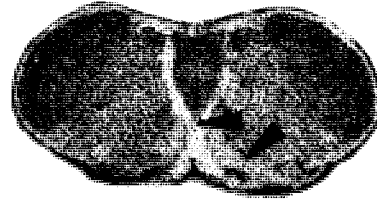
Atlas of Newborn Rat Medulla Oblongata

Abbreviations:

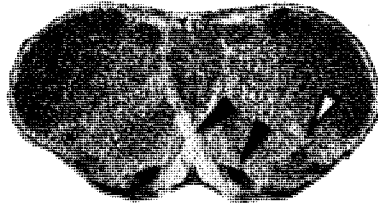
AP	area postrema
DC	medial nucleus of inferior olive, dorsal cap
DMCC	dorsomedial cell column
DMX	dorsal motor nucleus of the vagus nerve
IO	inferior olive
IOA/B	medial inferior olive, subnucleus A and B
IO β	medial inferior olive, subnucleus β
IOD	dorsal inferior olive
IOM	medial inferior olive
IOP	principal inferior olive
LRN	lateral reticular nucleus
LRNdiv	lateral reticular nucleus divided into medial and lateral subnucleus
NA	nucleus ambiguus, compact formation
NTB	nucleus of the trapezoid body
PD	pyramidal decussation
OBEX	Obex, the point where the central canal opens to the 4 th ventricle
V4	4 th ventricle
VII	facial nucleus
VII _{dor}	dorsal nucleus of the facial nucleus
VII _{med}	medial nucleus of the facial nucleus
VII _{lat}	lateral nucleus of the facial nucleus
XII	hypoglossal nucleus



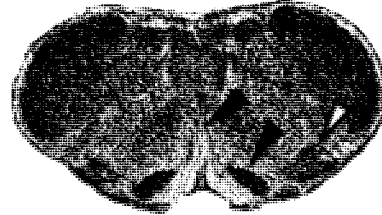
-1.60 mm *spinal-medullary transition-zone*



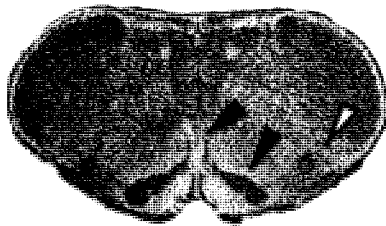
-1.55 mm *IOM: caudal end*



-1.50 mm *LRN: caudal end*



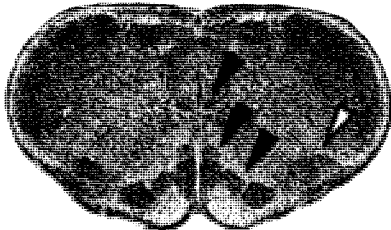
-1.45 mm *IOM: 1 nucleus*



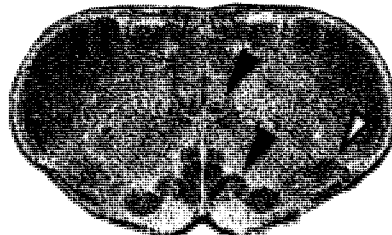
-1.40 mm *PD: rostral end
IOM: 2 nuclei (IOA/B)*



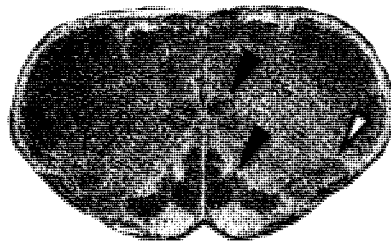
-1.35 mm *IOM: 3 nuclei (IOA/B, IOβ)
LRN: small*



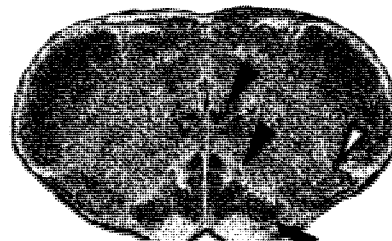
-1.30 mm *IOM: 4 nuclei (IOA/B, IOβ, DC)
XII: caudal end*



-1.25 mm *IOM: small loop in 2nd nucleus (IOB)
LRN: medium*

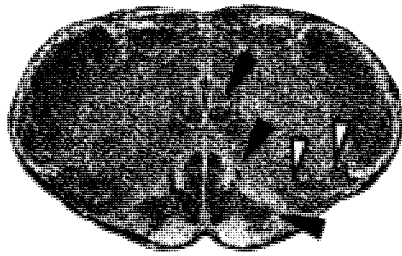


-1.20 mm *LRN: big*

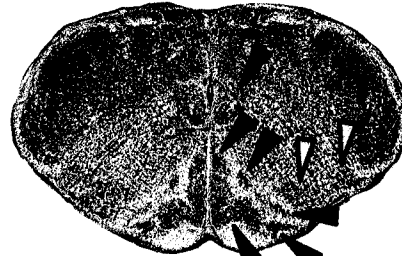


-1.15 mm *IOD: caudal end*

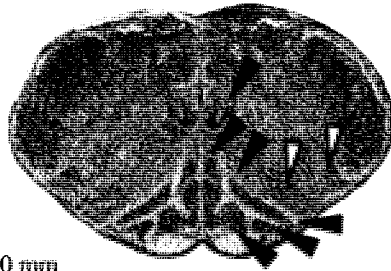
◄ PD ◄ IOM ◄ IOP ◄ IOD ◄ LRN ◄ XII



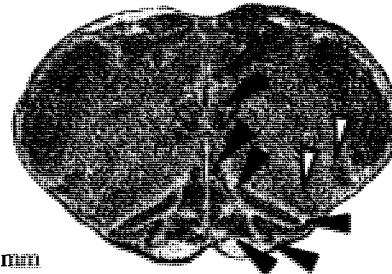
-1.10 mm LRN: medial and lateral nuclei



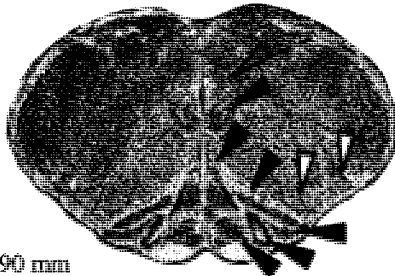
-1.05 mm IOD: broken band towards ventral surface
IOP: caudal end



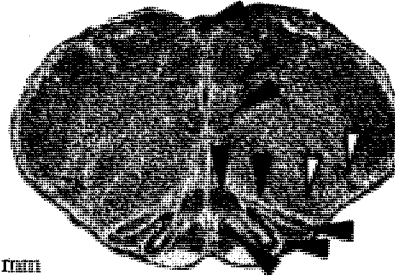
-1.00 mm IOD: big dorsal band
LRN: divided in medial and lateral nuclei



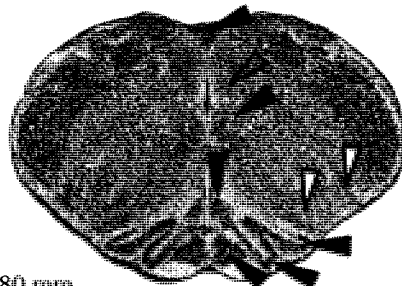
-0.95 mm IOM: sharp tip of dorsal cap
IOP: caudal end of 1st loop, DMX: caudal end



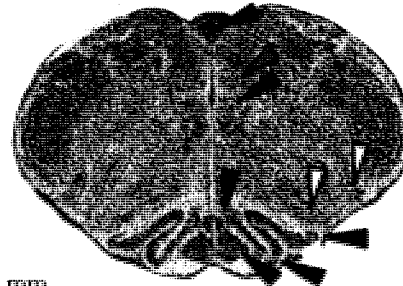
-0.90 mm IOM: rostral end of dorsal cap
IOP: small 1st loop



-0.85 mm IOD: small dorsal band, forms 2nd loop
IOP: small 1st loop, AP: caudal end

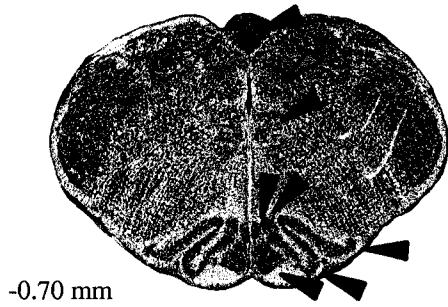


-0.80 mm IOM: rostral end of dorsal part
IOD: rostral end of dorsal band



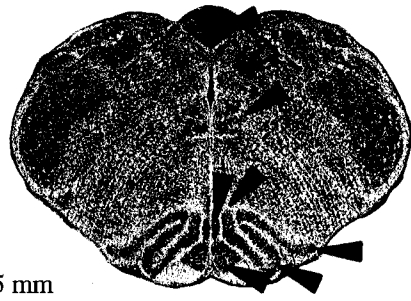
-0.75 mm DMCC: caudal end, IOD: rostral end of 2nd loop
LRN: rostral end of medial and lateral nuclei

▲ IOM ▲ DMCC ▲ IOP ▲ IOD
 ▲ LRN ▲ LRN_{div} ▲ AP ▲ XII ▲ DMX



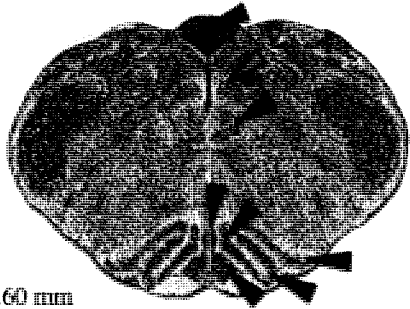
-0.70 mm

*IOP: caudal end of dorsal part
IOD: lateral part forms hook*



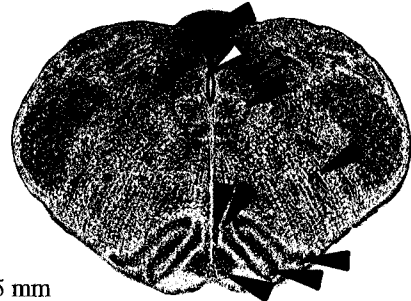
-0.65 mm

*DMCC: big, IOD: lateral part flat
IOP: 1st loop big, dorsal part big*



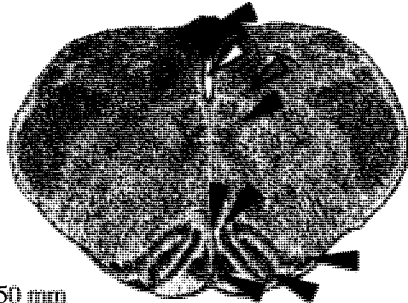
-0.60 mm

*DMCC: medium, IOM: big
IOP: dorsal part forms medial edge*



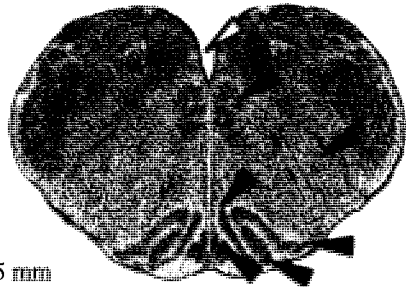
-0.55 mm

*DMCC: small, IOP: 1st loop big
Central canal opens to 4th ventricle = Obex*



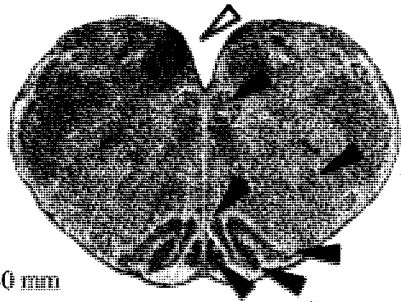
-0.50 mm

*DMCC: units with IOM, IOP: dorsal part round
IOD: lateral part long and flat, AP: rostral end*



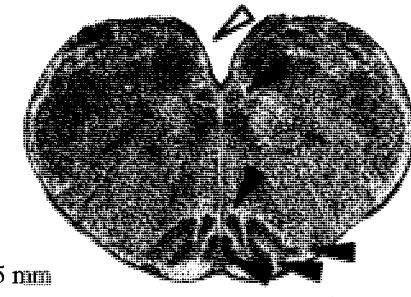
-0.45 mm

*IOM: dorsal tip, IOP: 1st loop medium
IOD: lateral part flat*



-0.40 mm

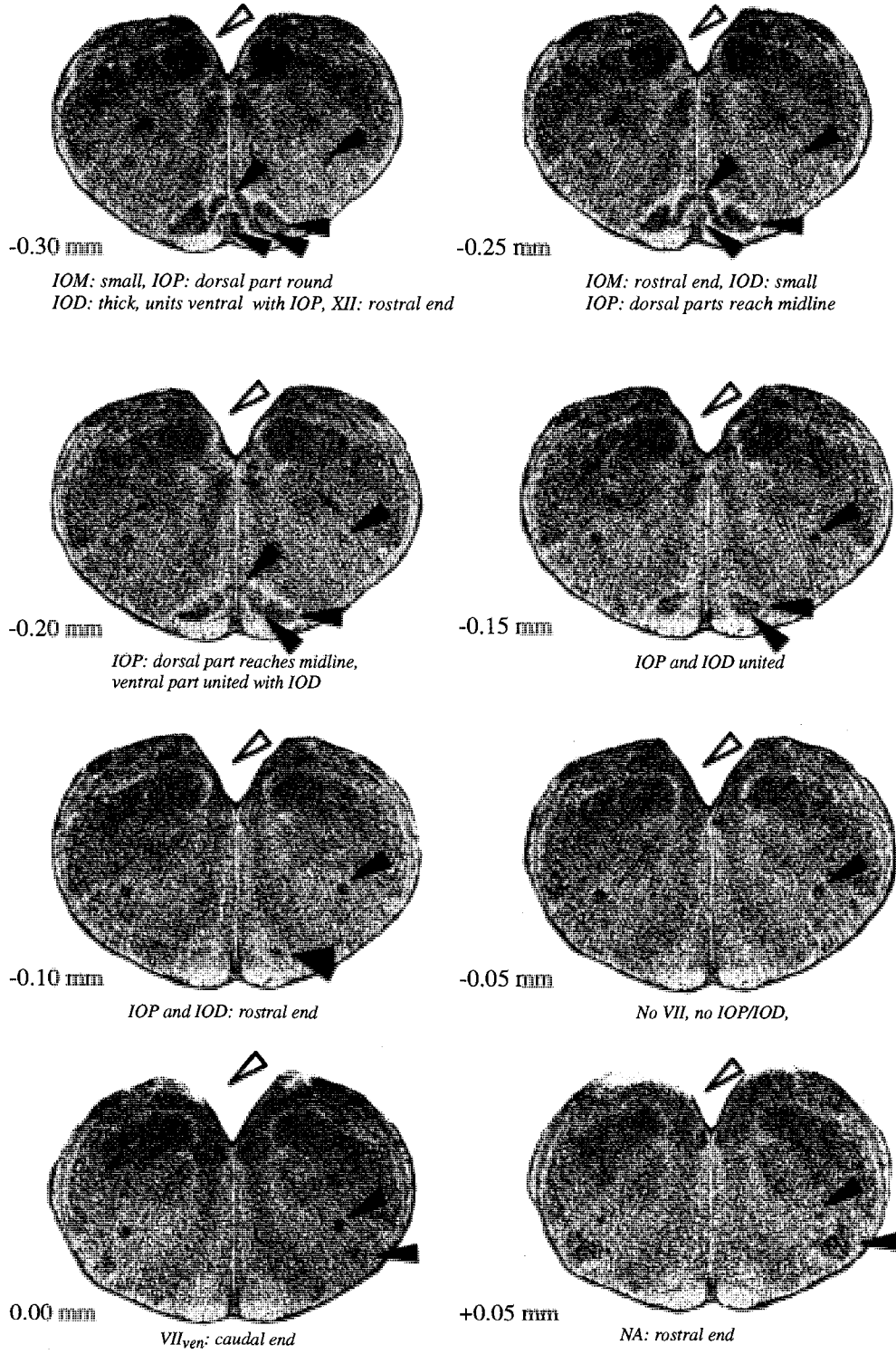
*IOM: medium, triangular, IOP: 1st loop small
IOD: rostral end of lateral part*

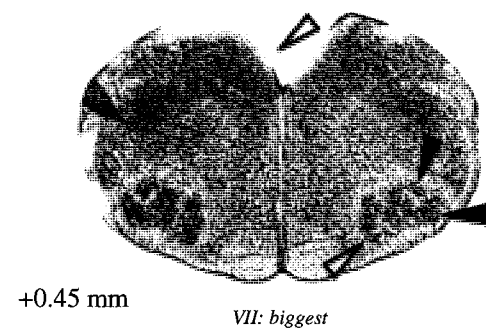
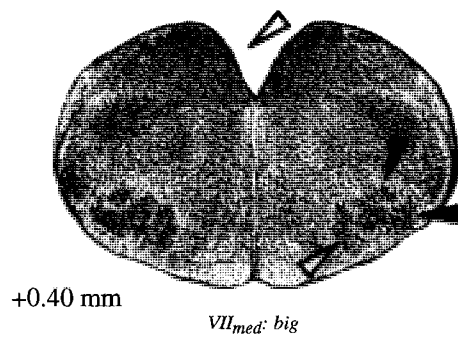
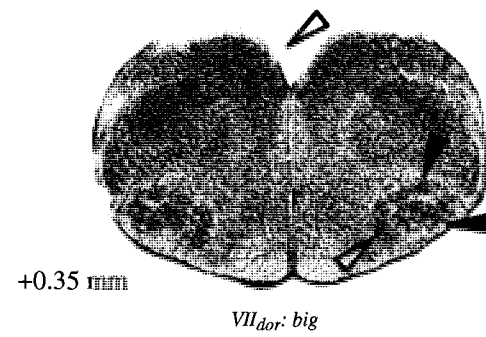
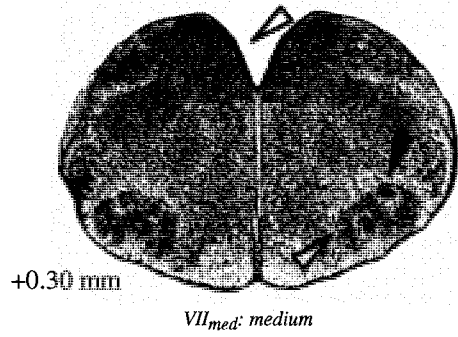
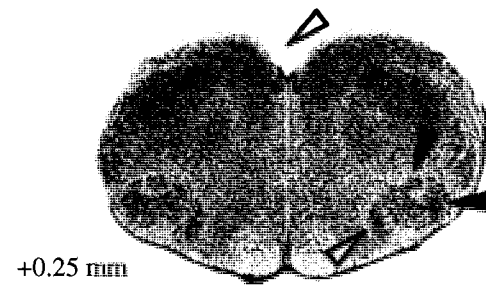
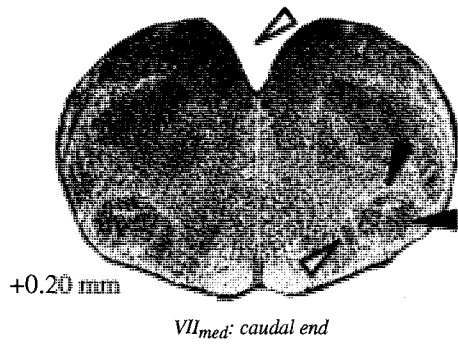
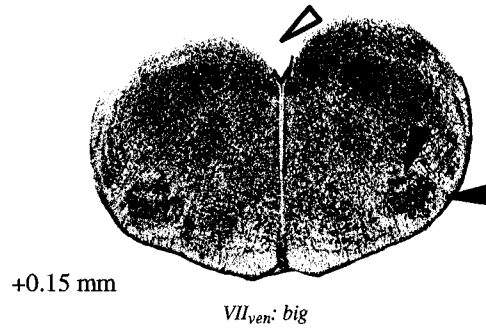
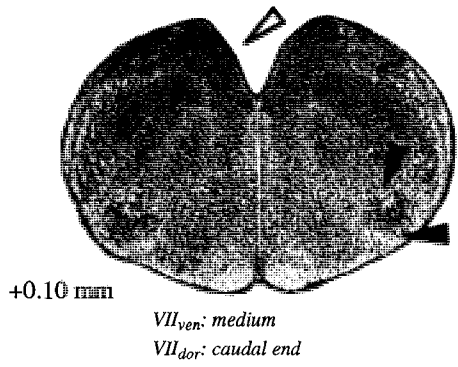


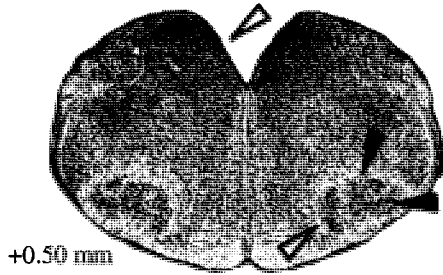
-0.35 mm

*IOM: small, IOP: rostral end of 1st loop
IOD: thin, ventral divided from IOP*

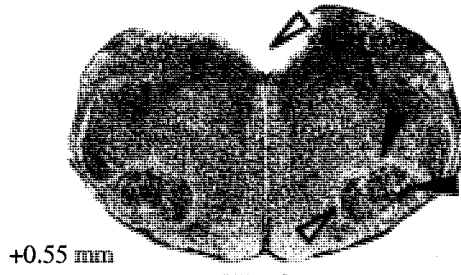
◀ IOM ◀ DMCC ◀ IOP ◀ IOD ◀ AP ◀ XII ◀ DMX ◀ NA ◀ V4





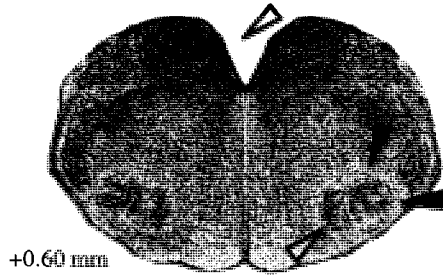


+0.50 mm



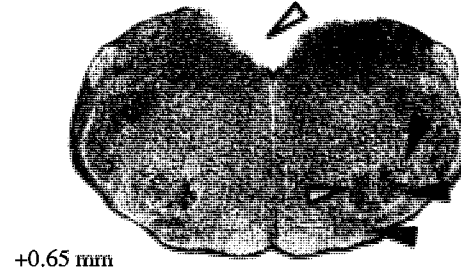
+0.55 mm

VII_{dor}: big



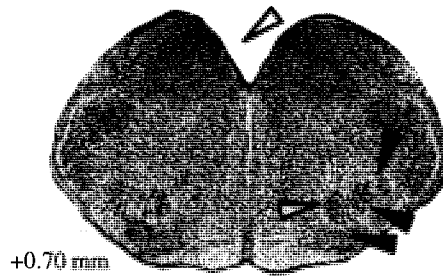
+0.60 mm

VII_{med}: big and flat



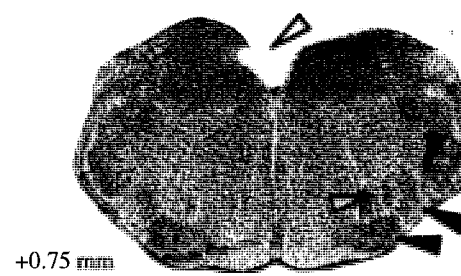
+0.65 mm

*VII_{ven}: small, VII_{dor}: small
NTB: caudal end*



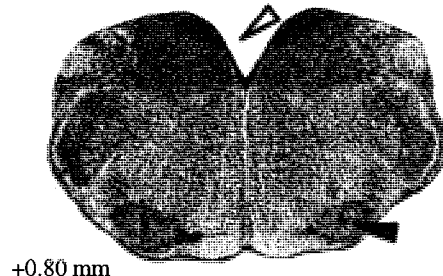
+0.70 mm

NTB: medium

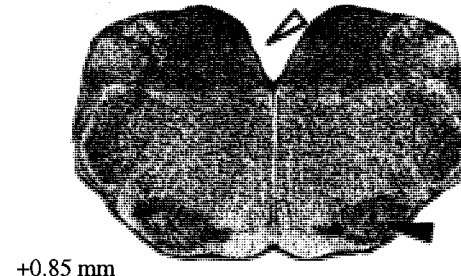


+0.75 mm

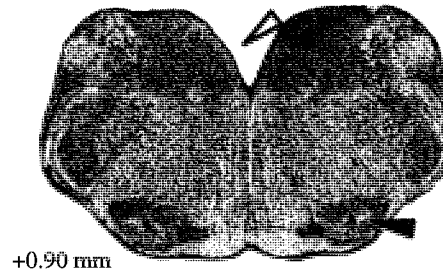
VII: rostral end



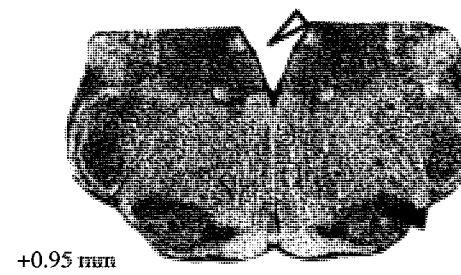
+0.80 mm



+0.85 mm



+0.90 mm



+0.95 mm

◀ NTB ◀ VII_{med} ◀ VII_{ven} ◀ VII_{dor} ◀ V4

Appendix II

Inspiratory burst patterns in 3 mM K⁺ in newborn rat preBötC slices

(For references, see chapter III)

One major aim of our study was to analyze in solution of physiological (3 mM) K⁺ whether inspiratory-related burst patterns in newborn rat brainstem slices depend on structures that rostrocaudally surround rhythmogenic inspiratory networks of the preBöttinger Complex (preBötC). For this purpose, the preBötC has been explored by systematically varying slice boundaries and/or thickness. In subgroups of these novel “calibrated” slices with a thickness ranging from 175 to 700 μm , patterns of inspiratory activity differed notably from robust bursting in 500 or 600 μm thick slices with the preBötC in the middle (“m-preBötC slices”) (Ruangkittisakul et al., 2006). Thus, we outline here properties that discriminate these distinct inspiratory-related burst patterns as well as inspiratory from putative non-respiratory activities. Moreover, we establish with suction electrodes that rhythmic activity within the ventral aspect of the slices derives only from the ventrolateral region corresponding to the preBötC, and in this way distinguish inspiratory from non-respiratory activities. Because the longevity of rhythm in 3 mM K⁺ varies as a function of slice thickness, burst properties in all slices are described based on the activity produced between 20 and 80 min after the start of recording when most activities remain stable (see chapter III for details).

In vitro inspiratory burst patterns

Isolated newborn rodent brainstem preparations generate various patterns of inspiratory-related bursts. In mouse preBötC slices in 8 mM K⁺ (Lieske et al., 2000), the predominant activity recorded at the slice surface, within a region that likely corresponds to the ventral respiratory column (Alheid et al., 2004), consists of events with a regular rate (5-15 bursts/min) and rather uniform amplitude. The temporal relation with intracellular respiratory bursting suggests that the extracellular neuronal population discharge corresponds to “fictive eupnea” (Figure A2-1A) (Lieske et al., 2000). At intervals of 1-5 min, the fictive eupnea burst pattern is interrupted by a burst that merges with a distinct, higher amplitude component. The subsequent eupneic burst is delayed by 1.5-3 cycles (Figure A2-1A). Because of the similarity of the enhanced bursts with sighs in vivo, they were labeled “fictive sighs” (Lieske et al., 2000).

Similarly, in newborn rat brainstem-spinal cords in 6.2 mM K⁺ inspiratory-related “fictive eupnea” nerve bursts of regular rate and amplitude are interrupted at 1-7 min intervals by one “biphasic burst” (Figure A2-1B) (Shvarev et al., 2003). This burst resembles the sigh in the mouse slices because it begins with a eupnea-like event and the peak of this initial phase is followed by a second component. The difference, however, is

that the second component of this biphasic event is similar in amplitude to the first (Figure A2-1B) (Shvarev et al., 2003). The difference between large amplitude sighs in the mouse slices and biphasic bursts in the en bloc model is not related to the fact that recordings were from the ventrolateral slice surface and cervical nerves, respectively. A burst pattern, similar to that in the en bloc medullas, can also be recorded in 3 mM K^+ from the ventrolateral surface of 500 or 600 μm thick newborn rat m-preBötC slices (Ruangkittisakul et al., 2006). Specifically, fictive eupnea-like “S-bursts” of regular amplitude and rate (~ 9 bursts/min) are interrupted by single biphasic “intermingled” events (“I-bursts”) of similar amplitude, which occur more frequently (at >2 bursts/min) than biphasic bursts in the en bloc model (Figure A2-1C).

In a subgroup of the latter 500 or 600 μm thick m-preBötC slices, the inspiratory pattern consists of one large amplitude event followed by a pause of activity (Figure A2-1C). The first burst after this inhibitory period is typically small and the amplitude of subsequent bursts often increases progressively until the onset of another large amplitude burst. The large amplitude events were referred to as “sighs” based on their prominent amplitude and the subsequent period of inactivity similar to the burst pattern in mouse slices (Lieske et al., 2000). The amplitude of bursts between consecutive sighs sometimes varies between slices and also between burst cycles in a given slice (Figure A2-1C). Because of this difference from the constant amplitude eupneic bursts in the mouse slices, these activities in the rat slices were labeled “intersigh bursts” (Ruangkittisakul et al., 2006). During longer recording periods in 3 mM K^+ , sighs can become the predominant type of rhythmic activity in rat slices due to a partial disappearance of the intersigh eupneic bursts (Figure A2-1C) (Ruangkittisakul et al., 2006).

For a unifying terminology of rhythmic activities in preBötC-containing brainstem slices, we assume that both S-bursts and intersigh bursts are subtypes of eupneic bursts, whereas intermingled bursts correspond to biphasic bursts. The greater variability of eupneic burst amplitude in rat compared to mouse slices may be due to differences between species, experimental conditions such as elevated superfusate K^+ in mice, or slice dimensions. We propose that newborn rat preBötC slices are capable of 3 inspiratory-related activities in oxygenated 3 mM K^+ saline: (i) “eupnea (bursts)”, (ii) “sigh (bursts)” and (iii) “biphasic bursts”. In rat preBötC slices, 2 of these activities can occur at a given time: (i) eupneic bursts plus sighs constitute a “eupnea-sigh (burst) pattern”, whereas (ii) eupneic bursts plus biphasic events generate a “eupnea-biphasic (burst) pattern”.

Discrimination of inspiratory and non-respiratory activity in the preBötC area

Below, criteria are given for discrimination of inspiratory versus non-respiratory activities monitored with suction electrodes from the surface of the ventral portion of the slices. A pivotal criterion is the region from which inspiratory population activity is recorded. In the above mouse slices, both eupneic and sigh bursts have maximal amplitudes in the same “hot spot” within the ventrolateral medulla (Figure A2-2A) (Lieske et al., 2000), whereas rhythmic activity is lost if the suction electrode is displaced by >300 μm . Thus, a most important criterion for lack of inspiratory-related activity in preBötC slices is the absence of rhythmic bursts (with a rate, duration or rise time similar to those described below) within this ventrolateral region that has a very similar location

in various studies (for references see Funk et al., 1993; Richter and Spyer, 2001; Ramirez et al., 2002). Importantly, lack of rhythmic activity within this area can be due to the fact that inspiratory bursting in 3 mM K⁺ arrests spontaneously after time periods of one to several hours (Figure A2-3) (for references, see chapter II and III). Thus, activities in 3 mM K⁺ should be assessed immediately after generating the slices.

Synchrony of bursting between the 2 sides of the bilaterally-organized preBötC (and with inspiratory-related hypoglossal nerve or nucleus activity) is a further criterion for inspiratory rhythm (Figures A2-1, A2-2, A2-3). Lack of synchrony, in contrast, does not imply that rhythmic activity is non-respiratory. In thin slices, a difference between the rostrocaudal boundaries of the ipsi- and contralateral sides of the slice (“lateral tilt”) could sever mutual axonal connections that are necessary for synchronous rhythm, or remove more of the critical region on one side than the other. As a result, similar but unsynchronized rhythm may be recorded, or activity may only be detected unilaterally. Furthermore, the definition of the minimal network that is sufficient for rhythm generation based on recording of population field potentials may actually overestimate the minimal slice thickness. This simply reflects that, as slice thickness is reduced, rhythmic burst amplitude also decreases because fewer neurons are expected to discharge in synchrony. Thus, the possibility cannot be excluded that slices ≤ 175 μm thin (i.e. the minimal substrate in our study) are capable of generating rhythm, but that suction electrodes lack the sensitivity required to detect these small signals.

In thin slices, and possibly also in thicker slices with an exposed (and reduced) preBötC, the signal-to-noise ratio of inspiratory bursts may be another critical parameter which depends partly on electrode characteristics. Consequently, it is difficult to compare burst amplitudes and signal-to-noise ratios between slices.

Distinguishing inspiratory burst patterns in 500 and 700 μm thick m-preBötC slices

Previously, only unilateral activities were assessed in the ventrolateral aspect of 500 or 600 μm thick m-preBötC slices in 3 mM K⁺, and the recording sites were not analyzed (Ruangkittisakul et al., 2006). Here, burst patterns were assessed from bilateral recordings on the slice surface over the identified respiratory hot spot in 14 m-preBötC[500] slices with mean caudal and rostral boundaries 0.71 ± 0.05 and 0.23 ± 0.09 mm caudal to the caudal end of the facial (VII) motor nucleus, VII_c, respectively. The purpose of these measurements was to establish the baseline behavior of slices in which the preBötC had not been disturbed, to facilitate a comparison of inspiratory-related burst parameters (e.g. pattern or duration) with those generated by slices in which the preBötC was exposed at one surface or reduced. Four of the above m-preBötC[500] slices showed a eupnea-biphasic burst pattern, in which 1-15 bilaterally-synchronous eupneic bursts were followed by 1 biphasic burst. After >1.5 h, eupneic bursts became shorter and their rate slowed (Figure A2-3A). In 2 other slices, a eupnea-biphasic burst pattern developed 15 and 20 min after initial eupnea, whereas 2 slices showed only eupneic bursts. In 2 further slices, an initial eupnea-biphasic burst pattern turned into a eupnea-sigh pattern after 15-20 min (Figure A2-3B, compare Figure A2-1). Further 4 slices showed a eupnea-sigh pattern from the start of recording. In 2 of these cases, a time-dependent slowing of sigh rate was accompanied by a decrease of eupneic burst amplitude until primarily sighs

remained. Similar to our previous study (Figure 2-4), there was no correlation between the boundaries of the above m-preBötC[500] slices and (i) occurrence of distinct burst patterns, (ii) burst rate and (iii) longevity of rhythms (means 133 ± 18 min in 8 slices without sighs compared to 118 ± 11 min in 6 slices with sighs).

Burst amplitudes were maximal over the region that was expected anatomically to correspond to the center of the ventral respiratory column. Electrode displacement from this hot spot by 100-300 μm caused a progressively smaller signal, and there was no difference between the area of maximal burst amplitude for slices with a eupnea, eupnea-biphasic or eupnea-sigh burst pattern (Figure A2-2B). Analysis of burst amplitude, rate, duration, rise time and shape at 20 and 80 min of recording revealed good signal-to-noise ratios (sighs: 7.2 ± 1.3 , n= 4; biphasic bursts: 5.3 ± 1.4 , n= 5; eupneic bursts between biphasic bursts: 4.9 ± 1.1 , n= 5; eupneic bursts between sighs: 3.7 ± 0.6 , n= 4). Sighs were significantly larger than associated eupneic bursts, whereas biphasic bursts were modestly (significant only at 20 min) larger than associated eupneic bursts (Figures A2-4, A2-5). Contrary to stable amplitudes of biphasic and associated eupnea bursts, eupneic burst amplitudes could vary greatly in slices with a eupnea-sigh pattern (Figures A2-1, A2-3).

As analyzed in 5 of the slices with a eupnea-biphasic burst pattern, mean total burst rate, and also eupneic burst rate, were regular and did not change between 20 and 80 min, whereas the rate of biphasic bursts decreased during that time period (Figure A2-5). Sigh rate also decreased significantly between 20 and 80 min in slices with a eupnea-sigh burst pattern, whereas the rate of associated eupneic bursts, and total eupnea-sigh burst rate, did not change (Figure A2-5). At both 20 and 80 min, sighs and biphasic bursts were significantly longer than their associated eupneic bursts, based on analysis of their half-width (Figures A2-4, A2-5). Importantly, there was a characteristic difference between the shape of sighs and biphasic bursts. Biphasic bursts showed an initial peak (modestly larger than that of eupneic bursts) followed by a partial recovery to baseline before the onset of a further event that was, on average, smaller than the first peak. In contrast, sighs showed a single, large amplitude peak (Figure A2-4). The difference between the shapes of both burst types was reflected by a longer rise time for sighs than biphasic bursts at both 20 and 80 min (Figure A2-5). Inspiratory-related bursting was also studied in 7 m-preBötC[700/-0.89] slices with mean caudal and rostral boundaries 0.89 ± 0.02 and 0.13 ± 0.09 caudal to VII_c, respectively, for a comparison of burst parameters in slices of identical thickness, in which the preBötC was exposed (and reduced) at one surface. All slices generated a eupnea-biphasic burst pattern for 203 ± 29 min, with a significant difference between the duration, but not amplitude or rise time, of eupneic and biphasic bursts at both 20 and 80 min (Figures A2-4, A2-5). The rate of eupneic bursts was stable, whereas the rate of biphasic bursts slowed down significantly between 20 and 80 min (Figure A2-5).

In summary, the above findings showed that m-preBötC slices with a thickness of 500 μm or greater are capable in 3 mM K⁺ of generating 3 patterns of long-term bilaterally-synchronous inspiratory-related activity in the typical ventrolateral respiratory region. These patterns are (i) a eupnea burst pattern, (ii) a eupnea-biphasic burst pattern and (iii)

a eupnea-sigh burst pattern. A burst was counted as a sigh, rather than associated eupneic bursts, if it had (i) a higher amplitude, (ii) a longer duration, (iii) a longer rise time plus (iv) a longer inter-burst interval following it (indicating post-sigh inhibition) than eupneic bursts in the same slice. Conversely, a burst was counted as a biphasic burst, rather than associated eupneic bursts, if it had (i) a longer duration and (ii) a secondary peak compared to eupneic bursts with a single peak in the same slice.

Burst patterns in slices with exposed or reduced preBötC

Based on the above criteria and the findings in the 500 and 700 μm thick m-preBötC slices, inspiratory-related burst patterns have been studied in 2 types of novel “calibrated” slices. First, inspiratory-related bursting was identified in m-preBötC slices of 250 μm or less thickness for determination of the minimal slice thickness that is sufficient for inspiratory rhythm. Second, distinct types of inspiratory-related bursting, specifically a eupnea versus a eupnea-sigh burst pattern, were revealed in c+preBötC[700] and r+preBötC[700] slices, which contained the preBötC plus either caudal or rostral tissue, respectively, for assessment of the minimal preBötC extent that is necessary for generation of rhythm in thicker slices. The specific properties of these slices are described in the main paper. Note, however, that quantitative information on recording sites or burst characteristics in these slices is included in the figures of the present supplemental document for a comparison with corresponding data acquired in the 500-700 μm thick m-preBötC slices.

No eupnea-sigh burst pattern was seen in m-preBötC[700] slices, whereas such a pattern was found in 27% of m-preBötC[600] slices (Ruangkittisakul et al., 2006) and 34% (12 of 35) of m-preBötC[500] slices (data were pooled from present study and those in Ruangkittisakul et al., 2006). This suggests that the probability of occurrence of a eupnea-sigh burst pattern may increase upon reduction of slice thickness.

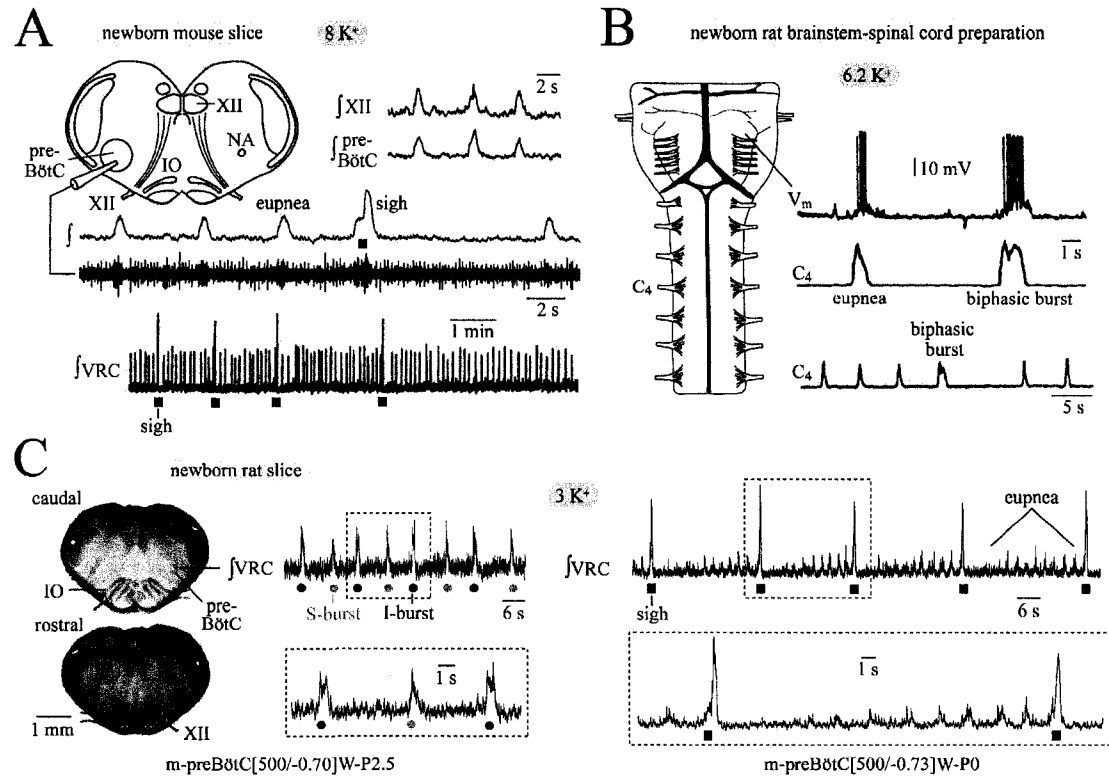


Figure A2-1 Inspiratory burst patterns in newborn rodent brainstem preparations. **A**, in transverse slices from 0-2 weeks-old mice containing the preBötzinger Complex (preBötC), inspiratory-related bursting (shown as raw differential and/or integrated signals) is monitored in 8 mM K^+ solution with suction electrodes from the ventrolateral region of the slice surface close to the nucleus ambiguus (NA), and hypoglossal (XII) nerve roots (upper right inset). The lowermost trace shows “fictive eupneic bursts” of regular rate and amplitude, interrupted at intervals $>1\text{ min}$ by larger amplitude “fictive sighs” and a postsigh period of inhibition. (With kind permission from Lieske et al., 2000.) **B**, In 6.2 mM K^+ , brainstem-spinal cords from 0-4 days-old rats generate fictive eupneic cervical (C_4) nerve bursts alternating with “biphasic bursts” of similar amplitude, likely comprising 2 partially-overlapping eupneic bursts. The lowermost trace shows that biphasic bursts are less frequent than eupneic bursts. (Recordings with kind permission from Shvarev et al., 2003.) **C**, “m-preBötC slices” from 0-4 days-old rats contain the preBötC in the middle. The $500\text{ }\mu\text{m}$ thick slice from a P2.5 Wistar rat with the caudal boundary 0.70 mm caudal to the posterior end of the facial (VII) nucleus, VII_c , is labeled “m-preBötC[500/-0.70]W-P2.5 slice”. The recording in 3 mM K^+ from the slice surface in the proposed region of the ventrolateral respiratory column (VRC) reveals a “eupnea-biphasic (burst) pattern”. Traces in the right panels show a “eupnea-sigh (burst) pattern” in a different slice, typical for $\sim 30\%$ of such cases. This burst pattern in 3 mM K^+ differs from that in the 8 mM K^+ mouse slices because of an initial postsigh depression of burst amplitude (see also Figure A2-3). (With kind permission from Ruangkittisakul et al., 2006.)

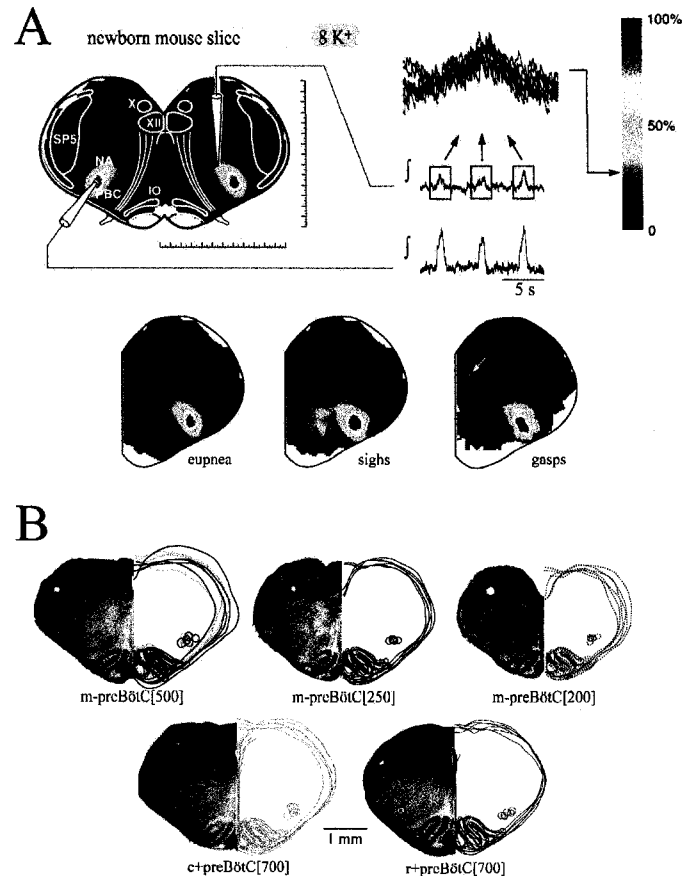


Figure A2-2 Ventrolateral respiratory region on the cut surface of transverse newborn rodent brainstem slices. **A**, Stereotaxic maps of the distribution of integrated rhythmic preBötC population activity in 0-2 weeks-old mice slices in 8 mM K^+ . The mapping electrode (right) was moved in 100 μ m steps, whereas a further electrode placed in the contralateral preBötC provided a time reference for averaging of the signals. The amplitude of the mean burst is represented by the color scheme (red indicating large burst amplitude). The lower row of images shows that distinct types of inspiratory-related behaviors, specifically eupnea, sighs and anoxic gasps, have their maximal amplitude in the same “hot spot”. (With kind permission from Lieske et al., 2000.) **B**, The left part of each image shows a fixed and thionin-stained rhythmic newborn rat preBötC slice after the experiment. The circular spot corresponds to the position of the suction electrode within the ventrolateral medulla with a maximal burst amplitude. Initial short-term (<2 min) tracking in more peripheral regions for optimal signals did not result in a notable “imprint” in contrast to the hot spot, in which the electrode was typically positioned for >3 h. The right aspect of images shows the superimposed shapes and recording sites of several slices of a given type. This analysis revealed that the respiratory hot spot had an almost identical location in all slice types, i.e. m-preBötC slices of 500 (n= 5 for eupnea-biphasic burst pattern; n= 5 for eupnea-sigh pattern), 250 (n= 6) or 200 μ m thickness (n= 6) and 700 μ m thick slices containing the preBötC plus either caudally- or rostrally-neighboring tissue, i.e., c+preBötC[700] (n= 6) or r+preBötC[700] slices (n= 6), respectively. Note that the hot spots for slices with a eupnea-biphasic (light green) or eupnea-sigh burst pattern (dark green) did not differ.

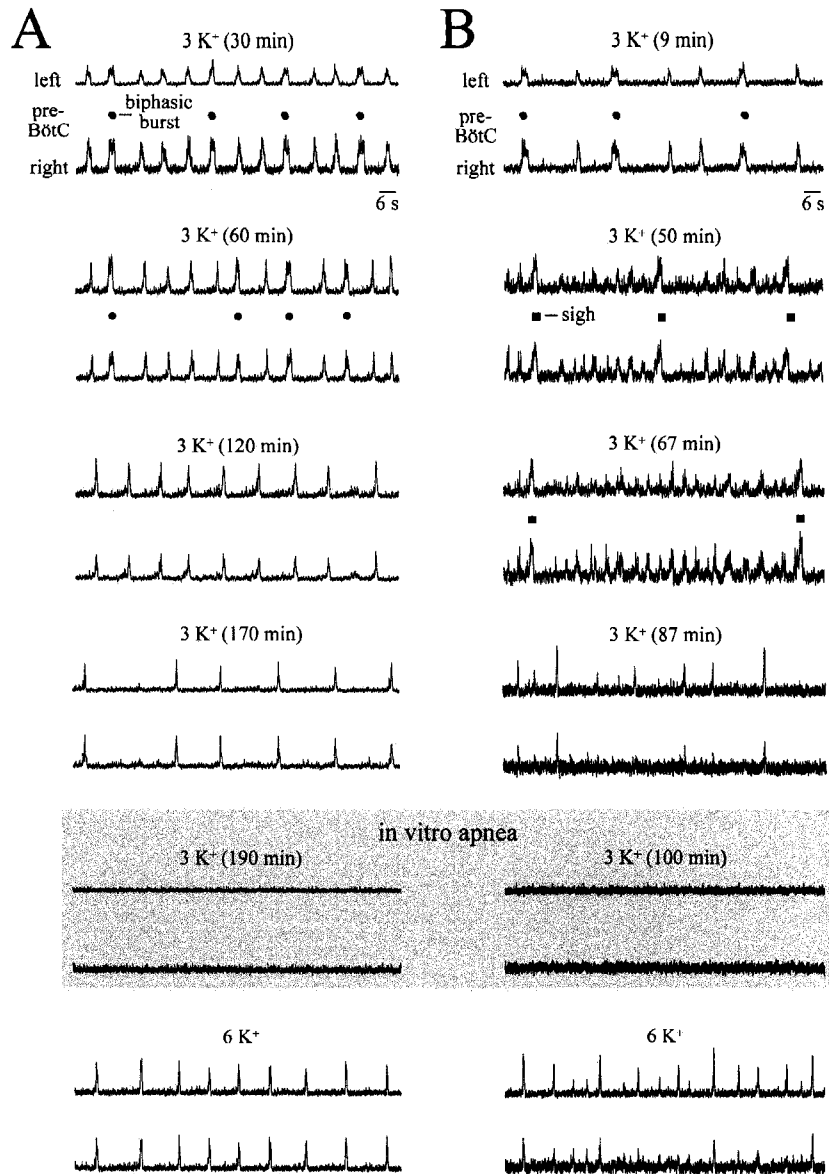


Figure A2-3 Burst patterns of inspiratory-related rhythm in m-preBötC[500] slices in 3 mM K⁺ solution. **A**, In a m-preBötC[500/-0.70]W-P3 slice, bilaterally-synchronous eupneic bursts alternated with biphasic bursts (filled circles; see Figure A2-1B,C). The rate of biphasic bursts decreased over time, until these events disappeared after ~2 h. In contrast, eupneic bursts persisted at a rate slightly lower than that during the initial phase of the recording. The rate of eupneic bursts decreased notably after ~3 h before rhythm arrested spontaneously after 190 min. Such “in vitro apnea” (Ruangkittisakul et al., 2006) was reversed by 6 mM K⁺ solution. **B**, A m-preBötC[500/-0.80]W-P3 slice showed initially a eupnea-biphasic burst pattern, which transformed after ~30 min into a eupnea-sigh burst pattern (see Figure A2-1C). After >1 h of recording, the rate of sighs was reduced, whereas the rate of eupneic bursts remained rather constant. The rhythm became irregular with a decrease in burst rate after >80 min and reversible in vitro apnea occurred after 100 min.

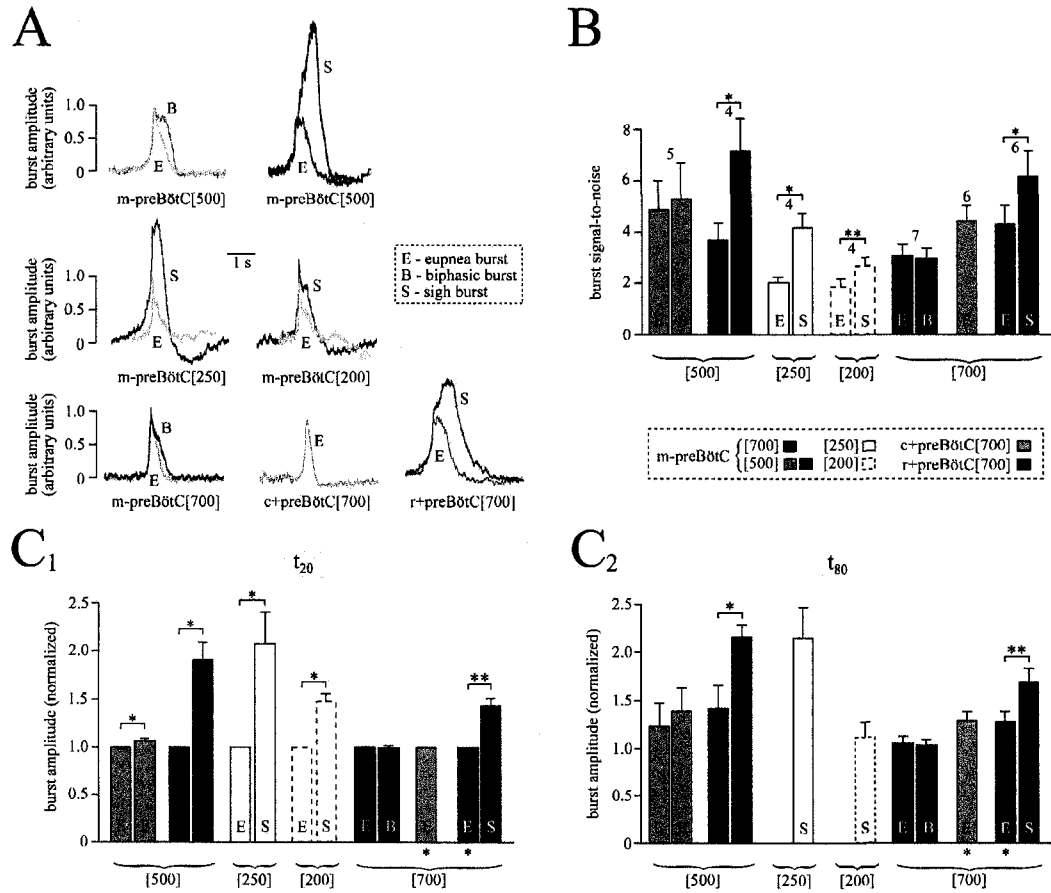


Figure A2-4 Inspiratory-related burst amplitudes in 3 mM K^+ . **A**, The mean amplitudes of eupneic (E), sigh (S) or biphasic (B) bursts from 4-12 events each (except 4-28 bursts in 200 and 250 μm slices) in 4 (200, 250, 500 μm thick m-preBötC), 5 (c+preBötC[700], r+preBötC[700]) or 6 (m-preBötC[700]) slices. Note that amplitudes were normalized to E bursts. Bursts were labeled as sighs, when they were notably larger than the associated eupneic bursts and did not show a secondary peak after the initial one as typical for biphasic bursts. Note that averaging of biphasic bursts resulted in transformation of the second peak into a reduced slope of recovery of the initial burst because of a jitter of the time of its occurrence. **B**, **C**, Comparison of burst amplitudes, referred to signal-to-noise ratio (**B**) or normalized to eupneic burst amplitudes at 20 min in a given slice (**C**) analyzed at 20 min (t_{20} , **C**₁) or 80 min (t_{80} , **C**₂) of recording. Note that eupneic bursts in 200 and 250 μm thin slices could not be analyzed at 80 min because of a progressive decrease of their amplitude. Significance: $P < 0.05$, *; $P < 0.01$, **; non-significant differences not shown. Significance for single burst types between 20 and 80 min is shown below bars. Bars represent means \pm SEM; digits above bars in **A** show the numbers of slices which were identical for **A-C**.

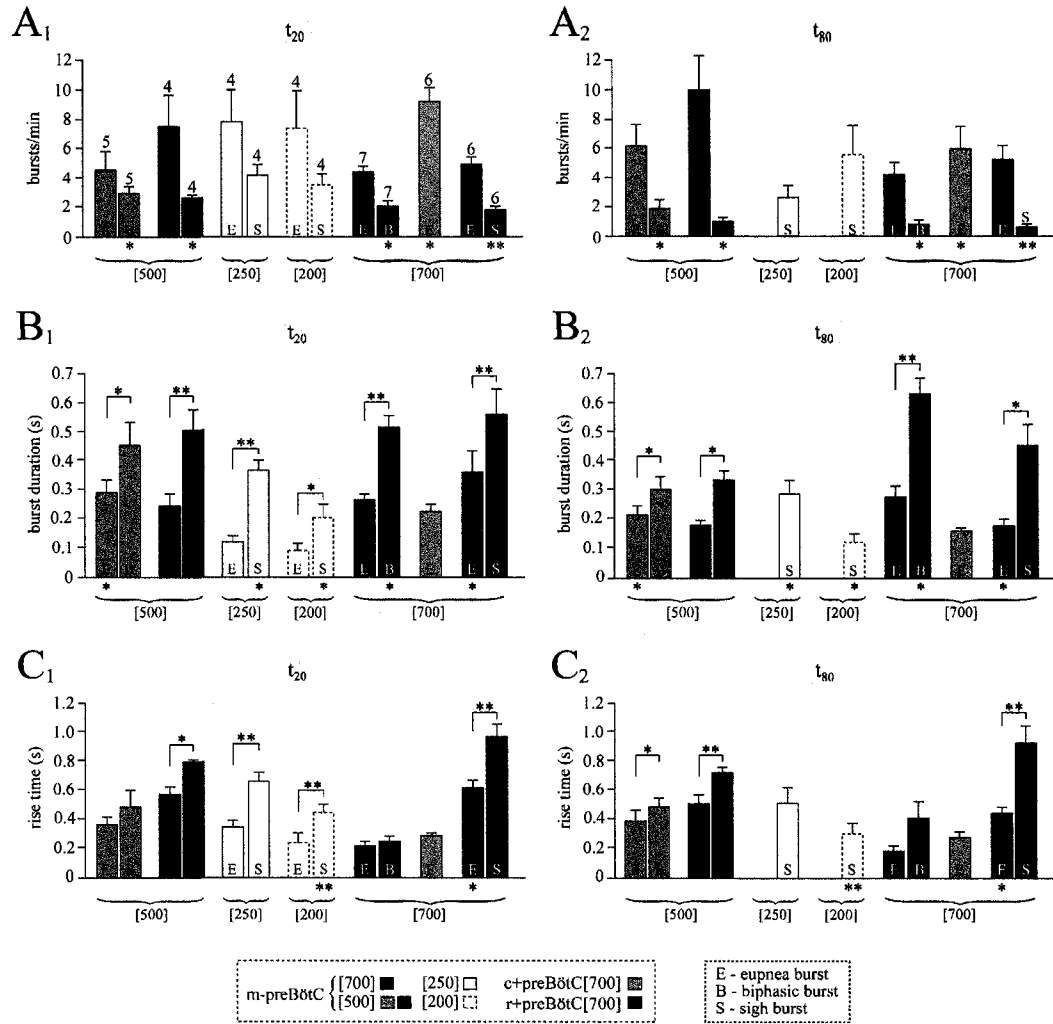


Figure A2-5 Inspiratory burst parameters of 3 mM K⁺ rhythms. A, Burst rates at 20 min (t_{20} , **A₁**) or 80 min (t_{80} , **A₂**) after the start of recording. The box below panels in **C** indicates the different slice types. Note the discrimination between eupneic (E) and biphasic bursts (B) for m-preBötC[700] slices and a subgroup of m-preBötC[500] slices. Sighs (S) and eupneic bursts between sighs were analyzed in a different subgroup of the m-preBötC[500] slices, in 250 and 200 μ m thin m-preBötC slices and r+preBötC[700] slices. Eupneic bursts were analyzed in c+preBötC slices. Significance was tested only between t_{20} and t_{80} for each burst type and not between burst types. **B**, **C**, Single burst duration (“half-width”) (**B**) and rise time (**C**) in the slices of **A**. Significance was tested between t_{20} and t_{80} for each burst type, and separately between 2 burst types in the same slice. For each slice, the average of >10 consecutive bursts was determined except for eupneic bursts in 200 or 250 μ m thin m-preBötC slices (> 5 bursts) or sighs, in which at least 3 bursts were analyzed in each slice. Note that eupneic bursts in 200 and 250 μ m thin slices could not be analyzed at 80 min because of a progressive decrease of their amplitude. Bars represent means \pm SEM; digits above bars show the numbers of slices which were identical for A-C. Significance: P < 0.05, *; P < 0.01, **.

Appendix III

Generation of newborn rat brainstem-spinal cord preparations with defined rostral boundary

(For references, see chapter IV)

The isolated brainstem-spinal cord preparation from newborn rats is an established model to study the neural control of breathing (Ballanyi et al., 1999). In this preparation, the activity of various respiratory networks is retained. Within the ventral respiratory column, these networks are the pre-Bötzinger Complex (preBötC) and the more rostrally located Bötzinger Complex (BötC) plus parafacial respiratory group (pFRG) that is presumably closely associated with the retrotrapezoid nucleus (RTN) (Feldman & Del Negro, 2006). The rostrocaudal extensions of respiratory marker brainstem nuclei are surprisingly constant in newborn rats of postnatal days (P) 0-4 (Ruangkittisakul et al., 2006). In this report, a representative brainstem atlas consisting of 50 μm fixed and thionin-stained transverse brainstem sections was introduced. In this “reference” atlas, the locations of marker structures were referred to their distance in mm from the caudal end of the facial motonucleus (VIIc), with a negative sign assigning a position caudal to VIIc. According to this terminology, the centre of the preBötC is presumably located close to -0.50 and extends $\sim 100 \mu\text{m}$ each in rostral and caudal direction, thus it is located between -0.40 to -0.60 (compare Figures A3-1, A3-2 with Figure 1 in Smith et al., 1991, Figure 2-2 in chapter II and Figure 4-1 of chapter IV). The rostrocaudal extension of the RTN/pFRG greatly overlaps with that of the VII nucleus, but appears to extend $\sim 200 \mu\text{m}$ caudal to VIIc (Onimaru & Homma, 2003, 2006). It should be noted that pre/post-inspiratory active neurons are also found within and caudal to the preBötC (Arata et al., 1990; Smith et al., 1990; Onimaru et al., 2003). Here, we describe a method for generation of newborn rat brainstem-spinal cord preparations with defined rostrocaudal boundaries that have either the preBötC more or less exposed to the rostral boundary or contain more rostral tissue with (portions of the) VII and thus, the BötC and RTN/pFRG. For their generation, we used structural landmarks on the ventral surface of the brainstem for positioning of a razor blade for manual transection. As shown in Figure A3-1, sectioning of brainstem-spinal cords at such landmarks revealed that the centre of the most rostral hypoglossal (XII) rootlet was located at -0.47 ± 0.04 (n= 6) while cutting just caudal to the vagal (X) nerve revealed a mean boundary of -0.06 ± 0.05 (n= 5). Transecting at the caudal end of the caudal cerebellar artery (CCA) (De Araujo & Campos, 2005) revealed a boundary of $+0.54 \pm 0.02$ (n= 5), whereas cutting just rostral to the CCA showed caudal structures of the medial nucleus of the trapezoid body (NTB) at $+0.79 \pm 0.06$ (n= 4). The CCA was located at $+0.74 \pm 0.16$ (n= 14) (Figure 4-1). A very caudal cutting position, where the vertebral arteries join to form the basilar artery (BA), revealed a boundary of -1.21 ± 0.08 (n= 5) (Figures 4-1, A3-1). The sectioning level of fixed and post-experiment thionin-stained brainstem-spinal cords with the proposed rostral boundary located between -0.20

and -0.50 was histologically identified by comparing structures of the inferior olive (IO) on their cut rostral surface with the complementary structures in the fixed and stained transected rostral aspect of the en bloc preparation (Figures 4-1, A3-1, A3-2). In ~40 % of 21 preparations with the rostral boundary presumably located between -0.15 and -0.30, IO structures were not revealed in the stained preparations. In those cases, sagittal sections of the transected rostral aspect of the preparations were inspected to determine the rostral boundary via the distance of the caudal end of the block from VIIc (Figure A3-3). In >70 % of cases, the histologically-identified boundary was close to that expected according to the surface landmarks.

The notable number of preparations without visible IO structures on the cut surfaces indicates that either the staining was sometimes poor or that the distance between VIIc and the rostral end of the IO may be more variable than indicated by our recent study based on transverse sections (Ruangkittisakul et al., 2006). To clarify this, we generated series of 200-250 μm thick sagittal sections of P2 rat brainstems (Figure A3-2). In the sagittal plane, VIIc is located >1 mm laterally, whereas the most rostral extension of the IO is located close to the midline (Ruangkittisakul et al., 2006). To determine the mean rostrocaudal distance between these regions in sagittal slices, we have used as reference the caudal end of the medial subregion of the NTB, which is located within the same mediolateral plane as the IO (Figure A3-2). This marker region is colocalized on the one hand with the caudal end of the superior olive and on the other hand with the rostral end of VII nucleus (Paxinos & Watson, 1982). In 5 sagittal sections, the mean distance between the rostral end of the IO and VIIc was 0.16 ± 0.03 mm, similar to that determined in transverse serial brainstem sections from P0-4 rats used to generate the atlas (0.13 ± 0.029 mm, $n=26$; Ruangkittisakul et al., 2006). According to data from that report, the mean distance between the caudal end of the NTB and the rostral end of the VII nucleus was 0 ± 0.05 mm ($n=10$). The analysis of transected slices revealed further that VII nucleus extended to $+0.76 \pm 0.07$ ($n=14$). Based on this, brainstem-spinal cord preparations transected at the rostral preBötC boundary (i.e., at the rostral proximal end the most rostral XII root) show pronounced IO structures at their rostral boundary. Conversely, preparations transected between the VI nerve and the CCA would contain the entire VII and thus the RTN/pFRG. Finally, preparations cut at the X nerve would have VIIc at the cut surface and thus contain the BötC. The brainstem-spinal cord (BSC) preparations can be labelled via the rostral boundary, i.e., in the above 3 cases BSC[-0.40], BSC[0], BSC[+0.74]. Our study revealed that preparations with the boundary caudal to -0.45 did not generate inspiratory-related rhythm (Figure A3-4).

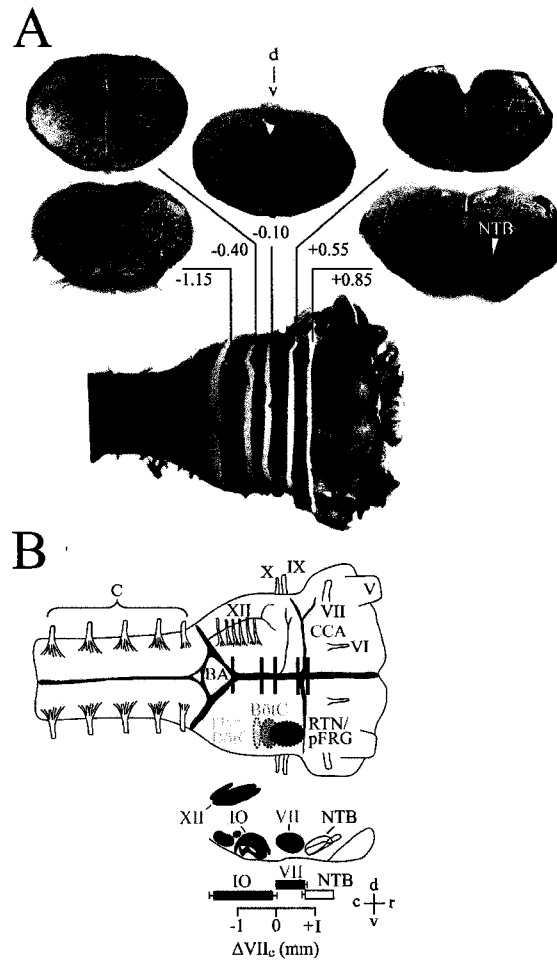


Figure A3-1 Ventral brainstem surface markers for the generation of brainstem-spinal cords (BSC) with identified boundaries. **A**, a fixed and thionin-stained BSC with pons attached was subjected to 5 consecutive manual transections using a razor blade. The 4 resulting transverse slices and the rostral brainstem block were exposed to thionin again for staining the cut surfaces (caudal slice boundaries are shown in the upper panels). Numbers indicate the distance of the caudal surface from VIIc as reference (compare Figure 4-1). **B**, schema of ventral brainstem surface marker structures. The centre of the most rostral XII rootlet was located 0.47 mm caudal to VIIc, thus at “-0.47” according to the terminology of Ruangkittisakul et al., (2006), whereas cutting just caudal to the vagal (X) nerve revealed a mean boundary at -0.06. Transecting just caudal to the caudal cerebellar artery (CCA, De Araujo & Campos, 2005) revealed a mean boundary at +0.54, whereas cutting caudal to the abducens (VI) nerve and rostral to the latter artery showed caudal structures of the nucleus of trapezoid body (NTB) at +0.79. A very caudal cutting position, specifically where the vertebral arteries joined to form the basilar artery, revealed a mean boundary of -1.21. The ovals labeled preBötC, BötC and pFRG indicate the positions of respiratory structures (compare Figure 4-1). Scale in **B** (in mm) also applies for **A**.

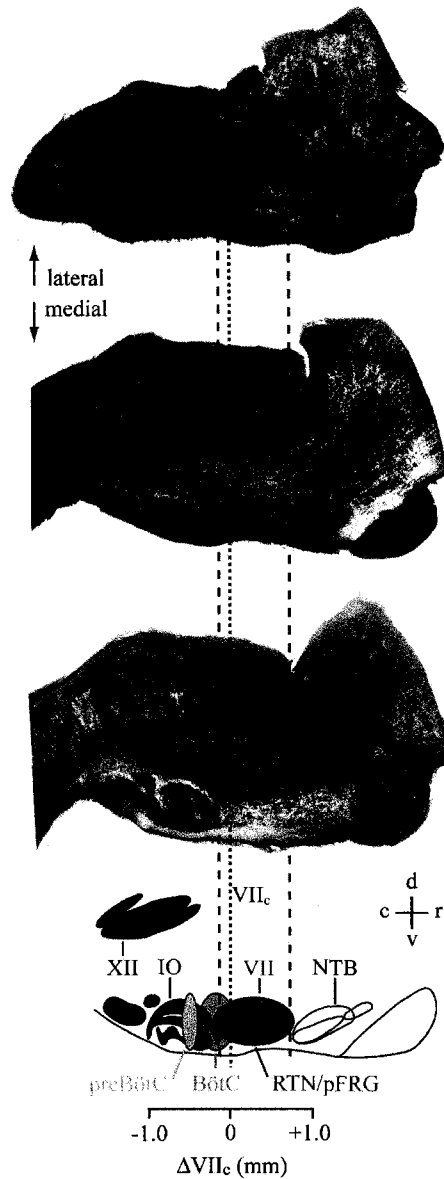


Figure A3-2 Brainstem marker nuclei for localizing respiratory structures in newborn rat brainstem-spinal cord preparations. Images show sagittal fixed and thionin-stained 200 μm sections from a postnatal day (P) 2 Wistar (W) rat brainstem, the uppermost photograph showing the most lateral section. The pair of dotted lines on the left indicates the rostral end of the inferior olive (IO) and the caudal end of the VII motonucleus (VIIc). The line on the right indicates the caudal end of the medial subregion of the NTB, which is colocalized in midline sections with the caudal end of the superior olive (Paxinos & Watson, 1982). The rostral end of the VII nucleus is colocalized with the caudal end of the medial NTB, though in a more lateral sagittal plane. This allows determination of the rostrocaudal extension of the VII nucleus, which proposedly greatly overlaps with the pFRG (see also Figures 4-1, A3-1). The centre of the $\sim 200 \mu\text{m}$ spanning preBötC is presumably located at $\sim 0.50 \text{ mm}$ caudal to VIIc (Smith et al., 1991; Ruangkittisakul et al., 2006). Note that the inspiratory active dorsally-located hypoglossal (XII) motonucleus has a rostrocaudal extension similar to that of the IO.

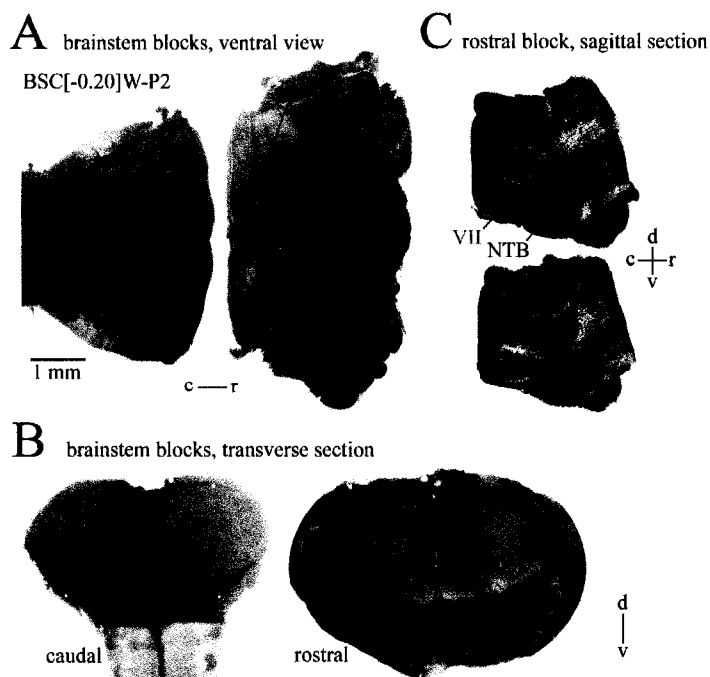


Figure A3-3 Determination of the rostral brainstem-spinal cord boundary for transection levels lacking histological respiratory marker regions. **A**, fixed and thionin-stained caudal and rostral brainstem tissue blocks from a P2 W rat after manual transection aiming to obtain a BSC[-0.20]. The rostral boundary could not be determined due to lack of presence (or lack of staining) of IO structures (**B**). **C**, serial sagittal sectioning (250 μ m) of the rostral brainstem block revealed that the closest distance of VIIc from the caudal boundary of the tissue block was 0.2 mm. Accordingly, the preparation could, indeed, be labeled BSC[-0.20]W-P2.

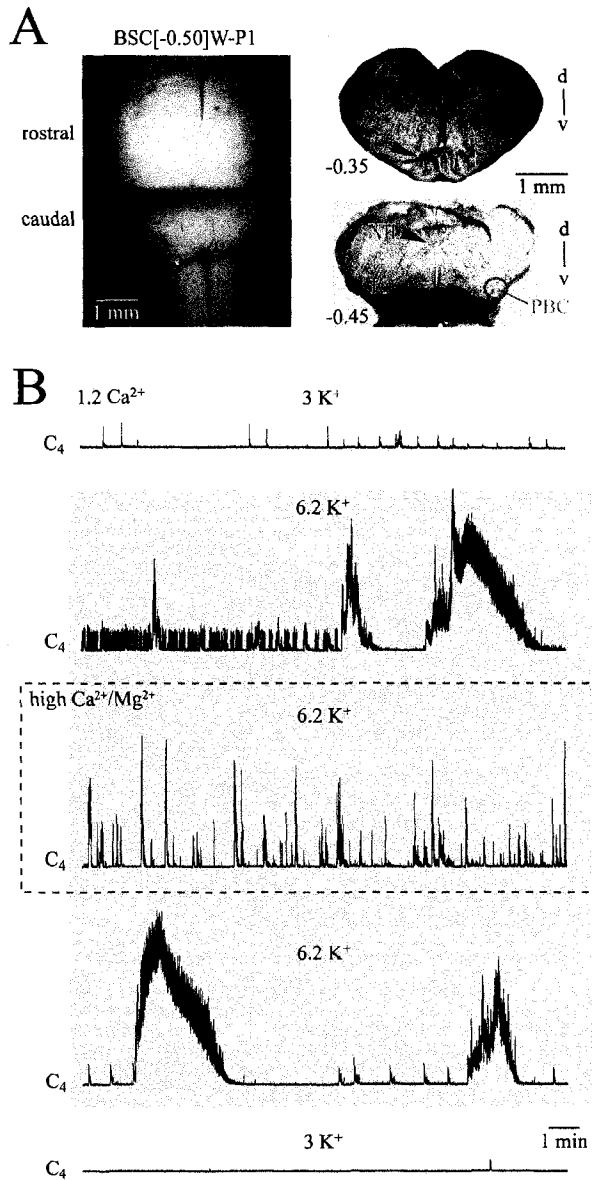


Figure A3-4 Absence of inspiratory rhythm in a brainstem-spinal cord preparation with the rostral boundary at the proposed centre of the preBötC. **A**, photographs of a transected live (left panel) and fixed plus thionin-stained (right panel) BSC[-0.50]W-P1 preparation. **B**, the uppermost trace shows non-respiratory cervical nerve (C₄) bursts occurring at irregular intervals and variable amplitude within the first 12 min of recording in 3 mM K⁺ before “rhythm” stopped (not shown). In 6.2 mM K⁺ solution, irregular small amplitude cervical bursts were intermingled with large amplitude, long duration (0.5–4 min) activity. The massive long duration discharge was reversibly suppressed in 6.2 mM K⁺ by “high Ca²⁺/Mg²⁺” superfusate in which Ca²⁺ was raised from 1.2 to 2.4 mM and Mg²⁺ from 1.0 to 1.3 mM. In that saline, large amplitude bursting occurred at variable strength and single burst duration of 1–10 s. Return to solution with physiological cation content abolished all activities. Similar to that example, 2 further BSC preparations with the boundary at -0.50 and one with a boundary at -0.55 did not show respiratory rhythm.